



TEZ ŞABLONU ONAY FORMU THESIS TEMPLATE CONFIRMATION FORM

1. Bu form, yalnızca FBE web sayfasında yer alan Word Tez Şablonu'nu kullanan öğrenciler tarafından doldurulacaktır. **Word şablonunu kullanmadığı halde bu formu dolduran öğrencilerin yaşayabileceği sıkıntılardan enstitümüz sorumlu değildir.**
2. Bu onay formunu takip eden sayfalarda, Tez Şablonu Dönüştürme Formu (TŞDF) yer almaktadır. TŞDF, üzerinde bulunan alanlara girilen verileri otomatik olarak FBE tez formatına dönüştürmektedir.
3. Bu şablon aracılığıyla oluşturulacak tezlerde herhangi bir sıkıntı yaşanmaması için **döküman boyunca yer alan tüm açıklamalara/uyarılara dikkat edilmesi gerekmektedir.** Bu nedenle, döküman içerisinde yer alan tüm yorumları dikkatli bir şekilde okuyup uygulayınız.
 - TŞDF aracılığıyla oluşturduğunuz tezinizi, [Tez Kontrol Formu](#)'nda yer alan tez formatı hakkındaki bilgilere göre tekrar kontrol edilmesi gerekmektedir. Bu konudaki tüm sorumluluk öğrenciye aittir.
5. TŞDF üzerinde düzeltme yapabileceğiniz alanlar sınırlıdır. Bu alanları görebilmek için, bu sayfanın alt kısmında yer alan **"Editable Fields On/Off"** butonuna tıklamanız gerekmektedir.
1. Aksi belirtilmediği sürece, TŞDF üzerinde yer alan tüm alanlar İngilizce doldurulmalıdır.
2. TŞDF aracılığıyla oluşturduğunuz tezinizdeki *İçindekiler, Tablolar Listesi ve Şekiller Listesi* gibi otomatik olarak oluşturulan bölümleri güncellemek için bu sayfanın alt kısmında yer alan **"Update Autofields"** butonuna tıklamanız gerekmektedir.
3. Bu sayfanın alt kısmında yer alan **"Confirmation Form"** butonuna tıklayarak tez şablonu onay formunuzu PDF dosyası olarak kaydediniz.
4. Bu sayfanın alt kısmında yer alan **"Converter Form"** butonuna tıklayarak TŞDF'nizi PDF dosyası olarak kaydediniz.
5. Bu sayfanın alt kısmında yer alan **"Thesis File"** butonuna tıklayarak tezinizi PDF dosyası olarak kaydediniz.
6. **Bu form aracılığıyla oluşturduğunuz PDF dosyalarının her birinin arkalı-önlü baskısını alarak tek bir spirallli cilt haline getiriniz.**
7. Spirallli hale getirdiğiniz tez taslağınızdaki ilgili alanları imzaladıktan sonra, Tez Juri Atama Formu'nuz ile birlikte bölüm sekreterliğine teslim ediniz.
8. Tez taslağınız bölüm sekreterliğiniz aracılığıyla format ve görünüm açısından kontrol edilmek üzere FBE'ye ulaştırılacaktır. Öğrenciler tarafından enstitüye getirilen tez taslakları kesinlikle kabul edilmeyecektir.
9. FBE tarafından kontrol işlemleri tamamlanan tez taslakları, öğrencilere teslim edilmek üzere bölüm sekreterliklerine iletilecektir.
10. Tez taslaklarının kontrol işlemleri tamamlandığında, bu durum öğrencilere METU uzantılı öğrenci e-posta adresleri aracılığıyla duyurulacaktır.
11. Tez taslakları bölüm sekreterlikleri tarafından öğrencilere iletileceği için öğrencilerimizin tez taslaklarını enstitümüzden elden alma konusunda ısrarcı olmamaları beklenmektedir.
12. Tez yazım süreci ile ilgili herhangi bir sıkıntı yaşarsanız, [Sıkça Sorulan Sorular \(SSS\)](#) sayfamızı ziyaret ederek yaşadığınız sıkıntıyla ilgili bir çözüm bulabilirsiniz.

1. This form will only be filled in by students who have used the Word Thesis Template on the FBE web page. **Our institute is not responsible for the difficulties that the students who have filled in this form although they do not use the Word template.**
2. The pages following this approval form contain the Thesis Template Converter Form (TTCF). TTCF automatically converts the data entered on the fields into the GSNAS thesis format.
 - In order to prevent any problems in the theses to be created through this template, it is **necessary to pay attention to all comments/warnings throughout the document.** For this reason, please **read and apply all comments/direction** in the document carefully.
4. You have to re-check your thesis, which you have created through the TTCF, according to the information about the thesis template contained in the [Thesis Control Form](#). All responsibility in this subject belongs to the student.
 - There are a limited number of editable fields on the TTCF. To see these fields, you need to click the **"Editable Fields On/Off"** button at the bottom of this count.
 - All of the fields in the form must be filled out in English unless it is not specified.
 - You need to click on the **"Update Autofields"** button at the bottom of this page to update automatically created sections such as *Table of Contents, List of Tables, and List of Figures* in your thesis created by TTCF.
- Click on the **"Confirmation Form"** button at the bottom of this page to save your thesis template confirmation form as a PDF file.
- Click on the **"Converter Form"** button at the bottom of this page and save your TTCF as a PDF file.
- Click on the **"Thesis File"** button at the bottom of this page to save your thesis as a PDF file.
- **Print both-side each of the PDF files that you have created through this form and make a single spiral bound.**
- Once you have signed the relevant fields in your thesis draft that you spiraled, submit it to the department secretary together with your Thesis Jury Assignment Form.
- Your thesis draft will be delivered to the GSNAS via your department secretary for controlling in terms of format and appearance. The thesis drafts submitted to the institute by students will not be accepted.
- The thesis drafts that are controlled by GSNAS, will be sent to the department secretary to be delivered to the students.
- This will be announced to the students via their METU students e-mail addresses when the control of the thesis drafts have been completed.
- As the thesis drafts will be delivered to the students by the department secretaries, we are expecting from our students no to insist about getting their theses drafts from the Institute.
- If you have any problems with the thesis writing process, you may visit our [Frequently Asked Questions \(FAQ\)](#) page and find a solution to your problem.

Yukarıda bulunan tüm maddeleri okudum, anladım ve kabul ediyorum. / I have read, understand and accept all of the items above.

Name : Ramin
Surname : Barzegar
E-Mail : ramin.barzegar@metu.edu.tr
Date : 10.09.2019
Signature : _____

Editable Fields On/O

Update AutoFields

Confirmation Form

Converter Form

Thesis File



THESIS TEMPLATE CONVERTER FORM

SECTION 1: GENERAL INFORMATION

STUDENT

Name : Ramin
Surname : Barzegar
Student ID : 2059772
Degree / Derece : Doctor of Philosophy / Doktora
Department / Bölüm : Mechanical Engineering / Makina Mühendisliği
Defense Date : 26.08.2019

HEAD OF DEPARTMENT

Title : Prof. Dr.
Name Surname : M. A. Sahir Arıkan
Department : Mechanical Engineering

SUPERVISOR

Title / Ünvan : Prof. Dr. / Prof. Dr.
Name Surname : Ahmet Yozgatlıgil

CO-SUPERVISOR

Title / Ünvan : Prof. Dr. / Prof. Dr.
Name Surname : Aysel Atımtay
Department, University : Environmental Engineering, METU



SECTION 2: EXAMINING COMMITTEE MEMBERS*

HEAD OF THE EX. COMMITTEE

Title : Assoc. Prof. Dr.
Name Surname : M. Metin Yavuz
Department, University : Mechanical Engineering, METU

MEMBER 1

Title : Prof. Dr.
Name Surname : Murat Köksal
Department, University : Mechanical Engineering, Hacettepe University

MEMBER 2

Title : Assist. Prof. Dr.
Name Surname : Feyza Kazanç
Department, University : Mechanical Engineering, METU

MEMBER 3

Title : Assoc. Prof. Dr.
Name Surname : Murat Aktaş
Department, University : Mechanical Engineering, TOBB ETU

* Your supervisor is one of the natural member of the examining committee. Therefore, please enter only the other committee members' information in this section.



SECTION 3: THESIS INFORMATION ON ENGLISH

THESIS TITLE

INVESTIGATION OF COMBUSTION OF LIGNITE AND TORREFIED BIOMASS IN A THERMOGRAVIMETRIC ANALYZER (TGA) AND IN A CIRCULATING FLUIDIZED BED (CFB) UNDER OXY-FUEL COMBUSTION CONDITIONS

ABSTRACT

In this study, the combustion of Turkish lignites (Orhaneli and Soma), torrefied woodchip, and their blends was studied under oxygen-enriched and oxy-fuel combustion conditions in a thermogravimetric analyzer. The iso-conversional kinetic methods were used to estimate the Arrhenius parameters and the uncertainty assessments associated with the kinetic calculations were considered. The co-combustion experiments showed a synergetic effect between the biomass samples and Orhaneli lignite. Based on the obtained results, Orhaneli lignite and the biomass torrefied at 300°C-30 min torrefaction conditions were selected for further analysis in a laboratory scale Circulating Fluidized Bed Combustor (CFBC). The CFBC experiments were conducted under oxygen-enriched and oxy-fuel combustion conditions and included the addition of calcium-based sorbents (Çan limestone and Eskişehir dolomite) for in-situ adsorption of sulfur dioxide emission. The conducted CFBC experiments showed that the sulfur dioxide removal was more effective with the addition of Çan limestone with the particle size of 1-2 mm and Ca/S ratio of 2. Also, increasing the oxygen concentration was an effective solution in sulfur retention. Furthermore, the combustion process in the CFBC was numerically simulated and the results were compared with the experiments. The simulation results showed a good agreement with the experimental data in estimation of the combustor temperature and carbon-based efficiency.

KEYWORDS

Oxy-fuel Combustion, Co-combustion, Torrefied biomass, CFBC, Sulfur Capture



SECTION 4: THESIS INFORMATION IN TURKISH

TEZ BAŞLIĞI

LİNYİT VE TORİFİYE EDİLMİŞ BİYOKÜTLENİN OKSİ-YANMA KOŞULARINDA YAKILMASININ TERMOGRAVİMETRİK ANALİZ CİHAZINDA VE DOLAŞIMLI AKIŞKAN YATAK YAKMA SİSTEMİNDE İNCELENMESİ

ÖZET

Bu çalışmada, Türkiye linyitlerinin (Orhaneli ve Soma), torefiye edilmiş odunun ve bunların karışımlarının oksijence-zenginleştirilmiş yanma ve oksii-yanmaları termogravimetric analiz cihazında incelenmiştir. Arrhenius parametrelerinin hesaplanmasında dönüşüm değerleri sabit alınarak (iso-conversional) kinetik metotları kullanılmıştır ve kinetik hesaplamalarında belirsizlik analizi dikkate alınmıştır. Karışımların yanma sonuçlarına göre, Orhaneli linyit ve biyokömür numuneleri arasında bir sinerji görülmüştür. Elde edilen sonuçlara göre, laboratuvar ölçekli Dolaşimli Akışkan Yatak (DAY) deneylerinde kullanmak üzere Orhaneli linyiti ve 300°C-30dakika koşulunda torefiye edilmiş biyokömür seçilmiştir. DAY sisteminde yapılan deneyler oksijence-zenginleştirilmiş ve oksii-yanma koşullarında gerçekleştirilmiştir. Bunun yanı sıra, kükürt dioksit emisyonunun yatakta tutulması için, kalsiyum bazlı tutucular (Çan kireçtaşı ve Eskişehir dolomit) yatağa eklenmiştir. DAY deney sonuçlarına göre, Çan kireçtaşının parçacık boyutu 1-2 mm ve Ca/S oranı 2 olduğunda kükürt dioksit emisyonunun yatakta tutulması daha etkin olmuştur. Bununla birlikte, oksijen konsantrasyonunun artırılmasının kükürt tutulmasında etkili olduğu görülmüştür. Bunlara ek olarak, DAY sistemindeki yanma prosesinin bir paket program kullanarak sayısal simülasyonu (modellemesi) yapılmıştır ve deney sonuçları ile karşılaştırılmıştır. Yatak sıcaklığı ve karbon-bazlı verimlilik için model sonuçları, deneysel veriler ile uyumludur.

ANAHTAR KELİMELER

Oksii-yanma, Birlikte Yakma, Torefiye Biyokütle, DAY, Kükürt Tutma



SECTION 5: THESIS DETAILS

NUMBER OF PAGES

Page number on the last page of this document: 208

DEDICATION

To My Beloved Wife and My Dear Parents

ACKNOWLEDGMENTS*

First and foremost, I would like to express my sincere gratitude towards my supervisor Prof. Dr. Ahmet Yozgatligil for his guidance, advice, criticism, encouragement and insight throughout the course of my studies.

I would like to express my deepest appreciation to my co-supervisor Prof. Dr. Aysel Atimtay for her sincere support, guidance and insightful suggestions during the completion of this work.

I would like to thank my Ph.D. committee and jury members, Professor Murat Köksal, Professor Feyza Kazanç, Professor M. Metin Yavuz and Professor Murat Aktaş for their valuable suggestions and helpful comments during the course of this study.

The financial support for this work by TUBITAK under the project “TUBITAK-1003-213M525: Oxy-combustion of Lignite and Torrefied Biomass in a Circulating Fluidized Bed (OXYCOMBUSTION)” is greatly acknowledged.

Special thanks goes to my dear colleagues and friends at DETS Dynamics Co. Mr. Niyazi Burak Tuncer, Mr. Umut Tektürk, Miss. Belgin Yaylacı, and Mr. Çağrı Metin for their help and support during this research.

My deepest gratitude is due all my friends and the staff in the Departments of Mechanical and Environmental Engineering, Dr. Sina Shafee, Mr. Levent Şahin, Mr. Duarte Magalhaes, and Miss. Sevil Avşaroğlu for their support during my research.

I also would like to extend my gratitude to the technical and scientific staff at TUBITAK-Marmara Research Center. Their help and support on this research especially on conducting the CFB experiments was invaluable.

And finally, I would like to show my profound gratitude to my kind and gracious wife, Faezeh, my beloved parents, and my dear family for their support and encouragement at every step of this endeavor. Their unshakeable confidence in me is invaluable.

* If you have received project support from TÜBİTAK, you must mention about it.

INVESTIGATION OF COMBUSTION OF LIGNITE AND TORREFIED
BIOMASS IN A THERMOGRAVIMETRIC ANALYZER (TGA) AND IN A
CIRCULATING FLUIDIZED BED (CFB) UNDER OXY-FUEL COMBUSTION
CONDITIONS

A THESIS SUBMITTED TO
THE GRADUATE SCHOOL OF NATURAL AND APPLIED SCIENCES
OF
MIDDLE EAST TECHNICAL UNIVERSITY

BY

RAMIN BARZEGAR

IN PARTIAL FULFILLMENT OF THE REQUIREMENTS
FOR
THE DEGREE OF DOCTOR OF PHILOSOPHY
IN
MECHANICAL ENGINEERING

AUGUST 2019

Approval of the thesis:

**INVESTIGATION OF COMBUSTION OF LIGNITE AND TORREFIED
BIOMASS IN A THERMOGRAVIMETRIC ANALYZER (TGA) AND IN A
CIRCULATING FLUIDIZED BED (CFB) UNDER OXY-FUEL
COMBUSTION CONDITIONS**

submitted by **RAMIN BARZEGAR** in partial fulfillment of the requirements for the degree of **Doctor of Philosophy in Mechanical Engineering Department, Middle East Technical University** by,

Prof. Dr. Halil Kalıpçılar
Dean, Graduate School of **Natural and Applied Sciences**

Prof. Dr. M. A. Sahir Arıkan
Head of Department, **Mechanical Engineering**

Prof. Dr. Ahmet Yozgatlıgil
Supervisor, **Mechanical Engineering, METU**

Prof. Dr. Aysel Atımtay
Co-Supervisor, **Environmental Engineering, METU**

Examining Committee Members:

Assoc. Prof. Dr. M. Metin Yavuz
Mechanical Engineering, METU

Prof. Dr. Ahmet Yozgatlıgil
Mechanical Engineering, METU

Prof. Dr. Murat Köksal
Mechanical Engineering, Hacettepe University

Assist. Prof. Dr. Feyza Kazanç
Mechanical Engineering, METU

Assoc. Prof. Dr. Murat Aktaş
Mechanical Engineering, TOBB ETU

Date: 26.08.2019

I hereby declare that all information in this document has been obtained and presented in accordance with academic rules and ethical conduct. I also declare that, as required by these rules and conduct, I have fully cited and referenced all material and results that are not original to this work.

Name, Surname: Ramin Barzegar

Signature:

ABSTRACT

INVESTIGATION OF COMBUSTION OF LIGNITE AND TORREFIED BIOMASS IN A THERMOGRAVIMETRIC ANALYZER (TGA) AND IN A CIRCULATING FLUIDIZED BED (CFB) UNDER OXY-FUEL COMBUSTION CONDITIONS

Barzegar, Ramin
Doctor of Philosophy, Mechanical Engineering
Supervisor: Prof. Dr. Ahmet Yozgatlıgil
Co-Supervisor: Prof. Dr. Aysel Atımtay

August 2019, 208 pages

In this study, the combustion of Turkish lignites (Orhaneli and Soma), torrefied woodchip, and their blends was studied under oxygen-enriched and oxy-fuel combustion conditions in a thermogravimetric analyzer. The iso-conversional kinetic methods were used to estimate the Arrhenius parameters and the uncertainty assessments associated with the kinetic calculations were considered. The co-combustion experiments showed a synergetic effect between the biomass samples and Orhaneli lignite. Based on the obtained results, Orhaneli lignite and the biomass torrefied at 300°C-30 min torrefaction conditions were selected for further analysis in a laboratory scale Circulating Fluidized Bed Combustor (CFBC). The CFBC experiments were conducted under oxygen-enriched and oxy-fuel combustion conditions and included the addition of calcium-based sorbents (Çan limestone and Eskişehir dolomite) for in-situ adsorption of sulfur dioxide emission. The conducted CFBC experiments showed that the sulfur dioxide removal was more effective with the addition of Çan limestone with the particle size of 1-2 mm and Ca/S ratio of 2. Also, increasing the oxygen concentration was an effective solution in sulfur retention. Furthermore, the combustion process in the CFBC was numerically simulated and the

results were compared with the experiments. The simulation results showed a good agreement with the experimental data in estimation of the combustor temperature and carbon-based efficiency.

Keywords: Oxy-fuel Combustion, Co-combustion, Torrefied biomass, CFBC, Sulfur Capture

ÖZ

LİNYİT VE TORİFİYE EDİLMİŞ BİYOKÜTLENİN OKSİ-YANMA KOŞULLARINDA YAKILMASININ TERMOGRAVİMETRİK ANALİZ CİHAZINDA VE DOLAŞIMLI AKIŞKAN YATAK YAKMA SİSTEMİNDE İNCELENMESİ

Barzegar, Ramin
Doktora, Makina Mühendisliği
Tez Danışmanı: Prof. Dr. Ahmet Yozgatlıgil
Ortak Tez Danışmanı: Prof. Dr. Aysel Atımtay

Ağustos 2019, 208 sayfa

Bu çalışmada, Türkiye linyitlerinin (Orhaneli ve Soma), torefiye edilmiş odunun ve bunların karışımlarının oksijence-zenginleştirilmiş yanma ve oksiyenmaları termogravimetric analiz cihazında incelenmiştir. Arrhenius parametrelerinin hesaplanmasında dönüşüm değerleri sabit alınarak (iso-conversional) kinetik metotları kullanılmıştır ve kinetik hesaplamalarında belirsizlik analizi dikkate alınmıştır. Karışımların yanma sonuçlarına göre, Orhaneli linyit ve biyokömür numuneleri arasında bir sinerji görülmüştür. Elde edilen sonuçlara göre, laboratuvar ölçekli Dolaşimli Akışkan Yatak (DAY) deneylerinde kullanmak üzere Orhaneli linyiti ve 300°C-30dakika koşulunda torefiye edilmiş biyokömür seçilmiştir. DAY sisteminde yapılan deneyler oksijence-zenginleştirilmiş ve oksiyenma koşullarında gerçekleştirilmiştir. Bunun yanı sıra, kükürt dioksit emisyonunun yatakta tutulması için, kalsiyum bazlı tutucular (Çan kireçtaşı ve Eskişehir dolomit) yatağa eklenmiştir. DAY deney sonuçlarına göre, Çan kireçtaşının parçacık boyutu 1-2 mm ve Ca/S oranı 2 olduğunda kükürt dioksit emisyonunun yatakta tutulması daha etkin olmuştur. Bununla birlikte, oksijen konsantrasyonunun artırılmasının kükürt tutulmasında etkili olduğu görülmüştür. Bunlara ek olarak, DAY sistemindeki yanma prosesinin bir paket

program kullanarak sayısal simülasyonu (modellemesi) yapılmıştır ve deney sonuçları ile karşılaştırılmıştır. Yatak sıcaklığı ve karbon-bazlı verimlilik için model sonuçları, deneysel veriler ile uyumludur.

Anahtar Kelimeler: Oksi-yanma, Birlikte Yakma, Torefiye Biyokütle, DAY, Kükürt Tutma

To My Beloved Wife and My Dear Parents

ACKNOWLEDGEMENTS

First and foremost, I would like to express my sincere gratitude towards my supervisor Prof. Dr. Ahmet Yozgatligil for his guidance, advice, criticism, encouragement and insight throughout the course of my studies.

I would like to express my deepest appreciation to my co-supervisor Prof. Dr. Aysel Atimtay for her sincere support, guidance and insightful suggestions during the completion of this work.

I would like to thank my Ph.D. committee and jury members, Professor Murat Köksal, Professor Feyza Kazanç, Professor M. Metin Yavuz and Professor Murat Aktaş for their valuable suggestions and helpful comments during the course of this study.

The financial support for this work by TUBITAK under the project “TUBITAK-1003-213M525: Oxy-combustion of Lignite and Torrefied Biomass in a Circulating Fluidized Bed (OXYCOMBUSTION)” is greatly acknowledged.

Special thanks goes to my dear colleagues and friends at DETS Dynamics Co. Mr. Niyazi Burak Tuncer, Mr. Umut Tektürk, Miss. Belgin Yaylacı, and Mr. Çağrı Metin for their help and support during this research.

My deepest gratitude is due all my friends and the staff in the Departments of Mechanical and Environmental Engineering, Dr. Sina Shafee, Mr. Levent Şahin, Mr. Duarte Magalhaes, and Miss. Sevil Avşaroğlu for their support during my research.

I also would like to extend my gratitude to the technical and scientific staff at TUBITAK-Marmara Research Center. Their help and support on this research especially on conducting the CFB experiments was invaluable.

And finally, I would like to show my profound gratitude to my kind and gracious wife, Faezeh, my beloved parents, and my dear family for their support and encouragement at every step of this endeavor. Their unshakeable confidence in me is invaluable.

TABLE OF CONTENTS

ABSTRACT	v
ÖZ	vii
ACKNOWLEDGEMENTS	x
TABLE OF CONTENTS	xi
LIST OF TABLES	xv
LIST OF FIGURES	xviii
LIST OF ABBREVIATIONS	xxv
LIST OF SYMBOLS	xxviii
CHAPTERS	
1. INTRODUCTION	1
1.1. General	1
1.2. Motivation	4
1.3. Scope of the Thesis.....	5
2. LITERATURE REVIEW	7
2.1. Energy Review	7
2.2. Carbon Capture and Storage (CCS)	10
2.3. Fluidized Bed Combustion Technology	15
2.3.1. Oxy-fuel Combustion in FBC.....	19
2.3.2. Sulfur Dioxide Capture in FBC	22
2.3.3. Application of Biomass in FBC.....	26
2.4. CFB Simulation Studies	31
2.5. Thermogravimetric Analysis (TGA).....	36

3. MATERIALS AND METHODS	45
3.1. Coal and Biomass Samples	45
3.2. Experimental Study	50
3.2.1. TGA Studies	50
3.2.2. CFB Studies	55
3.3. Numerical Analysis	64
3.3.1. Kinetic Analysis	64
3.3.2. Uncertainty Assessment	68
3.3.3. CeSFaMB Simulation Software	69
3.4. Experimental Matrices	73
3.4.1. TGA Experiments	73
3.4.2. CFB Experiments	77
4. RESULTS AND DISCUSSIONS	79
4.1. Thermogravimetric Analysis	79
4.1.1. Combustion of Lignites under Oxygen-Enriched and Oxy-fuel Conditions	79
4.1.1.1. TGA Analysis	80
4.1.1.2. Kinetic Analysis	86
4.1.2. Combustion of Torrefied Biomass Under Oxygen-Enriched and Oxy-fuel Conditions	96
4.1.2.1. Torrefied Biomass Physical and Chemical Properties	96
4.1.2.2. TGA Analysis	98
4.1.2.3. Kinetic Calculations	106
4.1.3. Co-Combustion of Lignite and Biomass Under Oxygen-Enriched and Oxy-fuel Conditions	113

4.1.3.1. TGA Analysis	114
4.1.3.2. Kinetic Analysis	136
4.2. Circulating Fluidized Bed Experiments	143
4.2.1. Combustion of Orhaneli Lignite and Çan Limestone in Enriched Oxygen Atmosphere	144
4.2.1.1. Limestone Particle Size = 0-1 mm; Ca/S Ratio = 1.5	144
4.2.1.2. Limestone Particle Size = 0-1 mm; Ca/S Ratio = 2	147
4.2.1.3. Limestone Particle Size = 1-2 mm; Ca/S Ratio = 1.5	150
4.2.1.4. Limestone Particle Size = 1-2 mm; Ca/S Ratio = 2	152
4.2.2. Combustion of Orhaneli Lignite and Eskişehir Dolomite in Enriched Oxygen Atmosphere	156
4.2.2.1. Dolomite Particle Size = 0-1 mm; Ca/S Ratio = 1.5	156
4.2.2.2. Dolomite Particle Size = 0-1 mm; Ca/S Ratio = 2	159
4.2.2.3. Dolomite Particle Size = 1-2 mm; Ca/S Ratio = 1.5	161
4.2.2.4. Dolomite Particle Size = 1-2 mm; Ca/S Ratio = 2	164
4.2.3. Oxy-fuel combustion of Orhaneli lignite	167
4.2.3.1. Addition of Çan limestone	168
4.2.3.2. Addition of Eskişehir Dolomite	171
4.3. Circulating Fluidized Bed simulation	174
5. CONCLUSIONS	183
5.1. TGA Experiments	183
5.2. Circulating Fluidized Bed Experiments	186
6. FUTURE STUDIES	189
REFERENCES	191

CURRICULUM VITAE.....207

LIST OF TABLES

TABLES

Table 2.1. World primary energy demand by fuel and scenario (Mtoe) [1]	8
Table 3.1. Proximate and ultimate analysis of lignite samples	46
Table 3.2. Ash XRF analysis of the coal samples	46
Table 3.3. Proximate and ultimate analysis of the biomass samples	49
Table 3.4. XRF analysis of the adsorbents	49
Table 3.5. BET results of the adsorbents	50
Table 3.6. PerkinElmer Pyris-1 TGA specifications	52
Table 3.7. Teledyne HFC 202 mass flow controller specifications	53
Table 3.8. Thermocouple heights from the distributor plate inside the combustor and return leg	59
Table 3.9. Expressions of the applied kinetics models	68
Table 3.10. Experimental matrix of Orhaneli and Soma lignite samples combustion and oxy-combustion at different oxygen concentrations	74
Table 3.11. Experimental matrix of raw and torrefied biomass samples combustion under air and oxy-fuel conditions	75
Table 3.12. Experimental matrix of co-combustion of Orhaneli and Soma lignite samples and biomass mixtures under air and oxy-combustion conditions	76
Table 3.13. Experimental matrix of CFBC studies	78
Table 4.1. Reaction intervals of Orhaneli lignite under oxygen enriched air and oxy-fuel combustion conditions	82
Table 4.2. Reaction intervals of Soma lignite under oxygen enriched air and oxy-fuel combustion conditions	83
Table 4.3. Average activation energy values for Orhaneli lignite at different combustion environments	91

Table 4.4. Average estimated activation energy values for Soma lignite at different combustion environments	93
Table 4.5. Characteristic temperatures of raw and torrefied biomass under air combustion condition.....	103
Table 4.6. Characteristic temperatures of raw and torrefied biomass under oxy-fuel combustion condition.....	105
Table 4.7. Average estimated activation energy values for raw and torrefied biomass under air and oxy-fuel combustion conditions	111
Table 4.8. Pre-exponential factor ranges for raw and torrefied biomass under air and oxy-fuel combustion conditions	113
Table 4.9. Characteristic temperatures of Orhaneli and raw and torrefied biomass 50/50 blends at different heating rates under air and oxy-fuel combustion conditions	116
Table 4.10. Characteristic temperatures of Soma and raw and torrefied biomass 50/50 blends at different heating rates under air and oxy-fuel combustion conditions.....	126
Table 4.11. Relative error calculation for the 50/50 blends of Orhaneli with raw and 300°C-30min torrefied biomass under air and oxy-fuel combustion atmospheres .	134
Table 4.12. Relative error calculation for the 50/50 blends of Soma with raw and 300°C-30min torrefied biomass under air and oxy-fuel combustion atmospheres .	135
Table 4.13. Average estimated activation energy values for Orhaneli, 300°C-30min torrefied biomass and their 25, 50 and 75 wt.% blends under air combustion atmosphere.....	139
Table 4.14. Average activation energy values for the 50/50 blend of Orhaneli with raw and 300°C-30min torrefied biomass under air and oxy-fuel combustion atmosphere	141
Table 4.15. Average activation energy values for the 50/50 blend of Soma with raw and 300°C-30min torrefied biomass under air and oxy-fuel combustion atmosphere	142
Table 4.16. Emissions of Orhaneli lignite combustion at different oxygen concentrations	144

Table 4.17. Emissions of the combustion of Orhaneli lignite and Çan limestone at different conditions	155
Table 4.18. Emissions of the combustion of Orhaneli lignite and Eskişehir dolomite at different conditions	167
Table 4.19. Emissions of Orhaneli lignite under oxy-fuel combustion conditions at different excess air ratios	168
Table 4.20. Input data of the CFBC system.....	175
Table 4.21. Comparison of CO ₂ and SO ₂ emission data between the simulation and experiments under oxygen-enriched conditions.....	177
Table 4.22. Comparison of CO ₂ and SO ₂ emission data between the simulation and experiments under oxy-fuel combustion conditions	181

LIST OF FIGURES

FIGURES

Figure 2.1. Global energy demand by fuel types from 1980 to 2035 [20]	7
Figure 2.2. Turkey annual electricity consumption (<i>left</i>) and the capacity of electricity production by energy source type (<i>right</i>) [22].....	9
Figure 2.3. World primary energy demand and energy-related CO ₂ emission for different policies [1]	10
Figure 2.4. Three main carbon capture and storage methods [13]	12
Figure 2.5. Fuel types used in FBC [52].....	16
Figure 2.6. Fluidized bed types, a) BFB, b) CFB, c) PBFB, and d) PCFB [53].....	17
Figure 2.7. Thermodynamic equilibrium curve of CaCO ₃ calcination [72]	24
Figure 3.1. Orhaneli lignite proximate analysis results	47
Figure 3.2. Soma lignite proximate analysis results	47
Figure 3.3. PerkinElmer Pyris-1 TGA apparatus.....	51
Figure 3.4. Teledyne HFC 202 mass flow controller (<i>left</i>) and the gas mixing unit (<i>right</i>).....	52
Figure 3.5. Schematic diagram of the utilized system.....	54
Figure 3.6. Weight loss regions and characteristic temperatures in a TGA/DTG curve	55
Figure 3.7. Schematic and photograph of the CFBC system.....	56
Figure 3.8. Graphical user interface program of the CFBC system	57
Figure 3.9. Windbox	58
Figure 3.10. Distributor plate used in the combustor.	58
Figure 3.11. Technical drawing of Module-101	60
Figure 3.12. Technical drawing of Module-102 and Module-107	60
Figure 3.13. Technical drawing of Module-103, Module-104, Module-105, and Module-106.....	61

Figure 3.14. Technical drawing of Module-108	62
Figure 3.15. Scheme of a fluidized bed boiler components simulated by CeSFaMB software [181]	72
Figure 3.16. A simplified diagram of a CFBC in CeSFaMB software [178]	72
Figure 4.1. TGA and DTG curves of Orhaneli lignite combustion under air and equivalent air oxy-fuel combustion atmospheres.....	82
Figure 4.2. TGA and DTG curves of Soma lignite combustion under air and equivalent air oxy-fuel combustion atmospheres	83
Figure 4.3. Comparison of TGA and DTG curves of Orhaneli lignite under oxygen enriched air and oxy-fuel combustion conditions	85
Figure 4.4. Comparison of TGA and DTG curves of Soma lignite under oxygen enriched air and oxy-fuel combustion conditions	86
Figure 4.5. Kinetic plots of Orhaneli lignite combustion at 21%O ₂ -79%N ₂ and 21%O ₂ -79%CO ₂ atmospheres for the isoconversional methods of FWO, KAS and Friedman methods	87
Figure 4.6. Kinetic plots of Soma lignite combustion at 21%O ₂ -79%N ₂ and 21%O ₂ -79%CO ₂ atmospheres for the isoconversional methods of FWO, KAS and Friedman methods	88
Figure 4.7. Comparison of estimated E _α vs. α for different methods for Orhaneli lignite at (a) 21%O ₂ , (b) 30%O ₂ and (c) 40%O ₂ oxygen concentrations.....	90
Figure 4.8. Comparison of estimated E _α vs. α for different methods for Soma lignite at (a) 21%O ₂ , (b) 30%O ₂ and (c) 40%O ₂ oxygen concentrations.....	92
Figure 4.9. Comparison of average E _α using different methods for (a) Orhaneli and (b) Soma lignites	93
Figure 4.10. Comparison of average E _α using different methods for (a) Orhaneli and (b) Soma lignites	94
Figure 4.11. Comparison of estimated pre-exponential factor by FWO method for (a) Orhaneli and (b) Soma lignites at different combustion and oxy-fuel combustion conditions	95
Figure 4.12. Variation of chemical components of biomass during torrefaction.....	98

Figure 4.13. Van Krevelen’s diagram for raw and torrefied biomass	98
Figure 4.14. TGA and DTG curves of raw and torrefied biomass combustion under air combustion atmosphere at 20°C/min heating rate	100
Figure 4.15. Characteristic temperatures for raw biomass at 20°C/min	101
Figure 4.16. DDTG curves of raw and torrefied biomass combustion under air combustion atmosphere at 20°C/min heating rate	102
Figure 4.17. Comparison of (a) TGA, (b) DTG, and (c) DDTG curves of raw and torrefied biomass combustion under air and oxy-fuel combustion atmospheres	104
Figure 4.18. Comparison of estimated $E\alpha$ vs. α for different methods for the raw and torrefied biomass samples under air combustion condition	107
Figure 4.19. Comparison of estimated $E\alpha$ vs. α by FWO method for the raw and torrefied biomass samples under air and oxy-fuel combustion conditions.....	109
Figure 4.20. Comparison of average uncertainty values for different methods at (a) air combustion and (b) oxy-fuel combustion conditions	112
Figure 4.21. TGA and DTG curves of Orhaneli lignite and 300°C-30min torrefied biomass co-combustion under air atmosphere.....	115
Figure 4.22. TGA and DTG curves of Orhaneli lignite and raw biomass 50/50 blend co-combustion at different heating rates under air and oxy-fuel combustion conditions	117
Figure 4.23. Comparison of 50/50 blend of Orhaneli lignite and raw biomass with its parent fuels at 10°C/min heating rate under air and oxy-fuel combustion atmospheres	118
Figure 4.24. Comparison of characteristic temperatures of 50/50 blend of Orhaneli lignite and raw biomass with its parent fuels at 10°C/min heating rate under air and oxy-fuel combustion atmospheres	119
Figure 4.25. TGA and DTG curves of Orhaneli lignite and 300°C-30min torrefied biomass co-combustion under air and oxy-fuel combustion conditions	121
Figure 4.26. TGA and DTG curves of Orhaneli lignite and 300°C-30min torrefied biomass co-combustion under air and oxy-fuel combustion conditions	123

Figure 4.27. Comparison of characteristic temperatures of 50/50 blend of Orhaneli lignite and 300°C-30min torrefied biomass with its parent fuels at 10°C/min heating rate under air and oxy-fuel combustion atmospheres	124
Figure 4.28. TGA and DTG curves of Soma lignite and raw biomass co-combustion under air and oxy-fuel combustion conditions.....	125
Figure 4.29. TGA and DTG curves of Soma lignite and raw biomass co-combustion under air and oxy-fuel combustion atmospheres	127
Figure 4.30. Comparison of characteristic temperatures of 50/50 blend of Soma lignite and raw biomass with its parent fuels at 10°C/min heating rate under air and oxy-fuel combustion atmospheres	128
Figure 4.31. TGA and DTG curves of Soma lignite and 300°C-30min torrefied biomass co-combustion under air and oxy-fuel combustion conditions.....	129
Figure 4.32. TGA and DTG curves of Soma lignite and 300°C-30min torrefied biomass co-combustion under air and oxy-fuel combustion conditions.....	131
Figure 4.33. Comparison of characteristic temperatures of 50/50 blend of Soma lignite and 300°C-30min torrefied biomass with its parent fuels at 10°C/min heating rate under air and oxy-fuel combustion atmospheres	132
Figure 4.34. Experimental and theoretical DTG profiles for the 50/50 blends of (a) Orhaneli and raw biomass and (b) Orhaneli and 300°C-30min torrefied biomass under air and oxy-fuel combustion atmospheres	134
Figure 4.35. Experimental and theoretical DTG profiles for the 50/50 blends of (a) Soma and raw biomass and (b) Soma and 300°C-30min torrefied biomass under air and oxy-fuel combustion atmospheres.....	135
Figure 4.36. Activation energy curves of 50/50 blends of Orhaneli and Soma lignites with raw and 300°C-30min torrefied biomass samples with respect to conversion degree under air and oxy-fuel combustion atmospheres.....	137
Figure 4.37. Comparison of the activation energies for Orhaneli, 300°C-30min torrefied biomass and their 25, 50 and 75 wt.% blends under air combustion atmosphere	138

Figure 4.38. Comparison of the activation energies for Orhaneli and (a) raw biomass and (b) 300°C-30min torrefied biomass under air and oxy-fuel combustion atmospheres	140
Figure 4.39. Comparison of the activation energies for Soma and (a) raw biomass and (b) 300°C-30min torrefied biomass under air and oxy-fuel combustion atmospheres	142
Figure 4.40. Temperature profile along (a) combustor and (b) return leg in the combustion of Orhaneli lignite and Çan limestone at Ca/S = 1.5 and Particle size of 0-1 mm	145
Figure 4.41. Effect of oxygen concentration on flue gas emissions in the combustion of Orhaneli lignite and Çan limestone at Ca/S = 1.5 and Particle size of 0-1 mm ..	147
Figure 4.42. Temperature profile along (a) combustor and (b) return leg in the combustion of Orhaneli lignite and Çan limestone at Ca/S = 2 and Particle size of 0-1 mm	148
Figure 4.43. Effect of oxygen concentration on flue gas emissions in the combustion of Orhaneli lignite and Çan limestone at Ca/S = 2 and Particle size of 0-1 mm	149
Figure 4.44. Temperature profile along (a) combustor and (b) return leg in the combustion of Orhaneli lignite and Çan limestone at Ca/S = 1.5 and Particle size of 1-2 mm	151
Figure 4.45. Effect of oxygen concentration on flue gas emissions in the combustion of Orhaneli lignite and Çan limestone at Ca/S = 1.5 and Particle size of 1-2 mm ..	152
Figure 4.46. Temperature profile along (a) combustor and (b) return leg in the combustion of Orhaneli lignite and Çan limestone at Ca/S = 2 and Particle size of 1-2 mm	153
Figure 4.47. Effect of oxygen concentration on flue gas emissions in the combustion of Orhaneli lignite and Çan limestone at Ca/S = 2 and Particle size of 1-2 mm	154
Figure 4.48. Temperature profile along (a) combustor and (b) return leg in the combustion of Orhaneli lignite and Eskişehir dolomite at Ca/S = 1.5 and Particle size of 0-1 mm	157

Figure 4.49. Effect of oxygen concentration on flue gas emissions in the combustion of Orhaneli lignite and Eskişehir dolomite at Ca/S = 1.5 and Particle size of 0-1 mm	158
Figure 4.50. Temperature profile along (a) combustor and (b) return leg in the combustion of Orhaneli lignite and Eskişehir dolomite at Ca/S = 2 and Particle size of 0-1 mm	160
Figure 4.51. Effect of oxygen concentration on flue gas emissions in the combustion of Orhaneli lignite and Eskişehir dolomite at Ca/S = 2 and Particle size of 0-1 mm	161
Figure 4.52. Temperature profile along (a) combustor and (b) return leg in the combustion of Orhaneli lignite and Eskişehir dolomite at Ca/S = 1.5 and Particle size of 1-2 mm.....	162
Figure 4.53. Effect of oxygen concentration on flue gas emissions in the combustion of Orhaneli lignite and Eskişehir dolomite at Ca/S = 1.5 and Particle size of 1-2 mm	163
Figure 4.54. Temperature profile along (a) combustor and (b) return leg in the combustion of Orhaneli lignite and Eskişehir dolomite at Ca/S= 2 and Particle size of 1-2 mm	165
Figure 4.55. Effect of oxygen concentration on flue gas emissions in the combustion of Orhaneli lignite and Eskişehir dolomite at Ca/S = 2 and Particle size of 1-2 mm	166
Figure 4.56. Temperature profile along (a) combustor and (b) return leg under oxy-fuel combustion of Orhaneli lignite and Çan limestone at Ca/S= 2 and Particle size of 0-1 mm	169
Figure 4.57. Flue gas emissions under oxy-fuel combustion of Orhaneli lignite and Çan limestone at Ca/S = 2 and Particle size of 0-1 mm.....	171
Figure 4.58. Temperature profile along (a) combustor and (b) return leg under oxy-fuel combustion of Orhaneli lignite and Eskişehir dolomite at Ca/S= 2 and Particle size of 0-1 mm.....	172

Figure 4.59. Flue gas emissions under oxy-fuel combustion of Orhaneli lignite and Eskişehir dolomite at Ca/S = 2 and Particle size of 0-1 mm	173
Figure 4.60. Comparison of experimental and simulation results for combustion of Orhaneli lignite under air atmosphere	175
Figure 4.61. Simulation results for the combustion of Orhaneli lignite under oxygen-enriched atmosphere	176
Figure 4.62. Change of CO ₂ and SO ₂ emissions along the combustor height under oxygen-enriched conditions.....	177
Figure 4.63. Comparison of experimental and simulation results for combustion of Orhaneli lignite under oxy-fuel combustion condition.....	178
Figure 4.64. Simulation results for the oxy-fuel combustion of Orhaneli lignite at different excess air ratios	179
Figure 4.65. Change of CO ₂ and SO ₂ emissions along the combustor height under oxy-fuel combustion conditions.....	180

LIST OF ABBREVIATIONS

ABBREVIATIONS

WEO	World Energy Outlook
GHG	Greenhous Gases
FBC	Fluidized Bed Combustion/Combustor
CCS	Carbon Capture and Sequestration/Storage
CFB	Circulating Fluidized Bed
CFBC	Circulating Fluidized Bed Combustor
TGA	Thermogravimetric Analyzer
DTG	Derivative Thermogravimetry
FWO	Flynn-Wall-Ozawa
KAS	Kissinger-Akahira-Sunose
GWh	Gigawatt Hour
Mtoe	Megaton Oil Equivalent
UNFCCC	United Nations Framework Convention on Climate Change
IGCC	Integrated Gasification Combined Cycle
ASU	Air Separation Unit
KW _{th}	Kilowatt (thermal)
MW _{th}	Megawatt (thermal)
MW _e	Megawatt (electric)
PFBC	Pressurized Fluidized Bed Combustor

BFB	Bubbling Fluidized Bed
METU	Middle East Technical University
SEM	Scanning Electron Microscope
FB	Fluidized Bed
Ca/S	Calcium Sulfur Ratio
HCl	Hydrogen Chloride
CFD	Computational Fluid Dynamics
1-D	One Dimensional
2-D	Two Dimensional
3-D	Three Dimensional
MW	Megawatt
kW	Kilowatt
DDPM	Dense Discrete Phase Model
UDF	User Defined Functions
LES	Large Eddy Simulation
DEM	Discrete Element Method
TFM	Two Fluid Model
DSC	Differential Scanning Calorimetry
FTIR	Fourier Transform Infrared Spectroscopy
H/C	Hydrogen Carbon Atomic Ratio
O/C	Oxygen Carbon Atomic Ratio
CCF	Combustion Characteristic Factor

ASTM	American Society for Testing and Materials
XRF	X-Ray Fluorescence
HHV	Higher Heating Value
LHV	Lower Heating Value
TÜBİTAK	Scientific and Technological Research Council of Turkey
BET	Brunauer-Emmett-Teller
MFC	Mass Flow Controller
T_i	Initial Temperature
T_{ig}	Ignition Temperature
T_{max}	Maximum Temperature
T_b	Burnout Temperature
MRC	Marmara Research Center
TT	Temperature Transmitter
FD	Force Draft
ID	Induced Draft
DAEM	Distributed Activation Energy Method
ICTAC	the international confederation for thermal analysis and calorimetry
TA	Thermal Analysis
MJ	Megajoule
DDTG	Second Derivative of Weight Loss
DTG_{exp}	Experimental Derivative Thermogravimetry
DTG_{th}	Theoretical Derivative Thermogravimetry

LIST OF SYMBOLS

SYMBOLS

λ	Excess air ratio
α	Conversion Degree
T	Temperature
t	Time
$f(\alpha)$	Conversion Function
$k(T)$	Rate Constant
m_i	Initial Mass of the Sample
m_t	Sample Mass at Time t
m_f	Final Mass of the Sample
E_a	Activation Energy
A	Pre-exponential Factor
R	Universal Gas Constant
n	Reaction Order
T_0	Initial Temperature
β	Heating Rate
$p(x)$	Temperature Integral
m	Slope
δm	Standard Deviation of the Slope
x_i	Mass Fraction of Sample

CHAPTER 1

INTRODUCTION

1.1. General

Increasing world population over the last century, the continuous improvements in living standards, industrialization and technological developments have led to drastic increase in the world energy consumption. According to World Energy Outlook (WEO2018), even if new energy consumption policies are adopted, the world primary energy demand will increase by over 25% between 2017 to 2040 and will reach to 17715 Mtoe [1]. Fossil fuels account for 81% of primary energy demand in 2017, however it is projected that its share declines to 74% by 2040. In order to reduce the reliance on fossil fuels, many efforts in developing renewable energy and alternative fuels have been carried out and substantial progress have been made. Although lately, the application of renewable energy has grown rapidly, their usage is still limited due to the high cost, poor technology reliability, and inadequate resource availability. Therefore, the conventional fossil fuels will still be the major energy source in the foreseeable future.

Coal is one of the most broadly distributed energy source in the world and due to its proven stability, ease of supply and economically attractive cost, it is estimated that coal will maintain its position in energy matrix of the world [2]. Today, with 891.5 billion tons of proven reserves [3], coal is the source of about 40% of all electricity generated in the world [4]. Nearly 55% of all coal reserves in the world are lignite and sub-bituminous which are characterized as low-rank coals [3]. Due to different geological age and formation mechanism, mined lignite in different regions have different characteristics and kinetic parameters. Hence, understanding kinetics and thermal decomposition mechanism of lignites are of great importance [5].

Coal-firing power plants are accounting for 40% of total global carbon dioxide emissions. Carbon dioxide is considered as the major greenhouse gas (GHG) and its release from the coal-firing industries is the most important cause of irreversible global warming and the associated impacts on climate change [6]. Moreover, pollutants such as sulfur dioxide and nitric oxides are emitted from coal-firing power plants as well having negative consequences on the climate such as rain acidification and ozone layer depletion. To tackle these problems, two major approaches are suggested: improving the combustion process and considering the use of alternative energy sources.

Fluidized Bed Combustion (FBC) as an emerging and advanced combustion technology was introduced in 1970s in order to improve the combustion process and provide cleaner energy [7]. It is a suitable technology for burning low-rank, high ash and high sulfur solid fuels and offers an alternative approach to the conventional emission abatement measures. FBC technology has excellent fuel flexibility, inherently low NO_x production, and the potential to achieve SO₂ emissions reductions of 90% or more by in-situ addition of calcium-based sorbents. Limestone and dolomite are proven to be the successful sorbents for in-bed removal of SO₂ in fluidized bed combustion systems. Countries that have abundant quantities of low-grade coal or biomass resources are very interested in FBC technology.

Application of renewable energy sources is another approach towards clean energy production. Renewable energy sources such as wind, solar, biomass, and hydropower have an increasing share of the energy production in recent years. The global energy obtained from renewables was almost 9700 Mtoe in 2017 and it is projected to reach to 12600 Mtoe by 2040 in the new policies scenario [1]. Among them, biomass which is categorized as a CO₂ neutral fuel, is one of the promising sources to match the requirements of substituted fossil fuels for GHG emissions reduction. Co-combustion of biomass with coal is a relatively easy way of reducing CO₂ emission from the conventional fossil fuel fired power plants [8].

Carbon Capture and Sequestration (CCS) is one of the most promising and effective solutions towards clean coal combustion [9]. CCS technology which complements the two other approaches in GHG reduction can be categorized under three main methods: pre-combustion capture, post-combustion capture, and oxy-fuel combustion technique. The first and second methods are applied to the conventional power plants where the CO₂ concentration in the flue gas is low (about 15% by volume). Oxy-fuel combustion technique, in which air is replaced by a mixture of oxygen (greater than 95% purity) and recycled flue gas to produce almost pure CO₂ is another approach in CCS technology [10]. Oxy-fuel combustion takes place in O₂/CO₂ atmosphere rather than in O₂/N₂ atmosphere as in conventional air fired combustion systems.

Oxy-fuel combustion provides a nitrogen free combustion environment and is one of the new technologies for enrichment of CO₂ in the flue gas. However, due to differences between the characteristics of N₂ and CO₂, switching from conventional air fired systems to oxy-fuel combustion system could result in changes in combustion parameters such as flame ignition, burning stability, char burnout, gas temperature profile, emission and ash properties [11], [12]. Increasing the oxygen concentration in oxy-fuel combustion atmosphere is a method to achieve comparable results as seen for conventional combustion in air [13].

Application of oxygen enriched air and oxy-fuel combustion technologies in FBC systems are the methods applied to coal combustion process in order to improve coal combustion efficiency [14], [15]. The advantages of FBC system combined with the advantages of producing high CO₂ concentration in the flue gas makes the oxy-fuel FBC combustion technology a great potential for both the utility and industrial markets [16].

Lignite is widely used in coal power plants and industries, hence, its applicability in oxy-fuel combustion needs to be thoroughly accessed. The successful commissioning of lignite in oxy-fuel combustion systems will promise the electricity generation in an environmentally friendly manner in the long term. Oxy-fuel combustion of

biomass/coal blends induces the potential of achieving an overall negative CO₂ emission from the power plant [17]. Oxy-fuel combustion and co-combustion of low-quality coal with biomass are promising methods for clean combustion technology.

In the light of these needs and potentials, application of low-rank coals as the main fuel and biomass as supplementary fuel in an FBC system with in-situ addition of calcium-based sorbents under oxygen-enriched and oxy-fuel combustion conditions seems to be promising for energy production.

1.2. Motivation

Most of the coal reserves in Turkey are low-grade lignite with nearly 10 billion tons of reserves which makes it the main indigenous energy source and plays a major role in Turkey's energy sector and power mix. Moreover, Turkey's geographic location has several advantages for extensive use of the renewable energy resources such as biomass. In order to investigate the potential of application of these resources in an FBC system operating under oxy-fuel combustion conditions, a TUBITAK project was proposed on "Oxy-fuel Combustion of Lignite and Torrefied Biomass in a Circulating Fluidized Bed (OXYCOMBUSTION)" (Project Code: 113M003) in 2013 [18]. The collaborators on this project were:

1. ITU, Department of Chemical Engineering,
2. METU, Departments of Mechanical and Environmental Engineering,
3. Marmara Research Center, Institute of Energy,
4. EGE University, Institute of Solar Energy,
5. Karabuk University, Faculty of Technology.

The main objectives of this TUBITAK project were: designing an equipment for CO₂ capture, building a torrefied biomass production system, retrofitting a laboratory scale CFB to operate under oxy-fuel combustion conditions, conducting in-situ adsorption of SO₂ in the CFB, and conducting techno-economic and feasibility assessments.

These objectives were categorized and each team was assigned to carry out an specific task on the project. The assigned sub-project for METU included the following tasks:

- Characterization of Lignite and Biomass Samples in a TGA under Oxygen-enriched and Oxy-fuel Combustion Conditions,
- Characterization of Limestone and Dolomite Samples in a TGA,
- SO₂ Capture in the CFB under Oxygen-enriched and Oxy-fuel Combustion Conditions.

The first and the last objectives were the subjects of the present thesis, and the second objective was considered as an M.Sc. thesis which was carried out at Environmental Engineering Department, METU [19].

1.3. Scope of the Thesis

This PhD research was proposed under the abovementioned TUBITAK project aiming at improving the knowledge on oxy-fuel combustion of Turkish indigenous lignite coals, biomass and coal/biomass blends in a laboratory scale Circulating Fluidized Bed (CFB). In order to achieve this, at first, a thorough investigation on combustion, oxygen-enriched combustion and oxy-fuel combustion of coal, biomass and their blends were experimentally conducted by means of Thermogravimetric analyzer (TGA). The kinetic analysis was performed in order to extract the Arrhenius parameters for the aforementioned reactions. Following that, CFB experiments were conducted in order to investigate the effects of addition of calcium-based sorbents for in-situ SO₂ adsorption. Finally, the obtained data for CFB experiments was used in order to numerically simulate the combustion process in the CFB. The main objectives of this study were suggested as follows:

- 1- The combustion experiments were conducted to investigate the combustion characteristics of the two Turkish indigenous lignites as well as raw and torrefied wood biomass at different atmospheres by means of TGA. The

- experiments were carried out under oxygen-enriched air and oxy-fuel combustion conditions with 21, 30, and 40% by vol. oxygen concentrations.
- 2- Co-combustion experiments of raw and torrefied biomass blended with lignites was conducted for three different blending ratios of 25, 50, and 75 wt.% under air and oxy-fuel combustion conditions.
 - 3- Three different isoconversional kinetic methods were used to calculate the Arrhenius parameters (activation energy and pre-exponential factors). Flynn-Wall-Ozawa (FWO), Kissinger-Akahira-Sunose (KAS), and Friedman methods were considered.
 - 4- A laboratory scale CFB combustor was used to conduct the experiments regarding the study of the effects of calcium-based sorbents addition for in-situ SO₂ adsorption.
 - 5- The obtained data of the CFB experiments was used in order to conduct a numerical study by means of CeSFaMB code. CeSFaMB is a comprehensive mathematical model and simulation program for bubbling and circulating fluidized-bed as well as downdraft and updraft moving-bed equipment.

CHAPTER 2

LITERATURE REVIEW

2.1. Energy Review

The population and economic growth in the recent decade have resulted in a significant increase in the world's energy demands. Figure 2.1 shows the U.S. Department of Energy report projection of the world energy consumption over time, based on a selection of available energy sources [20]. As illustrated in Figure 2.1, the global energy consumption is expected to increase by 80% in 2035. Fossil fuels, such as coal, natural gas and liquid petroleum, are the main energy sources, providing almost 80% of the total world energy demand between 1980 and 2035. Of all types of fossil fuels, liquid fuels are estimated to remain as the largest sources of energy for the next two decades, although their world-wide share of energy consumption is likely to decline from 35% in 2007 to 30% in 2035.

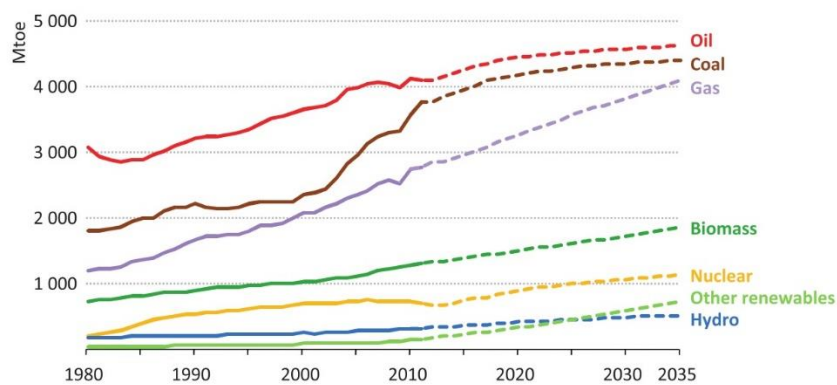


Figure 2.1. Global energy demand by fuel types from 1980 to 2035 [20]

Coal is one of the most important energy sources in the world to meet the rapidly growing energy needs and is expected to last for about 190 years which is longer than other types of fossil fuels [21]. The demand for coal will escalate over time, particularly due to the quick growth in China’s coal industry. According to WEO 2018 [1] three energy consumption policies can be executed: continuing with the current policies, adopting new policies, and sustainable development policy. The effect of these policies on the world primary energy demand and their contribution on CO₂ emissions are presented in Table 2.1. Coal powered 27% of the total energy demand in 2017, and will remain as the popular choice for the power generation industry towards 2040. Unless adopting the sustainable development policies, coal will still play the major role in the energy matrix of the world. Utilization of coal is not only in electricity production, but also in other industrial activities such as steel and cement production.

Table 2.1. World primary energy demand by fuel and scenario (Mtoe) [1]

			New Policies		Current Policies		Sustainable Development	
	2000	2017	2025	2040	2025	2040	2025	2040
Coal	2 308	3 750	3 768	3 809	3 998	4 769	3 045	1 597
Oil	3 665	4 435	4 754	4 894	4 902	5 570	4 334	3 156
Gas	2 071	3 107	3 539	4 436	3 616	4 804	3 454	3 433
Nuclear	675	688	805	971	803	951	861	1 293
Renewables	662	1 334	1 855	3 014	1 798	2 642	2 056	4 159
Hydro	225	353	415	531	413	514	431	601
Modern bioenergy	377	727	924	1 260	906	1 181	976	1 427
Other	60	254	516	1 223	479	948	648	2 132
Solid biomass	646	658	666	591	666	591	396	77
Total	10 027	13 972	15 388	17 715	15 782	19 328	14 146	13 715
<i>Fossil fuel share</i>	<i>80%</i>	<i>81%</i>	<i>78%</i>	<i>74%</i>	<i>79%</i>	<i>78%</i>	<i>77%</i>	<i>60%</i>
CO₂ emissions (Gt)	23.1	32.6	33.9	35.9	35.5	42.5	29.5	17.6

Notes: Mtoe = million tonnes of oil equivalent; Gt = gigatonnes. Solid biomass includes its traditional use in three-stone fires and in improved cookstoves.

Turkey has the second highest energy consumption growth after China. Energy imports in Turkey are 75% of its energy needs and energy demand in the country is forecasted to double by 2017. According to 2013 Turkey Energy Report published on February 2014 [22], in comparison with 2012, annual electricity consumption in Turkey has risen by 1.3% and increased to 245K GWh. Figure 2.2 illustrates Turkey’s annual energy consumption and the capacity of electricity production by energy source types.

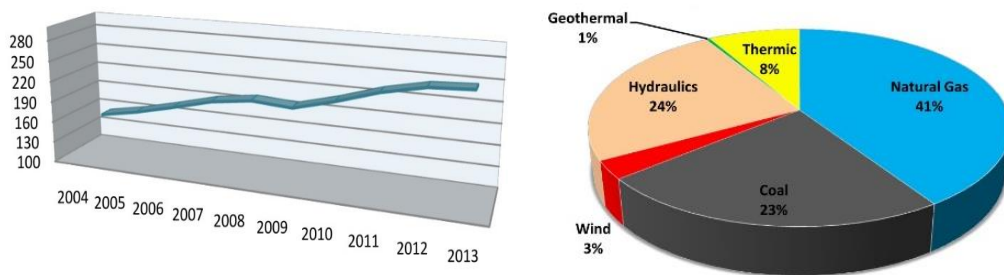


Figure 2.2. Turkey annual electricity consumption (*left*) and the capacity of electricity production by energy source type (*right*) [22]

In Turkey, most of the indigenous coal reserves are low-rank lignite (brown coal) with nearly 10 billion tons of reserves [23] which makes it the main indigenous energy source and plays a major role in Turkey’s energy sector and power mix. Turkey is ranked as seventh in the world with 2% of lignite reserves [24]. The imported hard coal combining with domestic lignite is accounted for 25.7% of total electricity generation in 2013 [25]. The government has begun a policy to encourage exploitation of Turkey’s domestic lignite reserves instead of natural gas for electricity generation. A distinctive characteristic of Turkish lignite coals is their relatively high (around 40-50%) volatile matter content [26], [27].

Turkey’s geographic location has several advantages for extensive use of most of the renewable energy sources [28]. It has a potential of producing 30% of its electricity demand from the renewable sources by 2023. Among them, biomass is considered as

the major source of renewable energy and fuel wood seems to be the most abundant type of biomass since it accounts for a considerable 21% share of the total energy production of Turkey. The total biomass energy potential of Turkey is about 32 Mtoe and approximately 17 Mtoe of that is usable [22].

2.2. Carbon Capture and Storage (CCS)

Carbon dioxide is the major GHG contributor in global warming and the associated impacts of climate change. The economic growth and global energy-related CO₂ emission are strongly linked in the current policies scenario. Adopting the new policies would weaken this link, however, the CO₂ emission keeps rising up to 36 Gigatons by 2040. The sustainable development scenario which cuts the fossil fuel share from the primary energy mix is the only option that would lead to a decrease in CO₂ emission by 2040 [1]. Figure 2.3 shows the relationship between the world primary energy demand and energy-related CO₂ emission for different policies.

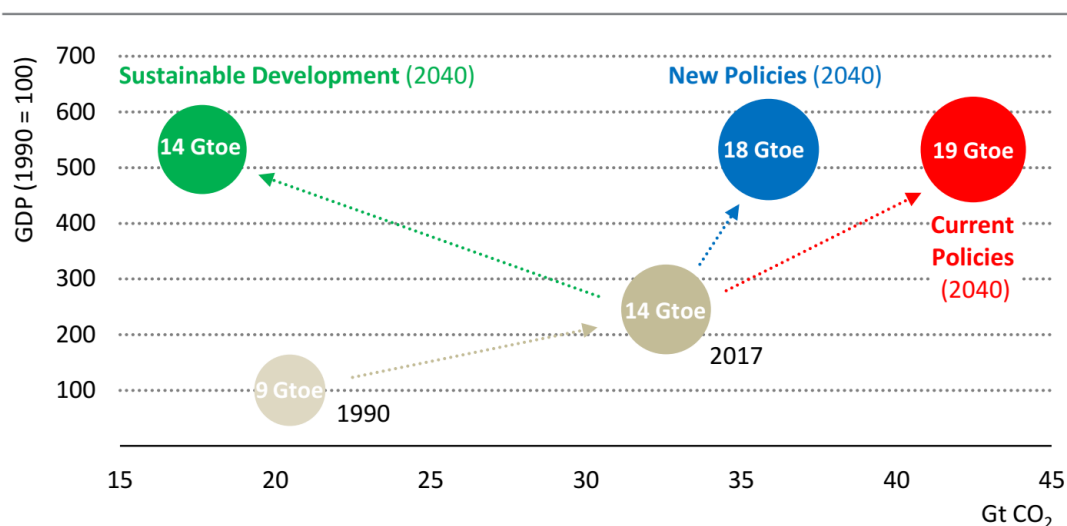


Figure 2.3. World primary energy demand and energy-related CO₂ emission for different policies [1]

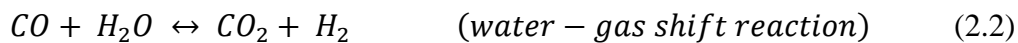
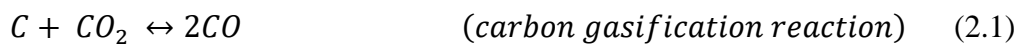
The United Nations Framework Convention on Climate Change (UNFCCC) in 2004 and the Kyoto Protocol, effective since 2005, were ratified by most of the countries all over the world. These treaties provided the basis for mutual international actions to mitigate climate change, to adapt to its impacts, and to comply with emission targets for the countries in their commitment period. The Paris agreement was the world's first comprehensive treaty concerning climate change issues and adopted by consensus on December 2015 dealing with GHG emissions abatement, adaptation and finance starting in the year 2020 [29].

The mitigation of GHG emissions from fossil fuel-fired power generation could be accomplished by increasing the efficiency of coal combustion (e.g. utilization of ultra-supercritical boilers, Fluidized Bed Combustion reactors, oxygen-enriched technology, and catalytic combustion), switching to lower carbon fuels or carbon neutral fuels such as biomass, and Carbon Capture and Storage (CCS) technology [30], [31]. CCS technology can be implemented to conventional power generation systems as a step change method to reduce CO₂ emission making it possible to continue the use of fossil fuels but with much less CO₂ concern. CCS is divided into four different categories: pre-combustion, post-combustion, oxy-fuel combustion and newly emerging technologies [32]–[34]. The plants configurations for the three main carbon capture and storage methods are shown in Figure 2.4 [13].

- Pre-combustion

Pre-combustion capture is commonly applied to the Integrated Gasification Combined Cycle (IGCC) power plants and termed as IGCC-CCS. Coal gasification is used to produce synthesis gas mixture (syngas) mainly containing CO, CO₂, and H₂. CO₂ is produced by a direct reaction of carbon and oxygen. The carbon gasification reaction takes place via the reaction with CO₂ and produce CO. The CO is converted into CO₂ by the water-gas shift reaction and can then be separated from the hydrogen-rich stream of flue gas before it is combusted in a gas turbine. The process of separation of

CO₂ before combustion is referred to as fuel decarbonization. The carbon gasification and water-gas shift reactions are:



IGCC power plants has promising process economics and high efficiency characteristics [35]–[37]. However, due to the fact that an IGCC plant construction have high capital costs and they are much more complicated systems than fluidized beds, only few IGCC electricity generation units exist and none of which are equipped with CCS [36], [38], [39].

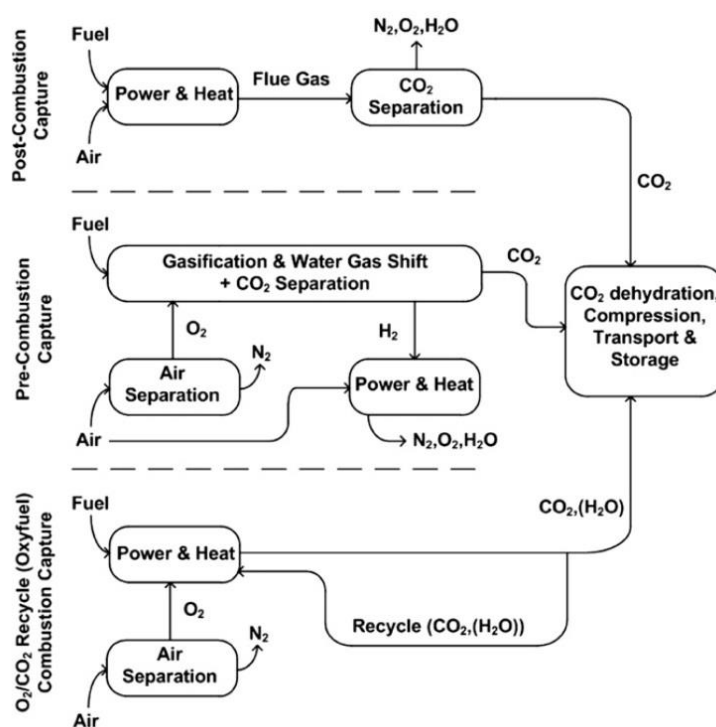


Figure 2.4. Three main carbon capture and storage methods [13]

- Post-combustion

In this method, CO₂ is separated from the flue gas of conventional coal-fired power plants just before they emitted to the atmosphere. This process is done by wet scrubbing with aqueous amine solutions such as mono-ethanol amine [33]. The carbon dioxide is then removed from the solvent during the regeneration process and finally the separated CO₂ is dried, compressed and stored in a safe storage. However, applying the post combustion method to the power plants impose serious penalties to the plant efficiency (around 10-14%) [40]. Retrofitting the existing plants is relatively simple since the capture unit can be added downstream of the boiler and flue gas cleaning systems without significant changes to the original plant [41].

- Oxy-fuel combustion

The idea of oxy-fuel combustion technology was first proposed by Abraham in 1982 in order to produce relatively pure CO₂ for enhanced oil recovery [42]. The concept of producing high concentrations of CO₂ for oil recovery application did not pick up on a large scale. However, the global warming awareness and the fact that CO₂ plays the major role in it, has renewed the interest in this technology.

Applying an air separation unit (ASU) to remove nitrogen from the air stream and introducing pure oxygen (95-97%) to the combustion medium causes the flue gas to consist mainly of CO₂ and water. The plant configuration typically involves flue gas recirculation (containing mostly CO₂) to the burners to moderate the adiabatic flame temperature to the acceptable limits of the boiler construction materials. As a result, the combustion process takes place in an O₂/CO₂ ambient, instead of O₂/N₂. Despite the fact that applying an ASU as an auxiliary unit to separate O₂ and N₂ has negative impact on power plant efficiency, several techno-economic assessment studies showed that oxy-fuel combustion is the most energy and cost efficient method of the CCS technology [43]–[46]. Due to high concentrations of CO₂ in the flue gas stream, CO₂ capture and sequestration technique can be readily achieved.

Technically, oxy-fuel combustion is not considered as a capture technology but rather a process during which a mixture of oxygen with high purity (greater than 95 %) and recycled flue gas is used for combustion. Hence, the combustion process takes place in O₂/CO₂ atmosphere rather than in conventional O₂/N₂ mixture. At the first step toward realizing this technology, an oxy-fuel boiler system in which oxygen is mixed with recirculating flue gas to achieve the same boiler heat transfer and adiabatic flame temperature as with air-firing, is employed and used as a reference when retrofitting existing boilers is being considered [10]. Some of the advantages of oxy-fuel combustion are as follows:

- 1- CO₂ concentration in exhaust gas is very high (up to 95% percent) and easy to capture and storage.
- 2- The emission control of the flue gas is easy because of low quantity and volume.
- 3- Heat loss is significantly lower than air-fired combustion system, therefore, the system size can be scaled down.
- 4- NO_x concentration decreases due to nitrogen elimination from the inlet flow into the boiler.

On the contrary, some of the most important challenges to tackle are:

- 1- On the oxy-fuel combustion process, the adiabatic flame temperature reaches higher values. This situation, makes this technology unadaptable to air-fired combustion systems. This problem requires further research and investigations.
- 2- The ASU which feeds pure oxygen to the process is an extra cost and impose energy penalty.

- Emerging technologies

Technologies such as membrane separation, chemical looping combustion, carbonation-calcination cycles, enzyme-based systems, ionic liquids, mineralization, etc. impose the possibility to drastically reduce the cost of electricity and the energy penalty concerned with carbon capture from power plants. However, these technologies have not been demonstrated at sufficient scales for industrialization [47], [48].

2.3. Fluidized Bed Combustion Technology

The fluidization process is based on the principal of changing the solid particle status from stationary to fluid status by applying an upward flow of a gas which its velocity exceeds the required critical velocity [49]. Fluidized Bed Combustion (FBC) is one of the advanced combustion technologies and offers an alternative approach to the conventional emission abatement measures. FBC plants are capable of burning a variety of low-grade solid fuels, including most types of coal, coke, municipal solid waste, plastics, wood and other biomass, at high efficiency and without the need for costly fuel preparation processes (e.g. pulverizing). From the emission point of view, FBC also reduces the amount of sulfur emitted in the form of SO_2 by means of limestone or dolomite addition which precipitate out sulfate during combustion [50], [51]. Also, due to the fact that combustion performs at lower temperatures compared to conventional power plants, less NO_x is emitted. It also eliminates the ash melting problems related to high combustion temperature. Figure 2.5 shows the application of FBC for several fuels based on their net calorific values [52]. As can be seen, burning different types of coals in FBC can be done without any particular challenges. Biomass fuels face some issues such as high moisture content and low calorific values. The thermal power for combustion in fluidized bed ranges from 30 to 900 MW_{th} and for gasification ranges from 8 to 10 MW_{th} . FBCs are usually used in the higher thermal range and have the capability to operate in a very wide range.

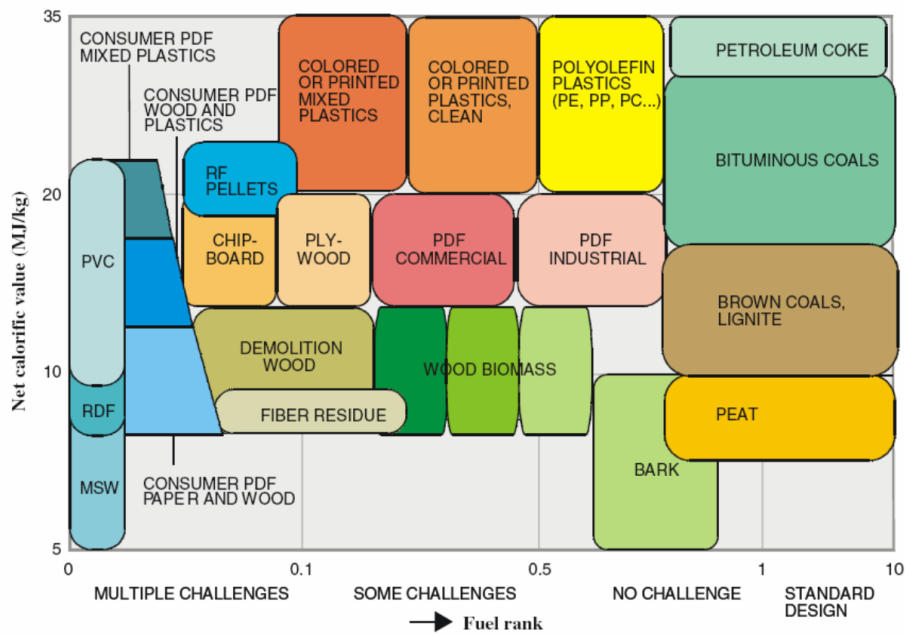


Figure 2.5. Fuel types used in FBC [52]

FBC systems generally fit into two major groups, atmospheric systems (FBC) and pressurized systems (PFBC), and two minor subgroups, bubbling (BFB) and circulating fluidized bed (CFB). Figure 2.6 illustrates the different types of fluidized bed combustors [53]. Atmospheric fluidized beds operate at atmospheric pressure and jets of air suspend the mixture of sorbent and burning fuel during combustion, converting the mixture into a suspension of red-hot particles that flow like a fluid. The PFBC systems operate at elevated pressures and produce a high-pressure gas stream at temperatures that can drive a gas turbine. Steam generated due to heat generated in the fluidized bed is utilized in a steam turbine, producing a highly efficient combined cycle system.

Stationary or bubbling bed is the classical approach where the gas at low velocities is used and fluidization of the solids is relatively stationary, with some fine particles being entrained. In CFB, the larger kinetic energy of the gases is sufficient enough to

suspend the particle bed. The surface of the bed is less smooth and larger particles can be entrained to the bed compared to stationary beds. Entrained particles are recirculated via an external loop back into the reactor bed. Depending on the process, the particles may be classified by a cyclone separator and removed from/returned to the bed, based on particle size. Compared to BFBs, CFBs can be used for a wide variety of fuels and operate at higher thermal power [52].

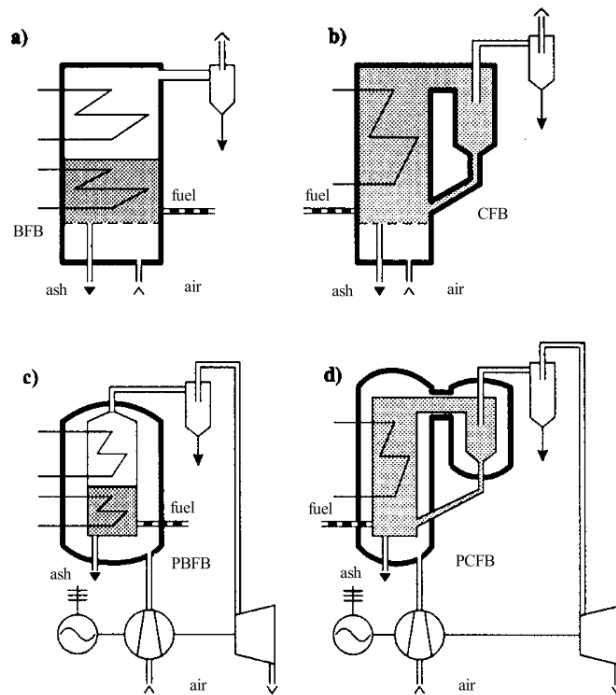


Figure 2.6. Fluidized bed types, a) BFB, b) CFB, c) PBFB, and d) PCFB [53]

Combustion in fluidized bed systems have several advantages compared to conventional pulverized coal combustion systems. These advantages are:

- 1- FBCs have higher combustion efficiency and higher availability than pulverized coal combustion systems.

- 2- Due to fluidization mechanism, fuel particles show a fluid-like behavior. Therefore, the control of the system is relatively easy.
- 3- The heat transfer between solid particles and the surface of heat exchangers are higher. Because of that, smaller heat exchangers can be utilized. This makes the FBC systems more compact compared to conventional pulverized coal combustion systems.
- 4- The fuel preparation process for FBC is easier because the complete pulverization of fuels is not required.
- 5- Due to good mixing of solid particles in the combustor, the temperature distribution is uniform and hot spots do not occur.
- 6- FBCs have excellent fuel flexibility and even can operate with inferior fuels with high moisture and low calorific values.
- 7- NO_x formation in FBC is lower than conventional combustors because the lower operational temperature (about 850°C).
- 8- Adsorption of SO₂ by in-situ addition of limestone and dolomite is possible.
- 9- Ash removal from the FBC is easier than pulverized coal combustion systems.
- 10- Because of the quick thermal equilibrium establishment between fuel particles and combustor, the response time to changes in load demands is fast.

In spite of these advantages, there are some challenges in application of FBCs that need to be addressed:

- 1- In order to maintain the fluidization of fuel particles, a continuous supply of high velocity flow is necessary which requires high fan power.
- 2- The flue gas of FBCs contains higher concentrations of particles. In order to separate these particles, auxiliary units such as cyclone, electrostatic precipitator, and bag filter are required.
- 3- Non-uniform residence time of solid particles can occur due to high rates of solid mixing.
- 4- High velocities of solid particles can result in erosion of heat exchanger pipes and inner walls of the furnace.

- 5- Combustion of fuels with high alkali content such as biomass can result in agglomeration of ash.

The studies regarding the application of fluidized bed technology on combustion of Turkey's indigenous lignites were started in early 1980s. A laboratory scale bubbling fluidized bed with thermal capacity of 0.3 MW_{th} was established at the Chemical Engineering Department in METU. Based on the valuable knowledge and experiences obtained from this system, Alkim Inc. has established a bubbling fluidized bed boiler in 2001. The first pilot circulating fluidized bed was built at Mechanical Engineering Department in Gazi University in the late 80s with 125 mm in diameter and 1.8 m in height [54]. A larger pilot CFB was constructed at Department of Chemical Engineering, METU in 2000s with 250 mm in diameter and 6.5 m in height with thermal capacity of 150 kW_{th} [55]. There is only one CFB power plant in operation in Turkey with the total capacity of 320 MW_e. It is designed to use Turkish lignite and has been commissioned by Turkish Electricity Generation Company since 2004.

The FBC technology is being studied in three major areas in order to meet the emission regulations and become a viable alternative for conventional power plants: compatibility with retrofitting to oxy-fuel combustion, flue gas desulfurization, and compatibility to operate with biomass fuel. These are the main subjects of study for most of the researches in this area.

2.3.1. Oxy-fuel Combustion in FBC

Oxy-fuel combustion technology has been investigated thoroughly in literature for pulverized coal combustion [12], [56]–[58], however, it has received relatively little attention for oxy-fuel FBC [59]. FBC technology has excellent fuel flexibility, inherently low NO_x production, and the potential to achieve SO₂ emissions reductions of 90% or more by in-situ addition of calcium-based sorbents. These inherent advantages combined with the advantages of producing high CO₂ concentration in the

flue gas allows the oxy-fuel FBC technology to have a great potential for both utility and industrial markets [16].

CFB combustion technology has the potential to improve the performance characteristics by using higher air flows to entrain and move the bed material, and recirculating nearly all the bed material with adjacent high volume and hot cyclone separators [60]. The advantage of CFB combustion technology in the context of oxy-fuel firing is in using external solid heat exchanger to extract heat from the combustion process. This allows a significant reduction of the amount of recycled flue gas required for combustion temperature control.

In CFB, fuel is combusted in a hot bed of solid particles (sorbent and ash) fluidized by combustion air that is introduced from below through a series of nozzles. CFB operates at gas velocities high enough to entrain a large portion of the solids (4–8 m/s), which are then separated from the flue gas and recycled back to the fluidized bed combustor. In addition to flue gas recycle, the solid circulation provides an effective means of controlling the combustion. Oxy-fuel CFB combustion can also use external solid heat exchangers to extract heat from the circulating solids to maintain combustor temperature. As a consequence, oxy-fuel CFB can significantly reduce the amount of recycled flue gas or alternatively permit much higher oxygen concentration in the combustor. This allows the economics of oxy-fuel firing in CFB boilers to be improved over pulverized coal firing because recirculated gas flow can be reduced significantly [61].

A hybrid of oxy-fuel and CFB have both the advantage of capturing CO₂, decreasing NO_x emission, and operating with a variety of fuels. In order to mitigate SO_x (SO₂ and SO₃) emission, and have a highly clean combustion, adsorption of SO_x has been investigated thoroughly in literature. Mathieu et.al [62] have provided a review paper about the types of sorbents systems, especially oxide materials, which are currently either in use or under laboratory investigations. They concluded that an ideal SO_x sorbent must ally four essential quantities: a strong affinity of the sorbent towards SO_x

along with fast kinetics, a large specific surface, a high physical/thermal/chemical stability, and the capability for multiple regenerations at a reasonable temperature and with performance recoveries close to 100%.

Leckner and Barea [63] have considered two different cases to understand the conditions of CO₂ capture in a CFB boiler: a situation when an air-fired CFB boiler is built prepared for conversion to CO₂ capture, and a new-design case where a new boiler is built particularly for CO₂ capture. They have concluded that at a given fuel load, the relevant parameters for maintaining the CFB performance (bed temperature and fluidization velocity) in the ready-to-convert case, cannot be kept entirely equal to those in the air-fired case. For bituminous coal under stoichiometric conditions, an oxygen volume–concentration of 0.30 is suitable when the nitrogen in air is replaced by recycling gas at constant bed temperature. The most potentially attractive option is the design of entirely new CFB boiler dedicated to oxy-combustion, employing high input oxygen concentration. The new design offers several advantages, resulting in considerably smaller boilers than in the air-fired case at the same power. Sizing of the new design units is suggested, based on a simplified analysis of the required heat transfer surfaces. The input excess oxygen to the plant can be lowered compared to that of a corresponding air-fired plant.

The emission of N₂O in oxy-fuel CFB combustion can be high enough to raise some related environmental issues. Li et.al [64] have experimentally investigated N₂O emission in O₂/CO₂ CFB combustion with a high oxygen concentration. A 0.1 MW_{th} oxy-fuel CFB was employed to study the operating parameters including the average temperature, overall oxygen concentration, excess oxygen ratio, gas staging, and oxygen staging. It was found that increasing the combustion temperature and overall oxygen concentration can lead to lower N₂O emission, while increasing the excess oxygen ratio can lead to higher N₂O emission levels. Gas staging and oxygen staging had a negative effect on the emission of N₂O, but the net growth of N₂O was small.

New developments in fluidized bed combustion and gasification processes have been investigated by Leckner [65]. It was found that bubbling fluidized beds are not suitable for combustion of coal because of various drawbacks, but circulating fluidized bed boilers can be considered as the most important coal converters and presently the increments in size and efficiency are the most important development tasks. The CO₂ removal is the most important challenge for further development. Several routes are proposed using FB both in single and dual reactor systems: oxy-combustion, chemical looping combustion, calcium cycling, alkali cycling, and amine absorption with solid sorbents. It was concluded that the research for CO₂ capture in FB is still on the laboratory scale and pilot scale plants have not yet been built.

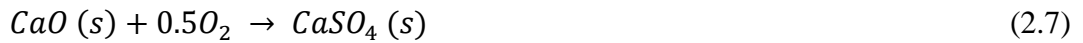
A recent detailed review summarizing the current knowledge on oxy-fuel combustion in fluidized bed combustors have been presented by Matheka et.al [66] in order to evaluate the existing literature in heat transfer, char combustion and pollutant emissions of oxy-fuel combustion in fluidized beds, as well as modelling of oxy-fuel in FB boiler and identify the gaps for further research direction. The review showed that currently there is no full scale or industrial power plants that operate on oxy-combustion using fluidized bed technology. Experimental work on heat transfer performance is still lagging. There are still very few studies focusing on the ash deposition, emission of major and trace elements during oxy-fuel combustion of coal in fluidized combustors. Few models have been developed to predict the performance of oxy-fluidized bed combustors.

2.3.2. Sulfur Dioxide Capture in FBC

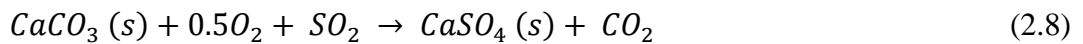
The Sulfur content inside coal is in the form of sulfides, organic sulfur compounds, sulfates, and traces of elemental sulfur [67]. The sulfur content and the way sulfur is bound depends on the type, age and location of the coal source [68]. Pyrite (FeS₂) is usually the main fraction of sulfides in coal and its reaction in combustion is according to the following reactions [69]:



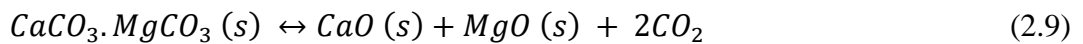
An ideal SO_x sorbent must ally four essential quantities: a strong affinity of the sorbent towards SO_x along with fast kinetics, a large specific surface, a high physical/thermal/chemical stability, and the capability for multiple regenerations at a reasonable temperature and with performance recoveries close to 100% [62]. Calcium (Ca) has a dominant role in sulfur self-retention by ash and the Ca/S molar ratio in the coal is, therefore, an important factor [70]. Calcium-based sorbents such as limestone (CaCO₃) and dolomite (CaCO₃·MgCO₃) are proved to be the successful sorbents for in-bed removal of SO₂ in fluidized bed combustion systems. Depending on the partial pressure of carbon dioxide, the calcium carbonate calcines to lime (CaO), which this process is called indirect sulfation, or remains un-calcined and the reaction between SO₂ and limestone takes place directly (direct sulfation) [71]. Thus, for calcined or un-calcined limestone, the reactions taking place are:



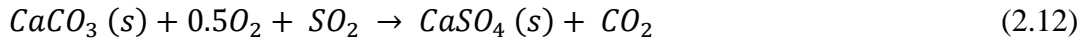
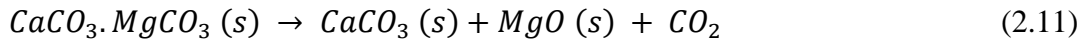
Or:



In dolomite utilization, the magnesium carbonate in the dolomite calcines to magnesium oxide both under typical atmospheric and pressurized FBC conditions, giving half calcined dolomite. However, the formed magnesium oxide does not react with sulfur dioxide [71]. Thus, depending on whether or not the calcium carbonate fraction of the dolomite calcines, the chemical reactions taking place are:



Or:



Sulfur capture with these sorbents is a process highly dependent on the temperature and CO_2 concentration according to the equilibrium curve of CaCO_3 calcination delineated in Figure 2.7 [72]. In oxy-fuel combustion, CO_2 concentration in the flue gas may be enriched between 60% and 90%. Due to high CO_2 concentration, the calcination and sulfation behavior of the sorbent is different from that in conventional coal combustion with air (about 15% CO_2).

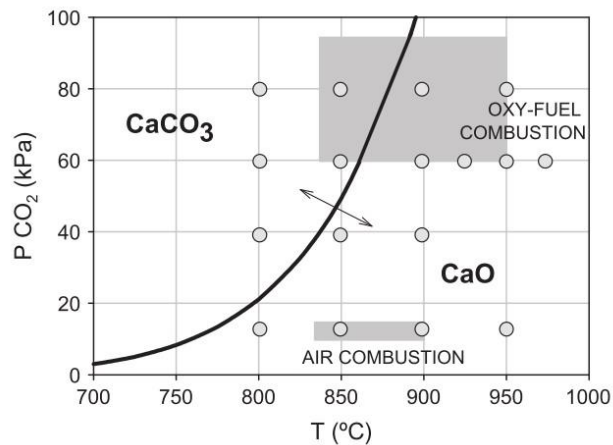


Figure 2.7. Thermodynamic equilibrium curve of CaCO_3 calcination [72]

Sulfur dioxide emission mitigation in air-fired fluidized bed combustion by means of limestone addition has been investigated by Lyngfelt et.al [50] and the optimum temperature for sulfur capture was obtained to be between 800 and 850°C. Below 800°C the sulfur capture process is inhibited due to slow or incomplete calcination and at temperature above the 900°C the porous structure of lime filled with CaSO_4 and reduces the theoretical sulfation potential of CaO particles. In general, the

sulfation efficiency is better in small CaO particles than in large ones. Additional studies about the mechanism of the sulfation of calcined limestone can be found elsewhere [73]–[75]. At temperatures below 900°C and at atmospheric pressure, the direct sulfation of CaCO₃ takes place in oxy-fuel combustion because of the high CO₂ partial pressure [76] and the longer calcination time compared to air firing [77].

The optimum temperature for the highest sulfur retention in FBC operating under oxy-fuel condition was found to be around 900°C [78], [79], whereas operating in conventional air-firing has the optimum temperature by about 850°C. Working at the optimum temperature, the SO₂ retentions were lower in oxy-fuel combustion.

Simultaneous removal of NO_x and SO₂ from coal-fired flue gases in oxy-fuel combustion by means of scrubbing with aqueous acidic solutions containing hydrogen peroxide (H₂O₂) to oxidize NO_x and SO₂ in HNO₃ and H₂SO₄, forming a mixture which can be reused or separated have been proposed by Liemans et al. [80]. It was found that, in oxido-acidic solutions, a rise in H₂SO₄ concentration resulted a decrease in SO₂ absorption efficiencies, while HNO₃ has only a slight negative effect on performances.

Modifying CaCO₃ by addition of CO(NH₂)₂ for flue gas desulfurization during oxygen enriched FB combustion in O₂/CO₂ atmosphere has been carried out by Kochel et al. [81] and resulted a positive impact in the case of an increased CO₂ concentration. The increased CO₂ concentration that accompanies the oxy-combustion inhibits the indirect sulfation process, while the addition of CO(NH₂)₂ to CaCO₃ compensates for its adverse effect, whereby the indirect sulfation process becomes feasible.

A morphological characterization of limestone and dolomite sorbents, during the sulfation process in both calcining and non-calcining conditions have been carried out at oxy-fuel CFB combustion by means of TGA [82]. Analyzing the sulfated samples by Scanning Electron Microscope (SEM) showed that for limestone two different structures of CaSO₄ product layer is formed. The first one, corresponding to the inner part of particles, was composed of small CaSO₄ crystals. In contrast, the space

limitations as a consequence of the higher molar volume of CaSO_4 compared to CaO in the external surface of the particles make that the CaSO_4 product layer tend to grow outwards to form a honeycomb-shaped structure. This structure was observed both in calcining and non-calcining conditions. The honeycomb-shaped structure was never found during dolomite sulfation because the extra porosity developed during MgCO_3 calcination have led to the lack of space limitations. In this case, high sulfation conversions were reached in semi-calcining ($\text{CaCO}_3\cdot\text{MgO}$) and calcining ($\text{MgO}\cdot\text{CaO}$) conditions.

The effect of water vapor on limestone calcination reaction rate and degree of conversion in a FB combustion has been investigated in a laboratory scale FB by Guo et al. [83]. The results showed that the water vapor improved the calcination rate and shortened the reaction time, and those influences were stronger for higher impurity limestone possibly because of more defects in the crystal structure. Water vapor directly influenced the chemical reaction of calcination without affecting the diffusion property of CO_2 . Higher water vapor content resulted in slightly lower ultimate degree of conversion of limestone, but for different kinds of limestone the difference was not obvious. Another study [84] regarding the effect of water vapor on simultaneous calcination and sulfation of limestone showed that SO_2 capture capability of Ca-based sorbent can be improved by more steam. The effect of steam on the calcination of limestone was much stronger at higher temperatures (880°C). For smaller limestone particles the effect of 15% steam was more significant on their sulfation than on their calcination. The CaO sulfurization could be enhanced by water vapor, and an optimum water vapor concentration was 5% for the reaction [85]. Meanwhile, the pore structure could also be affected by water vapor, enlarging the pore size.

2.3.3. Application of Biomass in FBC

Generally, any organic material that can be used as fuel such as wood, wood processing residues, crops, and animal and plant wastes can be categorized under

Biomass. Among the renewable energy and alternative fuels under development, biomass energy or bioenergy is one of the most promising resources to match the requirements of substituted fossil fuels for reducing GHG emissions. Biomass can be considered as one of the solar energy resources. All carbon contained in biomass is gained from carbon dioxide; in other words, the incineration of biomass releases the CO₂ emission that had been absorbed from atmosphere beforehand. Therefore, biomass is referred to as a carbon neutral fuel when it is burned [86].

Biomass as a sustainable energy source have recently attracted more interest from both political and scientific perspectives. However, application of biomass has some serious challenges to tackle. From the resources point of view, a rapid shift from fossil fuels to biomass may result in considerable conflicts concerning water and land use for either food production or biomass for energy generation [87]. In addition to that, biomass energy resources need special attention and more expensive solutions in terms of storage, handling, milling, and feeding compared to existing systems used for coal [88]. Other challenges with biomass include low energy density and great inhomogeneity of biomass fuels. In the past, a number of biomass pretreatment methods have been developed to address the aforementioned disadvantages. Among the explored biomass upgrading methods, torrefaction and densification (or pelletization) are two noticeable routes for solid fuel production.

Torrefaction of biomass is a thermochemical treatment process that involves heating biomass at temperatures of 200–300°C in the absence of oxygen, and causes the decomposition of hemicellulose and releasing different types of volatiles while the cellulose and lignin fractions remain almost unaffected [89]. Torrefaction of biomass improves its physical properties like grindability, particle shape, size, pelletability, and composition properties like moisture, carbon and hydrogen contents, and calorific value. The already higher energy density can be increased further by a pelletizing step after torrefaction [90]. Torrefied biomass has several immediate benefits over untreated biomass:

- Higher calorific value
- More homogeneous product
- Higher bulk density
- Excellent grindability (brittleness)
- Durability
- Hydrophobic nature/water resistance
- No biological activity.

Co-firing of biomass/coal blends for power generation combining with CCS technology opens up the possibility of CO₂ remission from the atmosphere. Oxy-fuel combustion of biomass/coal blends is an interesting and relatively young framework for research especially when its combustion is realized in FBC systems.

Torrefaction promises to deliver a solid biofuel which (when densified) has superior characteristics similar to coal in terms of handling, milling and transport [91]. This has potential to vastly improve the competitiveness of biomass as a renewable energy carrier (provided production costs decline over time following a typical technological learning curve). Over the last decade, the process of torrefaction has received renewed interest as a possible pre-processing technology for biomass driven by a potentially huge market for biomass for electricity production through co-firing or converting coal power plants to biomass entirely [92]. Biomass is the only renewable resource that can directly substitute coal in many applications [93]. If torrefied biomass becomes a market success, it could become an important CO₂ mitigation option.

Khan et al. [94] have performed a review article and presented the major issues concerned with biomass combustion with special reference to the small scale fluidized bed systems. They concluded that the biggest technical challenges that biomass today faces are all related to its ash content (especially alkali metals like potassium) which causes serious problems such as fouling, deposition, corrosion, slagging, and agglomeration in fluidized bed combustion systems. However, none of these issues represents an insurmountable obstacle for biomass.

Sun et al. [95] have carried out an experimental study on the combustion and heat transfer characteristics of wide size biomass co-firing in 0.2 MW fluidized bed reactor. Their results showed that the increase of biomass share had little effect on bed pressure and porosity, but axis temperature profiles in the dense zone became more uniform, the heat release enhanced by about 10% at the upper section of the dense zone, while that at the bottom weakened. Lower temperature at the bottom reduced the decomposition of CaSO_4 , which was advantageous to retention of SO_2 . They concluded that co-firing of biomass in CFB may reduce emissions, improve combustion efficiency and enhance heat transfer at the same time.

The role of minerals in co-firing applications of low rank coals and biomass materials on lignite and their blends with biomass in a lab-scale fluidized bed have been investigated by Vamvuka et al. [96]. It has been shown that combustion of raw fuels produced fly ashes rich in Ca, Si and Fe minerals, as well as K and Na minerals in the case of biomass samples. The results implied that combustion of each fuel alone could provoke medium or high deposition problems. However, biomass addition in the lignite fuel up to 20% wt. could reduce slagging/fouling and corrosion problems.

Varol et al. [97], [98] have investigated the effects of excess air ratio and secondary air injection in a co-combustion of lignite coal and woodchips in a CFB. They concluded that the required amount of excess air should be increased by increasing the woodchip share to obtain minimum CO emission, but further increase cannot be done because it resulted in NO increase. Also, they showed that increasing secondary air ratio lowered the recirculation rate which was followed by an increase in temperature of the dense phase and a decrease in the temperature of the dilute phase in the combustor.

Duan et al. [99] have investigated NO emission during co-firing of coal and three kinds of biomass (rice husk, wood chips, and dry wood flour) in an 10 kW_{th} oxy-fuel CFB. The indicated Results showed that burning biomass separately produced higher NO emissions and a higher fuel nitrogen conversion ratio than burning coal without

biomass addition was noticed due to the higher volatile matter content of the biomass. However, in oxy-fuel combustion, it was seen that NO emission was lower than that of air combustion, because CO₂ replacing N₂ reduces the yield of NO precursors like NH₃ during the devolatilization process. They showed that oxygen staging succeeded in controlling NO emission in a comparatively low level at high overall oxygen concentration condition.

A recent study on air and oxy-fuel combustion of biomass in a CFB on the combustion characteristics of biomass (willow) showed that replacing N₂ in the combustion environment by CO₂ caused slight delay (higher ignition temperature, burnout temperature and lower maximum mass loss rate) in the combustion of wooden biomass. However, when the concentration of oxygen in O₂/CO₂ mixtures is larger than 30%, the ignition and burnout temperatures decreased with increasing O₂ content [100]. They also concluded that combustion process in O₂/CO₂ mixtures at 30% and 40% O₂ was faster and shorter than that at lower O₂ concentrations. The total combustion time (volatiles + char) in the 40%O₂ + 60%CO₂ mixture was approximately 42% shorter than that of combustion in air.

Atimtay et al. [101] have conducted a comprehensive study on an air-firing CFB combustion with two types of Turkish lignites (Bursa-Orhaneli and Bolu-Göynük), addition of limestone to reduce SO₂ emissions as well as co-firing of pine chips and lignite. Their results showed that lignite combustion in CFB produced SO₂ emissions higher than limits, however, addition of limestone decreased SO₂ concentration down to 800-1000 mg/m³ for both lignites. Increasing the excess air ratio resulted in lower CO emission due to complete combustion. During co-firing experiments, the temperature in the freeboard region was 100–150 °C higher compared to coal combustion. From the efficiency point of view, the combustion efficiency from carbon balance was between 92 and 96% for the studied cases. The boiler efficiencies calculated based on indirect methods of ASME were found between 76.9 and 79.03% for Bursa-Orhaneli lignite, and between 69.6 and 71.5% for Bolu-Göynük lignite.

The impact of limestone on oxy-combustion of coal and biomass (corn stover) in a lab-scale fluidized bed has been investigated by Lupianez et al. [102]. Different kinds of limestone with various Ca/S molar ratios were tested. It was found that SO₂ capture increased with the Ca/S ratio and bed temperature, but to a different extent depending on the limestone fragmentation. The amount of NO emitted increased with the Ca/S ratio and the presence of calcined limestone (indirect desulfurization). In spite of the fact that operation under calcining conditions for oxy-combustion requires higher bed temperatures, due to the risk of agglomeration when introducing biomass in the blend, no agglomeration was found for any of the tested conditions. In comparison to air-firing, oxy-firing reduced the corrosion risk and did not affect deposition.

2.4. CFB Simulation Studies

The mathematical modeling and simulation approaches are reliable and cost-effective tools for process description, techno-economical evaluation, and providing information on the behavior of a given system. The fluidized bed boiler design can be supported by the mathematical models. However, the developed models require validation against experimental data. Therefore, both the experiments and numerical models play an important role in the design process. Reh [103] has presented a detailed review regarding CFB combustion modeling arguing that there has to be a balance between the computational modeling and experiments in the studies in this field.

Simulation of the particle transport and combustion process is computationally very demanding. High concentration of the solid phase significantly influences the particle behavior and the reactive flow. To deal with the complexity of these phenomena, special numerical techniques have to be used. In order to take into account a detailed information regarding the gas and solid fuel mixing dynamics, effects of various non-uniform geometries, impact of the coal-feed inlets and air-injection, a detailed mathematical model of the analyzed facility needs to be introduced in the model.

Sotudeh et al. [104] have developed a comprehensive CFBC model using Aspen Plus. The model was composed of hydrodynamic parameters, reaction models and kinetic subroutines. The furnace was divided into two regions, a dense region and an exponentially decaying region or freeboard. The reaction model was composed of devolatilization, volatile combustion, char combustion, NO_x formation and SO₂ adsorption. The obtained results were NO_x, CO and SO₂ emissions, O₂ concentration, and combustion efficiency. The results indicated good agreement with the experimental data.

Desroches et al. [105] have studied the combustion of municipal solid waste in a 25 kW_{th} pilot scale CFB. The dimensions of the pilot plant were 10 cm in diameter and 4 m in height. A 1-D model consisting gaseous pollutant (CO, NO, N₂O, SO₂, HCl) formation and destruction during the combustion of solid wastes has been developed and the results were compared with the experiments. The bed was divided into a dense region at the bottom of the furnace and a dilute zone above. The developed model included devolatilization, char combustion, volatile combustion, SO₂ adsorption, and NO and N₂O formation and reduction reactions. Different operation parameters such as temperature, excess air ratio, calcium addition, waste moisture and air staging was considered. Two different carbon combustion mechanisms were examined. The first model considered the shrinkage of char and the second model considered decrease in density of the char particles. The obtained results from both models showed satisfactory agreement with the experiments.

Zhou et al. [106] have employed a 2-D CFD approach to simulate the air-coal two phase flow and combustion characteristics of a 50 kW_{th} CFB combustor. The gas-solid hydrodynamics was modeled applying Eulerian-Granular multiphase model with a drag coefficient correction based on the extended energy minimization multiscale model. Moisture evaporation, coal devolatilization, volatile combustion, and char combustion and gasification reactions were considered. The temperature profiles in the furnace and concentration of the gases were validated with measurements.

Huilin et al. [107] have proposed a 1-D model for simulation of a 35 t/h commercial CFBC based on hydrodynamics, heat transfer and combustion. The flue gas temperature, the concentrations of O₂, H₂O, CO, CO₂, and SO₂ emissions, char concentration distribution in both dense and lean regions were calculated by the model. The model included SO₂ retention as well. The fluidization regime in the dense region was assumed to be turbulent bubbling regime. The drying and volatile combustion processes were assumed to be instantaneous and the devolatilization process of the char particles was time-dependent. The shrinking core model including both chemical reaction control and gas film diffusion was employed. The obtained results were validated by the experimental data showing that the developed model can be used to represent a CFBC unit in various applications.

Gnanapragasam and Reddy [108] have developed a CFB combustor model in order to study the influence of the shape of the riser exit geometry on the hydrodynamics of the riser column. Two different riser shapes (smooth and abrupt) under different operating conditions was examined to calculate the corresponding axial heat transfer coefficients. The core-annulus mass flux balance model was employed to estimate the axial voidage profile and the cluster renewal mechanistic model was used to predict the corresponding axial bed-to-wall heat transfer coefficient. The obtained results have provided fundamental understandings on the influence of the riser exit shape on the heat transfer characteristics of the CFBC.

The simulation of a 50 kW CFB combustor burning low grade Turkish lignites have been carried out by Gungor et al. [109], [110]. A 1-D model has been developed and the variations of CO, CO₂, SO₂ and NO_x emissions along the combustor height at different operational conditions such as particle diameter, bed operational velocity and excess air were studied. The bed region was assumed to be in turbulent fluidization regime and the lean region was modeled as core-annulus flow. No temperature profile along the combustor was obtained from the results. The model results were compared to the experimental data and good agreements were achieved.

Gungor [111], [112] has extended his work by developing a 2-D model for CFB combustion simulations. The analysis of the combustion system included fluid flow, heat transfer, and pollutant emissions. The model results were tested for three different size CFB, a 50 kW pilot scale CFB using Beypazari lignite, a 80 kW pilot scale using Tunçbilek lignite and an industrial scale 160 MW using Çan lignite. Overall SO₂ and NO_x emissions were calculated under different excess air (20-100%), bed operational velocity (4.15-6.50 m/s), particle size (540-852 µm) and inlet pressure (1.6-2.2 atm). The results indicated that with the increase in excess air, SO₂ and NO_x emissions were decreased. Increasing bed velocity resulted in increase of NO_x and decrease of SO₂ and increasing bed temperature resulted in decreasing both emissions.

Selcuk and Ozkan [113] have extended a previously developed comprehensive mathematical model to incorporate NO_x formation, reduction reactions and pressure drops around cyclone, downcomer and loop seal. A 150 kW_{th} CFB burning low calorific value Turkish lignite with high volatile matter and fixed carbon ration have been tested. The model included dense and lean region hydrodynamics, devolatilization and combustion, char combustion, char particles temperature and size distribution, and heat transfers to cooling water and refractory. O₂, CO, CO₂, H₂O, SO₂, NH₃ and NO components were considered in the model. The indicated results showed that at steady state performance of the combustor, temperature and pressure profiles, emissions, and char particle size distribution can be predicted reasonably well with mathematical simulations.

In the work of Zhang et al. [114] application of the Euler-Euler approach for modeling isothermal flow within large scale CFB boiler has been presented. Wischniewski et al. [115] have extended the standard two-fluid model for modeling the combustion process using a simplified geometrical model of the CFB boiler. An additional application of the Eulerian approach for modeling fluidization and combustion process has been presented by Myohanen [116], where part of the fluidization process was replaced by empirical models.

Adamczyk et al. [117] have simulated the oxy-fuel combustion in a CFB using ANSYS Fluent software. A unique approach of hybrid Euler-Lagrange model was implemented in Fluent as the Dense Discrete Phase Model (DDPM). The DDPM accounts for mutual particle-particle and fluid particle interactions characteristic for the dense solid particle flows by employing models derived from the Kinetic Theory of Granular Flows (KTGF). Their Performed simulations showed that the hybrid Euler Lagrange model can be used for predicting the particle transport in fluidized beds working under the oxy-fuel combustion regime. All evaluated results gave comparable tendencies to the experimental data.

The latter authors have conducted another study to improve the application of the hybrid Euler-Lagrange approach for modelling particle transport, air- and oxy-fuel combustion process in a large scale CFB [118]. The numerical results were validated against measured data. The main conclusion in their paper was proving that the very complex and non-uniform flow behavior combined with combustion process within the large scale CFB boiler can be modelled using commercial CFD ANSYS Fluent package extended by set of UDFs implemented into the solution procedure. The disadvantages of the simulations carried out using a 3D geometry were associated with very long simulation time required to obtain stable solutions.

The limestone behavior in air and oxy-fuel CFB processes were modelled by Rahiala et al. [119]. Different modeling methods were combined: the calculation of particle trajectories in a 3-D steady state CFB furnace model was utilized to investigate the real process environment which the particles experience and a stochastic Lagrangian particle flow model was used to study the effects of the transient environment on limestone reactions. For a selected typical particle size, their results were valid.

Luo et al. [120] have modeled a 3-D full-loop gas-solid flow in a CFB using CFD coupled with the discrete element method (DEM). They focused on the time-averaged flow characteristics and particle-scale details related to solid motion. The Navier-Stokes equations and large eddy simulation (LES) were utilized for gas motion and

turbulence in the CFB. LES has the potential for the gas combustion modeling due to its ability in modeling the multiphase flow. The indicated results of the simulations were in a good agreement with experiments. The results indicated that the solid motion showed an ‘S’ rising path in the riser but a spirally falling behavior in the cyclone. The vertical intensity of solid dispersion was several times of the radial one.

A CFB with a mechanical valve for on-line adjustment of solid flow rate has been numerically simulated using CFD by Liu et al. [121]. The two-fluid model (TFM) was utilized as the governing equations. The sliding mesh model which was used to simulate the opening or closing the valve, was able to successfully model the on-line closing of the mechanical valve. The simulation results revealed that the dynamic response of CFB when the valve was partially or fully closed agreed well with experimental observation. It has been concluded that the CFD simulation can be successfully implemented to CFB parametric analysis.

The research on the simulation of the CFB especially for co-combustion of coal and biomass and oxy-fuel combustion condition is still at its development phase having been conducted mostly in recent years [122]–[128].

2.5. Thermogravimetric Analysis (TGA)

Research on coal combustion characterization can be performed by means of laboratory scale equipment. The application of thermal analysis such as TGA, DTG (derivative thermogravimetry), and DSC (differential scanning calorimetry) in order to study the pyrolysis, gasification, and combustion behavior and kinetics of fossil fuel has an exceptional importance in energy research and developments. These techniques have significant part in the determination of the fossil fuel properties such as composition, decomposition characteristics, calorific effects, proximate analysis, and pyrite contents [129]. TGA is one of the simplest and practical techniques used to characterize the thermal stability and fraction of volatile components of materials by monitoring the weight change that occurs when the sample is heated. TGA allows to

perform iso-thermal and non-isothermal combustion tests at various ambient conditions and at wide range of temperatures which have great advantage in achieving the complete conversion of coal and biomass to delineate TGA/DTG curves and also calculate the kinetic parameters.

TGA analysis can be easily performed in various atmospheres such as Ar, N₂ and CO₂ for pyrolysis experiments, and air, oxygen-enriched air and oxy-fuel atmospheres for combustion experiments, etc. Research on combustion and oxy-fuel combustion of coal by means of TGA is prevalent in literature [11], [130]–[134]. Abbasi and Yozgatligil [130] have studied the effects of several catalysts on pyrolysis and combustion characteristics of Turkish lignite in oxy-fuel conditions via TGA-FTIR. Potassium carbonate, calcium hydroxide and iron (III) oxide were employed as catalysts precursors and impregnated to the lignite sample. The pyrolysis experiments were carried out under N₂ and CO₂ atmospheres and the combustion tests were conducted under different oxygen concentrations of 21% to 35%. Both N₂ and CO₂ were used as diluting gases. In pyrolysis experiments, the main difference was observed at temperature above 720°C attributed to char-CO₂ gasification. During the pyrolysis in CO₂ atmosphere, potassium carbonate was found to be the most effective catalyst in char gasification region. In oxy-fuel combustion experiments, the relative active sequence of catalysts to the reaction rates of devolatilization region was Fe >> K > Ca raw form for 30% oxygen concentration.

Meng et al. [134] have investigated pyrolysis and combustion behavior of a low-rank coal in O₂/N₂ and O₂/CO₂ mixtures using TGA and drop tube furnace. Different oxygen concentrations of 21%, 30%, 40%, and 60% was mixed with N₂ and CO₂ diluting gases. Isoconversional kinetic methods were also applied in order to calculate the Arrhenius parameters. It was found that the gasification reaction took place at temperatures higher than 800°C for pyrolysis in CO₂ atmosphere. The combustion rates of the coal increased with enhancing the oxygen concentration and the ignition and burnout points shifted to lower temperatures causing the complete combustion to achieve at lower temperatures and shorter times. The activation energy values

decreased with increasing the oxygen concentration under oxy-fuel conditions and were lower than that of air combustion conditions.

Selcuk and Yuzbasi [11] have studied the combustion behavior of a Turkish lignite with high sulfur and ash contents under air and oxy-fuel atmospheres by using TGA-FTIR. The considered oxygen concentrations were 21% and 30%. The obtained results indicated that replacing N₂ with CO₂ in the same oxygen concentration did not have a significant impact on the combustion process and only lead to a slight delay in combustion. However, oxygen concentration was an effective parameter on combustion by shifting the DTG profiles to lower temperature regions. Also, the peak and burnout temperatures decreased and the weight loss rate increased.

Characterization of two types of wood biomass and sewage sludge torrefaction have studied in a TGA by Wilk et al. [135]. The torrefaction process of the samples was carried out at different temperatures of 230°C, 260°C, and 290°C at different residence times of 30, 60, and 90 minutes. The pyrolysis process was conducted in argon and the combustion atmosphere was air. The obtained results indicated that the characteristics of the torrefied biomass and sewage were improved and the torrefaction resulted in more carbon content fuel with low moisture content and better strength. It was found that the effect of torrefaction temperature was greater than residence time in all samples. Additionally, the results showed that sewage sludge was not suitable for torrefaction.

Mi et al. [136] have investigate the pyrolysis and combustion characteristics of bamboo and pine wood biomass torrefied at 300°C for 2 hours in argon atmosphere. The analysis of raw and torrefied biomass as well as their blends was conducted in TGA. it was found that due to moisture and volatile removal and hemicellulose decomposition, the torrefied biomass had higher pyrolysis and combustion characteristic temperatures. Torrefied biomass samples had higher heating values, and lower H/C and O/C ratios.

TGA has also been used in a wide variety of areas in assessment of combustion characteristics of coal/biomass blends and evaluation of synergetic effect of their combination. Varol et al. [137] have studied the co-combustion of Turkish lignite and biomass (woodchip, olive cake and hazelnut shell) mixtures by means of TGA and showed that low rank coals can be burnt with biomass very beneficially. They concluded that biomass fuels were more reactive than lignite coals and the combustion characteristics of lignite can be improved by addition of biomass materials such as woodchips.

Vamvuka et al. [138] have investigated this experiment for blend of lignite with sewage sludge waste and some energy crops. The indicated results showed that lignite and cardoon biomass exhibited synergy, whereas lignite and pine needles showed more or less an additive behavior. Blending lignite with cotton, peach kernel and olive kernel increased its thermochemical reactivity. Sewage sludge, which is a more heterogeneous material in nature, showed a different combustion behavior than lignite.

The thermal characterization of wood, demolition wood, coffee waste and glossy paper and their mixtures have been studied using a TGA and a macro-TGA by Skreiberg et al. [139]. It was shown that the combustion characteristics of each single fuel was based on its main pseudo-components (hemicellulose, cellulose, and lignin) and their mixtures had quantitative and qualitative summative behavior based on the single fuels.

The co-combustion of coal blended with oil palm which was hydrothermally carbonized at different temperatures (150, 250, and 350°C) have been investigated by Parshetti et al. [140] in a TGA-FTIR system. Combustion characteristic factor (CCF) which includes the ease of ignition, the firing velocity and the burnout temperature was used as a criterion for combustion performance. Higher CCF values (greater than 2) indicate a good combustion performance. It was concluded that co-combustion of hydrothermally upgraded waste biomass with coal was an attractive option to consider in existing power plants for energy generation because of the major environmental

benefits such as reduction in the emission of greenhouse gases (CO_2 and CH_4), acidic gases (SO_2 and NO) and toxic gas (CO).

The combustion behavior of different kinds of torrefied biomass (lignocellulosic and animal wastes) and their blends with indigenous lignite was investigated via non-isothermal thermogravimetric method under air atmosphere Toptas et al. [141]. Characteristic combustion parameters for blends showed non-additivity behavior. It was found that the mixture of torrefied biomasses and lignite at a ratio of 1:1 had a lower ignition and burnout temperature than the pure coal sample. Although no interactions were observed between the lignite and torrefied biomass at initial step of combustion, a certain degree of interaction between the components occurred at char combustion step.

Co-combustion of coal with biomass under oxy-fuel combustion condition is a promising method for clean combustion technology. Yuzbasi et al. [142] have studied the air and oxy-fuel combustion characteristics of 50/50 wt.% blend of olive residue biomass and lignite in a TGA-FTIR. Combustion experiments were carried out in four different atmospheres; air, oxygen-enriched air environment (30% O_2 -70% N_2), oxy-fuel environment (21% O_2 -79% CO_2) and oxygen-enriched oxy-fuel environment (30% O_2 -70% CO_2). Combustion behavior of fuels and their blend in air and oxy-fuel conditions showed that burning process was slightly delayed in oxy-fuel conditions compared to air conditions at the same oxygen levels. However, as oxygen concentration increased, the DTG profiles shifted to lower temperatures, rate of weight loss increased and complete combustion was achieved at lower temperatures. A synergetic interaction has been found during co-combustion of olive residue and lignite blend. Another study by the latter authors [143] on the combustion behavior of petcoke/lignite blends under air and oxy-fuel conditions showed similar results.

Pickard et al. [17] have studied the co-firing of coal with biomass in oxygen and carbon dioxide enriched atmospheres by means of TGA and a 20 kW pulverized fuel combustor. TGA results showed that substituting N_2 as the combustion diluent with

CO₂ had little impact on the combustion properties of the fuels, but increasing the O₂ concentration accelerated the combustion of coal and biomass chars. Results from co-firing biomass with coal at 20 kW scale suggested substitution of N₂ with CO₂ significantly reduced the temperatures, carbon burnout and emissions of NO while combustion in O₂-enriched conditions had the opposite effects. Emissions of NO and SO₂ were found to reduce compared to air in combustion atmospheres enriched with O₂ and CO₂ while combustion temperatures and carbon burnout slightly increased.

Extracting the kinetics characteristics of coal and biomass from the data provided via TGA is the easiest and most cost effective technique [144]. Several published reports have focused on the combustion kinetics of coal and biomass applying this procedure [145]–[150]. Kinetic parameters are also required for CFD simulation for CFB design and maintenance [151].

Kok et al. [152] have studied the combustion behavior and kinetics of some biomass samples by means of TGA and three iso-conversional kinetic methods: Flynn-Wall-Ozawa (FWO), Kissinger, and ASTM I-II methods. The obtained activation energy values for Kissinger and ASTM I-II methods were in a good agreement, but the FWO method showed higher values for all biomass samples. They concluded that since each kinetic method has different assumptions in calculation, the results can vary accordingly. Thus, instead of focusing on activation energy values, it is better to focus on the comparative values when using the same kinetic method.

Irfan et al. [153] have evaluated the kinetics of bituminous coal and palm shells using TGA under air and oxy-fuel atmospheres. Doyle and Coats-Redfern kinetic models were applied. The activation energy was found to decrease with increasing palm shell composition in coal as well as increasing O₂ concentration in oxy-fuel. However, a reverse trend was observed for the pre-exponential factor.

Engin et al. [154] have studied the kinetics of Turkish lignite coals in air and oxy-fuel combustion by means of TGA. Four different kinetic methods were employed: Coats-Redfern (model fitting method), Friedman, FWO, and Kissinger-Akahira-Sunose

(KAS). It was found that the apparent activation energy of the coals predicted by the model fitting method (The Coats-Redfern) was lower for the oxy-fuel combustion in comparison to the air combustion and tend to decrease with increasing the O₂ concentration. The apparent activation energies of combustion process calculated by FWO method were slightly but systematically higher than that of calculated by the KAS and Friedman methods for the oxy-fuel atmospheres. The KAS method mostly predicted the lowest activation energy values.

Magalhaes et al. [155] have investigated the combustion behavior and kinetics of Turkish lignites and olive residue in a TGA at three heating rates of 15, 20, and 40°C/min. The characteristic temperatures were obtained based on TGA and DTG curves and the combustibility index was calculated for the main stage of combustion. Coats-Redfern method was applied to estimate the kinetic parameters. The results showed that the combustibility of olive residue was at least fivefold those of the lignites. Increasing the heating rate resulted in increase of the reactivity, combustibility and burnout temperatures of all fuels. The apparent activation energy values were approximately constant at the heating rates of 15 and 20°C/min and decreased with further increase of the heating rate to 40°C/min.

In the study conducted by Oyedun et al. [156], the pyrolysis characteristics and kinetics of plastics (polystyrene and high density polyethylene) and biomass (bamboo, empty fruit bunch and sawdust) blends have been investigated via TGA at the heating rate of 10°C/min. The activation energy and pre-exponential factors for the samples and their blends were estimated. In order to evaluate the synergetic interaction between of the blends, the relative error parameter was calculated based on the experimental and theoretical TGA data of the blends. It was found that while the thermal decomposition of the parent fuels can be characterized by one single reaction stage, the decomposition of the blends can be characterized by two reaction stages. The synergetic effect was seen at certain fractions of the blends. Increasing plastic fraction of the blends resulted in lower activation energy values, especially at the first stage of decomposition.

The combustion and oxy-fuel combustion of coal and biomass blends have been studied by Galina et al. [157] by means of thermogravimetric analyzer. The biomass samples were sugarcane bagasse and sorghum bagasse which were mixed with coal at fractions of 10, 25, 50, and 75%. The experiments were conducted at the heating rate of 10°C/min. based on the TGA data, parameters such as combustion index, synergism, and activation energy have been calculated. The synergism which was used to describe the interaction between biomass and coal samples was obtained by the difference between the experimental and theoretical DTG data. The relative error as a degree of synergism was also calculated. The obtained results indicated that there were certain levels of synergism in all mixtures in both air and oxy-fuel combustion atmospheres. Moreover, it was found that when N₂ was replaced with CO₂, an improvement in combustion performance was observed. Both sugarcane and sorghum bagasse showed similar trends making them suitable alternatives for application in clean energy generation.

CHAPTER 3

MATERIALS AND METHODS

3.1. Coal and Biomass Samples

The coals used in this study were two Turkish indigenous lignite samples (Orhaneli and Soma lignites) which were selected due to their different composition. Table 3.1 shows the proximate and ultimate analysis, and calorific values of the coals. The proximate analysis as an assay of the moisture, volatile matter, fixed carbon, and ash content of the lignite samples was conducted by means of PerkinElmer Pyris 1 TGA based on the procedure described in [158]. Elemental (C, H, N) analysis was carried out by METU Central Lab using a LECO CHNS-932 analyzer. The oxygen content was calculated by difference from the elemental analysis results. The calorific values of the samples were measured using AC-500 bomb calorimeter. In order to disclose the ash components of the samples, the X-ray Fluorescence (XRF) analysis was performed based on ASTM D-3682 and ASTM D-4326 test methods. The major contributors are listed in Table 3.2. The coals were sieved and a narrow particle size interval between 74-150 μm was selected in order to avoid the effect of heat and mass transfer during the process. The samples were dried at 105°C for about 2 hours and then stored in air tight vials in order to avoid contact with moisture.

In order to obtain the proximate analysis data of the samples the following procedure was carried out: about 10 mg of each sample was placed in TGA device and pure nitrogen gas was introduced to the chamber. The sample was weighed at 25°C, then heated to 110°C at 85°C/min and held for 6 minutes. Following that, the sample heated up to 950°C at 80°C/min where the temperature was kept until constant weight was achieved. Finally, the sample atmosphere was switched to air and the combustion of the fixed carbon took place and ultimately reached to a constant weight. The TGA and

DTG curves of this procedure for Orhaneli and Soma lignites are presented in Figure 3.1 and Figure 3.2 respectively.

Table 3.1. Proximate and ultimate analysis of lignite samples

	Orhaneli Lignite	Soma Lignite
<i>Proximate Analysis (wt.%, as received)</i>		
Moisture	3.82	2.69
Volatile Matter	43.69	30.01
Fixed Carbon	41.98	24.65
Ash	10.51	42.65
<i>Ultimate Analysis (wt.%, Dry Basis)</i>		
Carbon	55.35	30.82
Hydrogen	4.96	2.98
Nitrogen	0.97	0.78
Sulphur	1.73	0.57
Oxygen (by difference)	25.17	22.18
<i>Heating Values (kcal/kg, Dry Basis)</i>		
HHV	5920	3477
LHV	5718	3348

Table 3.2. Ash XRF analysis of the coal samples

<i>Components (wt.%)</i>	<i>CaO</i>	<i>Al₂O₃</i>	<i>Fe₂O₃</i>	<i>SO₃</i>	<i>SiO₂</i>	<i>MgO</i>	<i>Other Components</i>
Orhaneli Lignite	22.80	8.27	13.45	25.87	13.61	3.69	12.31
Soma Lignite	19.37	22.24	5.85	6.79	39.51	2.08	4.16

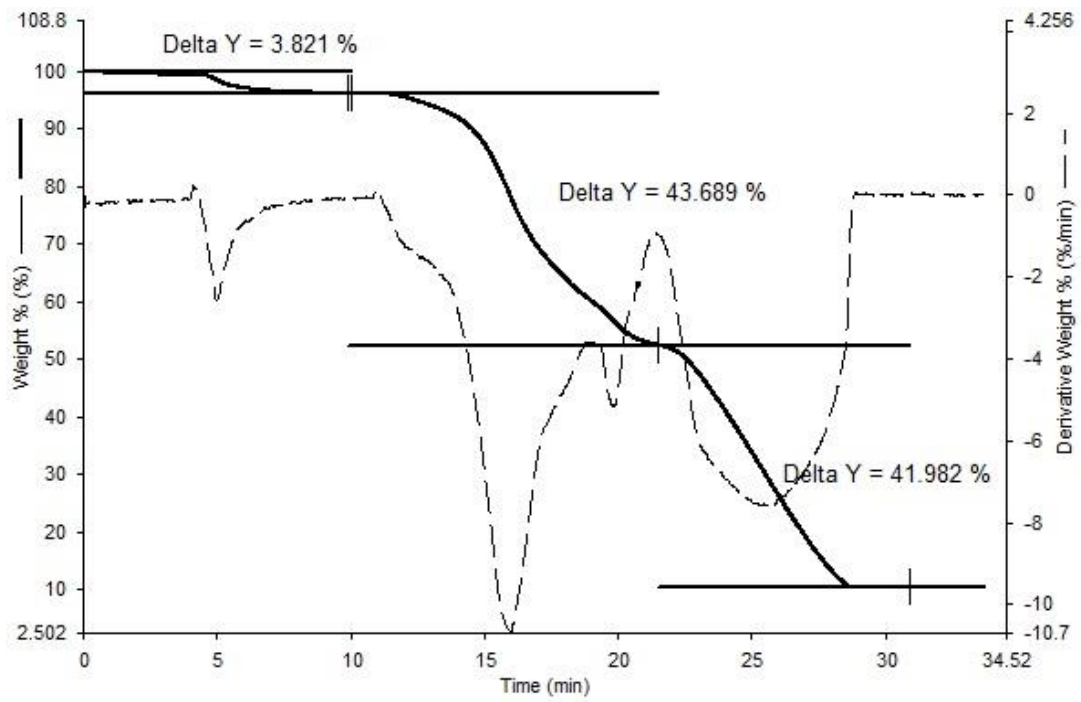


Figure 3.1. Orhaneli lignite proximate analysis results

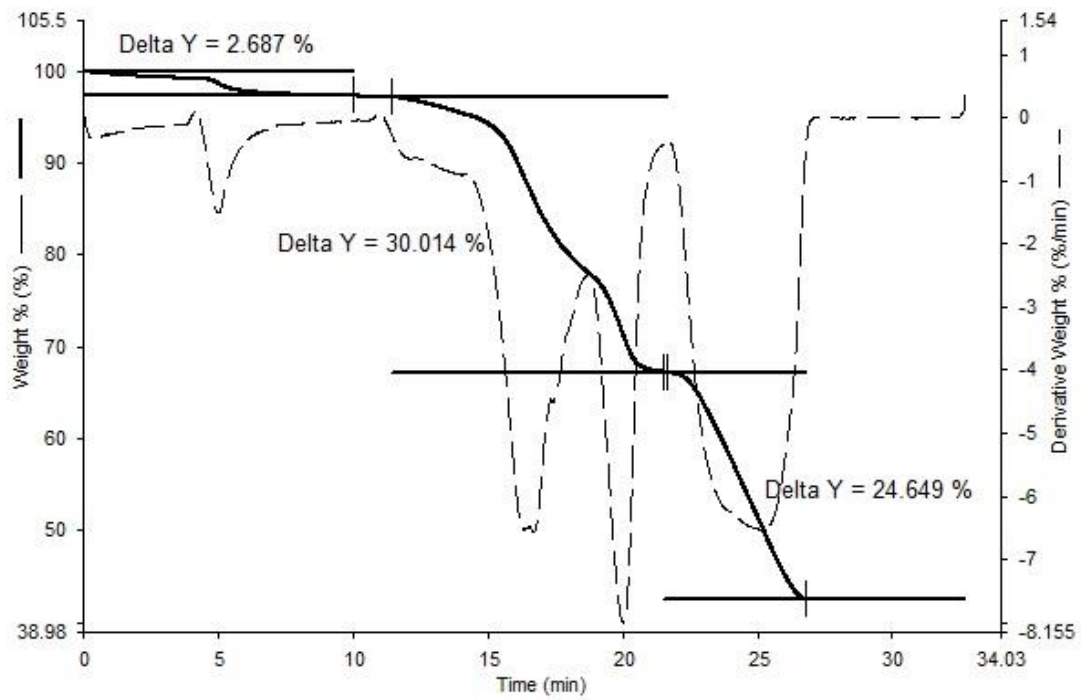


Figure 3.2. Soma lignite proximate analysis results

The biomass samples were prepared at EGE University under the TÜBİTAK 1003-113 M 003 project. The pine wood chips were provided from Kastamonu Entegre Ağaç Sanayi A.Ş. and torrefied in a specially designed biomass production system at different temperature and residence times. The device was a screw-type torrefaction system with a continuous fuel supply up to 5kg/hour. The residence time of the torrefaction process was controlled by changing the screw rotation speed and the torrefaction temperature was controlled by a thermostat control unit. The non-oxidative torrefaction method was used. In order to provide an inert atmosphere and keep the temperatures at the desired level, nitrogen was introduced into the torrefaction reactor section.

Originally, five torrefaction temperatures (225°C, 250°C, 275°C, 300°C, and 350°C) and three residence times (5, 15, and 30 minutes) were considered for the pine wood torrefaction process. Based on the results obtained in [159], three torrefaction temperature (250, 300, and 350°C) at two specified residence times (15 and 30 minutes) were selected for TGA analysis. The biomass samples were sieved and a narrow particle size interval of 74-150µm was selected. The samples were dried at 105°C for about 2 hours and stored in airtight vials. Table 3.3 shows the proximate and ultimate analysis and calorific values of the raw wood chip and torrefied biomass samples. The proximate analysis of the samples was conducted by means of PerkinElmer Pyris 1 TGA as for the coal samples. Elemental (C, H, N) analysis was carried out by Middle East Technical University (METU) Central Laboratory using a LECO CHNS-932 analyzer. The oxygen content was calculated by difference from the elemental analysis results. Table 3.3 also shows the H/C and O/C atomic ratios of the samples which were calculated based on the ultimate analysis.

In order to study the SO₂ removal in CFB combustion, two adsorbents were selected to be used in the experiments. These adsorbents were Çan limestone and Eskişehir dolomite with the characterizations given in Table 3.4. The adsorbent were used at particle sizes of 0-1 mm and 1-2 mm and Ca/S ratio of 1.5 and 2. The Brunauer–

Emmett–Teller (BET) analysis was also conducted to obtain the specific surface area of the adsorbents and the results are presented in Table 3.5.

Table 3.3. Proximate and ultimate analysis of the biomass samples

	Raw Biomass	250°C 15min	250°C 30min	300°C 15min	300°C 30min	350°C 15min	350°C 30min
Proximate Analysis (wt.%)							
Moisture	3.39	2.45	2.40	2.18	1.90	2.18	3.37
Volatile M.	79.48	76.56	70.91	57.59	55.67	36.15	31.76
Fixed C.	15.70	19.64	25.64	38.67	40.93	59.48	62.63
Ash	1.43	1.35	1.05	1.56	1.50	2.19	2.24
Ultimate Analysis (wt.%, Dry Basis)							
Carbon	48.35	51.87	55.78	65.87	65.29	71.86	70.34
Hydrogen	6.69	6.29	5.99	6.77	5.94	5.14	4.25
Nitrogen	0.19	0.21	0.21	0.29	0.28	0.35	0.35
Sulphur	0.02	0.01	0.02	0.06	0.03	0.09	0.14
Oxygen	44.75	41.62	38.00	27.01	28.46	25.56	24.92
Atomic Ratio							
H/C	1.66	1.46	1.29	1.23	1.09	0.86	0.72
O/C	0.69	0.60	0.51	0.31	0.33	0.26	0.26
Higher Heating Values (MJ/kg, Dry Basis)							
HHV	20.0	20.8	22.3	22.7	23.3	28.3	29.2

Table 3.4. XRF analysis of the adsorbents

Chemical Analysis (%)	Çan Limestone	Eskişehir Dolomite
CaO	97.78	75.77
SiO ₂	0.9932	0.0714
Al ₂ O ₃	0.6229	0.0503
MgO	0.2833	24.04
Fe ₂ O ₃	0.2167	0.0261
ZnO	0.0374	-
SO ₃	0.0367	-
MnO	0.0357	-
P ₂ O ₅	0.0174	-
K ₂ O	0.0133	-
SrO	-	0.0426
Loss on Ignition	41.2	45.1

Table 3.5. BET results of the adsorbents

	Çan Limestone	Eskişehir Dolomite
Before Calcination	0.5 m ² /g	1.5 m ² /g
After Calcination (@ 900°C)	13.45 m ² /g	20.26 m ² /g

3.2. Experimental Study

3.2.1. TGA Studies

TGA is used to characterize the physical and chemical properties of solid materials during dehydration, decomposition and oxidation processes based on changes in weight of a known quantity as a function of temperature at defined heating rate (dynamic measurement) or time at constant temperature (static measurement) in a controlled environment [160]. The measurements are used primarily to determine the thermal and/or oxidative stabilities of materials as well as their compositional properties.

The process environment is controlled by a sample purge gas which could be inert or a reactive flowing over the sample. A set of mass flow controllers are used to control the purge gas composition. In order to prevent the ultra-precision balance to be contaminated by volatile residue, a balance purge gas (usually nitrogen) is introduced to the device through a separate port to maintain a stable environment for the balance. The balance purge gas flow should always be higher than that of the sample purge. Sample and reference temperatures are measured directly with embodied thermocouples.

In TGA thermal curves, the x-axis can be displayed as time or temperature and the y-axis can be displayed as weight (mg) or weight percent (%). Deriving TGA curve with respect to time or temperature gives derivative thermogravimetry (DTG) curve which illustrates the rate of weight loss (mg/min or percentage per min). DTG curves are very useful in exploring the reaction rates and determining the different regions of a process.

The device utilized in this study was PerkinElmer Pyris-1 TGA apparatus which is shown in Figure 3.3. A platinum sample pan (8mm diameter, 2mm height) is suspended by a quartz hang-down from a precision balance ($\pm 0.001\text{mg}$) and resides in a furnace with the maximum operating temperature of 1000°C . The Pyris software manager was used to command the TGA and save the data. The specifications of the TGA are listed at Table 3.6.

The gas flow rates are measured and controlled by Teledyne Hastings HFC 202 Mass Flow Controller which is shown in Figure 3.4. The specifications of the mass flow controller are listed at Table 3.7. As it can be seen in Figure 3.4, four mass flow controllers are installed in the gas mixing unit including: CO_2 (max flow: 100 ml/min), N_2 (max flow: 30 ml/min), O_2 (max flow: 40 ml/min), and CO_2+SO_2 (max flow: 20 ml/min). The required mixture for the sample purge ambient is formed by mixing two gasses (N_2/O_2 or CO_2/O_2) in the desired ratios by utilizing CO_2 , N_2 , and O_2 mass flow controllers. Figure 3.5 represents the schematic diagram of the utilized system.



Figure 3.3. PerkinElmer Pyris-1 TGA apparatus

Table 3.6. PerkinElmer Pyris-1 TGA specifications

Sample Atmosphere	Standard or dynamic, including nitrogen, argon, helium, carbon dioxide, air, oxygen, or other inert or reactive gases. Analyses done at normal or reduced pressures.	
Standard Furnace	Temperature Range:	Sub-ambient to 1000°C
	Scanning Rates:	0.1°C/minute to 200°C/minute
	Temperature Precision:	±2°C
Balance	Tare:	Reproducible to ±2 µg
	Sensitivity:	0.1 µg
	Accuracy:	Better than 0.02%
	Precision:	0.001%
	Capacity:	1300 mg
Hang-down Wires	High temperature quartz, nichrome, or platinum	
Sample Pans	Standard Furnace:	Platinum or ceramic with capacity of 60 µL
Sample Mass Range	Up to 1300 mg	
Cooling	Forced air cooled with an external fan and internal booster purge	
	Standard Furnace:	1000°C to 40°C in less than 15 minutes under normal operation
User Control	Operates on Pyris software, fully tested on Windows operating system	
Hyphenated Techniques	Compatible with the Spectrum One as well as most other FT-IRs and mass spectrometers (MS)	
Gas Switching	Fast, thorough and efficient due to reduced furnace volume. Less than 3 minutes to purge the sample area of ambient gases (remove 99% of oxygen) and replace the volume with an inert purge gas. 10 minutes to achieve 99.99% of oxygen free environment.	
Quality Assurance	Developed under ISO 9000	
Dimensions (HxDxW)	67 x 28 x 60 cm	
Weight	40 kg	
Power Requirements	100 to 240 Volt, 50/60 Hz	



Figure 3.4. Teledyne HFC 202 mass flow controller (*left*) and the gas mixing unit (*right*)

Table 3.7. Teledyne HFC 202 mass flow controller specifications

Accuracy and Linearity	±1% F.S.
Repeatability	±0.05% F.S.
Std Pressure Rating	500 psig
High Pressure Option	Proof tested to 1500 psig
Pressure Coefficient	-0.0067%/psi (0-100 psig N2) typical
Control Valve DP	Per customer order
Leak Integrity	< 1x10e-9 sccs
Temperature Coefficient 3	Zero ±0.035% FS/°C (0-60°C) Span ±0.05% RDG/°C (0-60°C)
STP	0°C and 760 Torr
Power (±15 Volt controller)	±(14-16) VDC @ +60 mA/-185 mA (< 3 Watts)
Power (24 Volt controller)	(14-32) VDC < 4.2 Watts
Flow Signal	(inherently linear) 0-5.00 VDC or 4-20 mA
Command Signal	0-5.00 VDC or 4-20 mA
Wetted Material	316 SS, 302 SS, Nickel, Viton, 82/18 Au/Ni Braze, Trace Silver Solder, Kalrez
Connector	15-pin subminiature D/(9-pin for 24 Volt)
Fittings	% in. Swagelok, others available
Weight (approx.)	0.82 kg

The total sample purge gas flow rate was set to 100 ml/min during the experiments. In order to minimize the ambient temperature impact on the experiments, the sample purge gas passed through an electrically heated line before introducing to the TGA. The temperature of the heated line was kept constant at 100 °C. The balance purge should always be 10 ml/min more than sample purge to prevent the volatile gases from back streaming into the balance area.

Approximately 15 mg of a coal sample with particle size between 75-150 µm was used in each test within the temperature range of 50-950°C. In order to calculate the kinetic parameters, four different heating rates was considered; 5, 10, 15 and 20°C/min. The temperature and the sample weights were continuously recorded with the Pyris software manager. The repeatability of the experiments was checked by conducting the experiments three times.

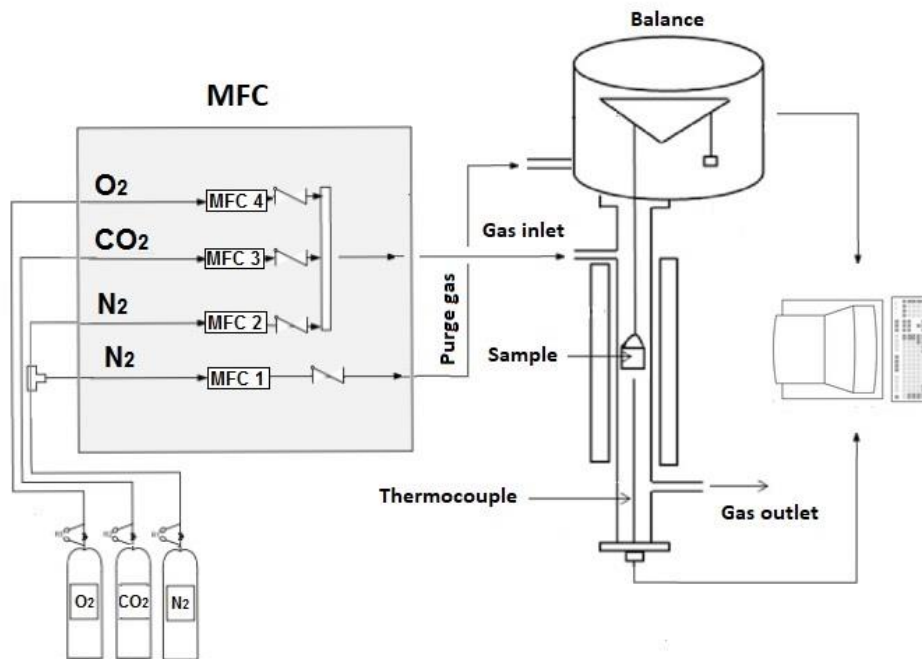


Figure 3.5. Schematic diagram of the utilized system

In combustion of solid fuels in TGA, usually three regions of weight loss appear. These weight loss regions show the thermal breakdown of organic materials and volatiles in the samples and can be determined according to DTG curves. In the case of coal and biomass combustion, the first region is due to moisture release of the sample which concludes in the temperatures up to 200°C. The second region which the main weight loss takes place is attributed to oxidation and devolatilization of the sample. The start and conclusion of this region depends on the type of the fuel and usually is between 250°C to 550°C. The third region is where the oxidation of char occurs and mainly depends on the ash components of the fuel. In fuels such as biomass which the ash content is very low, the third region does not appear in the TGA graph.

The characteristic temperatures describing the combustion of solid fuels can be obtained from TGA and DTG curves. The initial temperature (T_i) is assumed to correspond to weight percentage equal to 95% [161], the ignition temperature (T_{ig}) is

the temperature at which solid fuel starts burning which is the point that the weight loss curve in combustion diverges and a sudden decrease is seen in the DTG curve [133]. The peak temperature (T_{max}) is where the maximum weight loss occurs in the DTG curve, and the burnout temperature (T_b) represents the temperature at which combustion is completed. Figure 3.6 shows the weight loss regions and characteristic temperatures in a TGA/DTG graph.

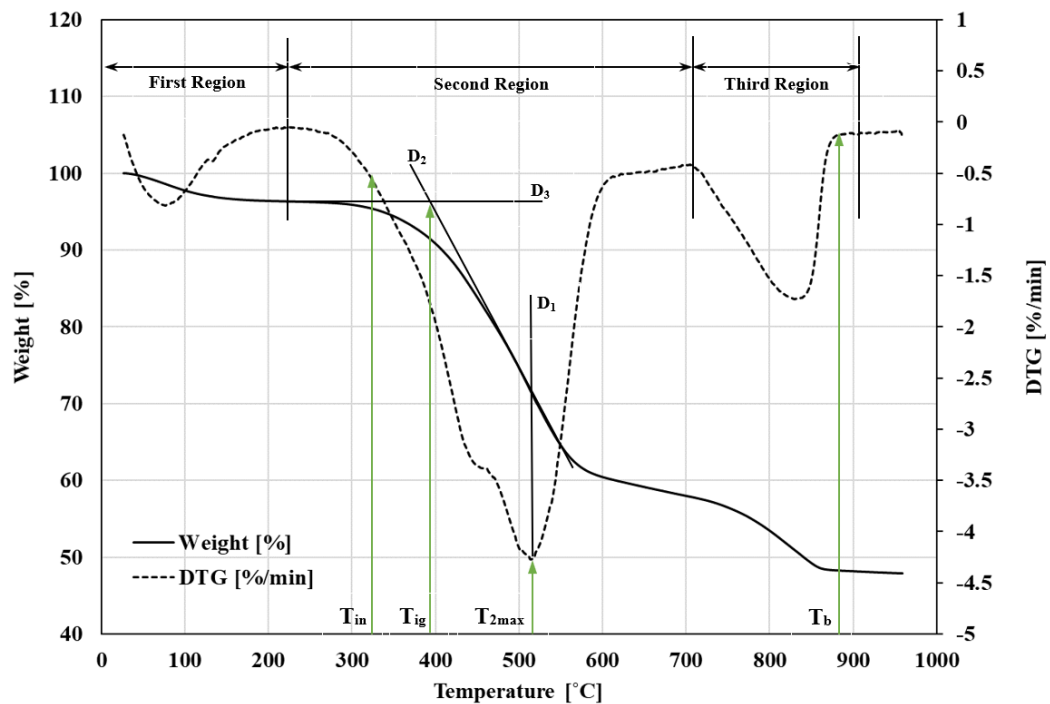


Figure 3.6. Weight loss regions and characteristic temperatures in a TGA/DTG curve

3.2.2. CFB Studies

The circulating fluidized bed combustor (CFBC) used in this thesis was designed and built in 2009 in Marmara Research Center (MRC) Energy Institute on the scope of a TÜBİTAK project proposed by Prof. Dr. A. Atımtay, Environmental Engineering Department, METU (Project Code: 105G023) [162]. Another TÜBİTAK project was

proposed by Prof. Dr. H. Okutan in 2013 (Project Code: 113M003) [18] to modify the existing system in order to study the co-combustion of lignite and torrefied biomass in oxy-fuel combustion conditions as well as the SO₂ removal experiments.

The 30 kW_{th} laboratory-scale CFBC was originally designed based on Orhaneli lignite. However, it was also possible to modify the system to operate properly with different types of fuels with different specifications. The setup is comprised of a circulating fluidized bed combustor, two fuel feeding hoppers, two cyclones, one return leg, primary and secondary air feeding systems, electrical heaters, ash hoppers, a flue gas cooling system, and a bag filter. Figure 3.7 displays the schematic and setup of the CFBC. The column height is 6 m with the internal diameter of 108 mm and the coal and biomass particle should be less than 2mm to fluidized.

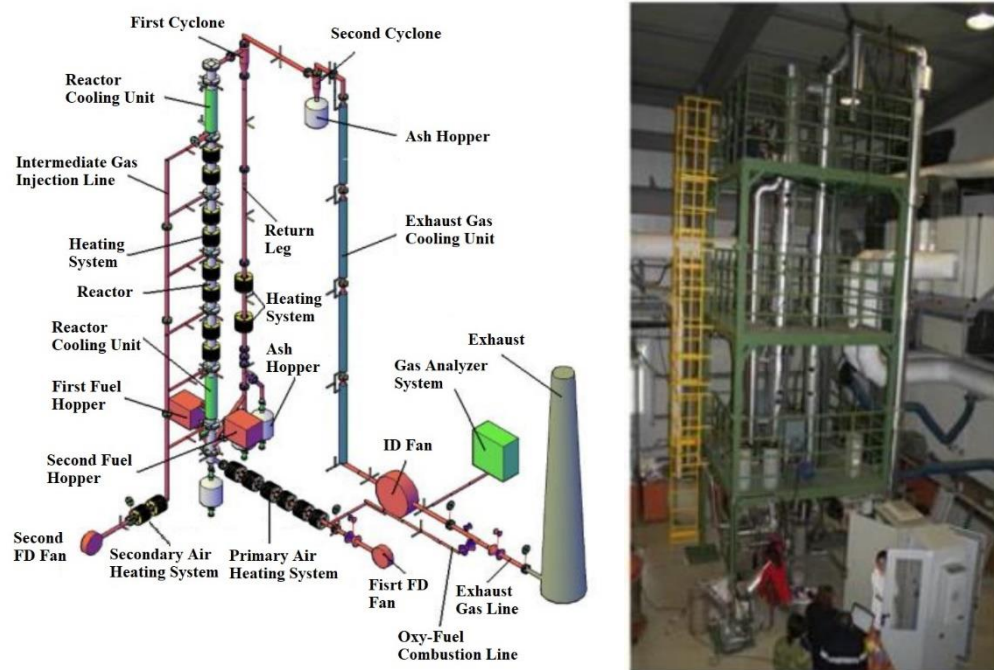


Figure 3.7. Schematic and photograph of the CFBC system

The control of air and fuel mass flow rates introducing to the system, the line control valves openness, process monitoring and recording the data such as the temperature, pressure and flue gas compositions is done by a computer control unit. The user graphical interface of the program is shown in Figure 3.8. The emission composition is analyzed by ABB-AO 2000 and GASMET-DX 4000 flue gas analyzers.

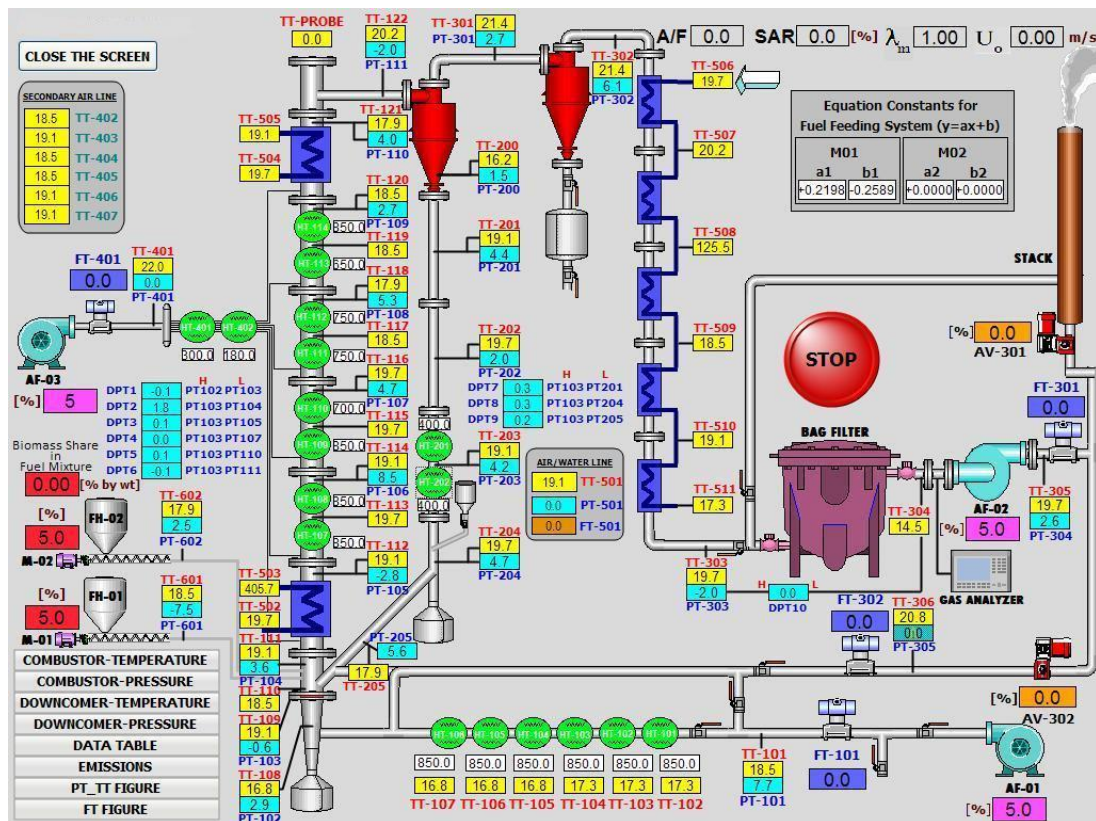


Figure 3.8. Graphical user interface program of the CFBC system

The bottom part of the combustor is called windbox which is a pipe with the diameter of 108 mm and the height of 150 mm. Air enters the windbox from sides with a pipe with the size of 36.6 mm. The windbox is connected to the bottom ash removal pipe through a conical part. The inlet temperature and pressure sensors are mounted in the windbox. Figure 3.9 delineates the windbox shape.



Figure 3.9. Windbox

The distributor is a perforated plate with 618 holes with the diameter of 1 mm and is fixed between the windbox and main body flanges. The diameter of the holes was determined in order to provide a gas flow velocity of around 30 m/s. Figure 3.10 shows the distributor plate.



Figure 3.10. Distributor plate used in the combustor.

The combustor's main body consists of eight modules with the diameter of 108 mm: Module-101 to Module-108. Each module has ports for temperature and pressure

measurements, gas sampling, and secondary air injection. The vertical distance of the thermocouple ports from the distributor plate are presented in Table 3.8. The thermocouples TT-109 to TT-121 are located in the combustor and TT-201 to TT-205 are in the return leg of the system.

Table 3.8. Thermocouple heights from the distributor plate inside the combustor and return leg

Combustor		Return Leg	
Thermocouple No	Vertical Height [cm]	Thermocouple No	Vertical Height [cm]
TT-109	4.0	TT-201	470.7
TT-110	24.0	TT-202	319.7
TT-111	32.0	TT-203	187.2
TT-112	125.0	TT-204	95.7
TT-113	170.5	TT-205	34.7
TT-114	216.0		
TT-115	261.5		
TT-116	307.0		
TT-117	355.0		
TT-118	398.0		
TT-119	443.5		
TT-120	498.0		
TT-121	580.0		

Module-101 is placed immediately after the distributor plate and has the total height of 425 mm. The fuel feeding hoppers are connected to this module at the height of 62.64 mm and 126.13 mm over the distributor plate. The recirculated gas injection position is 136 mm above the distributor plate. Module-101 is presented in Figure 3.11.



Figure 3.11. Technical drawing of Module-101

Module-102 and Module-107 have identical shape and are used for cooling purposes (if needed). The total height of these modules is 910 mm and are composed of two concentric cylinders which allows the air or water flow in between. Figure 3.12 shows the schematic of these modules.

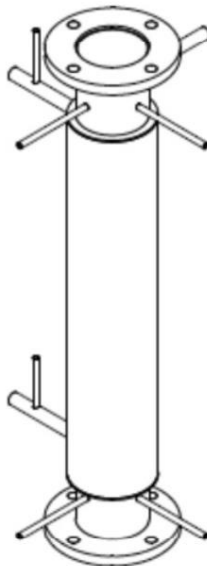


Figure 3.12. Technical drawing of Module-102 and Module-107

Modules 103 to 106 are identical with the total height of 910 mm. The outside of these modules is surrounded by eight electrical heaters in order to increase the air temperature over the ignition temperature of the fuel. These heaters are in operation during the transition stage and when the system reaches to the steady-state condition, they are turned off. The schematic of these modules is presented in Figure 3.13.

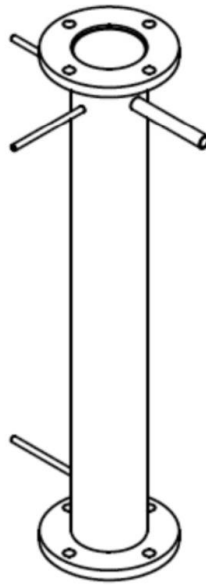


Figure 3.13. Technical drawing of Module-103, Module-104, Module-105, and Module-106

The last module of the combustor is Module-108 with the total height of 260 mm and the gases are directed from this module to the first cyclone. Figure 3.14 shows the drawing of this module.

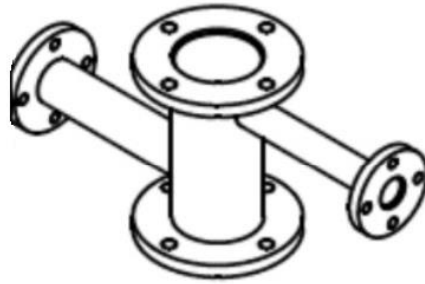


Figure 3.14. Technical drawing of Module-108

The first cyclone is comprised of a cylinder with the diameter of 108 mm and height of 216 mm and a conical part with the height of 216 mm. It is connected to the combustor via a pipe with diameter of 36.6 mm and captures the solid particles and feeds back to the combustor through a recycling tube. The recycling tube height is 5.55 m with the diameter of 36.6 mm. The particles that did not capture at the first cyclone, enter the second cyclone and captured there. The second cyclone is smaller than the first one (with the diameter of 84.24 mm and the total height of 337 mm) and is used to capture the finer particles escaping the first cyclone. The ash hopper is placed at the bottom of the second cyclone and the accumulated ash is collected and subjected to ash analysis. The micron size particles which are escaped from the cyclones are trapped by bag filters installed at the exhaust line.

The air is introduced to the system via a force draft (FD) fan and the pressure inside the combustor is controlled by an induced draft (ID) fan. By adjusting the flowrate and operational pressures of these fans, the system can operate at positive or negative pressure (gauge). In the combustion tests, the flow rate is adjusted so that the pressure at the exit of the second cyclone is zero. In order to protect the ID fan and bag filter from the high temperature flue gas, five water cooled heat exchangers are placed around the pipe connecting the second cyclone to the bag filter. These heat exchangers decrease the flue gas temperature below 200°C.

The first step to operate the system is to turn on the existing inlet and exhaust fans. The supplied air is heated by passing through six electrical heaters. Then, the air passes through holes created in the distributor plate. The electrical heaters around the combustor are operated in transition stage in order to increase the temperature of the bed. Silica sand is introduced from the return leg into the bed. 6 kg of sand with the diameter between 250-350 μm is used for each experiment. The minimum of 15 m^3/h flowrate is required in order to fluidize the bed sand and prevent the plugging of the distributor plate holes.

The fuels are prepared in advance and stored in the fuel hoppers. When the temperature in the dense region of the bed reaches 420-430 $^{\circ}\text{C}$, the fuel is fed into the combustor. The feeding lines are air-cooled in order to prevent the reaction of the fuel particles in the feeding line. The proper temperature for the feeding line is less than 200 $^{\circ}\text{C}$. It takes about 3 hours for the system to heat up. When the temperature profile along the combustor reaches 800 to 850 $^{\circ}\text{C}$ and combustion is self-sustained, the electrical heaters around the bed are turned off and the data recording is started. It takes around 5 hours for the system to reach to steady-state condition. The superficial velocity in the bed should be between 3-4 m/s in order to sustain the particle fluidization. The gas flow rate is around 25-30 m^3/h at the standard condition (20 $^{\circ}\text{C}$ and 1 atm).

The combustion process was carried out under oxygen-enriched air with oxygen concentrations of 21, 23, 25, and 27% and the excess air ratio (λ) was 1.4 throughout the experiments. The excess air ratio was adjusted by controlling the amount of feeding fuel. In order to adjust the oxygen concentration at the desired levels, an oxygen tank was connected to the inlet system and the flow was controlled by a mass flow controller and gas analyzer. Each test was started with air combustion (21% O_2) and after the system was reached to the steady state and the measurements were recorded, the oxygen was gradually introduced to the system to reach to 23% oxygen concentration. After the system reached to steady state, the measurements were

recorded. This process was repeated to the oxygen concentrations of 25 and 27% as well.

3.3. Numerical Analysis

3.3.1. Kinetic Analysis

In general, three methods are used to study the coal kinetics: model fitting method, iso-conversional or model free methods, and distributed activation energy method (DAEM) [163]. Model fitting methods are broadly used in solid-state kinetics and show an excellent fit to the experimental data, but produce uncertain kinetic parameters especially for non-isothermal conditions [164]. The international confederation for thermal analysis and calorimetry (ICTAC) has suggested that the kinetic data was first processed by applying various iso-conversional methods [165] such as Kissinger method, Kissinger-Akahira-Sunose (KAS) Method, Flynn-Wall-Ozawa (FWO) Method, and Friedman Method. Isoconversional kinetic methods can be applied reliably to calculate the activation energy of the process [166].

Non-isothermal kinetics methods introduced in the late 1950s as an outcome of the extensive development of thermo-analytical methods. Numerous empirical models for estimating the Arrhenius parameters (activation energy and pre-exponential factor) from the results of thermal analysis (TA) have been suggested to describe the process under consideration [167]. Model-fitting and model-free kinetic approaches can be applied to both isothermal and non-isothermal thermal decomposition data in order to calculate the aforementioned parameters. Model-fitting methods give excellent fits for both isothermal and non-isothermal data but yield a single value of Arrhenius parameters which is highly uncertain especially when applied to non-isothermal data. The values obtained by these methods are averages that do not reflect changes in the kinetics and mechanism with the temperature and the extent of conversion. On the other hand, the iso-conversional approach yields similar dependencies of the activation energy on the extent of conversion for isothermal and non-isothermal data.

The use of the iso-conversional method is recommended as a reliable way of extracting trustworthy and consistent kinetic information from both isothermal and non-isothermal data [168].

The decomposition of coal can be formulated as a single step kinetic equation in terms of temperature (T) and conversion degree (α) [169]:

$$\frac{d\alpha}{dt} = k(T) f(\alpha) \quad (3.1)$$

where $f(\alpha)$ is the conversion function of the reaction characterizing its mechanism and $k(T)$ is the rate constant. The conversion degree represents the decomposed amount of the sample at time t and is defined as follows:

$$\alpha = \frac{(m_i - m_t)}{(m_i - m_f)} \quad (3.2)$$

where m_i is the initial mass of the sample, m_f is the final mass of the sample, and m_t is the sample mass at time t which are obtained by TGA for any selected region. The rate constant is generally expressed by the Arrhenius equation [169]:

$$k(T) = A \exp\left(\frac{-E_a}{RT}\right) \quad (3.3)$$

where the term A is the pre-exponential factor, E_a is the activation energy, R is the universal gas constant and T is the absolute temperature. The decomposition kinetic relation can be obtained combining these equations:

$$\frac{d\alpha}{dt} = A \exp\left(\frac{-E_a}{RT}\right) f(\alpha) \quad (3.4)$$

The conversion function of the reaction is usually described as follows:

$$f(\alpha) = (1 - \alpha)^n \quad (3.5)$$

where n is the reaction order. The reaction order can be considered to be the first order mechanism in combustion process according to reports by other researchers [154], [170], [171].

The isoconversional principle states that at a constant extent of conversion, the reaction rate is only a function of the temperature [172]. Hence, deriving Eq. 3.4 with respect to $1/T$ gives:

$$\left[\frac{d \ln(d\alpha/dt)}{dT^{-1}} \right]_{\alpha} = -\frac{E_{\alpha}}{R} \quad (3.6)$$

Under non-isothermal conditions, where the sample is heated at a constant heating rate (β), the temperature at time t can be expressed as:

$$T = T_0 + \beta t \quad (3.7)$$

where T_0 is the initial temperature and β is the heating rate. For non-isothermal experiments, the following mathematical expression can be considered:

$$\frac{d\alpha}{dT} = \frac{d\alpha}{dt} \cdot \frac{dt}{dT} \quad (3.8)$$

where dt/dT is $1/\beta$. The differential form of the non-isothermal rate law can be obtained by substituting Eq. 3.8 into Eq. 3.4 as follows:

$$\frac{d\alpha}{dT} = \frac{A}{\beta} \exp\left(\frac{-E_a}{RT}\right) f(\alpha) \quad (3.9)$$

Applying the integral method is a simple practical approach to avoid the numerical differentiation by defining $g(\alpha)$ as the integral form of the reaction model:

$$g(\alpha) \equiv \int_0^{\alpha} \frac{d\alpha}{f(\alpha)} = \frac{A}{\beta} \int_0^T \left[\exp\left(\frac{-E_a}{RT}\right) \right] dT = \frac{AE_a}{\beta R} p(x) \quad ; \quad x = \frac{E_a}{RT} \quad (3.10)$$

where $p(x)$ is the temperature integral. The temperature integral is usually approached by estimation and therefore errors have been proved to occur in the results. By applying an iterative procedure, a more accurate activation energy value can be obtained [173]. Applying Doyle's approximation:

$$p(x) \cong \exp(-1.0518x - 5.331) \quad (3.11)$$

and rearranging Eq. 3.10, Flynn-Wall-Ozawa (FWO) equation can be developed:

$$\ln(\beta) = \ln\left(\frac{AE_a}{Rg(\alpha)}\right) - 5.331 - 1.052 \frac{E_a}{RT} \quad (3.12)$$

Kissinger-Akahira-Sunose (KAS) method can be developed by estimating $p(x)$ based on Coats-Redfern approximation:

$$p(x) \equiv \frac{\exp(-x)}{x^2} \quad (3.13)$$

Substituting in Eq. 3.10 gives the KAS method:

$$\ln\left(\frac{\beta}{T^2}\right) = \ln\left(\frac{AR}{E_a g(\alpha)}\right) - \frac{E_a}{RT} \quad (3.14)$$

FWO and KAS integral methods are developed based on non-isothermal rate equation. Friedman differential isoconversional method can be easily obtained by rearrangement of Eq. 3.4:

$$\ln\left(\frac{d\alpha}{dt}\right) = \ln(Af(\alpha)) - \frac{E_a}{RT} \quad (3.15)$$

Substituting Eq. 3.8 into Eq. 3.15 gives:

$$\ln\left(\beta \frac{d\alpha}{dT}\right) = \ln(Af(\alpha)) - \frac{E_a}{RT} \quad (3.16)$$

For each value of α , $\ln(\beta)$, $\ln(\beta/T^2)$, and $\ln(\beta d\alpha/dT)$ values are plotted versus $1000/T$ for FWO, KAS, and Friedman methods, respectively. Activation energies are calculated from the slope of the linear regression lines and pre-exponential factors are estimated from the intercepts. The non-isothermal kinetic methods are widely used owing to the apparent simplicity of processing experimental data according to the formal kinetic model described by Eq. 3.9. In the model free methods, the kinetic parameters are evaluated without any particular form of the reaction model and the results are the most reliable for the calculation of activation energies in thermally activated reactions [174]. The expressions of these methods are listed in Table 3.9.

Table 3.9. Expressions of the applied kinetics models

Method	Expression
FWO	$\ln(\beta) = \ln\left(\frac{AE_a}{Rg(\alpha)}\right) - 5.331 - 1.052 \frac{E_a}{RT}$
KAS	$\ln\left(\frac{\beta}{T^2}\right) = \ln\left(\frac{AR}{E_a g(\alpha)}\right) - \frac{E_a}{RT}$
Friedman	$\ln\left(\beta \frac{d\alpha}{dT}\right) = \ln(Af(\alpha)) - \frac{E_a}{RT}$

3.3.2. Uncertainty Assessment

The sources of uncertainty in a TGA device are the balance fluctuations, temperature measurement by the thermocouple and the sample preparation. However, due to the high accuracy of TGA for both measurements of mass and temperature, the works reporting the assessment of uncertainty for TGA suggested that these factors are relatively less of a concern [175], [176]. It has been suggested that the uncertainties in estimating kinetic parameters can be avoided for isoconversional methods [177]. Nonetheless, some imprecision in calculation of activation energies can be considered due to deviation from the regression lines plotted to obtain the slope and intercepts. The estimation of uncertainty in the activation energy values for the FWO kinetic method based on this procedure has been explained in ASTM 1641-13 standard method [178]. The slope of each line and its standard deviation can be obtained as follows:

$$m = \frac{\Delta \log(\beta)}{\Delta(1/T)} \quad (3.17)$$

$$\delta m = \left[\frac{n \sum (\delta y_i)^2}{(n-2)[n \sum x_i^2 - (\sum x_i)^2]} \right]^{1/2} \quad (3.18)$$

where:

$$x = 1/T \quad (3.19)$$

$$y = \Delta \log(\beta) \quad (3.20)$$

$n = \text{number of individual sets of } x \text{ and } y \text{ data}$

The uncertainty of activation energy is related to the imprecision of determination of the slope value:

$$\frac{\delta m}{m} = \frac{\delta E}{E} \quad (3.21)$$

This method was extended for KAS and Friedman method as well and used in this study.

3.3.3. CeSFaMB Simulation Software

The Comprehensive Simulator of Fluidized and Moving Bed (CeSFaMB) is a 1-D mathematical model and simulation code developed by Souza-Santos [179] for calculations regarding bubbling and circulating fluidized-bed as well downdraft and updraft moving-bed equipment. The software simulations developed to study steady state operations. The software can be utilized in modeling of different types of boiler, furnaces, gasifiers, dryers, and pyrolyzers, operating under different regimes. It is able to work with different types of fuels such as low and high rank coals, wood, biomass, oil shale, petroleum coke and others. As a reliable simulator, CeSFaMB is powerful tool for optimization and process design and is capable of simulating the following main types of equipment:

- Downdraft Moving Beds
- Updraft Moving Beds
- Bubbling Fluidized Beds
- Circulating Fluidized Beds
- Downdraft Entrained or Pneumatic Flow
- Updraft Entrained or Pneumatic Flow

The following operating parameters can be obtained from CeSFaMB software [180], [181]:

- Temperature profiles inside combustor,
- Particle size distribution,
- Concentrations and distributions of 20 gas components in the combustor including Ar, CO₂, CO, O₂, N₂, NO, N₂O, NO₂, SO₂, H₂O, H₂, CH₄, C₂H₆, C₂H₄, C₃H₆, C₃H₈, C₆H₆, HCN, H₂S, NH₃, and tar,
- Velocity and diameter of bubbles in the combustor,
- The minimum fluidization velocity,
- Superficial velocities in the combustor,
- Mass flow of gases and particles in the bed,
- Void fraction in the bed and freeboard.

Figure 3.15 shows a schematic of a fluidized bed boiler components simulated by CeSFaMB [182]. The simplified schematics of the mathematical model for a circulating fluidized bed is illustrated in Figure 3.16. Details regarding the mathematical model about the program can be found elsewhere [179]. For a 1-D modeling the following assumptions were made:

- 1- The flow regime is steady-state.
- 2- The gas flow throughout the chamber is plug-flow and irrotational.
- 3- Heat dissipation due to viscosity and diffusion are negligible.
- 4- Radiative heat transfer is negligible.
- 5- No gravity effects on the system.

The governing equations were presented in a cylindrical coordinate system. Based on the assumptions, the governing equations were simplified as follows:

Continuity equation:

$$\frac{d(\rho u)}{dz} = 0 \quad (3.22)$$

Continuity for the individual species (j):

$$u \frac{d\rho_j}{dz} = D_j \frac{d^2\rho_j}{dz^2} + R_{Mj} \quad (3.23)$$

Momentum conservation equation:

$$\rho u \frac{du}{dz} = \mu \frac{d^2u}{dz^2} - \frac{dP}{dz} \quad (3.24)$$

Energy balance equation:

$$u\rho c \frac{dT}{dz} = \lambda \frac{d^2T}{dz^2} + R_Q \quad (3.25)$$

Average particle diameter:

$$d_{P_{av}} = \frac{1}{\sum_{i=1}^n \frac{W_i}{d_{P_i}}} \quad (3.26)$$

Minimum fluidization velocity:

$$U_{mf} = \frac{N_{Re_{mf}} \mu_{G_{av}}}{d_{P_{av}} \rho_{G_{av}}} \quad (3.27)$$

Where:

$$N_{Re_{mf}} = (a_1^2 + a_2 N_{Ar})^{1/2} - a_1 \quad (3.28)$$

$$N_{Ar} = \frac{g d_{P_{av}}^3 \rho_{G_{av}} (\rho_{P_{av}} - \rho_{G_{av}})}{\mu_{G_{av}}^2} \quad (3.29)$$

For the case of coal combustion, the values for a_1 and a_2 were 25.25 and 0.0651, respectively [179].

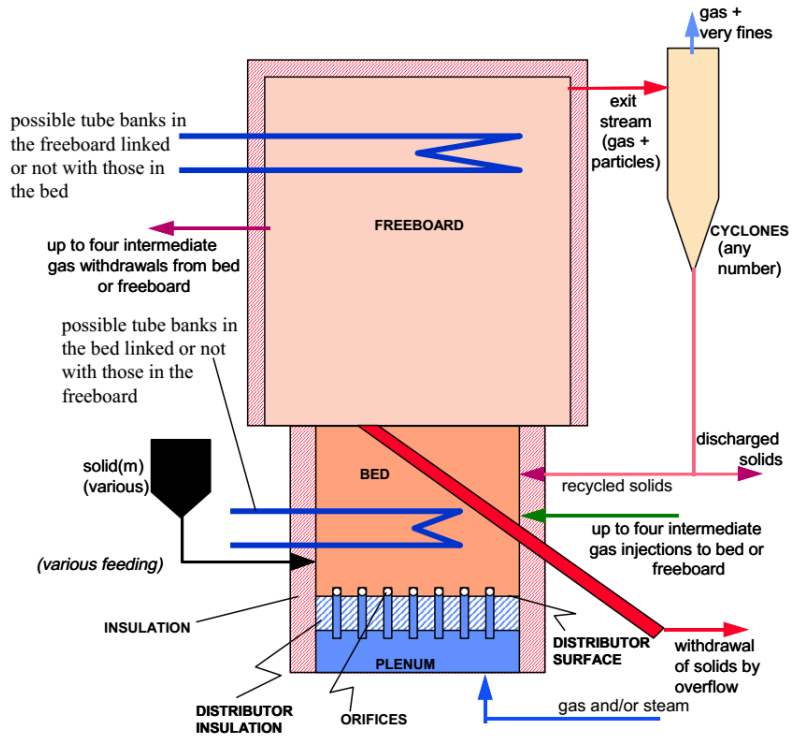


Figure 3.15. Scheme of a fluidized bed boiler components simulated by CeSFaMB software [182]

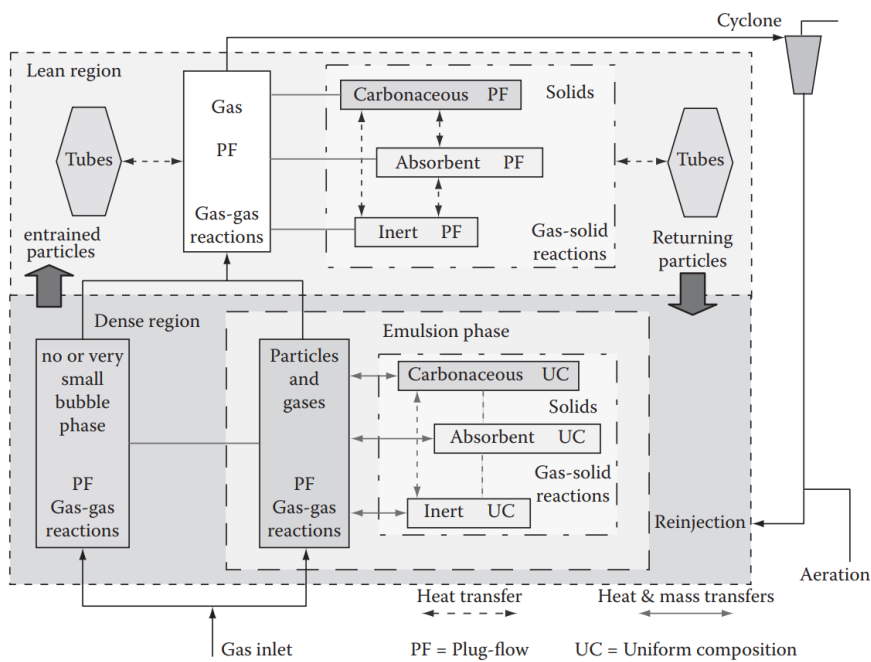


Figure 3.16. A simplified diagram of a CFBC in CeSFaMB software [179]

3.4. Experimental Matrices

3.4.1. TGA Experiments

The TGA experiments were carried out based on three groups of tests. The first set of experiments were conducted for combustion of Orhaneli and Soma lignites under oxygen-enriched and oxy-fuel combustion atmospheres in order to evaluate the most suitable lignite to be further analyzed in CFB. Different oxygen concentrations of 21, 30 and 40% were considered. The tests were carried out in three heating rates of 5, 10, and 20°C/min in order to estimate the iso-conversional kinetic parameters. Table 3.10 lists the experimental matrix including all possible experiments.

Torrefaction process of biomass have been taken place at different furnace temperature and residence times. In order to single out the most matching torrefied biomass to be mixed with lignite samples, a series of combustion experiments were conducted in TGA under air and oxy-fuel combustion conditions. The experimental matrix regarding this set of experiments are listed in Table 3.11.

Based on the obtained results from the combustion of the different torrefied biomasses, it was concluded that the sample torrefied at 300°C torrefaction temperature and 30min residence time had the closest characteristics to the utilized lignites. Therefore, the co-combustion of the mixtures was conducted for the lignite and 300°C-30min samples the different mass fractions of 25, 50, and 75 wt.%. Another set of experiments were performed with raw woodchip mixed with lignites as well in order to investigate the possibility of mixing the lignite with raw biomass. Table 3.12 lists the experimental matrix for co-combustion of the mixtures under the air and air-equivalent oxy-fuel combustion conditions.

Table 3.10. Experimental matrix of Orhaneli and Soma lignite samples combustion and oxy-combustion at different oxygen concentrations

Test No.	Sample	Atmosphere	Heating Rate (°C/min)
1	Orhaneli Lignite	Dry Air	5
2	Orhaneli Lignite	Dry Air	10
3	Orhaneli Lignite	Dry Air	20
4	Orhaneli Lignite	CO ₂ Air Equiv.	5
5	Orhaneli Lignite	CO ₂ Air Equiv.	10
6	Orhaneli Lignite	CO ₂ Air Equiv.	20
7	Soma Lignite	Dry Air	5
8	Soma Lignite	Dry Air	10
9	Soma Lignite	Dry Air	20
10	Soma Lignite	CO ₂ Air Equiv.	5
11	Soma Lignite	CO ₂ Air Equiv.	10
12	Soma Lignite	CO ₂ Air Equiv.	20
13	Orhaneli Lignite	%30 O ₂ +%70 N ₂	5
14	Orhaneli Lignite	%30 O ₂ +%70 N ₂	10
15	Orhaneli Lignite	%30 O ₂ +%70 N ₂	20
16	Orhaneli Lignite	%30 O ₂ +%70 CO ₂	5
17	Orhaneli Lignite	%30 O ₂ +%70 CO ₂	10
18	Orhaneli Lignite	%30 O ₂ +%70 CO ₂	20
19	Soma Lignite	%30 O ₂ +%70 N ₂	5
20	Soma Lignite	%30 O ₂ +%70 N ₂	10
21	Soma Lignite	%30 O ₂ +%70 N ₂	20
22	Soma Lignite	%30 O ₂ +%70 CO ₂	5
23	Soma Lignite	%30 O ₂ +%70 CO ₂	10
24	Soma Lignite	%30 O ₂ +%70 CO ₂	20
25	Orhaneli Lignite	%40 O ₂ +%60 N ₂	5
26	Orhaneli Lignite	%40 O ₂ +%60 N ₂	10
27	Orhaneli Lignite	%40 O ₂ +%60 N ₂	20
28	Orhaneli Lignite	%40 O ₂ +%60 CO ₂	5
29	Orhaneli Lignite	%40 O ₂ +%60 CO ₂	10
30	Orhaneli Lignite	%40 O ₂ +%60 CO ₂	20
31	Soma Lignite	%40 O ₂ +%60 N ₂	5
32	Soma Lignite	%40 O ₂ +%60 N ₂	10
33	Soma Lignite	%40 O ₂ +%60 N ₂	20
34	Soma Lignite	%40 O ₂ +%60 CO ₂	5
35	Soma Lignite	%40 O ₂ +%60 CO ₂	10
36	Soma Lignite	%40 O ₂ +%60 CO ₂	20

Table 3.11. Experimental matrix of raw and torrefied biomass samples combustion under air and oxy-fuel conditions

Test No.	Sample	Atmosphere	Heating Rate (°C/min)
1	Raw Biomass	Dry Air	10
2	Raw Biomass	Dry Air	20
3	Raw Biomass	Dry Air	40
4	Raw Biomass	CO ₂ Air Equiv.	10
5	Raw Biomass	CO ₂ Air Equiv.	20
6	Raw Biomass	CO ₂ Air Equiv.	40
7	250°C-15min Biomass	Dry Air	10
8	250°C-15min Biomass	Dry Air	20
9	250°C-15min Biomass	Dry Air	40
10	250°C-15min Biomass	CO ₂ Air Equiv.	10
11	250°C-15min Biomass	CO ₂ Air Equiv.	20
12	250°C-15min Biomass	CO ₂ Air Equiv.	40
13	250°C-30min Biomass	Dry Air	10
14	250°C-30min Biomass	Dry Air	20
15	250°C-30min Biomass	Dry Air	40
16	250°C-30min Biomass	CO ₂ Air Equiv.	10
17	250°C-30min Biomass	CO ₂ Air Equiv.	20
18	250°C-30min Biomass	CO ₂ Air Equiv.	40
19	300°C-15min Biomass	Dry Air	10
20	300°C-15min Biomass	Dry Air	20
21	300°C-15min Biomass	Dry Air	40
22	300°C-15min Biomass	CO ₂ Air Equiv.	10
23	300°C-15min Biomass	CO ₂ Air Equiv.	20
24	300°C-15min Biomass	CO ₂ Air Equiv.	40
25	300°C-30min Biomass	Dry Air	10
26	300°C-30min Biomass	Dry Air	20
27	300°C-30min Biomass	Dry Air	40
28	300°C-30min Biomass	CO ₂ Air Equiv.	10
29	300°C-30min Biomass	CO ₂ Air Equiv.	20
30	300°C-30min Biomass	CO ₂ Air Equiv.	40
31	350°C-15min Biomass	Dry Air	10
32	350°C-15min Biomass	Dry Air	20
33	350°C-15min Biomass	Dry Air	40
34	350°C-15min Biomass	CO ₂ Air Equiv.	10
35	350°C-15min Biomass	CO ₂ Air Equiv.	20
36	350°C-15min Biomass	CO ₂ Air Equiv.	40
37	350°C-30min Biomass	Dry Air	10
38	350°C-30min Biomass	Dry Air	20
39	350°C-30min Biomass	Dry Air	40
40	350°C-30min Biomass	CO ₂ Air Equiv.	10
41	350°C-30min Biomass	CO ₂ Air Equiv.	20
42	350°C-30min Biomass	CO ₂ Air Equiv.	40

Table 3.12. Experimental matrix of co-combustion of Orhaneli and Soma lignite samples and biomass mixtures under air and oxy-combustion conditions

Test No.	Sample	Atmosphere	Heating Rate (°C/min)
1	Orhaneli Lignite	Dry Air	10
2	Orhaneli Lignite	Dry Air	20
3	Orhaneli Lignite	Dry Air	40
4	Orhaneli Lignite	CO ₂ Air Equiv.	10
5	Orhaneli Lignite	CO ₂ Air Equiv.	20
6	Orhaneli Lignite	CO ₂ Air Equiv.	40
7	Soma Lignite	Dry Air	10
8	Soma Lignite	Dry Air	20
9	Soma Lignite	Dry Air	40
10	Soma Lignite	CO ₂ Air Equiv.	10
11	Soma Lignite	CO ₂ Air Equiv.	20
12	Soma Lignite	CO ₂ Air Equiv.	40
13	%25 300-30+%75 Orh.	Dry Air	10
14	%25 300-30+%75 Orh.	Dry Air	20
15	%25 300-30+%75 Orh.	Dry Air	40
16	%75 300-30+%25 Orh.	Dry Air	10
17	%75 300-30+%25 Orh.	Dry Air	20
18	%75 300-30+%25 Orh.	Dry Air	40
19	%50 Raw+%50 Orh.	Dry Air	10
20	%50 Raw+%50 Orh.	Dry Air	20
21	%50 Raw+%50 Orh.	Dry Air	40
22	%50 Raw+%50 Orh.	CO ₂ Air Equiv.	10
23	%50 Raw+%50 Orh.	CO ₂ Air Equiv.	20
24	%50 Raw+%50 Orh.	CO ₂ Air Equiv.	40
25	%50 300-30+%50 Orh.	Dry Air	10
26	%50 300-30+%50 Orh.	Dry Air	20
27	%50 300-30+%50 Orh.	Dry Air	40
28	%50 300-30+%50 Orh.	CO ₂ Air Equiv.	10
29	%50 300-30+%50 Orh.	CO ₂ Air Equiv.	20
30	%50 300-30+%50 Orh.	CO ₂ Air Equiv.	40
31	%50 Raw+%50 Soma	Dry Air	10
32	%50 Raw+%50 Soma	Dry Air	20
33	%50 Raw+%50 Soma	Dry Air	40
34	%50 Raw+%50 Soma	CO ₂ Air Equiv.	10
35	%50 Raw+%50 Soma	CO ₂ Air Equiv.	20
36	%50 Raw+%50 Soma	CO ₂ Air Equiv.	40
37	%50 300-30+%50 Soma	Dry Air	10
38	%50 300-30+%50 Soma	Dry Air	20
39	%50 300-30+%50 Soma	Dry Air	40
40	%50 300-30+%50 Soma	CO ₂ Air Equiv.	10
41	%50 300-30+%50 Soma	CO ₂ Air Equiv.	20
42	%50 300-30+%50 Soma	CO ₂ Air Equiv.	40

3.4.2. CFB Experiments

Based on the obtained results from the thermogravimetric analysis, it was concluded that Orhaneli lignite has superior characteristics than Soma lignite. Therefore, Orhaneli was selected to be used in the CFB experiments. The particle size of the Orhaneli lignite was in the range of 1-3 mm and the adsorbent samples were used in two particle size intervals of 0-1 mm and 1-2 mm. In order to remove the emitted SO₂ from the combustor, limestone and dolomite were used with Ca/S ratios of 1.5 and 2. The limestone sample was Çan limestone and the dolomite sample was Eskişehir dolomite. The combustion atmosphere was enriched oxygen with oxygen concentrations of 21, 23, 25, and 27 vol.% as well as oxy-fuel combustion condition. The experiment matrix is presented in Table 3.13.

Table 3.13. Experimental matrix of CFBC studies

Test No.	Sample	Atmosphere	Adsorbent	Adsorbent Particle Size (mm)	Ca/S ratio
1	Orhaneli Lignite	Air	Çan limestone	0-1	1.5
2	Orhaneli Lignite	23% O ₂	Çan limestone	0-1	1.5
3	Orhaneli Lignite	25% O ₂	Çan limestone	0-1	1.5
4	Orhaneli Lignite	27% O ₂	Çan limestone	0-1	1.5
5	Orhaneli Lignite	Air	Çan limestone	0-1	2
6	Orhaneli Lignite	23% O ₂	Çan limestone	0-1	2
7	Orhaneli Lignite	25% O ₂	Çan limestone	0-1	2
8	Orhaneli Lignite	27% O ₂	Çan limestone	0-1	2
9	Orhaneli Lignite	Air	Çan limestone	1-2	1.5
10	Orhaneli Lignite	23% O ₂	Çan limestone	1-2	1.5
11	Orhaneli Lignite	25% O ₂	Çan limestone	1-2	1.5
12	Orhaneli Lignite	27% O ₂	Çan limestone	1-2	1.5
13	Orhaneli Lignite	Air	Çan limestone	1-2	2
14	Orhaneli Lignite	23% O ₂	Çan limestone	1-2	2
15	Orhaneli Lignite	25% O ₂	Çan limestone	1-2	2
16	Orhaneli Lignite	27% O ₂	Çan limestone	1-2	2
17	Orhaneli Lignite	Air	Eskişehir dolomite	0-1	1.5
18	Orhaneli Lignite	23% O ₂	Eskişehir dolomite	0-1	1.5
19	Orhaneli Lignite	25% O ₂	Eskişehir dolomite	0-1	1.5
20	Orhaneli Lignite	27% O ₂	Eskişehir dolomite	0-1	1.5
21	Orhaneli Lignite	Air	Eskişehir dolomite	0-1	2
22	Orhaneli Lignite	23% O ₂	Eskişehir dolomite	0-1	2
23	Orhaneli Lignite	25% O ₂	Eskişehir dolomite	0-1	2
24	Orhaneli Lignite	27% O ₂	Eskişehir dolomite	0-1	2
25	Orhaneli Lignite	Air	Eskişehir dolomite	1-2	1.5
26	Orhaneli Lignite	23% O ₂	Eskişehir dolomite	1-2	1.5
27	Orhaneli Lignite	25% O ₂	Eskişehir dolomite	1-2	1.5
28	Orhaneli Lignite	27% O ₂	Eskişehir dolomite	1-2	1.5
29	Orhaneli Lignite	Air	Eskişehir dolomite	1-2	2
30	Orhaneli Lignite	23% O ₂	Eskişehir dolomite	1-2	2
31	Orhaneli Lignite	25% O ₂	Eskişehir dolomite	1-2	2
32	Orhaneli Lignite	27% O ₂	Eskişehir dolomite	1-2	2
33	Orhaneli Lignite	Oxy-fuel Comb.	Çan limestone	0-1	2
34	Orhaneli Lignite	Oxy-fuel Comb.	Eskişehir dolomite	0-1	2

CHAPTER 4

RESULTS AND DISCUSSIONS

4.1. Thermogravimetric Analysis

The TGA analysis in this thesis were carried out under three categories: first, the combustion experiments of the selected lignites were conducted under oxygen-enriched and oxy-fuel conditions. Then, the combustion tests regarding the raw and torrefied biomass were performed. Based on the obtained results, the biomass sample having the closest characteristics to the used lignites was obtained. Finally, the co-combustion of the lignites with raw and torrefied biomass was conducted under air and oxy-fuel combustion conditions.

4.1.1. Combustion of Lignites under Oxygen-Enriched and Oxy-fuel Conditions

Literature review revealed that there is not a comprehensive study regarding kinetics of combustion and oxy-fuel combustion of lignite at elevated oxygen concentrations. In particular, a study focused on kinetics of high and low ash lignites at oxy-fuel combustion conditions have not been found in open literature. Therefore, in this section, the combustion and oxy-fuel combustion characteristics of two Turkish lignites (Orhaneli and Soma) were investigated by Thermogravimetric Analysis method. Experiments were carried out under oxygen-enriched air and oxy-fuel combustion conditions with 21, 30, 40% oxygen concentrations. Three heating rates of 5, 10, and 20°C/min were considered and the isoconversional kinetic methods of FWO, KAS, and Friedman were employed to estimate activation energies. Additionally, the estimation of uncertainty in activation energy of the lignites was conducted for the aforementioned kinetics methods.

4.1.1.1. TGA Analysis

The TGA and DTG profiles for Orhaneli and Soma lignites combustion in air and air equivalent oxy-fuel combustion (21%O₂ + 79%CO₂) are given in Figure 4.1 and Figure 4.2, and the obtained characteristic temperatures are presented at Table 4.1 and Table 4.2, respectively. The first weight loss peak on DTG profile can be attributed to moisture release up to 200°C in air and oxy-fuel cases for both lignites. The combustion of volatiles and fixed carbon content of coals started at around 300°C for Orhaneli lignite and 350°C for Soma while indicating a slight increase with the increase of heating rate. The total weight loss during this stage was about 80% for Orhaneli and 50% for Soma irrespective of diluting gases or heating rates and can be attributed to the amount of the volatile matter and fixed carbon contents of the coals (Table 3.1). Orhaneli lignite, which has relatively superior quality owing to its higher volatile matter, higher fixed carbon, and lower ash contents, displayed a steeper weight loss profile indicating a more rapid combustion process.

The rate of weight loss became larger when the heating rate was increased because the combustion process proceeds faster at high heating rates [183]. Increasing the heating rate resulted in a shift in combustion profiles to higher temperature zones and higher weight losses. Due to differences in lignite samples properties, the effect of heating rate on combustion profiles were different. Table 4.1 and Table 4.2 also show that increasing the heating rate results in increasing the burnout temperatures for both coals at both combustion environments.

As can be seen in Figure 4.1 and Figure 4.2, the combustion behavior of the samples in both atmospheres were approximately identical at combustion stage indicating that both N₂ and CO₂ can be considered as inert gases at volatiles combustion [130], [154]. After the combustion process took place, the combustion behavior in air equivalent oxy-fuel combustion atmosphere deviated from the air combustion. The third peak occurred in air atmosphere combustion can be attributed to decomposition of calcium carbonate due to its presence in the ash: $CaCO_3(s) \rightarrow CaO(s) + CO_2(g)$ which occurs

in the temperature interval of 600-850°C [184]. This peak was not observed in oxy-fuel combustion condition as calcium carbonate decomposition was prevented by CO₂ [185]. This peak was small for Orhaneli lignite because of low ash content. The quantity of CaCO₃ in the sample can be easily calculated from the data in Table 3.2, which in the case of Orhaneli sample was about 4% of the total sample weight. Decomposition of the CaCO₃ caused the release of CO₂ by about 2% of the total weight. The calculation of CaCO₃ quantity for Soma lignite showed 13.3% CaCO₃ in the sample resulting a weight loss by about 7% due to the release of CO₂. For the case of air equivalent oxy-fuel condition, as can be seen from the DTG curves, another decomposition reaction took place at about 900°C. This reaction is believed to be the result of CaCO₃ decomposition reaction. This decomposition process cannot be accomplished in CO₂ atmosphere until the temperature is higher than 900°C [186].

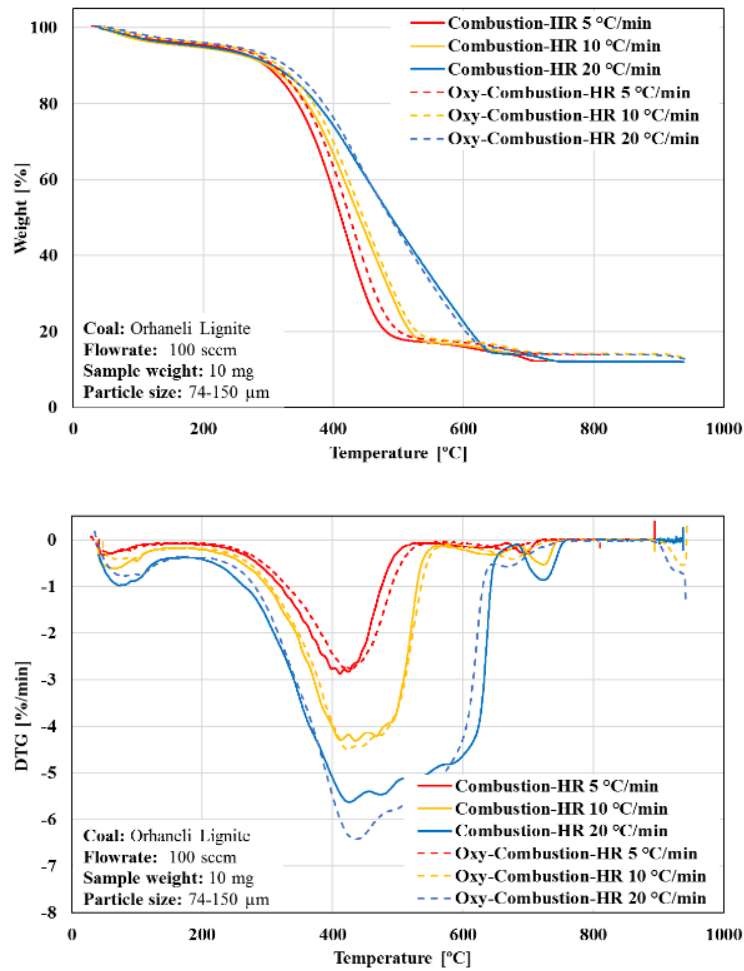


Figure 4.1. TGA and DTG curves of Orhaneli lignite combustion under air and equivalent air oxy-fuel combustion atmospheres

Table 4.1. Reaction intervals of Orhaneli lignite under oxygen enriched air and oxy-fuel combustion conditions

	<i>HR= 5°C/min</i>				<i>HR= 10°C/min</i>				<i>HR= 20°C/min</i>			
	T_i [°C]	T_{ig} [°C]	T_{max} [°C]	T_b [°C]	T_i [°C]	T_{ig} [°C]	T_{max} [°C]	T_b [°C]	T_i [°C]	T_{ig} [°C]	T_{max} [°C]	T_b [°C]
21%O₂-79%N₂	288	339	411	489	288	343	414	523	295	345	426	615
21%O₂-79%CO₂	300	342	420	511	307	345	423	536	318	349	431	608
30%O₂-70%N₂	283	332	411	478	290	335	413	498	301	337	434	548
30%O₂-70% CO₂	291	339	416	498	299	342	415	515	311	345	415	556
40%O₂-60%N₂	277	327	388	483	291	330	398	495	297	331	388	519
40%O₂-60% CO₂	291	335	409	498	307	340	406	524	308	339	392	532

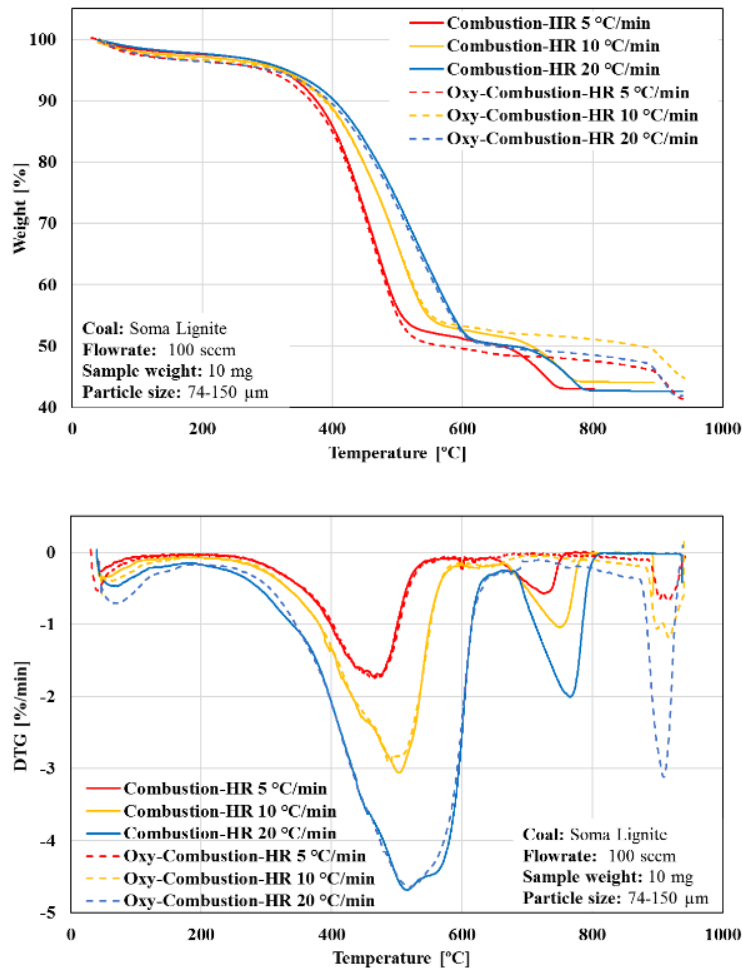


Figure 4.2. TGA and DTG curves of Soma lignite combustion under air and equivalent air oxy-fuel combustion atmospheres

Table 4.2. Reaction intervals of Soma lignite under oxygen enriched air and oxy-fuel combustion conditions

	<i>HR= 5°C/min</i>				<i>HR= 10°C/min</i>				<i>HR= 20°C/min</i>			
	T_i	T_{ig}	T_{max}	T_b	T_i	T_{ig}	T_{max}	T_b	T_i	T_{ig}	T_{max}	T_b
	[°C]	[°C]	[°C]	[°C]	[°C]	[°C]	[°C]	[°C]	[°C]	[°C]	[°C]	[°C]
21%O₂-79%N₂	358	364	465	745	370	401	504	768	381	405	520	786
21%O₂-79%CO₂	347	381	464	534	367	406	496	568	370	407	517	617
30%O₂-70%N₂	352	360	442	750	371	395	483	770	384	402	507	806
30%O₂-70% CO₂	372	376	464	537	385	399	504	575	402	404	530	601
40%O₂-60%N₂	352	357	443	768	358	378	454	775	374	400	497	793
40%O₂-60% CO₂	354	372	454	531	374	393	475	570	389	399	515	587

Combustion and oxy-fuel combustion tests of the samples were carried out at the elevated oxygen concentrations and their TGA and DTG curves are shown in Figure 4.3 and Figure 4.4. The indicated results showed that oxygen concentration impact on the combustion profiles was more significant than the effect of diluting gases. As it can be seen from the DTG curves, there was only a slight delay in combustion of the samples due to replacing N₂ by CO₂ for all oxygen concentrations. This result is in a good agreement with literature [11], [133]. Increasing the oxygen concentration in combustion environment shifted the weight loss curves to lower temperature zone and the maximum weight loss occurred at lower temperatures as it was shown in the Table 4.1 and Table 4.2. Similar results were reported elsewhere [187]. Although, elevated oxygen concentrations resulted in a faster combustion of the samples, no impact on the amount of weight loss was noticeable. The results also indicated that calcium carbonate decomposition reaction was independent of the oxygen concentration and took place when the temperature reached to a certain threshold at 700°C.

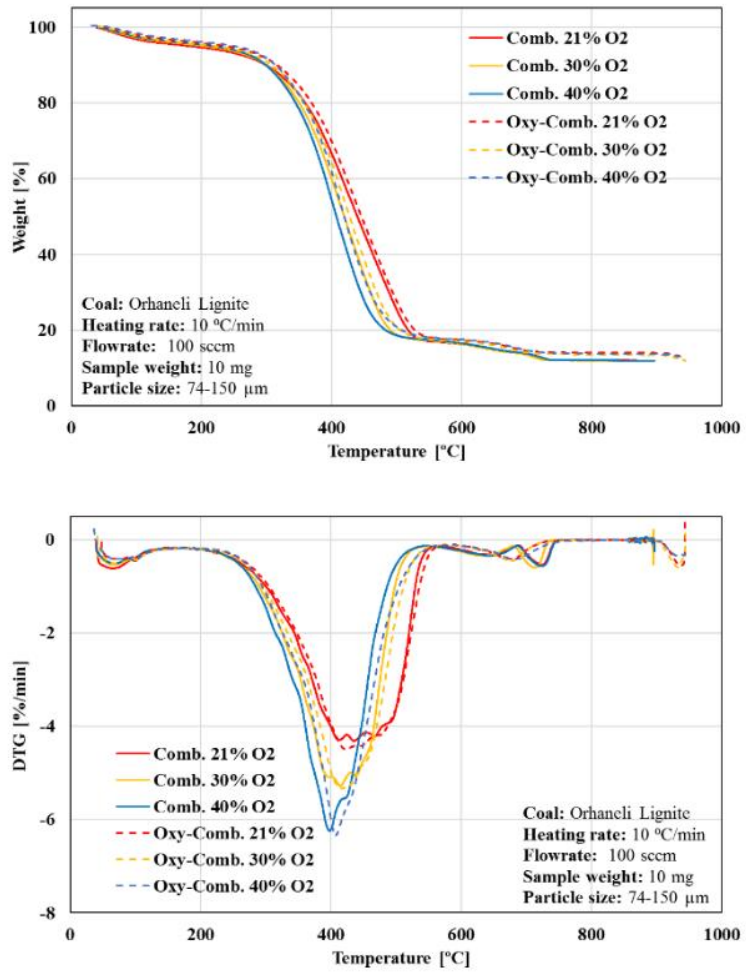


Figure 4.3. Comparison of TGA and DTG curves of Orhancli lignite under oxygen enriched air and oxy-fuel combustion conditions

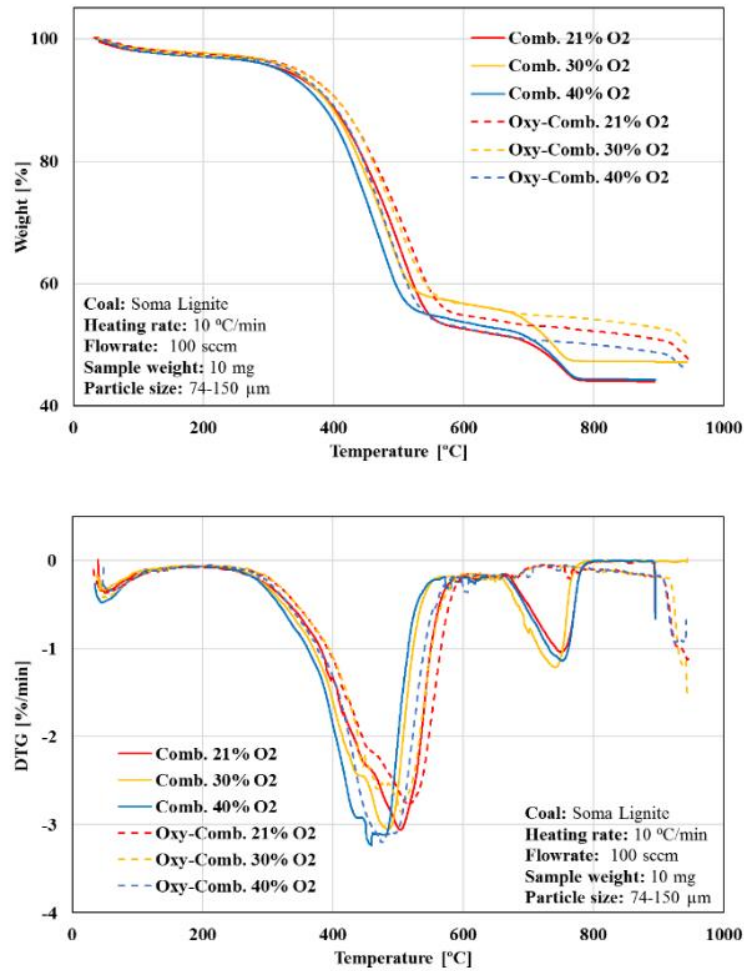


Figure 4.4. Comparison of TGA and DTG curves of Soma lignite under oxygen enriched air and oxy-fuel combustion conditions

4.1.1.2. Kinetic Analysis

In order to calculate the kinetic parameters of the lignite samples, three isoconversional methods of FWO, KAS, and Friedman were employed. The conversion degree (α) ranging from 0.10 to 0.90 with a step-size of 0.05 were applied for each case. The linearity of isoconversional curves was checked for each conversion by calculating the linear correlation coefficient. The obtained results are depicted in Figure 4.5 and Figure 4.6 for Orhaneli and Soma lignites during the combustion in air

and air equivalent oxy-fuel condition. The same figures had been plotted for the oxygen enhanced combustion conditions as well, but the figures are not presented here. Figure 6 shows similar trends in kinetic plots for Orhaneli lignite regardless of combustion environment. However, a difference at higher conversions ($\alpha > 0.70$) can be seen for Soma lignite. This was mainly due to decomposition of CaCO_3 in air combustion condition.

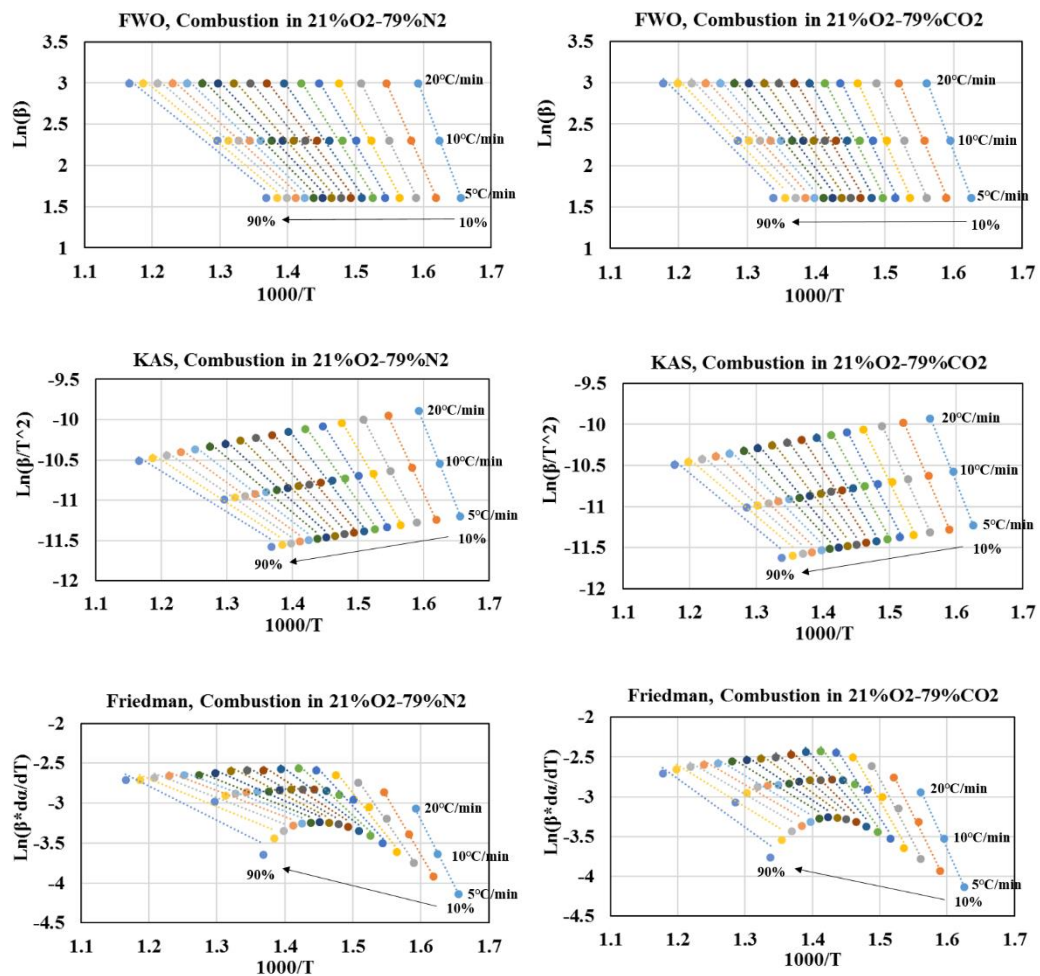


Figure 4.5. Kinetic plots of Orhaneli lignite combustion at 21% O_2 -79% N_2 and 21% O_2 -79% CO_2 atmospheres for the isoconversional methods of FWO, KAS and Friedman methods

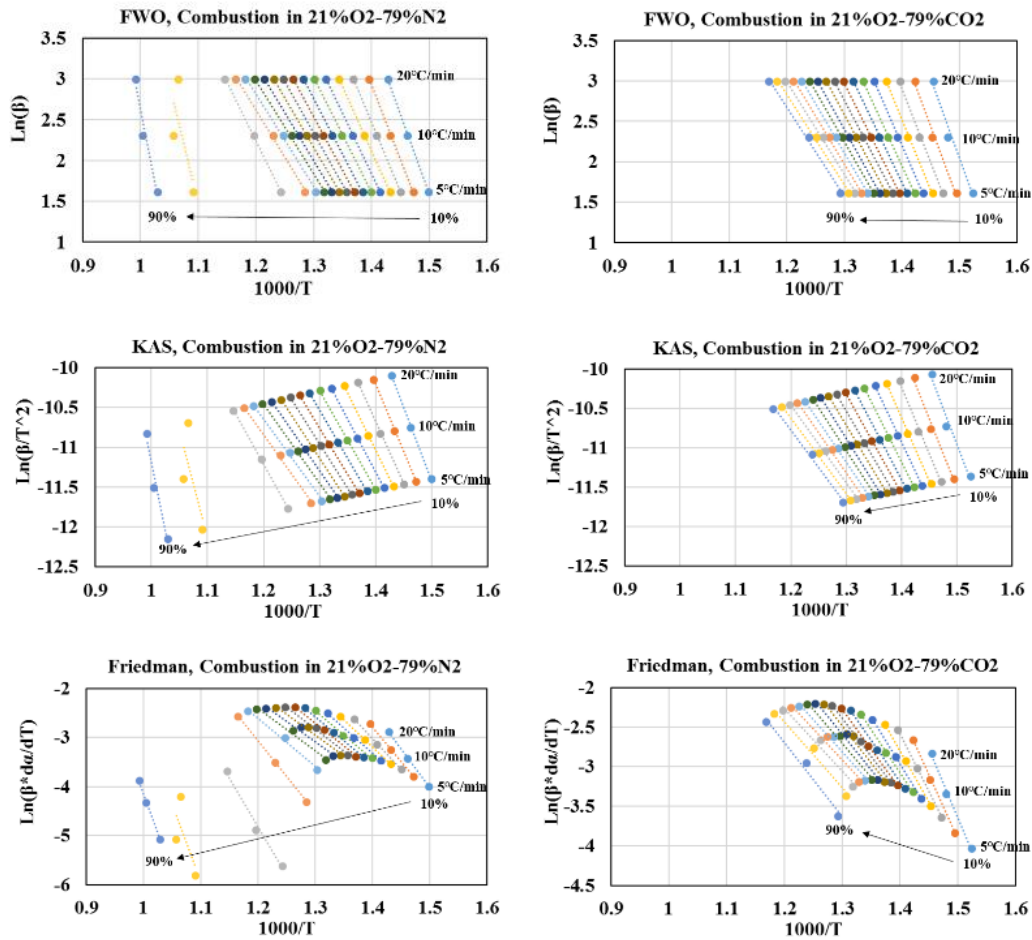


Figure 4.6. Kinetic plots of Soma lignite combustion at 21% O₂-79% N₂ and 21% O₂-79% CO₂ atmospheres for the isoconversional methods of FWO, KAS and Friedman methods

The variation of the activation energies with conversion degree for Orhaneli sample combustion and oxy-fuel combustion conditions are illustrated in Figure 4.7. As it can be seen, the three methods showed similar trends. The estimated activation energies via FWO and KAS methods were in a good accordance and produced relatively similar results. The values of the activation energies were not the same and changed with increase of the conversion factor because of the complicated multistep reaction nature of the combustion in lignite samples. For instance, the activation energy values for combustion in 21% oxygen concentration was 165 kJ/mole at $\alpha=10\%$ and decreased

to about 50 kJ/mole at $\alpha=90\%$. Diluting gas (N_2 to CO_2) showed no significant impact on the activation energy trends but the activation energy values changed. Combustion in N_2 diluting gas had lower activation energy levels than that of combustion in its CO_2 equivalent. That is because CO_2 has higher heat capacity than N_2 , which makes the combustion process more energy intense. The activation energy values were nearly the same at $\alpha=10\%$ regardless of oxygen concentration or combustion atmosphere at about 165 kJ/mole.

When combustion process took place in 21% oxygen concentration environment, the activation energy values tend to decrease with the increase of conversion degree, however, in 30% oxygen concentration, the activation energy values were nearly the same up to $\alpha=35\%$ and then started to decrease. At 40% oxygen concentration, the activation energies increased with increase of the conversion up to $\alpha=35\%$, then followed a decrease. The same trends have been obtained elsewhere [154], [188]. The average activation energy values and their associated errors for Orhaneli sample at different combustion environment were averaged and the results are presented at Table 4.3. The average activation energy values estimated by the three methods were in decreasing order of FWO > KAS > Friedman throughout different combustion conditions. It can be concluded that, combustion in oxy-fuel conditions had higher activation energy values comparing to conventional combustion atmosphere. Moreover, activation energies were higher at elevated oxygen concentrations. That is because combustion process took place at lower temperature zone resulting increase in activation energy levels.

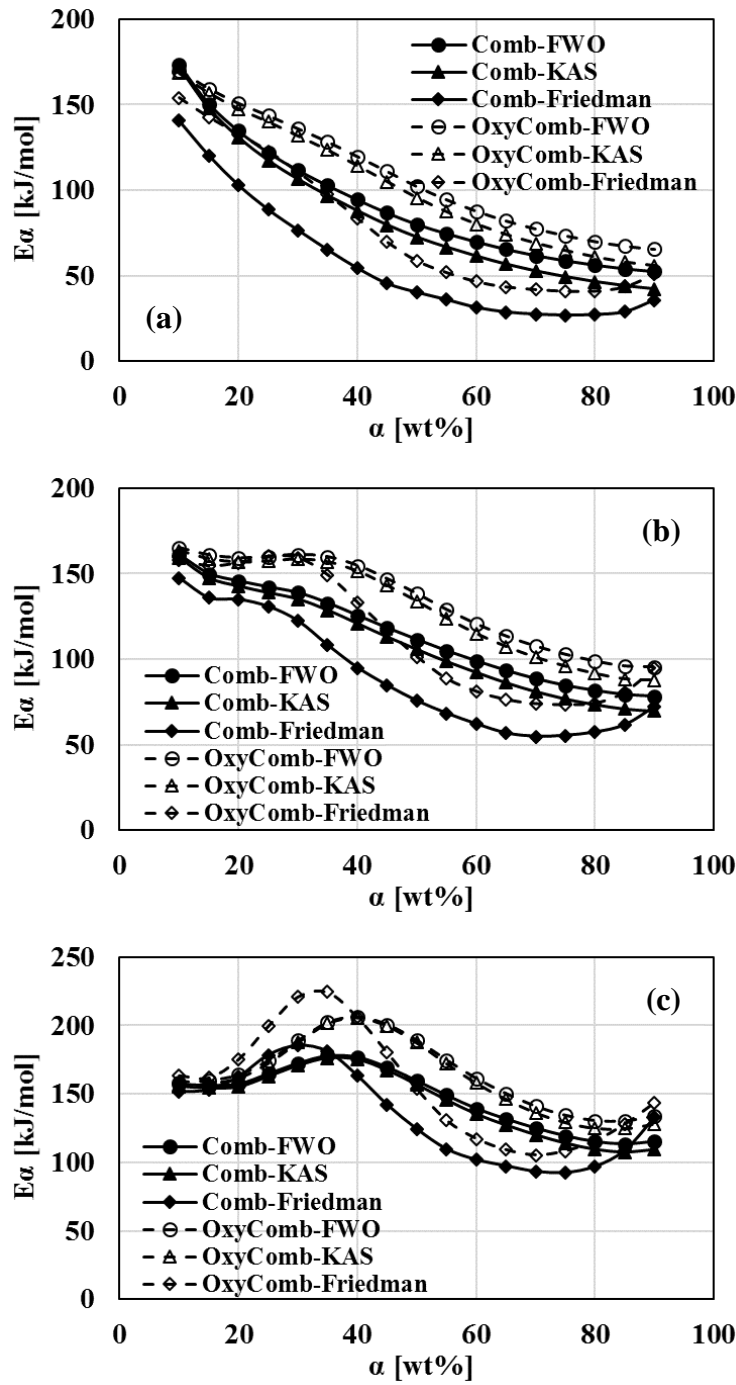


Figure 4.7. Comparison of estimated E_α vs. α for different methods for Orhaneli lignite at (a) 21% O_2 , (b) 30% O_2 and (c) 40% O_2 oxygen concentrations

Table 4.3. Average activation energy values for Orhaneli lignite at different combustion environments

	Average Activation Energy [kJ/mol]		
	FWO	KAS	Friedman
21%O₂-79%N₂	<i>91.19 ± 7.29</i>	<i>84.15 ± 8.42</i>	<i>57.48 ± 11.96</i>
21%O₂-79%CO₂	<i>108.19 ± 11.77</i>	<i>101.91 ± 12.96</i>	<i>78.43 ± 16.88</i>
30%O₂-70%N₂	<i>113.83 ± 13.93</i>	<i>108.29 ± 14.99</i>	<i>89.59 ± 18.49</i>
30%O₂-70% CO₂	<i>133.16 ± 20.99</i>	<i>128.79 ± 22.46</i>	<i>113.66 ± 26.73</i>
40%O₂-60%N₂	<i>147.15 ± 15.42</i>	<i>143.62 ± 16.27</i>	<i>133.75 ± 20.65</i>
40%O₂-60% CO₂	<i>164.75 ± 21.35</i>	<i>161.87 ± 22.66</i>	<i>155.55 ± 29.12</i>

The calculated activation energies versus conversion degree for Soma lignite at different combustion environments are depicted in Figure 4.8 and the average activation energy values and associated errors are given at Table 4.4. As it can be seen, the three kinetic methods were in a good agreement for various combustion environments. The activation energy values at $\alpha=10\%$ was nearly the same at about 150kJ/mole for all cases. As it can be seen, the estimated activation energies in oxy-fuel combustion conditions were almost consistent with the explanations given for Orhaneli lignite. That was the same for air and oxygen enriched air combustion up to $\alpha=60\%$. For $\alpha>65\%$, due to decomposition of CaCO₃ the activation energy values increased. These higher values also affected the average values resulting a contradictory estimation for activation energies regarding diluting gases. The average activation energy for Orhaneli and Soma lignites for all combustion conditions are summarized in Figure 4.9.

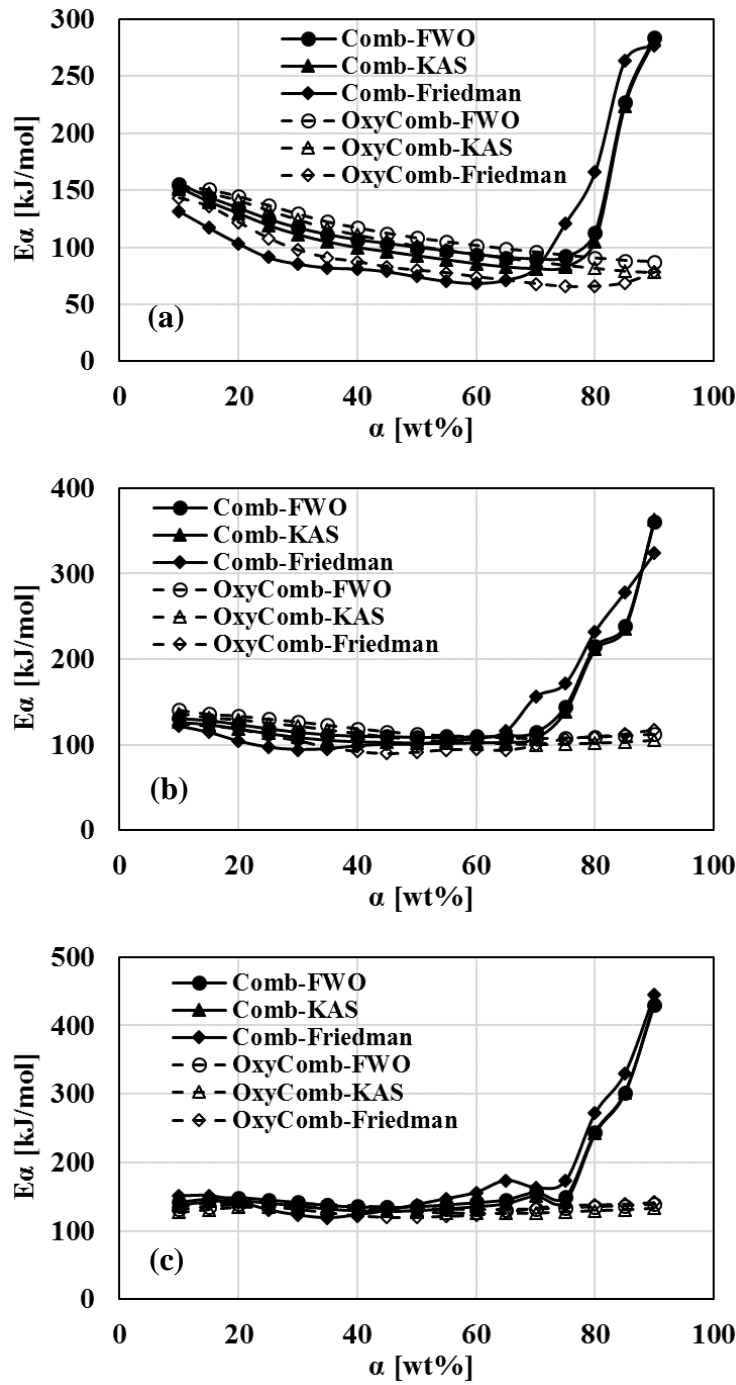


Figure 4.8. Comparison of estimated E_α vs. α for different methods for Soma lignite at (a) 21% O_2 , (b) 30% O_2 and (c) 40% O_2 oxygen concentrations

Table 4.4. Average estimated activation energy values for Soma lignite at different combustion environments

	Average Activation Energy [kJ/mol]		
	FWO	KAS	Friedman
21%O ₂ -79%N ₂	128.43 ± 11.30	122.10 ± 11.60	115.04 ± 13.46
21%O ₂ -79%CO ₂	113.85 ± 5.35	107.34 ± 5.69	89.16 ± 7.04
30%O ₂ -70%N ₂	144.98 ± 8.41	139.57 ± 8.93	142.15 ± 11.66
30%O ₂ -70% CO ₂	118.55 ± 8.06	112.24 ± 8.42	104.66 ± 8.37
40%O ₂ -60%N ₂	175.19 ± 38.05	171.37 ± 40.31	180.42 ± 41.68
40%O ₂ -60% CO ₂	135.30 ± 6.76	130.02 ± 7.02	131.61 ± 6.05

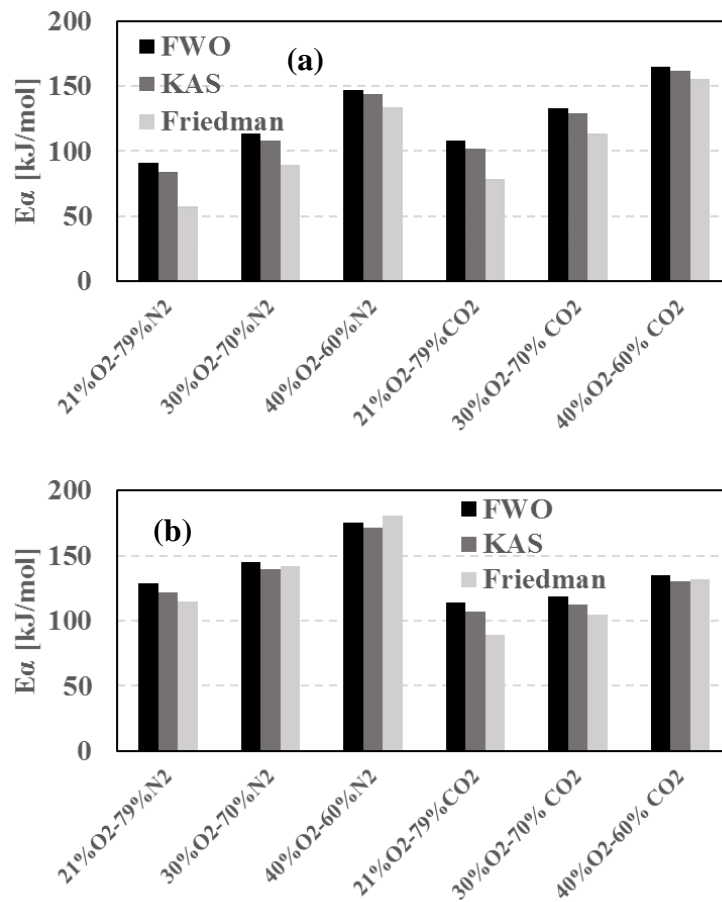


Figure 4.9. Comparison of average E_a using different methods for (a) Orhaneli and (b) Soma liginites

The standard ASTM 1641-13 method was applied to estimate the uncertainty of the FWO method. Furthermore, this method was extended to calculate the uncertainty values of KAS and Friedman methods as well. The estimated mean uncertainty values for the activation energies are presented in Figure 4.10 for Orhaneli and Soma lignites under combustion and oxy-fuel combustion conditions. It can be seen that the uncertainties related to FWO method are lower than KAS and Friedman methods. The uncertainty values for FWO and KAS methods were in the range of 8-17% and 5-10% for Orhaneli and Soma lignites, respectively. The maximum uncertainty value was 23% associated to the combustion 40% O₂-60% N₂ for Soma lignite.

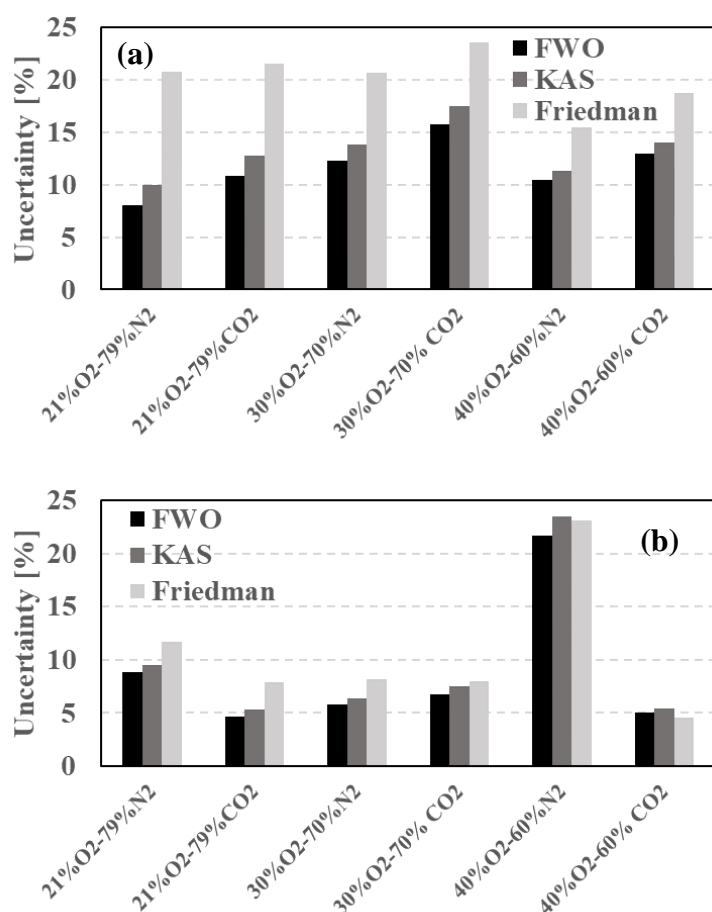


Figure 4.10. Comparison of average E_a using different methods for (a) Orhaneli and (b) Soma lignites

The pre-exponential factors were calculated using the activation energy values determined by FWO method for Orhaneli and Soma combustion at different environments. The reaction order was considered unity as described in section 3.3.1. Figure 4.11 illustrates the obtained results for pre-exponential factors at different conversion values. As it can be seen, the pre-exponential factors followed the activation energies trends.

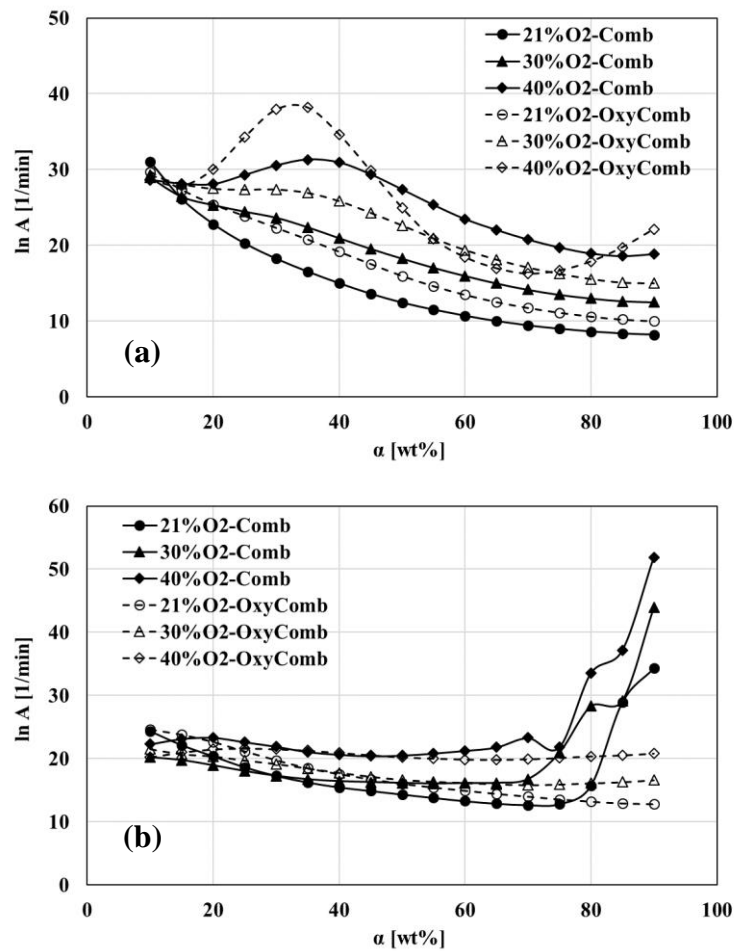


Figure 4.11. Comparison of estimated pre-exponential factor by FWO method for (a) Orhaneli and (b) Soma lignites at different combustion and oxy-fuel combustion conditions

4.1.2. Combustion of Torrefied Biomass Under Oxygen-Enriched and Oxy-fuel Conditions

In this section, the combustion and oxy-fuel combustion characteristics of torrefied pine wood chips were investigated by Thermogravimetric Analysis. Three torrefaction temperatures (250, 300, and 350°C) and two residence times (15 and 30 minutes) were considered. Experiments were carried out at three heating rates of 10, 20, and 40°C/min. The isoconversional kinetic methods of FWO, KAS, and Friedman were employed to estimate the activation energies. The assessment of uncertainty in obtaining the activation energy values was also considered.

4.1.2.1. Torrefied Biomass Physical and Chemical Properties

The temperature and residence time are considered the main factors affecting the torrefaction process of biomass. Hence, three torrefaction temperatures of 250, 300, and 350°C and two residence times of 15 and 30 minutes were considered. Torrefaction alters the chemical properties of biomass as seen in Table 3.3. Increasing the temperature and residence time resulted in decrease of volatile matter and increase of fixed carbon. Approximately 5% change in volatiles and fixed carbon contents was seen due to increase in residence time, while this was more than 15% for temperature increase. The decrease of volatiles was due to devolatilization of hemicellulose where its thermal degradation takes place at temperature interval of 180-340°C [189]. When the volatile matter in a fuel is high, the fuel is more reactive and has low calorific value. On the contrary, a higher fixed carbon gives a less reactive fuel with higher calorific value [190]. The fixed carbon content increased from 15.70% for the wood chip to 62.63% at 350°C-30min torrefaction condition. The HHV of the wood chip was 20.0 MJ/kg and torrefaction corresponded an increase of 4 to 46% compared to the raw biomass. It should also be noted that because of the low ash content of the wood chip, the ash content of the torrefied biomass did not change significantly and for all torrefaction conditions was approximately 1 to 2%.

Variation of the chemical components of biomass during torrefaction are depicted in Figure 4.12. The carbon content increased and hydrogen and oxygen contents decreased. The most significant increase in carbon content was up to 49% for 350°C-15min biomass compared to the raw sample. The hydrogen content decreased from 6.69% for wood chip to 4.25% for the most extreme torrefaction condition (350°C-30min). The nitrogen and sulfur contents were low and showed no major difference during torrefaction. The oxygen content declined from 44.75% to 24.92%. Torrefaction temperature affected the chemical components of biomass more significantly than residence time as can be seen in Figure 4.12. The same results can be found elsewhere [135].

Figure 4.13 illustrates the van-Krevelen's diagram of the raw and torrefied biomass samples. Due to torrefaction, carbon content increased and oxygen and hydrogen contents decreased resulting in decreased O/C and H/C atomic ratios. The red oval shape embodies biomass area and the blue one stands for lignite. At 250°C torrefaction temperature, the samples were in biomass region. However, the biomass atomic ratios inclined to lignite region at higher temperatures. 300°C-30min and 350°C-15min torrefied biomass were completely embedded in lignite region. The ultimate analysis results show that at 300°C torrefaction temperature, by increasing the residence time the oxygen content was increased while in the other cases the reduction of oxygen was noticed. This increase in oxygen content which might be due to measurement error has adversely affected the O/C trend. As it can be seen, the residence time did not affect the O/C ratios at higher temperatures but H/C ratios decreased. That is because by increasing the residence time, the hydroxyl groups degradation advances and leads to loss of hydrogen content of the biomass.

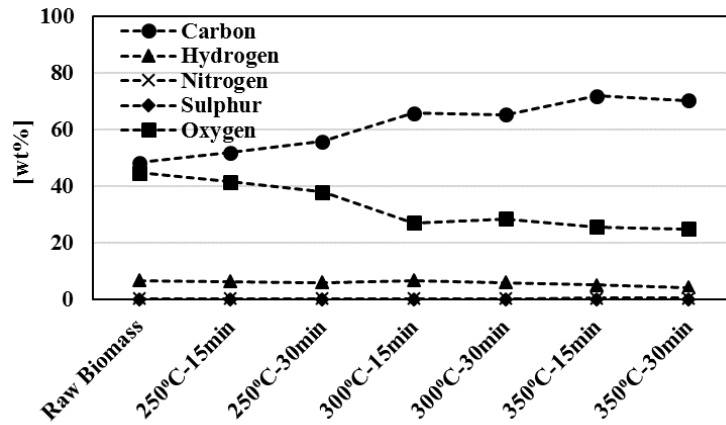


Figure 4.12. Variation of chemical components of biomass during torrefaction

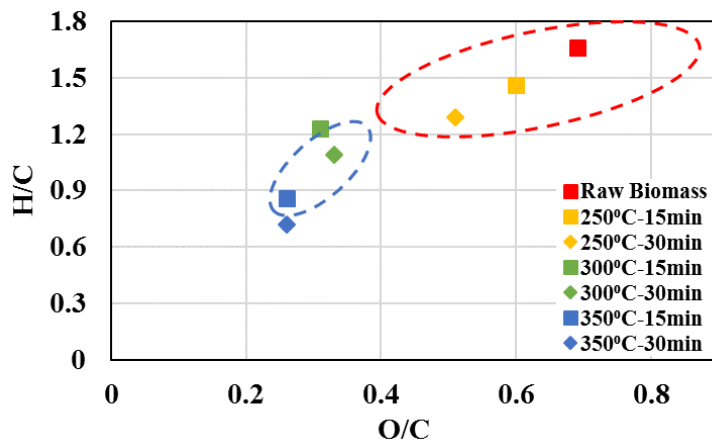


Figure 4.13. Van Krevelen's diagram for raw and torrefied biomass

4.1.2.2. TGA Analysis

The TGA and DTG profiles for combustion of raw and torrefied biomass for 20°C/min heating rate in air are shown in Figure 4.14. Generally, the first weight loss appearing in TGA data up to 200°C is attributed to moisture release. Nevertheless, the mass loss associated with dehydration was not observed for torrefied biomass samples confirming the hydrophobic nature of wood biomass. The main weight loss was due

to thermal and oxidative degradation of biomass. Depending on torrefaction temperature, this stage took place in one or two phases. Combustion in two phases were seen for raw biomass and biomasses torrefied at 250°C and 300°C temperatures. The first phase corresponded to combustion of hemicellulose and cellulose components taking place within the temperature range of 250-410°C. Following that, the second phase assigned to the decomposition of lignin which occurs in the temperature interval of 410-620°C. Due to complete decomposition of hemicellulose and cellulose during torrefaction at 350°C, only one phase of weight loss was appeared. The maximum weight loss appeared at approximately 370°C under air combustion for wood and biomasses torrefied at 250°C and 300°C temperatures. The weight loss at first phase was approximately 60% for raw biomass and decreased to about 20% for 300°C-30min sample. For biomass torrefied at 350°C, the peak representing the decomposition of hemicellulose did not appear.

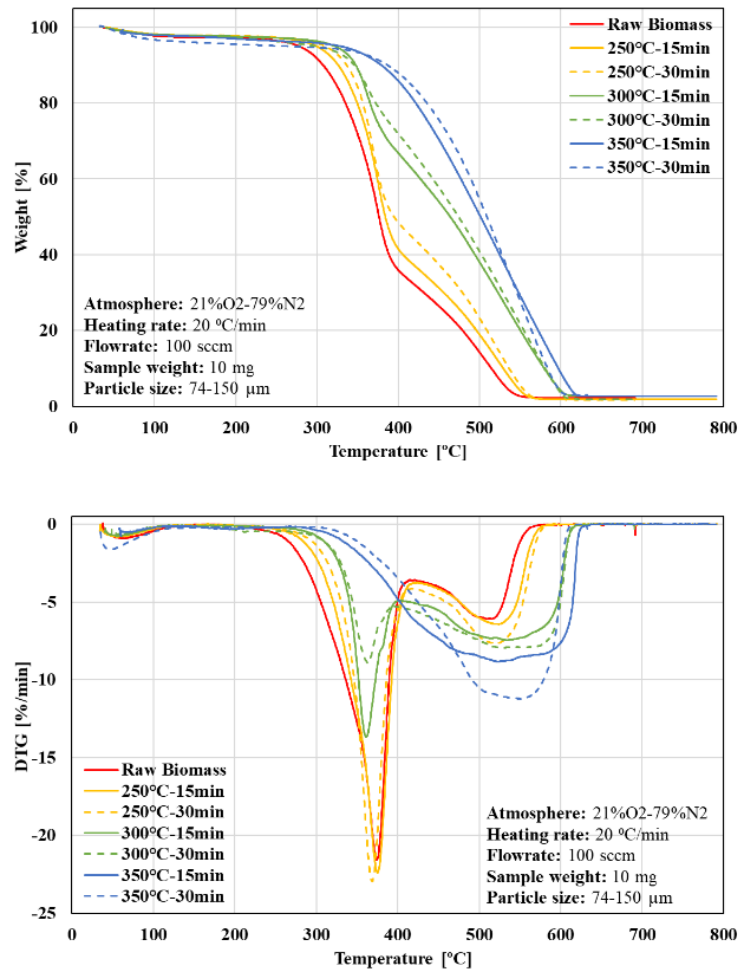


Figure 4.14. TGA and DTG curves of raw and torrefied biomass combustion under air combustion atmosphere at 20°C/min heating rate

Generally, the second derivative of weight loss curves (DDTG) for raw and torrefied biomass samples can be divided into three stages describing the behavior of lignocellulosic biomass. The first stage corresponds to degradation of hemicellulose, the second stage also sharing the DTG peak relates to cellulose degradation, and the third stage corresponds to decomposition of lignin [191]. The characteristic temperatures describing the biomass decomposition can be derived from the DTG and DDTG curves. The initial temperature (T_i) is assumed to correspond to weight

percentage equal to 95% [161], the ignition temperature (T_{ig}) is the temperature at which biomass starts burning which is the point that the weight loss curve in combustion diverges and a sudden decrease is seen in the DTG curve [192]. T_{S1} is assumed the temperature at which the cellulose combustion starts, the peak temperature (T_{max}) is where the maximum weight loss occurs in the DTG curve, T_{S2} is assumed the end of cellulose combustion, and T_b represents the temperature where combustion is completed. Figure 4.15 illustrates the characteristic temperatures for raw biomass combustion. The degradation of hemicellulose started at $T_i = 245^\circ\text{C}$ followed by a sharp decay at $T_{S1} = 333^\circ\text{C}$ where the decomposition of cellulose took place. At $T_{S2} = 415^\circ\text{C}$ the long tailing which is mainly associated with lignin degradation occurred. The same results can be found elsewhere [193], [194].

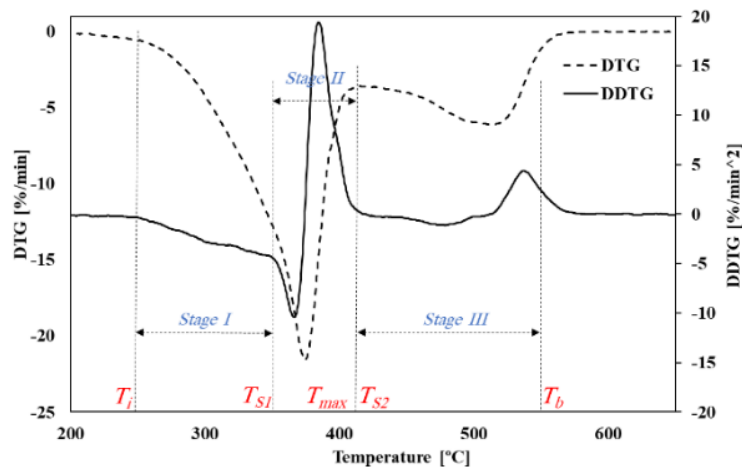


Figure 4.15. Characteristic temperatures for raw biomass at 20°C/min

The DDTG curves for torrefied biomass under air combustion are shown in Figure 4.16 at 20°C/min heating rate. Due to slight degradation of hemicellulose at 250°C-15min torrefaction condition, the DDTG curve was nearly identical to the raw biomass and the transition from hemicellulose to cellulose (T_{S1}) could be identified. However, by increasing the torrefaction temperature and residence time that resulted in

decomposition of hemicellulose during torrefaction process, a noticeable transition did not appear and T_{SI} could not be pinpointed. For the biomass samples torrefied at 300°C, the cellulose combustion completed earlier (lower T_{S2}). That is because the first local minimum of cellulose decomposition occurred at lower temperatures compared to 250°C torrefaction temperature. Giving that there was no hemicellulose and cellulose components for the cases of 350°C torrefaction temperature, there were no significant variation in their DDTG curves.

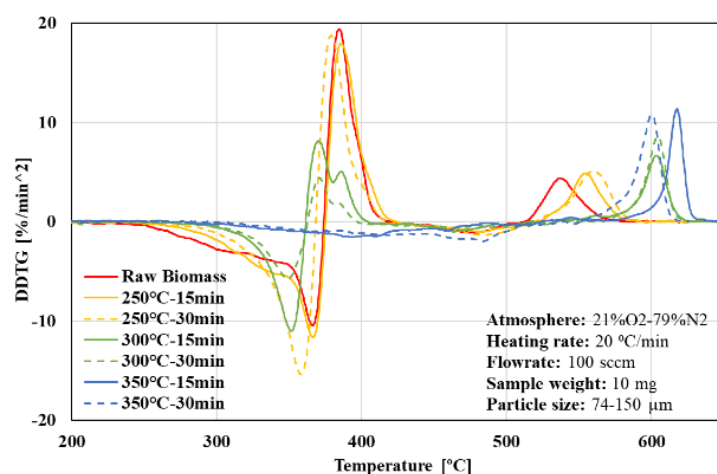


Figure 4.16. DDTG curves of raw and torrefied biomass combustion under air combustion atmosphere at 20°C/min heating rate

The calculated characteristic temperatures for raw and torrefied biomass combustion are provided in Table 3. As can be seen, torrefaction resulted in a delay in the ignition temperature by about 5°C for biomasses torrefied at 250 and 300°C. However, for 350°C torrefaction temperature, T_{ig} delayed to 402 and 428°C for 15 and 30 minutes residence times respectively. That is because at this torrefaction temperature the biomass component is mainly lignin which its decomposition takes place at temperatures above 410°C. Moreover, increasing the heating rate resulted in decreasing the initial temperature and increasing the ignition and peak temperatures.

Table 4.5. Characteristic temperatures of raw and torrefied biomass under air combustion condition

	T_i [°C]	T_{ig} [°C]	T_{s1} [°C]	T_{max} [°C]	T_{s2} [°C]	T_b [°C]
<i>HR= 10°C/min</i>						
Raw Biomass	253	319	-	362	-	531
250°C-15min	265	331	-	364	-	538
250°C-30min	286	335	-	361	-	542
300°C-15min	302	335	-	356	-	562
300°C-30min	301	325	-	351	-	560
350°C-15min	321	399	-	506	-	557
350°C-30min	335	421	-	514	-	563
<i>HR= 20°C/min</i>						
Raw Biomass	245	333	350	375	415	557
250°C-15min	265	340	350	375	420	570
250°C-30min	274	342	-	369	415	574
300°C-15min	290	340	-	361	402	602
300°C-30min	277	338	-	364	395	611
350°C-15min	310	402	-	523	-	623
350°C-30min	329	428	-	551	-	608
<i>HR= 40°C/min</i>						
Raw Biomass	230	338	-	386	-	621
250°C-15min	245	348	-	389	-	632
250°C-30min	255	351	-	382	-	672
300°C-15min	261	350	-	372	-	672
300°C-30min	196	342	-	367	-	699
350°C-15min	283	405	-	545	-	813
350°C-30min	281	432	-	600	-	743

Figure 4.17 compares the TGA, DTG and DDTG profiles of raw and torrefied biomass under air and oxy-fuel combustion atmospheres. The characteristic temperatures under oxy-fuel combustion atmosphere are displayed in Table 4. It can be observed that the initial temperature was not affected by combustion atmosphere and was approximately the same for all of the samples. According to this, it can be said that the degradation of hemicellulose was not affected by combustion environment. On the other hand, the DDTG curves in oxy-fuel conditions showed lower and delayed peaks compared to air combustion indicating that the presence of CO₂ affected the cellulose decomposition. The cellulose degradation temperature intervals increased by about 5°C for raw and torrefied biomass samples. In addition, it can be seen that the decomposition of lignin in oxy-fuel condition took place at a slower rate than that of air combustion. Moreover, the ignition temperature increased by about 5°C in oxy-

fuel condition. The peak and burnout temperatures increased as well indicating the delayed combustion in the presence of CO₂. The same results can be found elsewhere [142].

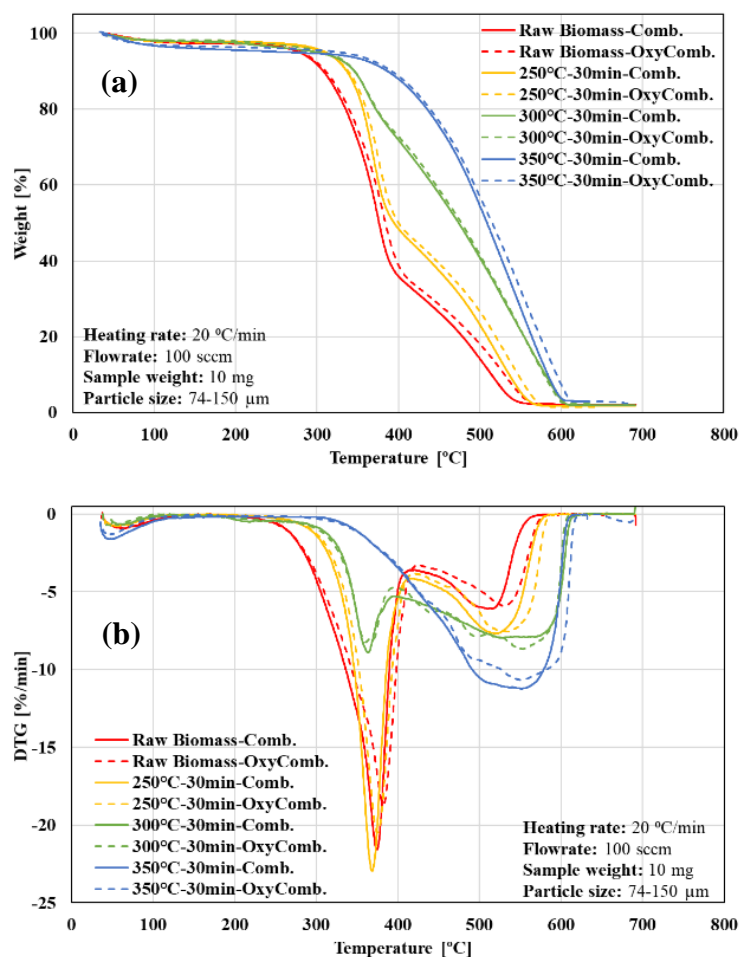


Figure 4.17. Comparison of (a) TGA, (b) DTG, and (c) DDTG curves of raw and torrefied biomass combustion under air and oxy-fuel combustion atmospheres

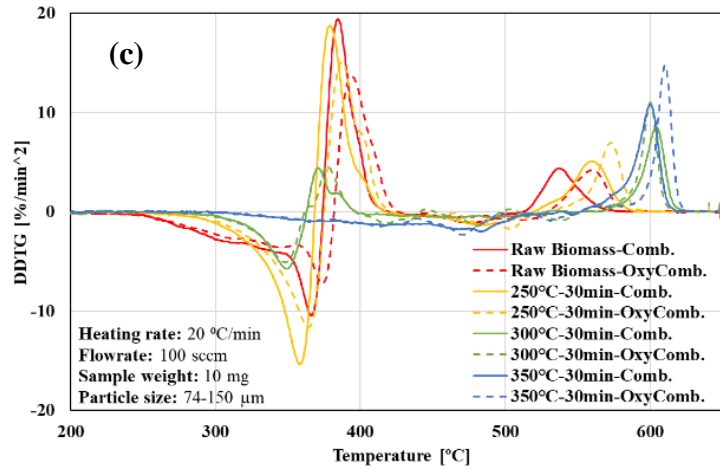


Figure 4.17. (continued)

Table 4.6. Characteristic temperatures of raw and torrefied biomass under oxy-fuel combustion condition

	T_i [°C]	T_{ig} [°C]	T_{s1} [°C]	T_{max} [°C]	T_{s2} [°C]	T_b [°C]
HR= 10°C/min						
Raw Biomass	251	324	-	371	-	545
250°C-15min	267	333	-	369	-	543
250°C-30min	285	337	-	364	-	550
300°C-15min	302	335	-	365	-	566
300°C-30min	299	329	-	353	-	562
350°C-15min	323	406	-	502	-	564
350°C-30min	336	429	-	517	-	571
HR= 20°C/min						
Raw Biomass	243	337	355	382	425	572
250°C-15min	266	346	355	383	426	574
250°C-30min	276	348	-	375	420	582
300°C-15min	294	349	-	373	404	608
300°C-30min	274	340	-	360	395	613
350°C-15min	313	410	-	534	-	629
350°C-30min	327	434	-	554	-	618
HR= 40°C/min						
Raw Biomass	231	340	-	396	-	625
250°C-15min	244	353	-	396	-	644
250°C-30min	258	355	-	385	-	671
300°C-15min	258	356	-	379	-	698
300°C-30min	202	344	-	368	-	701
350°C-15min	290	412	-	553	-	831
350°C-30min	285	438	-	603	-	773

4.1.2.3. Kinetic Calculations

In order to calculate the kinetic parameters of the raw and torrefied biomass samples, three isoconversional methods of FWO, KAS, and Friedman were employed. The conversion degree (α) ranging from 0.10 to 0.90 with a step-size of 0.05 were applied for each case. The linearity of isoconversional curves was checked for each conversion by calculating the linear correlation coefficient. The obtained results for evolution of the activation energies with conversion degree are depicted in Figure 4.18 under air combustion condition. As it can be seen, the three methods showed similar trends for all samples. The estimated activation energy distribution between FWO and KAS methods were in a good accordance and produced relatively comparable results. However, the calculated activation energies via Friedman method had lower values. The values of the activation energies changed with increase of the conversion factor due to the complicated multistep reaction nature of the combustion in biomass samples.

For the raw biomass, the activation energy value was 175kJ/mole at $\alpha=10\%$ and increased up to 200kJ/mole at $\alpha=35\%$. This stage (stage I) can be attributed to the hemicellulose combustion [195]. At stage II where the degradation of cellulose took place, the activation energy values remained approximately constant at 200kJ/mole through increasing the conversion factor up to 65%. Following that, at $\alpha=65\%$ the combustion of lignin started (stage III) and resulted in decrease of the activation energy value down to 90kJ/mole [196]. The 250°C-15min biomass sample had less amount of hemicellulose than that of the raw biomass. Therefore, the activation energy values indicating hemicellulose decomposition (stage I) were in a shorter conversion factor interval of 10-20%. The evolution of activation energy values for cellulose and lignin was comparable to the raw biomass.

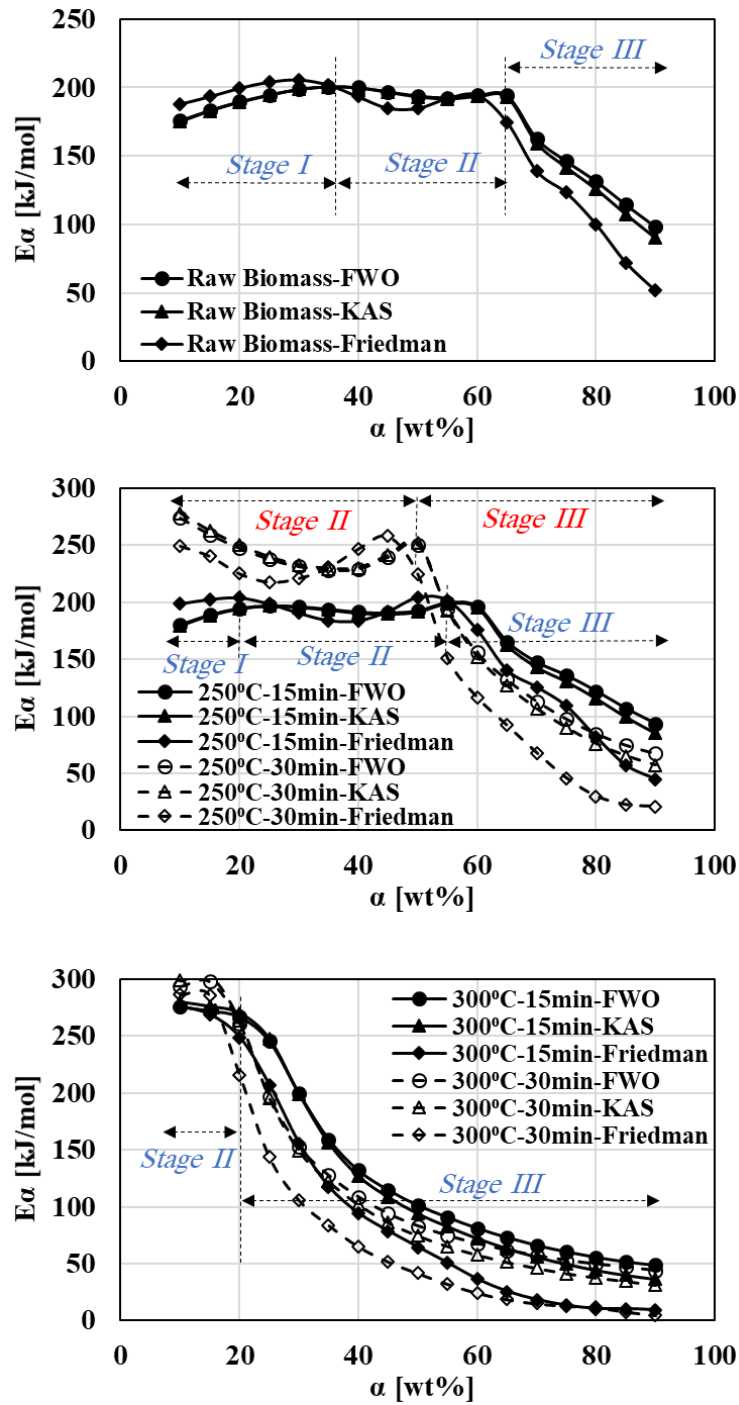


Figure 4.18. Comparison of estimated $E\alpha$ vs. α for different methods for the raw and torrefied biomass samples under air combustion condition

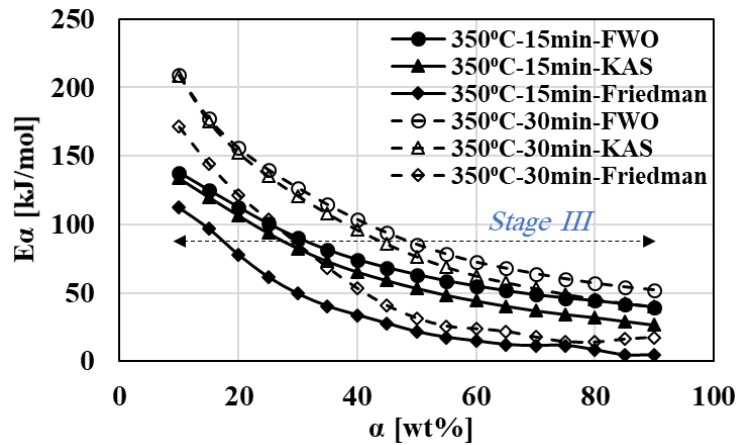


Figure 4.18. (Continued)

Due to the fact that the 250°C-30min biomass sample had only a slight amount of hemicellulose, the combustion process started by cellulose decomposition. The activation energy value of cellulose at the start of combustion was 275kJ/mole, decreased to 230kJ/mole at $\alpha=30\%$ and followed by an increase up to 250kJ/mole at $\alpha=50\%$. At this point, the combustion of lignin started causing a decrease in activation energy values down to 70kJ/mole. For 300°C torrefaction temperature, the cellulose quantity was very small, hence, the cellulose degradation stage completed at $\alpha=20\%$ and $\alpha=15\%$ for 15 and 30 minutes residence times respectively. The activation energy values for lignin combustion was decreased from 270kJ/mole to 50kJ/mole during conversion evolution. Biomass torrefaction at 350°C resulted in degradation of hemicellulose and cellulose completely. Therefore, the 350°C torrefied biomass was merely composed of lignin component. It can be seen that the activation energy evolution showed one stage of lignin decomposition in a decreasing interval of 130-40kJ/mole and 210-50kJ/mole for 15 and 30 minutes residence times respectively.

The calculated activation energies versus conversion degree for raw and torrefied biomass samples under different combustion environments are depicted in Figure 4.19. As can be seen, diluting gas (N_2 to CO_2) did not affect the activation energy trends; however, slight changes in activation energy values were noticed. At oxy-fuel

combustion condition, the activation energy values for hemicellulose and lignin combustion stages were slightly higher while cellulose combustion stage showed lower values of activation energies.

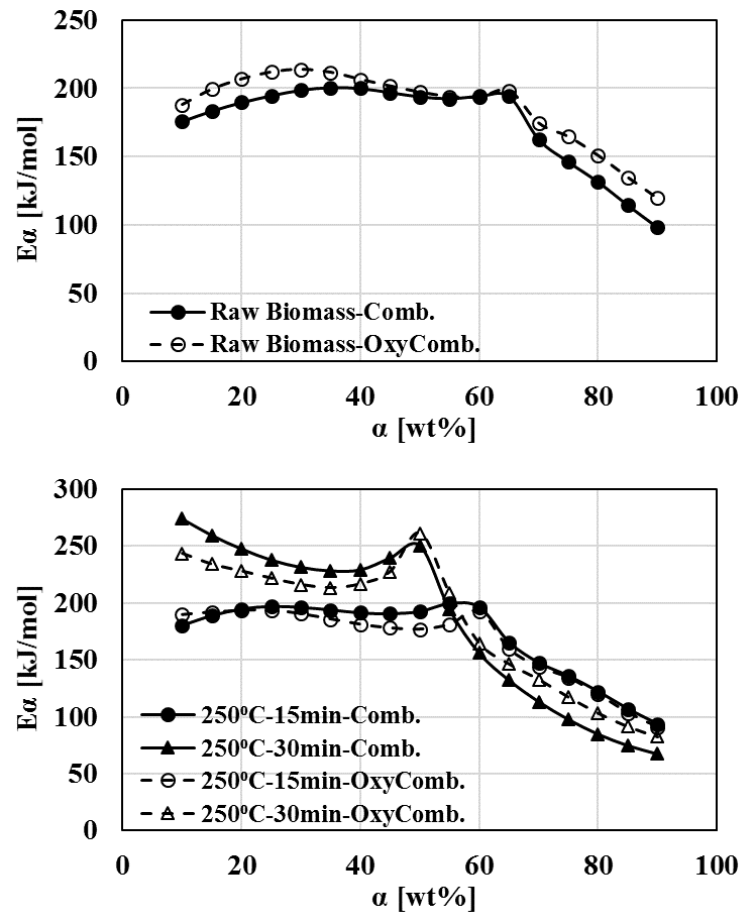


Figure 4.19. Comparison of estimated $E\alpha$ vs. α by FWO method for the raw and torrefied biomass samples under air and oxy-fuel combustion conditions

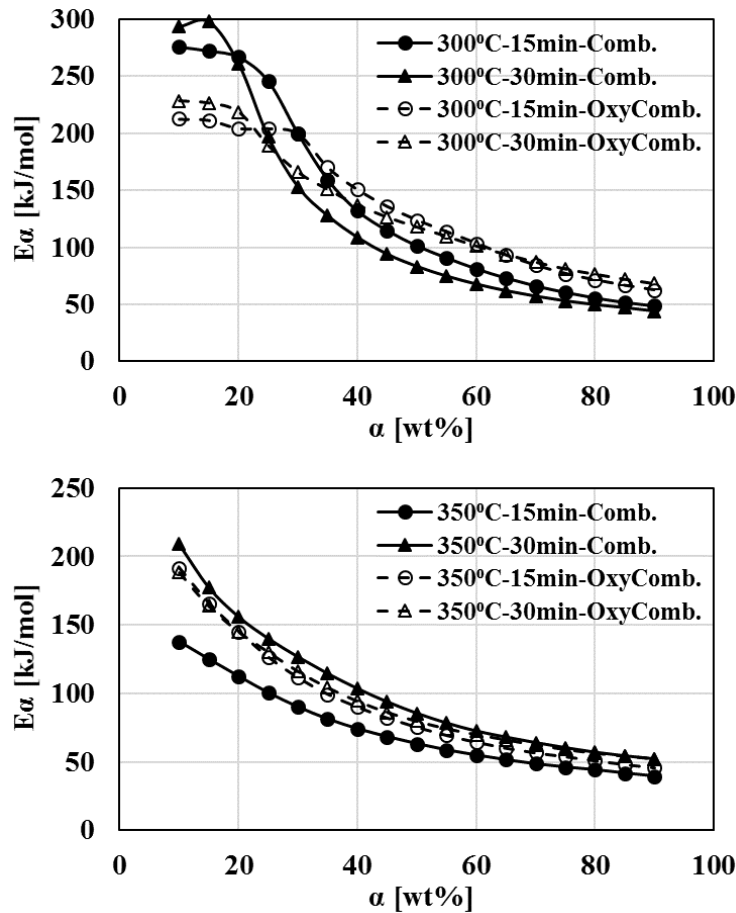


Figure 4.19. (Continued)

The averaged activation energy values for raw and torrefied biomass samples under air and oxy-fuel combustion conditions are given at Table 4.7. It can be deduced that the diluting gas impact on average activation energies were insignificant. The average activation energy values estimated by the three methods were in decreasing order of FWO > KAS > Friedman throughout different combustion conditions.

Intensifying the torrefaction conditions of biomass decreased the average values of activation energies. The lower values for torrefied biomass samples was due to their higher reactivity and higher specific surface area. Based on FWO method, the highest

average activation energy was obtained by 250°C-30min biomass at 183.40kJ/mole and the lowest value was 72.93kJ/mole for 350°C-15min biomass.

Table 4.7. Average estimated activation energy values for raw and torrefied biomass under air and oxy-fuel combustion conditions

	Air Combustion			Oxy-fuel Combustion		
	FWO	KAS	Friedman	FWO	KAS	Friedman
Raw Biomass	174.58	172.51	165.02	186.25	184.63	177.30
250°C-15min	172.12	167.55	158.47	165.16	162.20	149.26
250°C-30min	183.40	181.19	156.46	182.75	180.46	161.25
300°C-15min	135.02	129.53	99.12	134.43	128.87	103.81
300°C-30min	121.73	115.33	82.77	132.34	126.72	102.61
350°C-15min	72.93	63.54	35.72	90.54	82.12	48.96
350°C-30min	100.83	92.84	57.17	94.35	85.93	52.30

The standard ASTM 1641-13 method was applied to estimate the uncertainty of the FWO method. Furthermore, this method was extended to calculate the uncertainty values of KAS and Friedman methods as well. The estimated mean uncertainty values for the activation energies are presented in Figure 4.20 for biomass samples under air and oxy-fuel combustion conditions. It can be seen that the uncertainties related to FWO method are lower than KAS and Friedman methods. The same results has been found elsewhere [197]. Estimation of activation energy using Friedman method had higher uncertainties especially at higher torrefaction temperatures. The uncertainty values for FWO and KAS methods were in the range of 5-14% and 5-17% for air combustion and oxy-fuel combustion conditions, respectively.

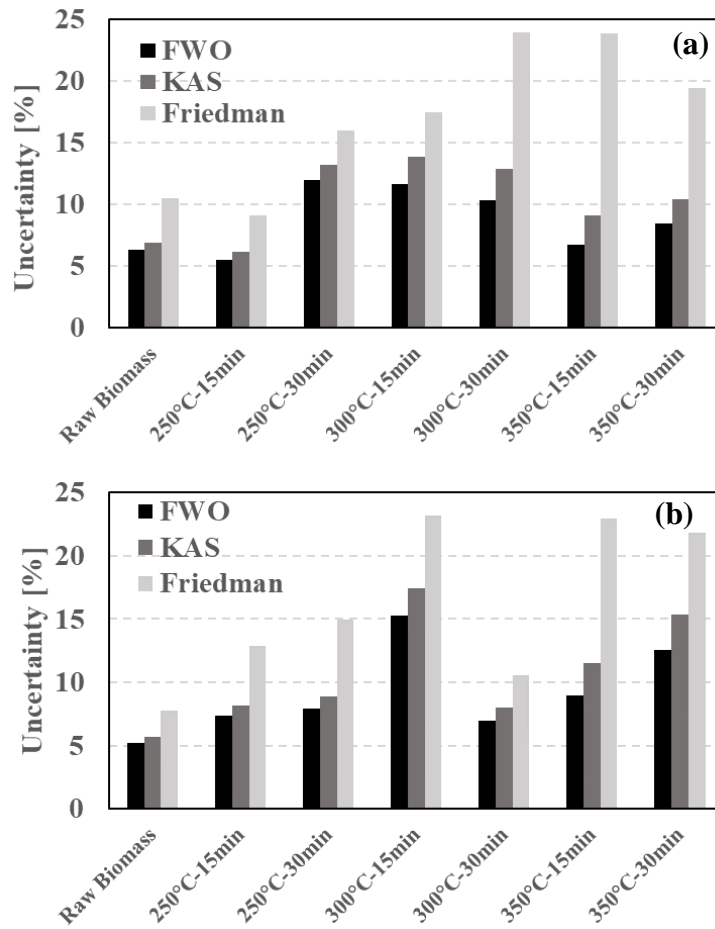


Figure 4.20. Comparison of average uncertainty values for different methods at (a) air combustion and (b) oxy-fuel combustion conditions

The pre-exponential factors were calculated using the activation energy values determined by FWO method for biomass samples at different environments. The obtained maximum and minimum pre-exponential factor data for combustion of raw and torrefied biomass samples under air and oxy-fuel combustion atmospheres are provided in Table 6. The pre-exponential factors were within the range of $5.76\text{E}+02$ to $5.71\text{E}+23$ depending on the type of biomass sample. The same results can be found elsewhere [152], [198].

Table 4.8. Pre-exponential factor ranges for raw and torrefied biomass under air and oxy-fuel combustion conditions

	Air Combustion		Oxy-fuel Combustion	
	A_{\min} [min^{-1}]	A_{\max} [min^{-1}]	A_{\min} [min^{-1}]	A_{\max} [min^{-1}]
Raw Biomass	<i>5.43E+06</i>	<i>1.64E+16</i>	<i>9.68E+07</i>	<i>1.68E+17</i>
250°C-15min	<i>2.08E+06</i>	<i>5.62E+15</i>	<i>1.14E+06</i>	<i>2.35E+15</i>
250°C-30min	<i>3.77E+04</i>	<i>2.21E+22</i>	<i>2.78E+05</i>	<i>4.13E+19</i>
300°C-15min	<i>1.98E+03</i>	<i>1.39E+22</i>	<i>1.35E+04</i>	<i>3.71E+16</i>
300°C-30min	<i>1.02E+03</i>	<i>5.71E+23</i>	<i>2.84E+04</i>	<i>1.24E+18</i>
350°C-15min	<i>5.76E+02</i>	<i>4.59E+09</i>	<i>1.31E+03</i>	<i>7.17E+13</i>
350°C-30min	<i>2.98E+03</i>	<i>1.08E+15</i>	<i>2.88E+03</i>	<i>1.95E+13</i>

4.1.3. Co-Combustion of Lignite and Biomass Under Oxygen-Enriched and Oxy-fuel Conditions

Blending fuels is a physical process which can be done mechanically or chemically (impregnation or ultrasonic treatment) in order to increase the combustion characteristics of the fuels. Usually, before feeding low-rank coals to power plant boilers, they are mixed with bituminous or anthracite coals to improve their chemical properties. Blending can result in economic benefits by mitigating problems such as corrosion, slagging and fouling. From the environmental perspective, a well-prepared fuel blend can also be beneficial in reduction of pollutions such as particulate matter, sulfur dioxide, nitrogen oxide and carbon dioxide.

Certain combustion characteristics of blended fuels including ignition temperature and the kinetics parameters do not reflect the weighted average of their parent fuels [199]. The ignition temperature and activation energy are the measure of the fuel reactivity and are a critical parameter in the assessment of the fuel blending. Therefore, it is essential to study the combustion characteristics of fuel blends beforehand.

Blending coals with renewable and sustainable resources such as biomass is used to generate a component of green power generation which is pursued as a consequence of current or future regulations. Furthermore, oxy-fuel combustion of biomass/coal

blends induces the potential of achieving an overall negative CO₂ emission from the power plant [17]. Oxy-fuel combustion and co-combustion of low-quality coal with biomass are promising methods for clean combustion technology.

In this study, based on the obtained results from the combustion of the different torrefied biomasses, it was concluded that the sample torrefied at 300°C torrefaction temperature and 30min residence time conditions indicates the closest characteristics to the utilized lignites. Therefore, Orhaneli and Soma lignites were blended with 300°C-30min sample at different mass fractions of 25, 50, and 75 wt.%. In order to investigate the possibility of mixing the lignite with raw biomass, another set of experiments were also conducted to study the raw woodchip and lignite blending. Since all of the considered fuels were solid fuels, the blending procedure was done mechanically.

4.1.3.1. TGA Analysis

The co-combustion process of the lignites and biomass blends was carried out at different mass fractions under air (21% O₂- 79% N₂) and air equivalent oxy-fuel (21% O₂ and 79% CO₂) combustion conditions by means of TGA. The samples were mixed thoroughly and 10 mg of the samples were used in each experiment. Figure 4.21 shows the TGA and DTG co-combustion results of Orhaneli and 300°C-30min torrefied biomass at different mass fraction of 25, 50, and 75 wt.% under air combustion condition. As can be seen, the obtained results for 25 and 75% mass fraction mixtures were close to that of 50% blend and concluding appreciable results between them would be arduous. Hence, in order to decrease the number of the experiments, the 50/50 blends were considered for the blends.

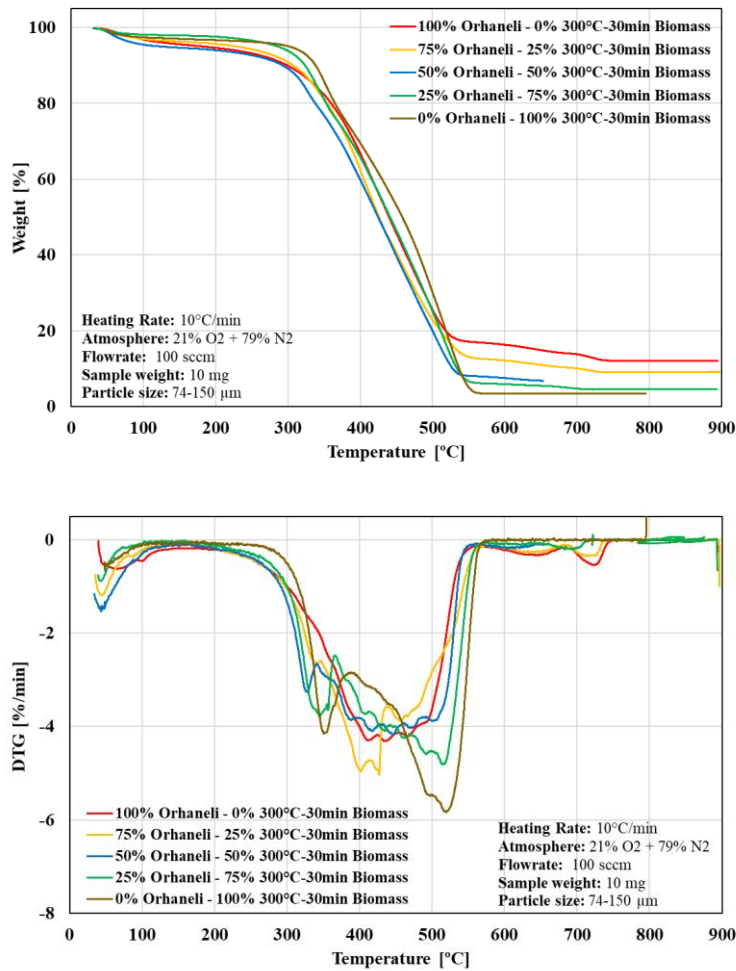


Figure 4.21. TGA and DTG curves of Orhaneli lignite and 300°C-30min torrefied biomass co-combustion under air atmosphere

The TGA and DTG profiles for combustion of 50/50 blend of Orhaneli lignite and raw biomass at different heating rates under air and air-equivalent oxy-fuel combustion atmospheres are presented in Figure 4.25. The characteristic temperatures of the blend are summarized in Table 4.9 . In both air and oxy-fuel cases, the moisture released in the first 200°C temperature zone. The second weight loss was attributed to the combustion of volatiles occurred in the temperature interval of 260 to 520°C at 10°C/min, 290 to 570°C at 20°C/min, and 300 to 760°C at 40°C/min. Increasing the

heating rate resulted in the delay of the characteristic temperatures as can be seen in Table 4.9. The total weight loss was 92% irrespective of heating rate or combustion atmosphere. From the DTG profiles it can be seen that the rate of weight loss became larger with the increase of heating rate due to faster combustion process.

Switching the combustion atmosphere diluting gas from N₂ to CO₂ delayed the initial temperature (T_i), ignition temperature (T_{ig}) and maximum temperature (T_{max}). However, the burnout temperature (T_b) was seen to be lower in oxy-fuel combustion condition indicating that the completion of combustion occurred faster. This phenomenon was more significant in higher heating rates.

Table 4.9. Characteristic temperatures of Orhaneli and raw and torrefied biomass 50/50 blends at different heating rates under air and oxy-fuel combustion conditions

	T_i [°C]	T_{ig} [°C]	T_{max} [°C]	T_b [°C]
<i>HR= 10°C/min</i>				
50/50 Orh.- Raw Bio.- Comb.	238	297	341	514
50/50 Orh.- Raw Bio.- Oxy-Comb.	248	307	347	515
50/50 Orh.- 300°C-30min Bio.- Comb.	285	323	444	537
50/50 Orh.- 300°C-30min Bio.- Oxy-Comb.	293	322	451	545
<i>HR= 20°C/min</i>				
50/50 Orh.- Raw Bio.- Comb.	224	307	358	586
50/50 Orh.- Raw Bio.- Oxy-Comb.	244	326	367	568
50/50 Orh.- 300°C-30min Bio.- Comb.	227	337	342	654
50/50 Orh.- 300°C-30min Bio.- Oxy-Comb.	252	335	406	594
<i>HR= 40°C/min</i>				
50/50 Orh.- Raw Bio.- Comb.	208	313	366	784
50/50 Orh.- Raw Bio.- Oxy-Comb.	226	330	371	632
50/50 Orh.- 300°C-30min Bio.- Comb.	246	329	364	847
50/50 Orh.- 300°C-30min Bio.- Oxy-Comb.	236	326	361	739

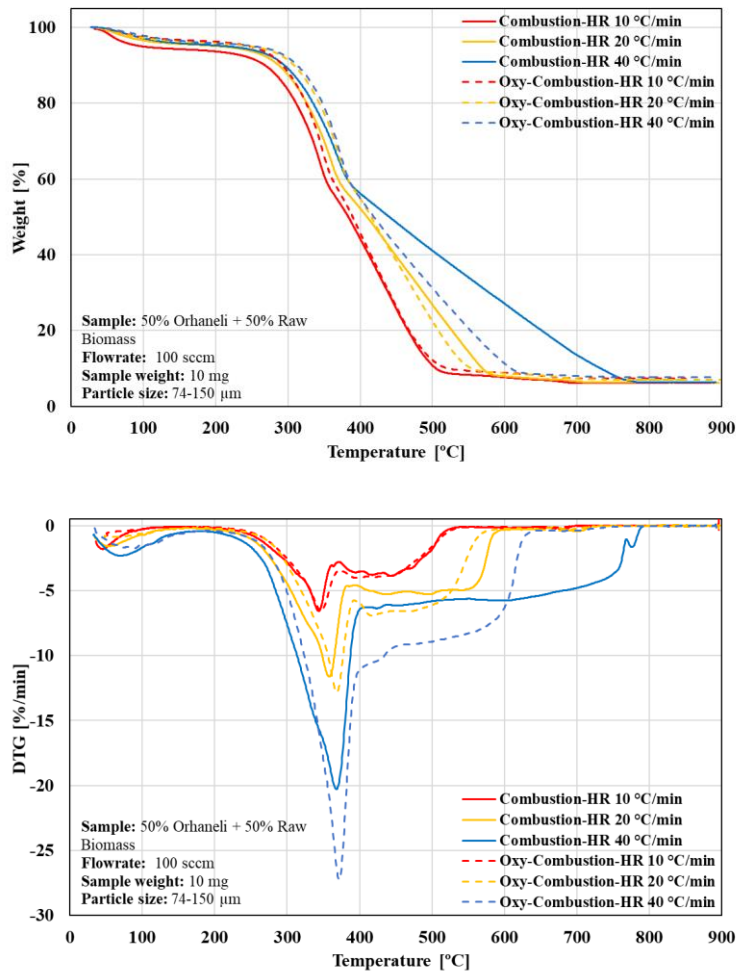


Figure 4.22. TGA and DTG curves of Orhaneli lignite and raw biomass 50/50 blend co-combustion at different heating rates under air and oxy-fuel combustion conditions

Figure 4.23 shows the comparison of the combustion of Orhaneli lignite, raw biomass and their 50/50 blend at 10°C/min heating rate under air and oxy-fuel combustion conditions. The DTG results for the blend indicated two peaks in the combustion region: the first peak was due to combustion of hemicellulose and cellulose inherited from the biomass content of the blend and the second region can be attributed to the combustion of volatiles and fixed carbon of the lignite part and the lignin content from the biomass part. In combustion of raw biomass, it was seen that the lignin content

decomposed in temperature interval of 420-530°C, but this phase did not appear in combustion of the blend. That is because the combustion of lignite part in the temperature interval of 375-510°C, resulted in the decomposition of lignin at lower temperatures. Therefore, it can be said that the synergetic effect in the co-combustion of the blend was more prominent in decomposition of lignin fraction of the biomass. Similar results can be found elsewhere [156].

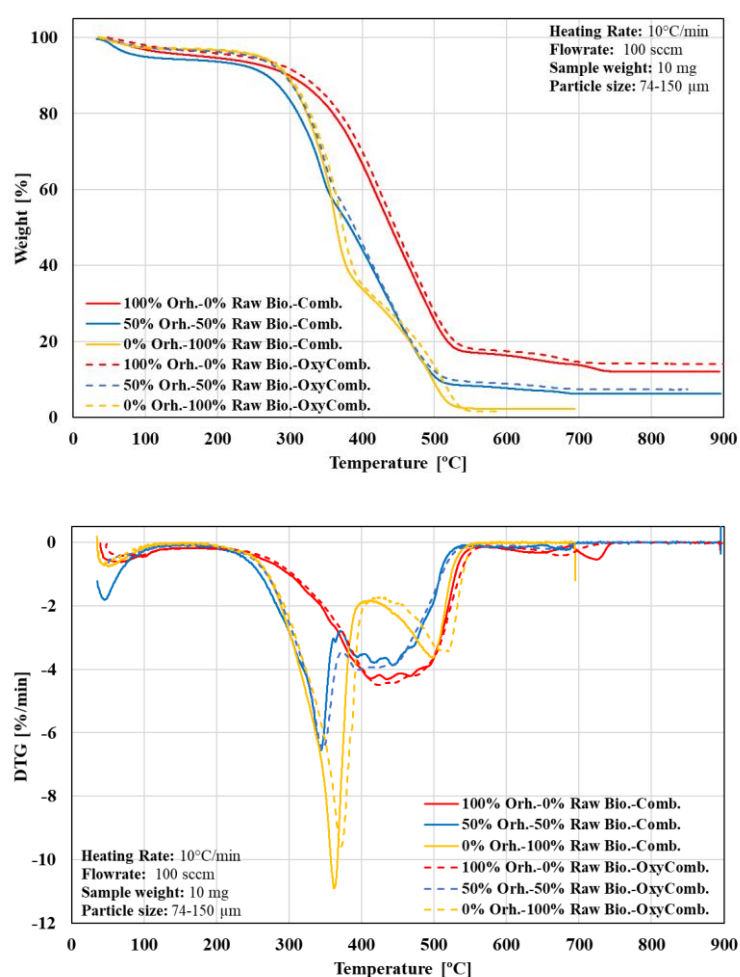


Figure 4.23. Comparison of 50/50 blend of Orhaneli lignite and raw biomass with its parent fuels at 10°C/min heating rate under air and oxy-fuel combustion atmospheres

Figure 4.24 represents the comparison of the characteristic temperatures regarding the blend and its parent fuels. It was seen that the characteristic temperatures of the blend were lower than its parent fuels under both air and oxy-fuel combustion conditions showing that the blend had higher reactivity than the parent fuels [199]. The ignition temperature of the blend was about 20°C and 40°C lower than that of raw biomass and Orhaneli lignite, respectively. This can be considered as an enhancement in the blend combustion. The completion of combustion of the blend also occurred at lower temperatures than the parent fuels. These results showed a synergetic effect in co-combustion of lignite and raw biomass.

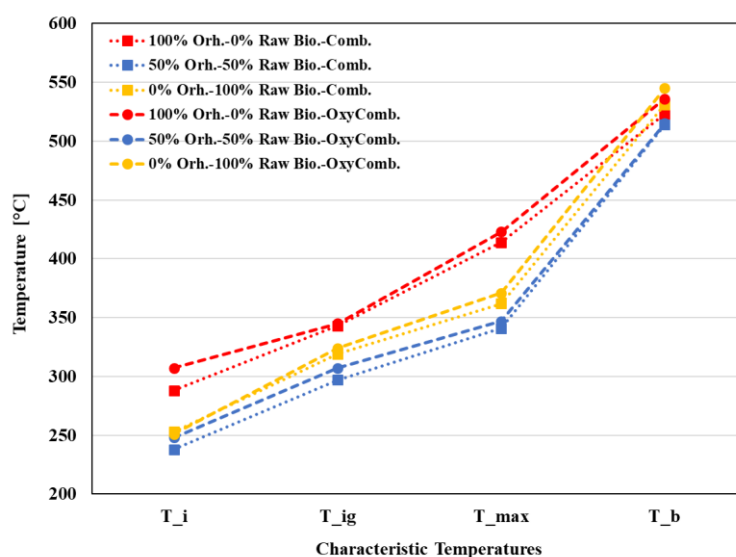


Figure 4.24. Comparison of characteristic temperatures of 50/50 blend of Orhaneli lignite and raw biomass with its parent fuels at 10°C/min heating rate under air and oxy-fuel combustion atmospheres

The TGA and DTG profiles for the co-combustion of 50/50 blend of Orhaneli lignite and 300°C-30min torrefied biomass at different heating rates under air and air-equivalent oxy-fuel combustion atmospheres are presented in Figure 4.25. The characteristic temperatures of the blend are summarized in Table 4.9 . In both air and

oxy-fuel cases, the moisture released in the first 200°C temperature zone. The second weight loss can be attributed to the combustion of volatiles and fixed carbon content. The first peak in this region was due to decomposition of cellulose content in the blend followed by combustion of lignite and lignin contents. The total weight loss was about 92% irrespective of heating rate or combustion atmosphere. Increasing the heating rate caused the combustion occurred at higher temperatures.

The combustion characteristic temperatures were followed the general increase trend due to switching atmospheres from air to oxy-fuel conditions at 10°C/min heating rate representing the combustion delay under oxy-fuel conditions. However, the obtained results indicated that the combustion process under oxy-fuel condition occurred faster at higher heating rates and was more significant at 40°C/min.

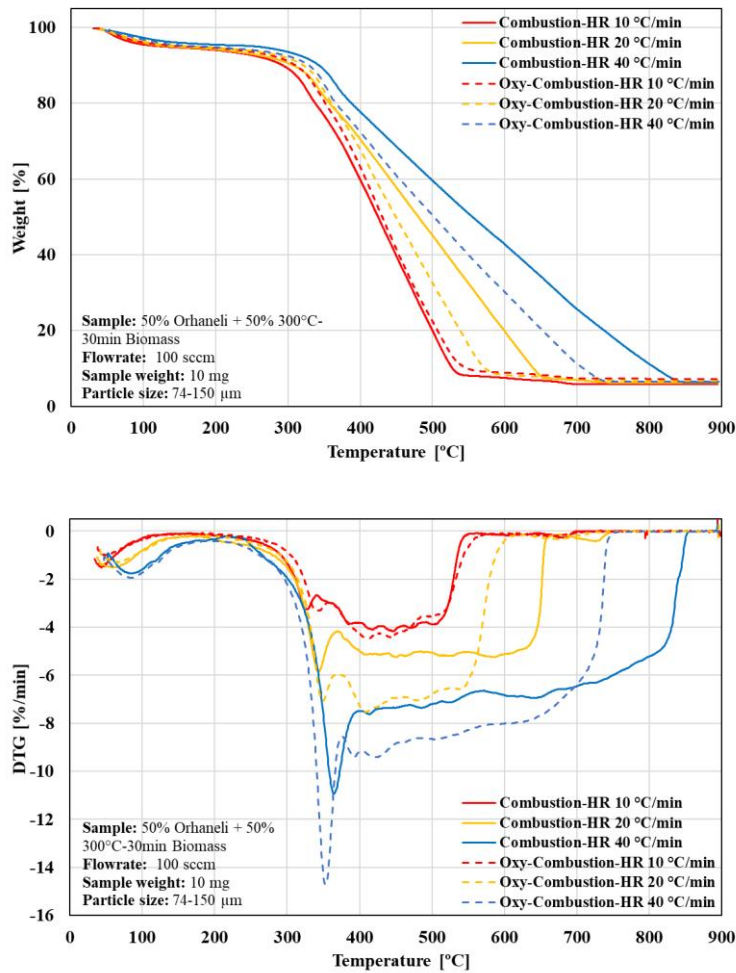


Figure 4.25. TGA and DTG curves of Orhaneli lignite and 300°C-30min torrefied biomass co-combustion under air and oxy-fuel combustion conditions

The TGA and DTG comparison of air and oxy-fuel combustion of Orhaneli lignite and 300°C-30min torrefied biomass with their 50/50 blend are presented in Figure 4.26. The first peak in the combustion region was attributed to the decomposition of cellulose content and the second peak was the decomposition of volatiles and fixed carbon content of the blend as well as lignin combustion. It was found that the cellulose combustion in blend took place at lower temperatures than in 100% biomass. Also, the peak related to lignin combustion in 100% biomass did not occur in the

blend showing that the lignin content in the blend was decomposed at lower temperatures along with combustion of lignite components. A small peak which appeared in air combustion can be attributed to the degradation of CaCO_3 content. This decomposition process did not appear in oxy-fuel condition due to presence of CO_2 .

The characteristic temperature comparison of 50/50 blend of Orhaneli lignite and 300°C-30min torrefied biomass and its parent fuels are illustrated in Figure 4.27. The initial temperature (T_i) for Orhaneli lignite under air and oxy-fuel combustion conditions were 288°C and 307°C, and for 300°C-30min torrefied biomass were 299°C and 301°C, respectively. T_i for their 50/50 blend was 285°C and 393°C which was close to that of Orhaneli lignite initial temperature. It was seen that the initial temperature of the blend was lower than that of the parent fuels. The ignition temperature (T_{ig}) of the blend was around 322°C at both combustion atmospheres and the value was also seen to be lower than its parent fuels. It can be concluded that the 50/50 blend of lignite and torrefied biomass has higher reactivity. The ignition of the blend was occurred at temperatures close to the ignition temperature of 300°C-30min biomass which can be attributed to the combustion of cellulose component of the blend.

In 100% biomass combustion, the maximum temperature (T_{max}) where the maximum weight loss occurs was associated to the lignin component. However, in combustion of the blend, since the degradation of lignin took place at lower temperatures along with lignite volatile matter, T_{max} was significantly lower than that of 100% biomass. Moreover, it can be seen that switching the combustion atmosphere from air to oxy-fuel resulted in increase in initial temperature in Orhaneli lignite by about 19°C. However, this increase was not significant in case of 300°C-30min biomass. The initial temperature difference between air and oxy-fuel combustion atmospheres for the blend was about 8°C.

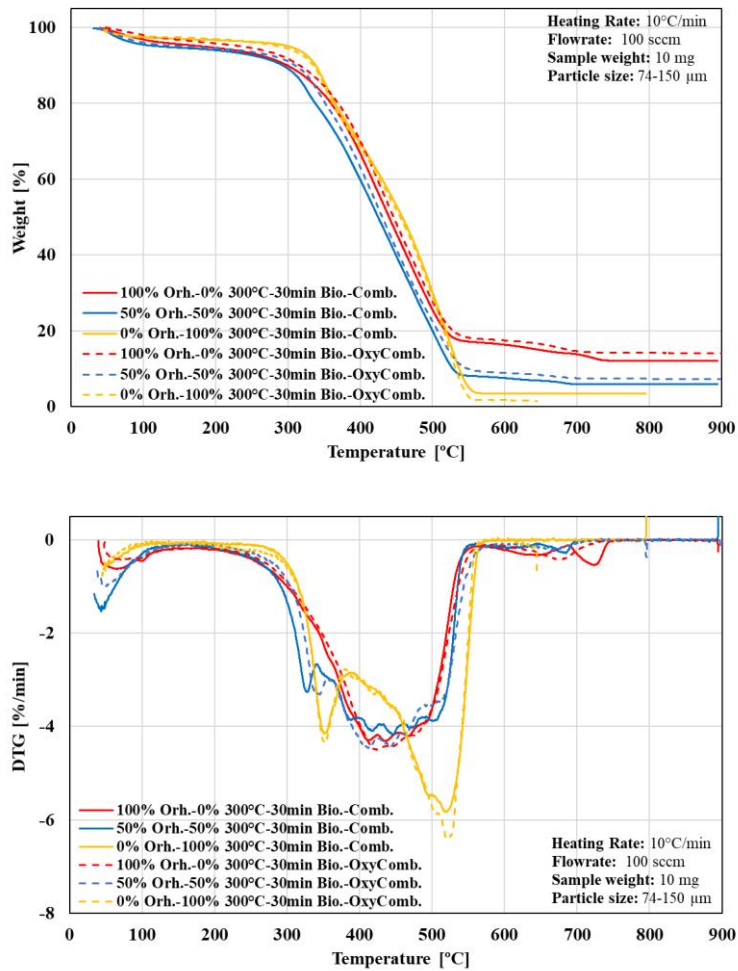


Figure 4.26. TGA and DTG curves of Orhaneli lignite and 300°C-30min torrefied biomass co-combustion under air and oxy-fuel combustion conditions

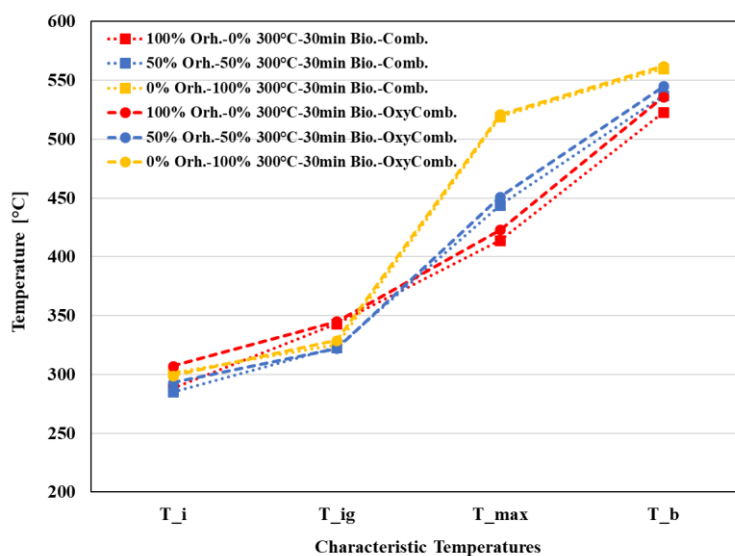


Figure 4.27. Comparison of characteristic temperatures of 50/50 blend of Orhaneli lignite and 300°C-30min torrefied biomass with its parent fuels at 10°C/min heating rate under air and oxy-fuel combustion atmospheres

The TGA and DTG profiles for combustion of 50/50 blend of Soma lignite and raw biomass at different heating rates under air and air-equivalent oxy-fuel combustion atmospheres are depicted in Figure 4.25. The characteristic temperatures are presented in Table 4.10. The moisture release process completed in the first 200°C for both air and oxy-fuel conditions. The major weight loss occurred at the second combustion region attributed to combustion of volatiles. Two separate weight losses were seen in this region: the first one was due to combustion of hemicellulose and cellulose components present in the blend occurring in the interval of 260 to 400°C, and the second peak was attributed to the combustion of lignite components as well as the lignin content occurring in the temperature interval of 400 to 700°C. The last weight loss region which was occurred only in air combustion condition was due to decomposition of CaCO₃ present in the ash. This peak did not appear in the presence of CO₂. By increasing the heating rate, the combustion process shifted to higher temperature regions. However, the total weight loss was irrespective of heating rate

and was about 78% and 74% under air and oxy-fuel combustion conditions, respectively.

Table 4.10 shows that switching the combustion atmosphere to oxy-fuel condition resulted in the delay of T_i , T_{ig} , and T_{max} characteristic temperatures. However, T_b decreased indicating that the completion of the combustion occurred faster in oxy-fuel condition. This phenomenon was more significant in higher heating rates.

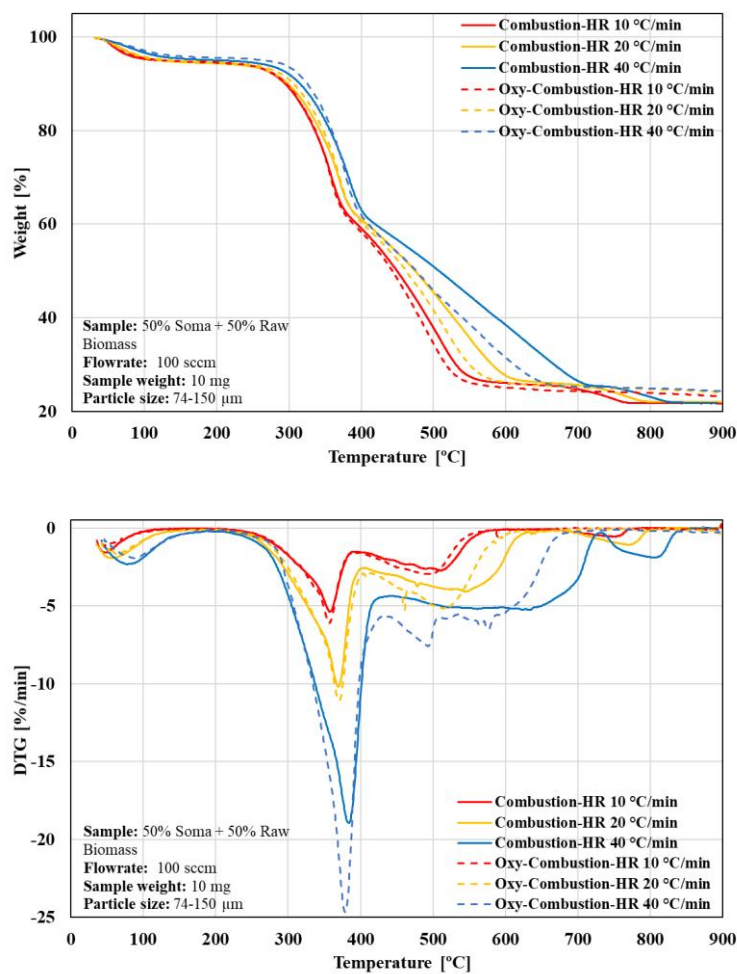


Figure 4.28. TGA and DTG curves of Soma lignite and raw biomass co-combustion under air and oxy-fuel combustion conditions

Table 4.10. Characteristic temperatures of Soma and raw and torrefied biomass 50/50 blends at different heating rates under air and oxy-fuel combustion conditions

	T_i [°C]	T_{ig} [°C]	T_{max} [°C]	T_b [°C]
	<i>HR= 10°C/min</i>			
50/50 Soma- Raw Bio.- Comb.	259	314	356	558
50/50 Soma- Raw Bio.- Oxy-Comb.	259	317	354	545
50/50 Soma- 300°C-30min Bio.- Comb.	294	330	500	544
50/50 Soma- 300°C-30min Bio.- Oxy-Comb.	297	332	503	552
	<i>HR= 20°C/min</i>			
50/50 Soma- Raw Bio.- Comb.	244	319	367	617
50/50 Soma- Raw Bio.- Oxy-Comb.	257	325	369	598
50/50 Soma- 300°C-30min Bio.- Comb.	245	334	365	847
50/50 Soma- 300°C-30min Bio.- Oxy-Comb.	291	372	528	614
	<i>HR= 40°C/min</i>			
50/50 Soma- Raw Bio.- Comb.	237	331	382	720
50/50 Soma- Raw Bio.- Oxy-Comb.	256	335	379	670
50/50 Soma- 300°C-30min Bio.- Comb.	283	328	551	641
50/50 Soma- 300°C-30min Bio.- Oxy-Comb.	248	329	355	673

The TGA and DTG comparison of the combustion of Soma lignite, raw biomass and their 50/50 blend at 10°C/min heating rate under air and oxy-fuel combustion conditions are presented in Figure 4.29. The main combustion region for 100% raw biomass occurred in two distinct sections which were the hemicellulose and cellulose combustion section and lignin combustion section. Soma biomass combustion showed one major combustion peak which was in the interval of 400°C to 570°C. For the combustion of their 50/50 blend, two distinct weight loss in the main combustion region can be seen. Due to the fact that the combustion of lignin occurs in the temperature interval of 420-530°C, the lignin decomposition peak coincided with the Soma main combustion interval, hence the impact of blending on lignin decomposition enhancement could not be seen for this blend. The decomposition of

CaCO₃ which appeared in the range of 680-780°C did not affected by the presence of biomass in the blend.

Figure 4.30 illustrates the comparison of the characteristic temperatures regarding the blend and its parent fuels. The ignition and maximum temperatures were lower than its parent fuels under both air and oxy-fuel combustion conditions showing that the blend had higher reactivity than the parent fuels. The ignition temperature of the blend was about 5°C and 85°C lower than that of raw biomass and Soma lignite, respectively.

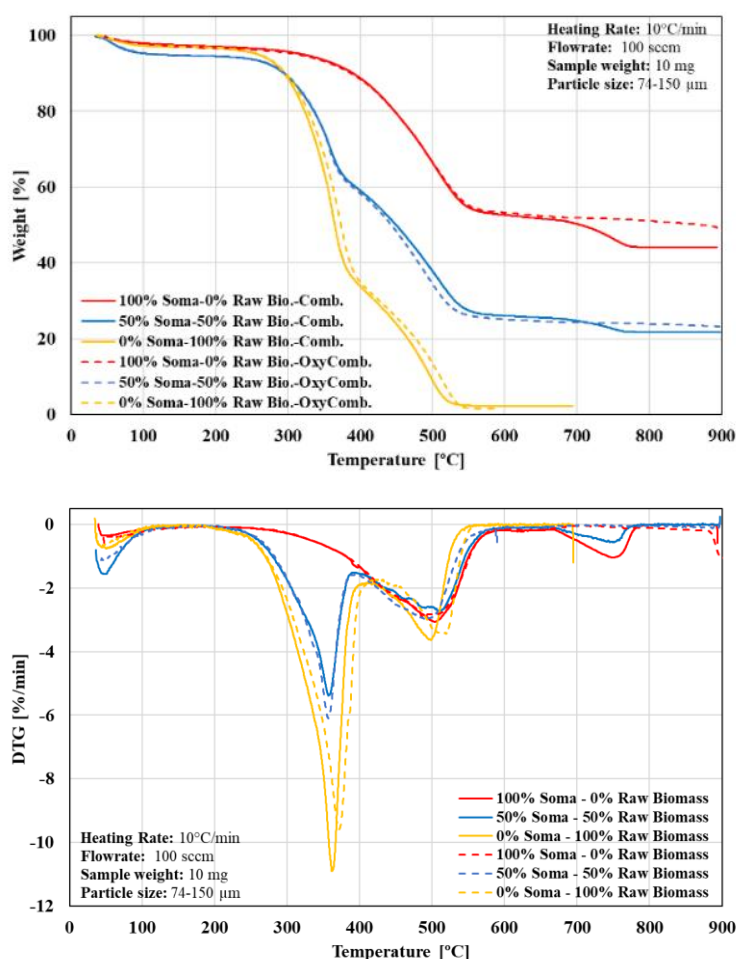


Figure 4.29. TGA and DTG curves of Soma lignite and raw biomass co-combustion under air and oxy-fuel combustion atmospheres

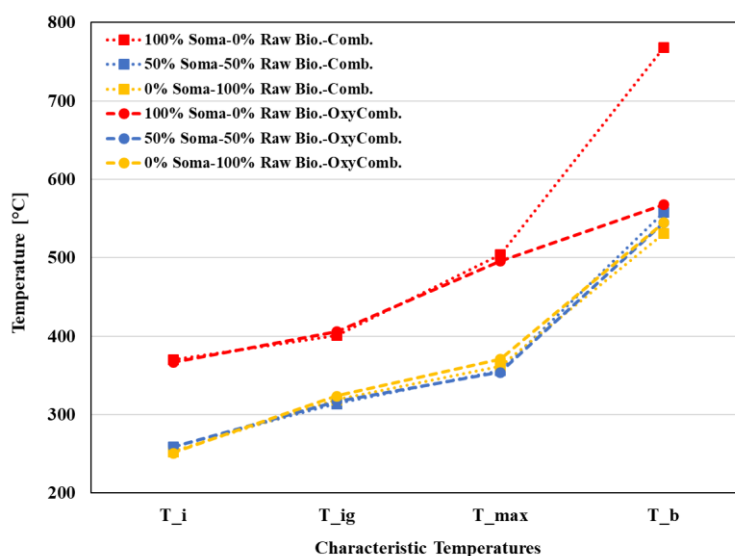


Figure 4.30. Comparison of characteristic temperatures of 50/50 blend of Soma lignite and raw biomass with its parent fuels at 10°C/min heating rate under air and oxy-fuel combustion atmospheres

The TGA and DTG profiles for the co-combustion of 50/50 blend of Soma lignite and 300°C-30min torrefied biomass at different heating rates under air and air-equivalent oxy-fuel combustion atmospheres are presented in Figure 4.31. The characteristic temperatures of the blend are summarized in Table 4.10. In both air and oxy-fuel cases, the moisture released in the first 200°C temperature zone. The second weight loss can be attributed to the combustion of volatiles and fixed carbon content. The first peak in this region was due to decomposition of cellulose content in the blend followed by combustion of lignite and lignin contents. The last weight loss at temperatures higher than 670°C was due to decomposition of CaCO₃ under in air atmosphere. By increasing heating rate, the combustion process shifted to higher temperature regions. However, the total weight loss was irrespective of heating rate and was about 75% and 71% under air and oxy-fuel combustion conditions, respectively.

The combustion characteristic temperature trends were comparable to the blend of 300°C-30min torrefied biomass with Orhaneli lignite. The obtained results indicated that the combustion process under oxy-fuel condition occurred faster at higher heating rates and was more significant at 40°C/min.

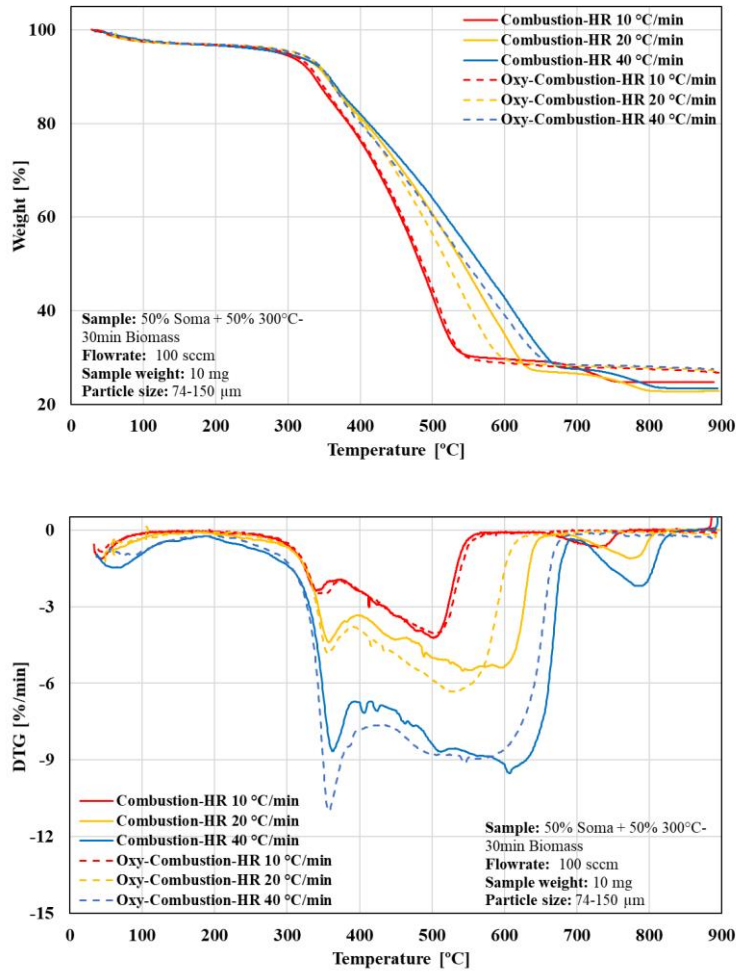


Figure 4.31. TGA and DTG curves of Soma lignite and 300°C-30min torrefied biomass co-combustion under air and oxy-fuel combustion conditions

The TGA and DTG comparison of air and oxy-fuel combustion of Soma lignite and 300°C-30min torrefied biomass with their 50/50 blend are presented in Figure 4.32. It was seen that the cellulose combustion in the blend took place at lower temperatures than in 100% biomass combustion. The decomposition of lignin did not appear in the blend due to its decomposition temperature overlap with the main weight loss region of the Soma lignite. This result was similar to the co-combustion of Soma and raw biomass. The decomposition of CaCO₃ which appeared in the range of 680-780°C did not affected by the presence of biomass in the blend as well.

The characteristic temperature comparison of 50/50 blend of Soma lignite and 300°C-30min torrefied biomass and its parent fuels are shown in Figure 4.33. The initial temperature (T_i) for Soma lignite under air and oxy-fuel combustion conditions were 370°C and 367°C, and for 300°C-30min torrefied biomass were 301°C and 299°C, respectively. T_i for their 50/50 blend was 294°C and 297°C which was close to biomass initial temperature. It was seen that the initial temperature of the blend was lower than that of the parent fuels. The ignition temperature (T_{ig}) of the blend was around 330°C under both combustion atmospheres and the value was also seen to be identical to its biomass parent. The ignition temperature of the blend can be attributed to combustion of cellulose component. Blending Soma lignite and 300°C-30min torrefied biomass did not show a considerable effect on fuel reactivity.

Similar to co-combustion of Soma lignite and raw biomass, the impact of blending on lignin decomposition could not be distinguished in Soma and 300°C-30min torrefied biomass either. That was because the temperature interval related to lignin decomposition was coincided with the Soma main combustion interval. The maximum weight loss temperature (T_{max}) occurred at temperatures comparable with Soma lignite.

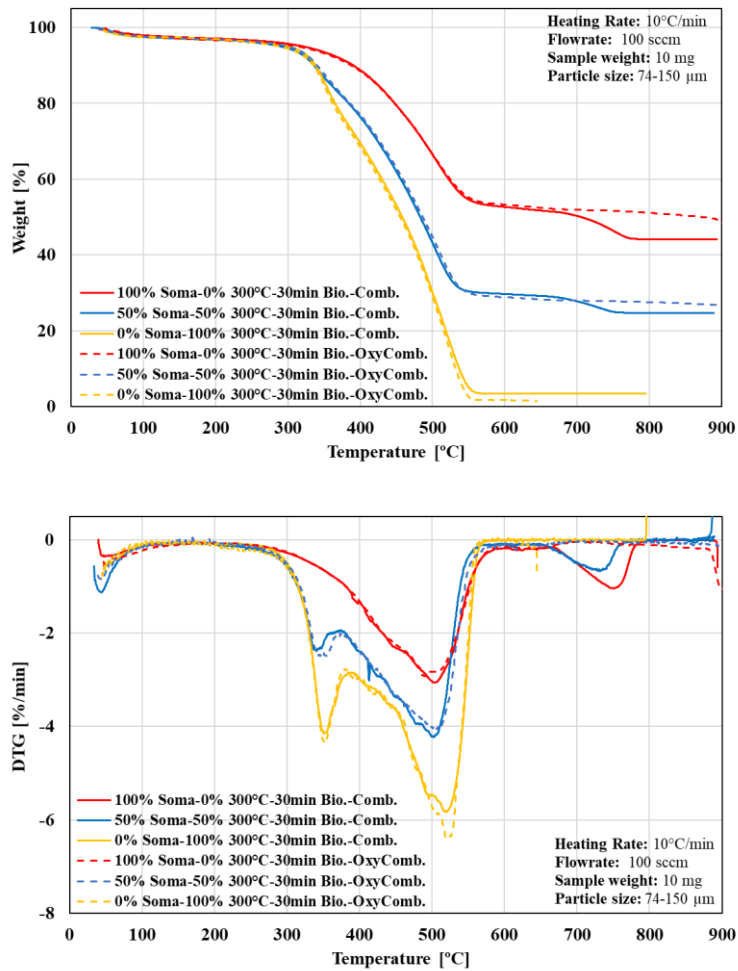


Figure 4.32. TGA and DTG curves of Soma lignite and 300°C-30min torrefied biomass co-combustion under air and oxy-fuel combustion conditions

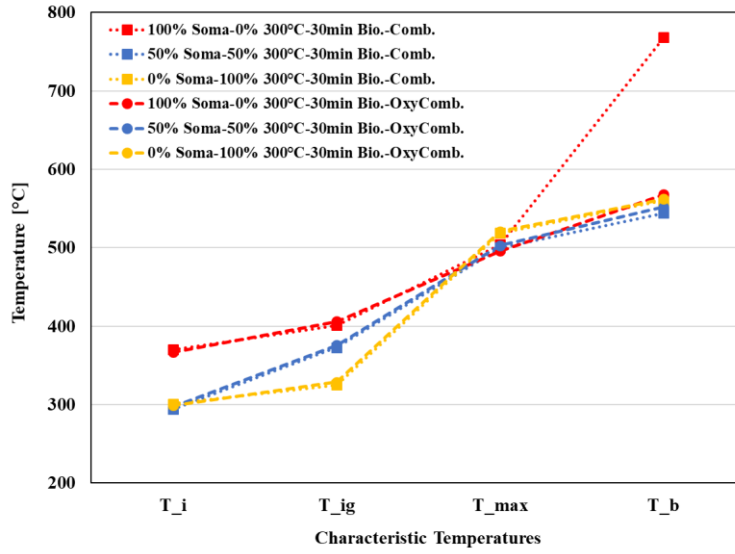


Figure 4.33. Comparison of characteristic temperatures of 50/50 blend of Soma lignite and 300°C-30min torrefied biomass with its parent fuels at 10°C/min heating rate under air and oxy-fuel combustion atmospheres

In order to describe the interaction between the distinct samples that made a mixture, the synergism term was used which is based on the difference between theoretical DTG and experimental DTG profiles [157]. Theoretical DTG of a blend is calculated according to Eq. 4.1:

$$DTG_{th} = \sum_{i=1}^n x_i \cdot DTG_{exp,i} \quad (4.1)$$

Where x_i is the mass fraction of each sample in the mixture and DTG_{exp} is the experimental mass loss rate of each sample. The degree of synergism is determined according to the relative error which was described in [156]:

$$\Delta m_{error} = \left[\frac{m_{blend} - (x_1 \cdot m_1 + x_2 \cdot m_2)}{m_{blend}} \right] \cdot 100 \quad (4.2)$$

Where Δm_{error} is the relative error, m is the mass loss of pure components of the mixture. Greater values of the relative error denote the greater interaction between the blend components.

The experimental and calculated DTG profiles for 50/50 blends of Orhaneli with raw and 300°C-30min torrefied biomass are given in Figure 4.34 and the relative errors are presented in Table 4.11. The difference between the experimental and theoretical results indicated a synergetic effect between the components. It can be seen that the characteristic temperatures are decreased in the experiments denoting an improvement in combustion process of the mixtures. The average relative error was higher in air combustion and the results showed that the highest degree of synergism was in the blend of Orhaneli and 300°C-30min torrefied biomass where the average relative error was 21.41%. The synergism phenomena for coal and biomass co-combustion can be found elsewhere [157], [200], [201].

The experimental and calculated DTG profiles for 50/50 blends of Soma with raw and 300°C-30min torrefied biomass are given in Figure 4.35 and the relative errors are presented in Table 4.12. The theoretical DTG profiles were similar to experimental DTG meaning that the synergetic effect between the Soma and biomass samples were insignificant compared to that of Orhaneli blends. The highest average relative error was 7.17% for the case of Soma and raw biomass blend combustion in oxy-fuel condition. The average relative error regarding 50/50 blend of Soma lignite with 300°C-30min torrefied biomass was about 1.34% showing that the blend had no significant synergetic effect.

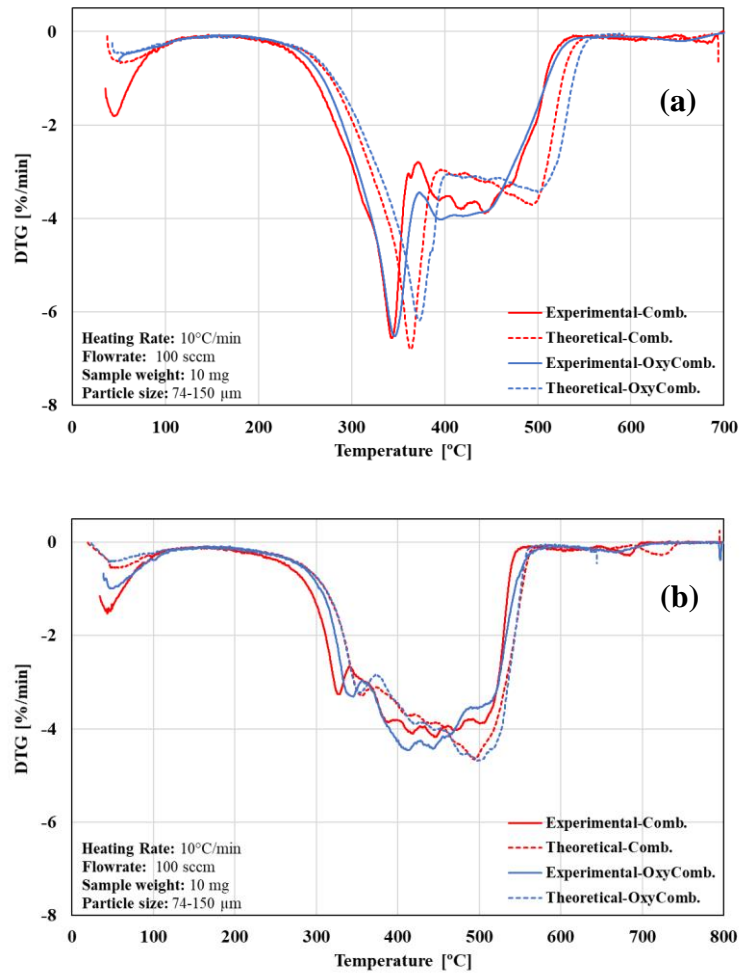


Figure 4.34. Experimental and theoretical DTG profiles for the 50/50 blends of (a) Orhaneli and raw biomass and (b) Orhaneli and 300°C-30min torrefied biomass under air and oxy-fuel combustion atmospheres

Table 4.11. Relative error calculation for the 50/50 blends of Orhaneli with raw and 300°C-30min torrefied biomass under air and oxy-fuel combustion atmospheres

	<i>T</i> [°C]	Max. Δm_{error} [%]	Average Δm_{error} [%]
50% Orh.- 50% Raw Bio.- Comb.	490	71.14	17.98
50% Orh.- 50% Raw Bio.- Oxy-Comb.	490	85.35	17.02
50% Orh.- 50% 300°C-30min Bio.- Comb.	527	73.43	21.41
50% Orh.- 50% 300°C-30min Bio.- Oxy-Comb.	515	36.35	9.59

**T*: the temperature at which the maximum relative error occurred

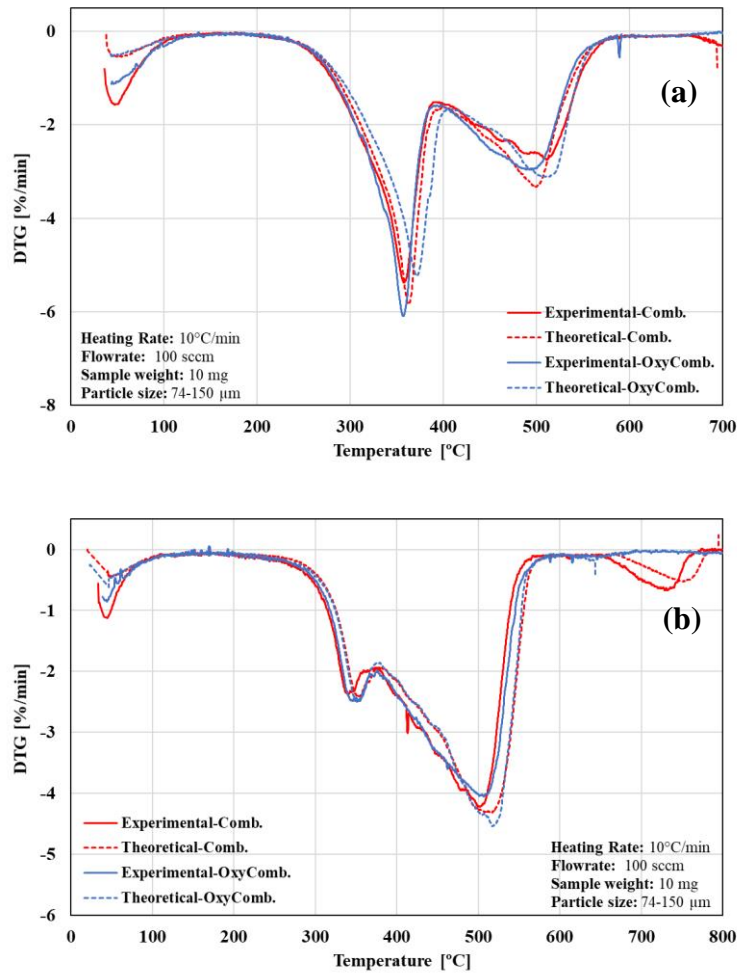


Figure 4.35. Experimental and theoretical DTG profiles for the 50/50 blends of (a) Soma and raw biomass and (b) Soma and 300°C-30min torrefied biomass under air and oxy-fuel combustion atmospheres

Table 4.12. Relative error calculation for the 50/50 blends of Soma with raw and 300°C-30min torrefied biomass under air and oxy-fuel combustion atmospheres

	$^*T [^{\circ}C]$	$Max. \Delta m_{error} [\%]$	$Average \Delta m_{error} [\%]$
50% Soma- 50% Raw Bio- Comb.	358	10.17	4.26
50% Soma- 50% Raw Bio.- Oxy-Comb.	507	21.08	7.17
50% Soma- 50% 300°C-30min Bio.- Comb.	512	16.95	1.34
50% Soma- 50% 300°C-30min Bio.- Oxy-Comb.	511	12.01	1.45

*T : the temperature at which the maximum relative error occurred

4.1.3.2. Kinetic Analysis

In order to calculate the kinetic parameters of the 50/50 blends of Orhaneli and Soma lignites with raw and 300°C-30min torrefied biomass samples, three isoconversional methods of FWO, KAS, and Friedman were employed. The conversion degree (α) ranging from 0.10 to 0.90 with a step-size of 0.05 were applied for each case. The linearity of isoconversional curves was checked for each conversion by calculating the linear correlation coefficient. The assessment of uncertainty was carried out by applying the standard ASTM 1641-13 for FWO method. Furthermore, this method was extended to calculate the uncertainty values of KAS and Friedman methods as well.

The evolution of the activation energies with conversion degree for the blends are depicted in Figure 4.36 under air and oxy-fuel combustion conditions. As it can be seen, the three methods showed similar trends for all samples. Similar to calculations for the lignite and biomass pure samples, the estimated activation energy distribution between FWO and KAS methods were in a good accordance and produced relatively comparable results. However, the calculated activation energies via Friedman method resulted in lower values. The values of the activation energies changed with increase of the conversion factor due to the complicated multistep reaction nature of the combustion in the blend samples.

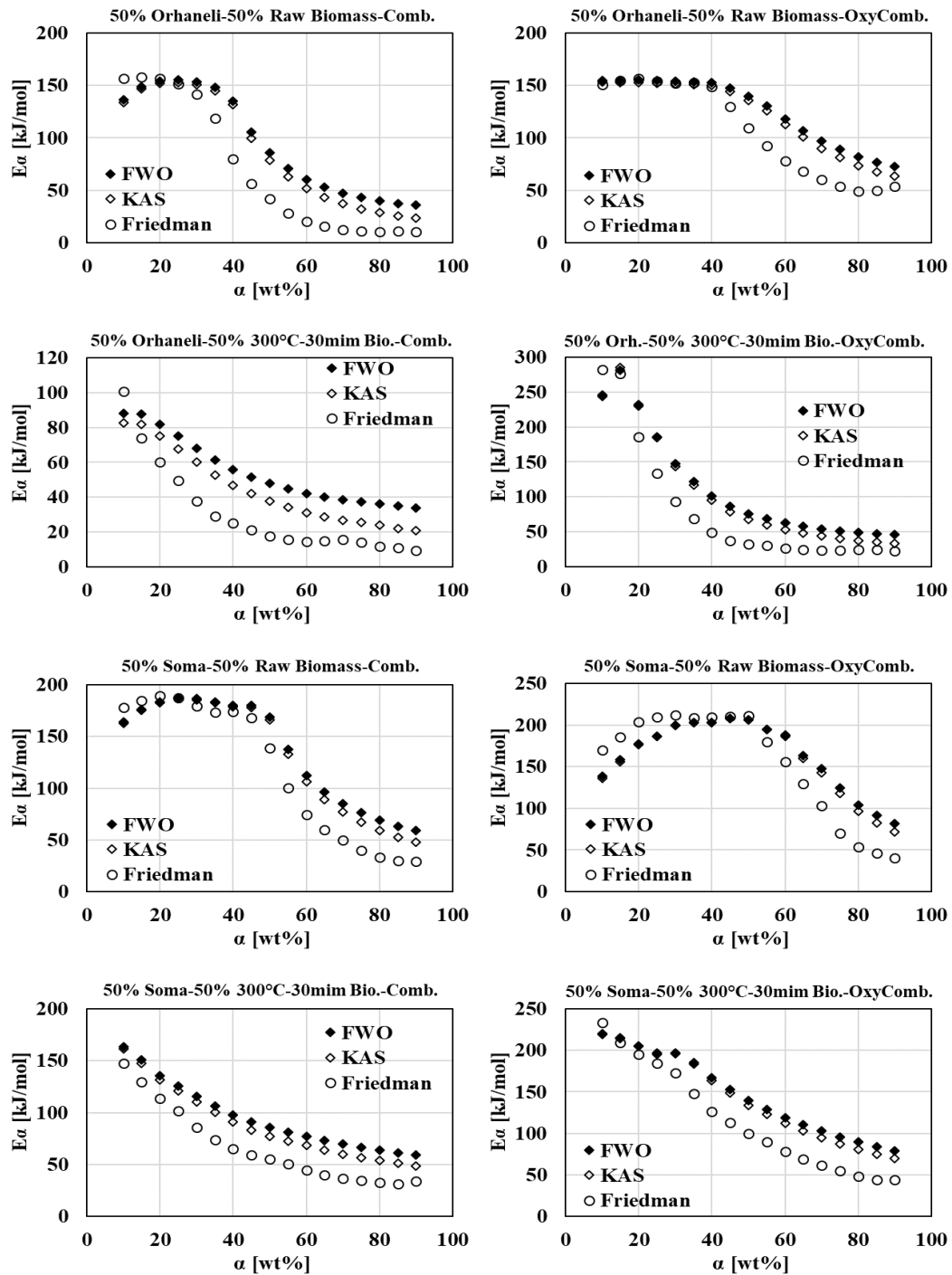


Figure 4.36. Activation energy curves of 50/50 blends of Orhaneli and Soma lignites with raw and 300°C-30min torrefied biomass samples with respect to conversion degree under air and oxy-fuel combustion atmospheres

Figure 4.37 represents the evolution of the activation energy values with respect to conversion degree for Orhaneli, 300°C-30min torrefied biomass and their 25, 50 and 75 wt.% blends under air combustion atmosphere. The average activation energy values and the corresponding uncertainties are given in Table 4.13. As can be seen, all blends exhibited approximately comparable values of activation energy especially after the start of combustion ($\alpha > 30\%$). The activation energy values at the start of combustion ($\alpha = 10\%$) were 290 kJ/mol for 300°C-30min torrefied biomass and 175 kJ/mol for the Orhaneli lignite. However, the activation energy values for the blends were in the range of 90-140 kJ/mol. The average activation energy values of the blends were lower than their parent fuels indicating the higher reactivity of the blends [202].

The evolution of activation energy of the blends was similar to that of the Orhaneli and decreased with the increase of conversion factor. The lowest activation energy was obtained at 50/50 blend of Orhaneli and 300°C-30min biomass showing the highest reactivity than the other mixtures. The estimated uncertainty values were in the range of 3.35% to 49.43% which the highest value was obtained for the 25/75 blend of Orhaneli and biomass sample. Comparing the uncertainty values for different kinetic methods, it was seen that FWO method resulted in lowest and Friedman method had the highest uncertainty values.

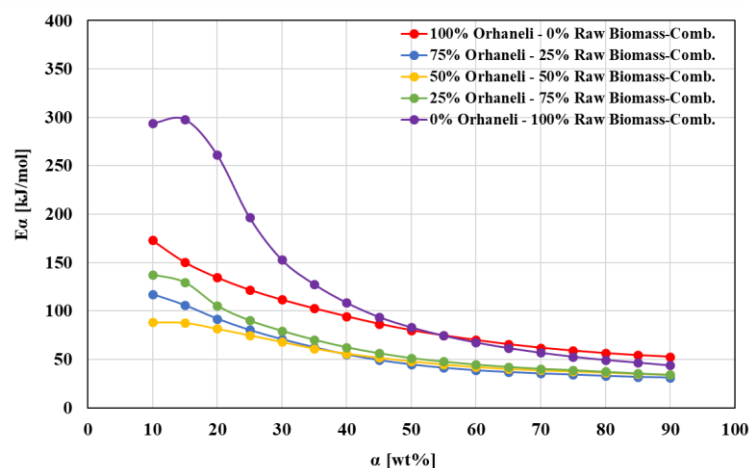


Figure 4.37. Comparison of the activation energies for Orhaneli, 300°C-30min torrefied biomass and their 25, 50 and 75 wt.% blends under air combustion atmosphere

Table 4.13. Average estimated activation energy values for Orhaneli, 300°C-30min torrefied biomass and their 25, 50 and 75 wt.% blends under air combustion atmosphere

	FWO		KAS		Friedman	
	<i>E_a</i> [kJ/mol]	Uncertainty [%]	<i>E_a</i> [kJ/mol]	Uncertainty [%]	<i>E_a</i> [kJ/mol]	Uncertainty [%]
Orhaneli lignite- Comb.	91.19	8.00	84.95	10.00	57.48	20.81
75% Orh.- 25% 300°C-30min Bio.- Comb.	56.55	5.35	46.85	6.88	26.36	25.28
50% Orh.- 50% 300°C-30min Bio.- Comb.	54.47	3.57	44.74	4.67	30.80	5.25
25% Orh.- 75% 300°C-30min Bio.- Comb.	64.98	19.12	55.56	24.96	33.50	49.43
300°C-30min biomass- Comb.	121.73	10.31	115.33	12.91	82.77	23.91

The comparison of the activation energies of the 50/50 blends of Orhaneli lignite with the raw and 300°C-30min torrefied biomass samples and parent fuels under air and oxy-fuel combustion atmospheres are given in Figure 4.38. Generally, the evolution of the activation energy values was below the biomass samples. The activation energy values of the 50/50 blend of Orhaneli with raw biomass were lower than parent fuels in air combustion and close to the values of Orhaneli lignite under oxy-fuel condition. For the case of 50/50 blend of Orhaneli and 300°C-30min torrefied biomass, the activation energy was below the parent fuels under air combustion at all conversion degrees. Under oxy-fuel combustion conditions, the activation energy of the blend was lower than its parent fuels at conversion degrees higher than 35% ($\alpha > 35\%$).

The average activation energy values of the blends and their associated uncertainties are summarized in Table 4.14. The average activation energy values estimated by the three methods were in decreasing order of FWO > KAS > Friedman throughout different co-combustion conditions. The 50/50 blend of Orhaneli and raw biomass combustion resulted in average activation energy values comparable to Orhaneli lignite under both atmospheres at approximately 94 and 126kJ/mol, respectively. The blend of Orhaneli and 300°C-30min torrefied biomass showed similar results at about 112kJ/mol. However, the average value regarding this blend under air combustion conditions showed a value significantly below the activation energies of its parent fuels at about 54kJ/mol. It can be concluded that blending Orhaneli lignite with 300°C-30min torrefied biomass resulted in higher reactivity of the fuel.

The calculated uncertainty values were in the range of 3.57% to 33.53%. The highest uncertainty values were obtained in Friedman method and the lowest values were in FWO method. Comparing the uncertainty values of the blends and their portions, it can be said that the calculations regarding the activation energy of the parent fuels had lower uncertainty than their blends.

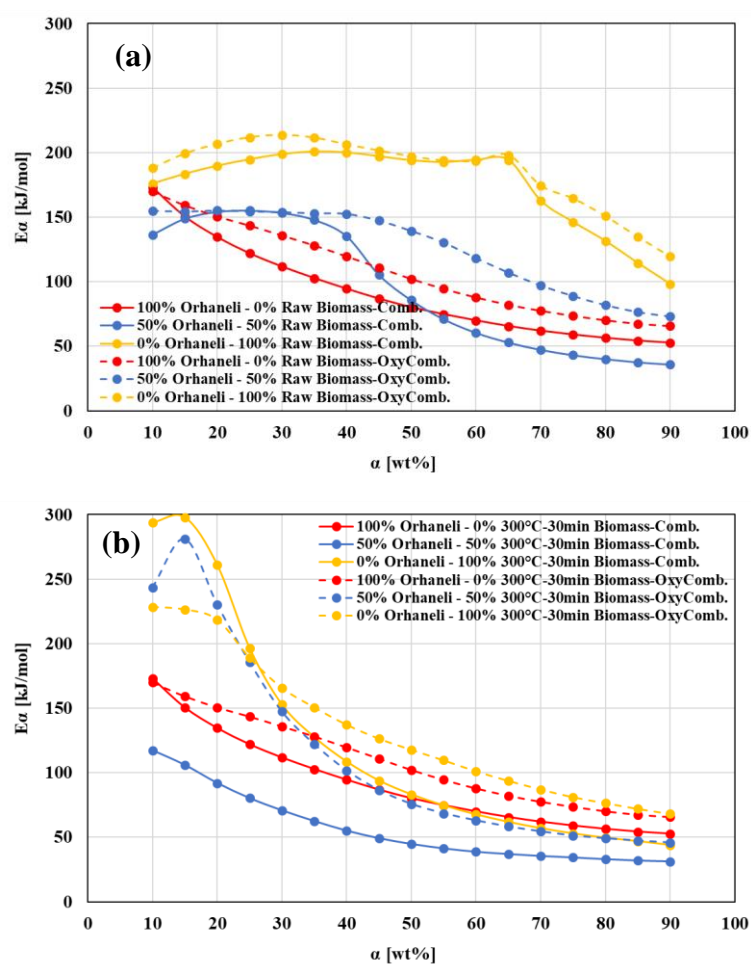


Figure 4.38. Comparison of the activation energies for Orhaneli and (a) raw biomass and (b) 300°C-30min torrefied biomass under air and oxy-fuel combustion atmospheres

Table 4.14. Average activation energy values for the 50/50 blend of Orhaneli with raw and 300°C-30min torrefied biomass under air and oxy-fuel combustion atmosphere

	FWO		KAS		Friedman	
	E_a [kJ/mol]	Uncertainty [%]	E_a [kJ/mol]	Uncertainty [%]	E_a [kJ/mol]	Uncertainty [%]
50% Orh.- 50% Raw Bio- Comb.	94.77	12.45	88.16	16.25	69.51	32.50
50% Orh.- 50% Raw Bio.- Oxy-Comb.	125.79	7.78	121.04	8.61	106.80	15.36
50% Orh.- 50% 300°C-30min Bio.- Comb.	54.47	3.57	44.74	4.67	30.80	5.25
50% Orh.- 50% 300°C-30min Bio.- Oxy-Comb.	112.48	11.61	106.08	14.43	80.07	33.53

The comparison of the activation energies of the 50/50 blends of Soma lignite with raw and 300°C-30min torrefied biomass samples and parent fuels under air and oxy-fuel combustion atmospheres are given in Figure 4.39. The average activation energies for the different blends are shown in Table 4.15. In contrast with the obtained results for the blends of Orhaneli lignite, in cases of Soma blends, the evolution of the activation energy was similar to the biomass samples especially for the combustion in oxy-fuel conditions. The average activation energy value for the 50/50 blend of Soma and raw biomass was 135.86kJ/mol which was close to that of Soma lignite value at 128.43kJ/mol. In oxy-combustion condition, the average activation energy value of the blend was 164.64kJ/mol which was close to that of raw biomass value at 186.25kJ/mol. The air combustion of the blend of Soma and 300°C-30min torrefied biomass resulted in lower activation energy values of its portions at 95.57kJ/mol. However, in oxy-fuel combustion conditions, this value was higher than its parent fuels at about 145.41kJ/mol.

The estimated uncertainty values showed that the uncertainties related to FWO method were lower than KAS and Friedman methods. The uncertainty values for the blends of Soma and the biomass samples were in the range of 6.95% to 23.12% and were higher than the values related to their parents.

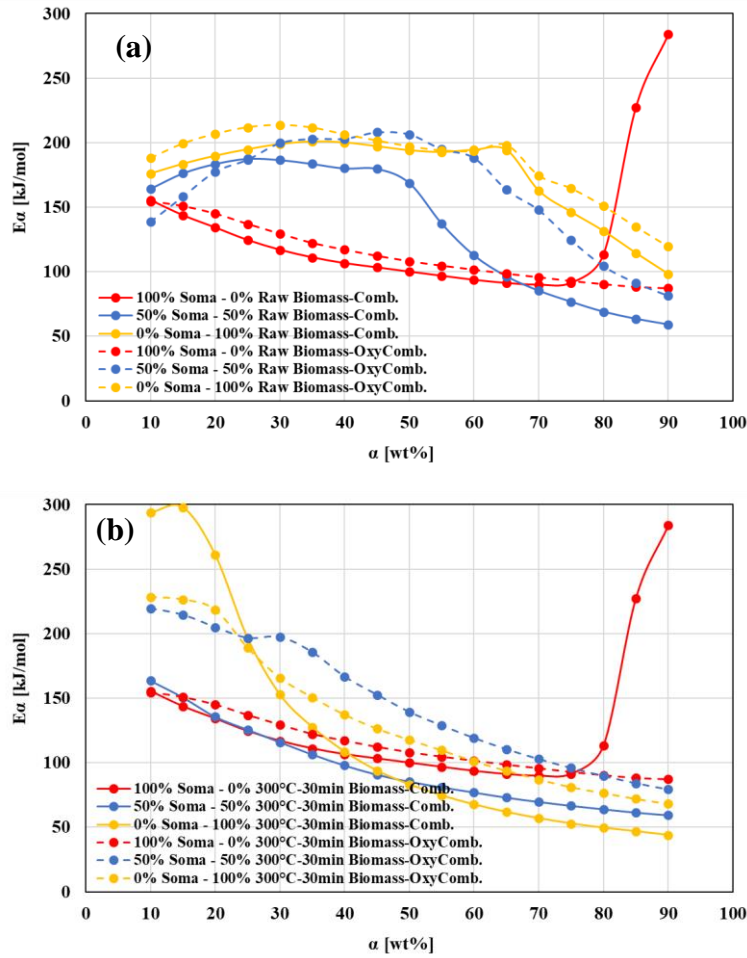


Figure 4.39. Comparison of the activation energies for Soma and (a) raw biomass and (b) 300°C-30min torrefied biomass under air and oxy-fuel combustion atmospheres

Table 4.15. Average activation energy values for the 50/50 blend of Soma with raw and 300°C-30min torrefied biomass under air and oxy-fuel combustion atmosphere

	FWO		KAS		Friedman	
	E_a [kJ/mol]	Uncertainty [%]	E_a [kJ/mol]	Uncertainty [%]	E_a [kJ/mol]	Uncertainty [%]
50% Soma- 50% Raw Bio.- Comb.	135.86	8.81	131.24	9.95	117.09	12.44
50% Soma- 50% Raw Bio.- Oxy-Comb.	164.64	8.32	161.70	9.09	154.85	15.81
50% Soma- 50% 300°C-30min Bio.- Comb.	95.57	11.13	88.17	12.67	66.84	23.12
50% Soma- 50% 300°C-30min Bio.- Oxy-Comb.	145.41	6.95	140.67	7.71	115.00	10.09

4.2. Circulating Fluidized Bed Experiments

Based on the obtained results from the TGA experiments, Orhaneli lignite was chosen to be used in the CFBC system. The sulfur content of the Orhaneli lignite is relatively high (1.73%), hence, addition of sorbents for SO₂ retention is required. Calcium-based sorbents such as limestone (CaCO₃) and dolomite (CaCO₃·MgCO₃) are proved to be successful sorbents for in-situ removal of SO₂ in fluidized bed combustion systems. Therefore, Çan limestone and Eskişehir dolomite were selected in order to study the SO₂ adsorption process. As can be seen in Table 3.4, Çan limestone has higher content of CaO than Eskişehir dolomite which makes it potentially superior adsorbent. The adsorbents were used at different particle sizes of 0-1 mm and 1-2 mm and Ca/S ratios of 1.5 and 2. The particle size of Orhaneli lignite was in the range of 1-3 mm. The combustion process was carried out under oxygen-enriched air with oxygen concentrations of 21, 23, 25, and 27% and the excess air ratio (λ) was 1.4 throughout the experiments. The excess air ratio was adjusted by controlling the amount of feeding fuel.

In order to adjust the oxygen concentration at the desired levels, an oxygen tank was connected to the inlet system and the flow was controlled by a mass flow controller and gas analyzer. Each test was started with air combustion (21% O₂) and after the system was reached to the steady state and the measurements were recorded, the oxygen was gradually introduced to the system to reach to 23% oxygen concentration. After the system reached to steady state, the measurements were recorded. This process was repeated to the oxygen concentrations of 25 and 27% as well. Finally, the combustion atmosphere was switched to oxy-fuel condition and the combustion process was studied under this condition as well. The experimental matrix regarding these experiments are given in Table 3.13.

The emission values in the combustion of Orhaneli lignite at different oxygen concentrations are given in Table 4.16. These results were obtained when no sulfur adsorbent was introduced to the bed. As can be seen, the SO₂ concentrations were in

the range of 1223mg/MJ and 1650mg/MJ and increased with the increase of the oxygen concentration. The main aim of the addition of Ca-based sorbents was the removal of SO₂ emission.

Table 4.16. Emissions of Orhaneli lignite combustion at different oxygen concentrations

Atmosphere	Bed temperature [°C]	NO _x [mg/MJ]	CO [mg/MJ]	SO ₂ [mg/MJ]	CO ₂ [%]
Air	767	92	269	1223	16
23% O ₂	816	101	201	1354	18
25% O ₂	862	124	195	1515	18
27% O ₂	870	150	191	1650	21

4.2.1. Combustion of Orhaneli Lignite and Çan Limestone in Enriched Oxygen Atmosphere

4.2.1.1. Limestone Particle Size = 0-1 mm; Ca/S Ratio = 1.5

The combustion test of Orhaneli lignite and Çan limestone adsorbent was performed in the CFBC under different oxygen-enriched environments. At the steady-state condition, fuel feeding rate was about 4.5 kg/h. The superficial velocity inside the bed was 2.60 m/s and the carbon-based efficiency was 96.5%. Figure 4.40 represents the temperature profiles along the combustor and the return leg. The highest temperature value was measured at about 32 cm above the distributor plate for the oxygen concentration of 25% at 910°C. The highest temperature at the top of the reactor was about 730°C at oxygen concentration of 21% indicating that the combustion process was completed at higher levels inside the reactor. The temperature profiles along the return leg were measured from the bottom of the cyclone at 4.7 m above the distributor plate down to gas recirculation point at 0.136 m. The highest temperature profile was measured for the 21% oxygen concentration and was about 650°C at the top of the return leg and decreased to 400°C at the re-entry location. Increasing the oxygen

concentration caused the combustion to take place at lower levels of the combustor, hence the temperatures inside the return leg were lower. Due to high temperatures in the return leg, it can be said that a good recirculation of the gases was taking place in the system.

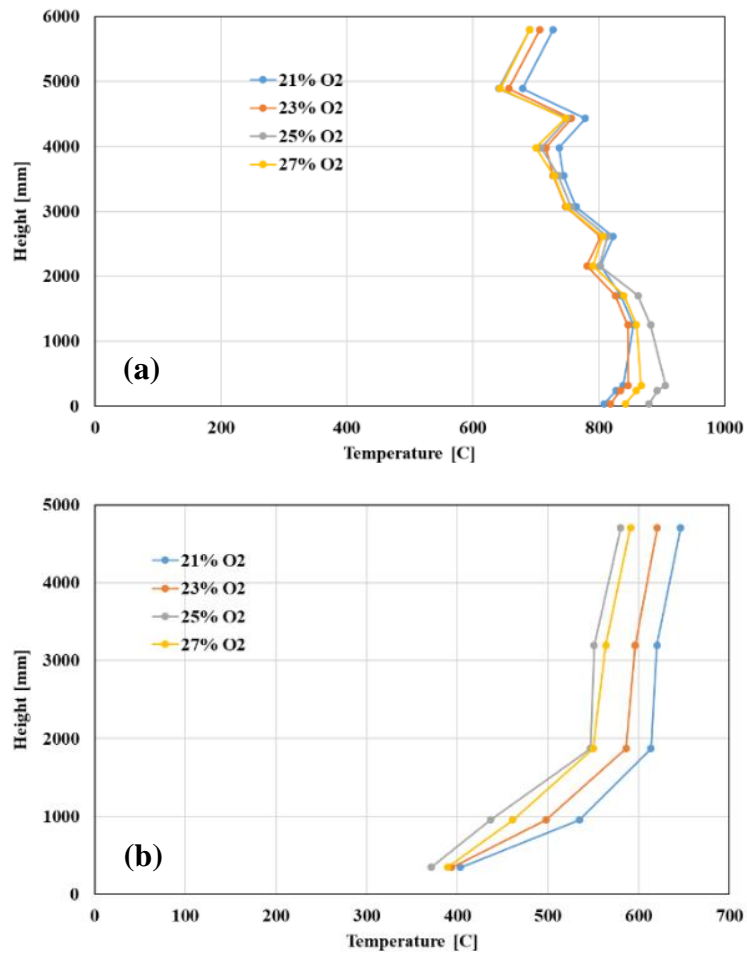


Figure 4.40. Temperature profile along (a) combustor and (b) return leg in the combustion of Orhaneli lignite and Çan limestone at Ca/S = 1.5 and Particle size of 0-1 mm

The effect of oxygen concentration on NO_x, CO, SO₂, and CO₂ emissions are shown in Figure 4.41. The secondary ordinate represents the average temperature of the dense

region of the bed. NO_x, CO, and SO₂ concentrations are given in mg/MJ at standard temperature and pressure. Flue gas measurements were performed during the steady state period of the experiments. It can be seen that the variation of NO_x emission was approximately constant at different oxygen concentrations and were about 160mg/MJ. That was because the bed temperature did not change by changing the oxygen concentration and was constant at around 850°C. CO emission showed a slight decrease from 165mg/MJ to 155mg/MJ by increasing oxygen concentration due to complete combustion.

Depending on the partial pressure of CO₂ and bed temperature, the calcium carbonate calcines to lime (indirect sulfation), or remains un-calcined and the reaction between SO₂ and limestone takes place directly (direct sulfation). Based on CaCO₃ thermodynamic equilibrium curve (Figure 2.7), it can be seen that the indirect adsorption process took place inside the bed. The SO₂ concentration was 591mg/MJ at 21% oxygen concentration, increased up to 724mg/MJ at 25% O₂, then decreased down to 272mg/MJ. The small particle size of the adsorbents resulted in their fast leaving of the bed before their complete reaction with SO₂ emission. CO₂ emission increased from 14% to 19% due to increase in oxygen concentration. That was because combustion in oxygen-enriched atmosphere resulted in complete combustion of the fuel.

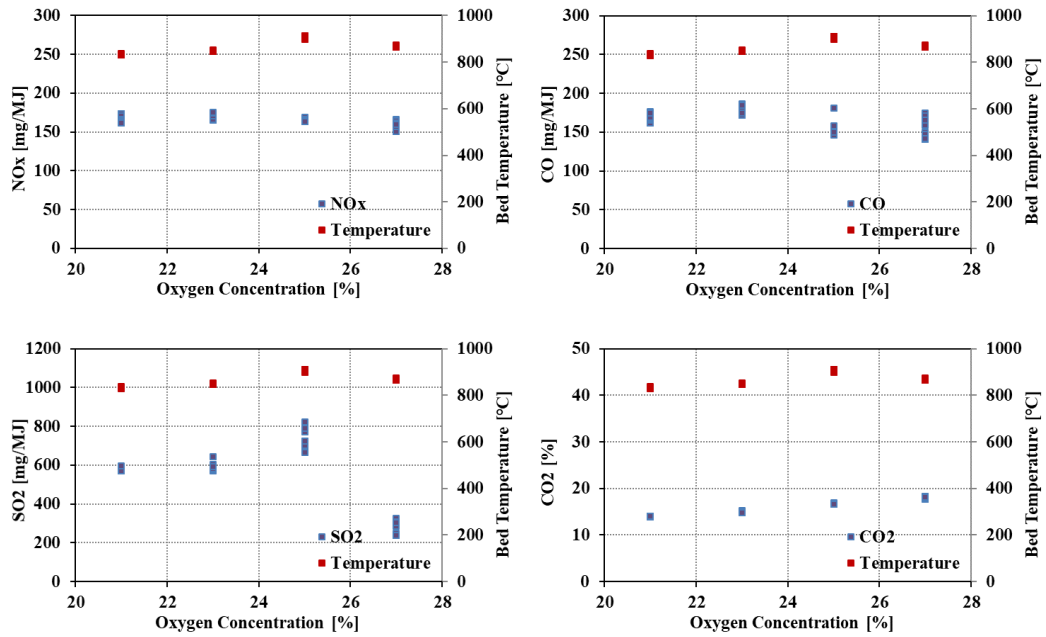


Figure 4.41. Effect of oxygen concentration on flue gas emissions in the combustion of Orhaneli lignite and Çan limestone at Ca/S = 1.5 and Particle size of 0-1 mm

4.2.1.2. Limestone Particle Size = 0-1 mm; Ca/S Ratio = 2

In the next case, the Ca/S ratio was increased from 1.5 to 2 while all other parameters were kept the same as before. The results of the temperature profiles along the combustor and the return leg are given in Figure 4.42. The highest temperature value was measured at about 1.2 m above the distributor plate for the oxygen concentration of 25% as 847°C. The maximum temperature decreased by increasing the Ca/S ratio by about 30°C and the height at which this maximum occurred shifted from 32 cm above the distributor plate to 1.2 m. This can be explained by increasing the amount of adsorbent in the bed which caused the slower combustion process. The highest temperature at the top of the bed was about 770°C at oxygen concentration of 21% which was higher than the combustion at Ca/S=1.5 by about 40°C. The temperature profiles at the return leg decreased with the increase of oxygen concentration. Due to increase in the amount of Ca-based sorbent in the bed, the carbon-based efficiency

was decreased from 96.5% to 93.57%. It can be concluded that increasing the Ca/S ratio resulted in decrease of the bed temperature at the dense region and its increase at the top of the bed.

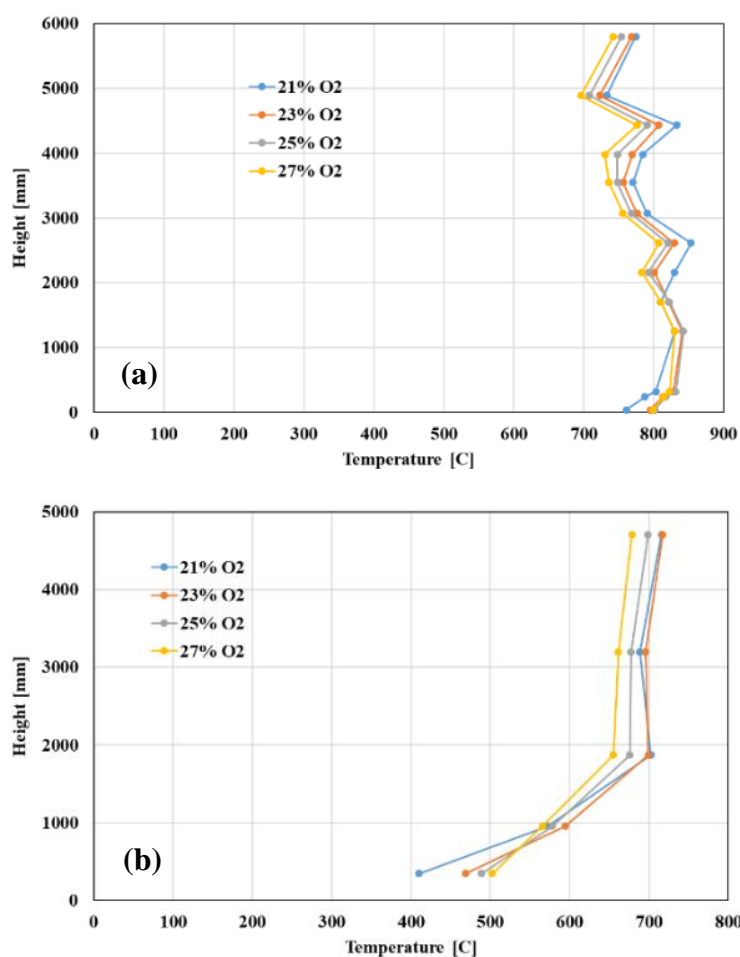


Figure 4.42. Temperature profile along (a) combustor and (b) return leg in the combustion of Orhaneli lignite and Çan limestone at Ca/S = 2 and Particle size of 0-1 mm

The effect of oxygen concentration on NO_x, CO, SO₂, and CO₂ emissions are shown in Figure 4.43. NO_x emission values slightly decreased from 162mg/MJ to 143mg/MJ with the increase of oxygen concentration. This decrease can be explained by lower

temperature due to increase of Ca/S ratio. On the other hand, CO emission values showed a slight increase from about 89mg/MJ to 136mg/MJ with the increase in oxygen concentrations. The adverse trend of NO_x and CO can be attributed to NO reduction reactions [105]. The concentration of CO was lower than that of the Ca/S=1.5 which can be attributed to lower carbon-based efficiency. SO₂ emission decreased from about 521mg/MJ at 21% O₂ to around 204mg/MJ at 27% O₂. Comparison of the Figure 4.41 and Figure 4.43 showed that increasing the Ca/S ratio from 1.5 to 2 resulted in the decrease in SO₂ emission by about 50%. CO₂ emission increased from about 14% to 19% by increasing the oxygen concentration. In summary, it can be concluded that increasing Ca/S ratio from 1.5 to 2 resulted in the decrease of NO_x, CO, and SO₂ emissions.

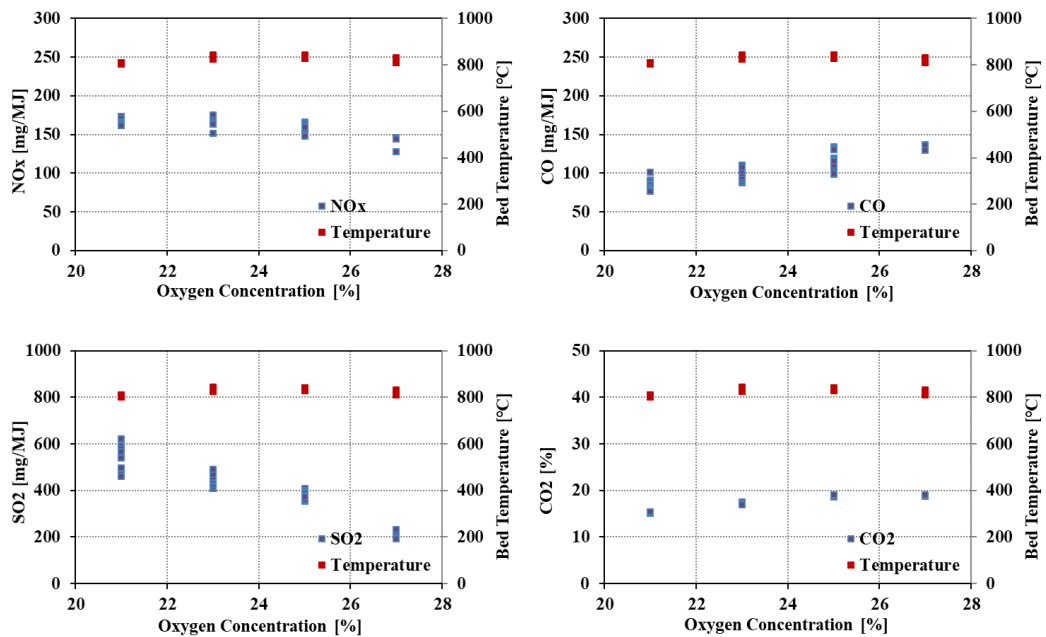


Figure 4.43. Effect of oxygen concentration on flue gas emissions in the combustion of Orhaneli lignite and Çan limestone at Ca/S = 2 and Particle size of 0-1 mm

4.2.1.3. Limestone Particle Size = 1-2 mm; Ca/S Ratio = 1.5

In this set of experiments, bigger particle sizes of the adsorbent were used (1-2 mm). The fuel feeding rate was about 4.5 kg/h at steady state condition. The superficial velocity inside the bed was 2.60 m/s and the carbon-based efficiency was 96.3%. Increasing the adsorbent particle size did not have a significant impact on the combustion efficiency. The temperature profiles throughout the bed and the return leg for the combustion of Orhaneli lignite and Çan limestone at Ca/S ratio of 1.5 are shown in Figure 4.44. The highest temperature value was measured at about 32cm above the distributor plate for the oxygen concentration of 27% as 892°C. The highest temperature at the top of the bed was about 770°C at oxygen concentration of 21%. The temperature profiles at the return leg decreased with the increase of oxygen concentration. Increasing the adsorbent particle size did not have a significant impact on the bed temperature distribution and the results were comparable with the case of smaller particle size experiments.

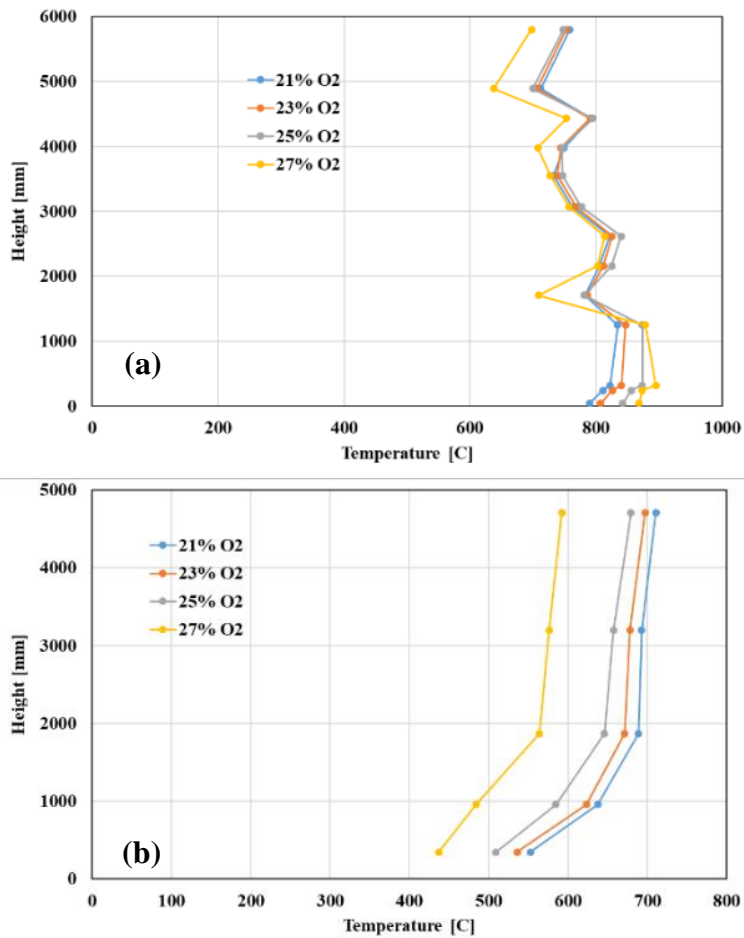


Figure 4.44. Temperature profile along (a) combustor and (b) return leg in the combustion of Orhaneli lignite and Çan limestone at Ca/S = 1.5 and Particle size of 1-2 mm

Figure 4.45 shows the effect of oxygen concentration on NO_x, CO, SO₂, and CO₂ emissions. The variation of NO_x and CO emissions at different oxygen concentrations were in the range of 101mg/MJ to 152mg/MJ and 107mg/MJ to 146mg/MJ, respectively. NO_x emission was highest at 27% oxygen concentration which can be attributed to high temperature of the bed at around 840°C. Increasing the particle size enhanced the adsorption of SO₂ emission by about 60%. The highest SO₂ emission in this case was 223mg/MJ at 21% oxygen concentration and decreased to 189mg/MJ by increasing O₂ to 27%. That was because the bigger particle sizes remained longer in the bed which allowed them for further reaction with SO₂ emission. CO₂ emission was in the range of 15% to 20%.

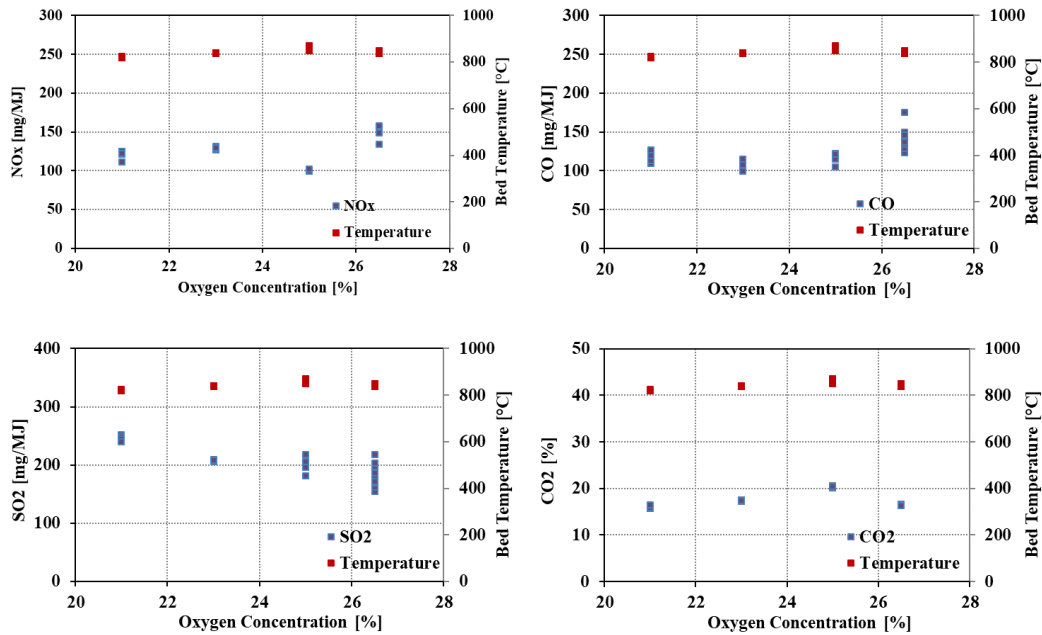


Figure 4.45. Effect of oxygen concentration on flue gas emissions in the combustion of Orhaneli lignite and Çan limestone at Ca/S = 1.5 and Particle size of 1-2 mm

4.2.1.4. Limestone Particle Size = 1-2 mm; Ca/S Ratio = 2

In this set of experiments, bigger particle sizes of the adsorbent were used (1-2 mm) and the Ca/S ratio was increased to 2. The fuel feeding rate was about 4.8 kg/h at steady state condition. The superficial velocity inside the bed was 2.80 m/s and the carbon-based efficiency was 94.06%. Increasing the Ca/S ratio showed a negative impact on the combustion efficiency and decreased its value by about 2%. Figure 4.46 represents the temperature profiles along the combustor and the return leg for the combustion of Orhaneli lignite and Çan limestone at Ca/S = 2 and adsorbent particle size of 1-2 mm. The highest temperature value was measured at about 1.2 m above the distributor plate for the oxygen concentration of 27% as 853°C. The maximum temperature decreased by increasing the Ca/S ratio by about 40°C and the height at which this maximum occurred, shifted from 32 cm above the distributor plate to 1.2 m. Increasing the adsorbent particle size did not have a significant impact on the

temperature distribution of the bed. The highest temperature at the top of the bed was about 720°C which was lower than the combustion at Ca/S=1.5 by about 25°C.

The temperature profiles at the return leg decreased with the increase of oxygen concentration. The highest temperature profile was measured for the 21% oxygen concentration and was about 655°C at the top of the return leg and decreased to 490°C at the re-entry location. It can be concluded that increasing the Ca/S ratio resulted in decrease of the reactor temperature at the dense region and top of the bed.

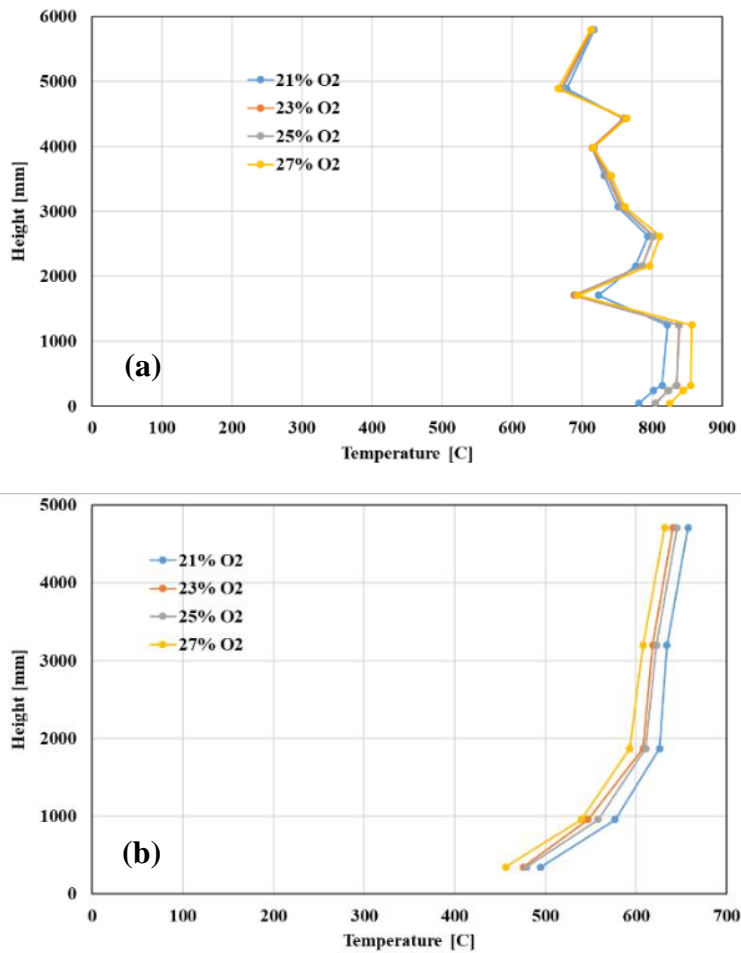


Figure 4.46. Temperature profile along (a) combustor and (b) return leg in the combustion of Orhaneli lignite and Çan limestone at Ca/S = 2 and Particle size of 1-2 mm

The effect of oxygen concentration on NO_x, CO, SO₂, and CO₂ emissions are shown in Figure 4.47. NO_x emission values were approximately similar to that of the Ca/S=1.5 and were changed from 121mg/MJ to 149mg/MJ by increasing the oxygen concentration. On the other hand, at Ca/S=2, CO emission doubled comparing to Ca/S=1.5. This increase was more significant at lower oxygen concentrations. CO emission values ranged from 178mg/MJ to 277mg/MJ with the minimum in oxygen concentration of 25%. Comparing the results between Ca/S ratios of 1.5 and 2 at particle size of 1-2 mm, it can be seen that there was a significant improvement in SO₂ retention especially at higher oxygen concentrations. SO₂ emission decreased dramatically from 294mg/MJ at 21% O₂ to 49mg/MJ at 27% O₂. It can be concluded that the Ca/S ratio of 2 and adsorbent particle size of 1-2mm had superior effect on SO₂ adsorption. CO₂ emission increased from about 15% to 19% due to increase in oxygen concentration.

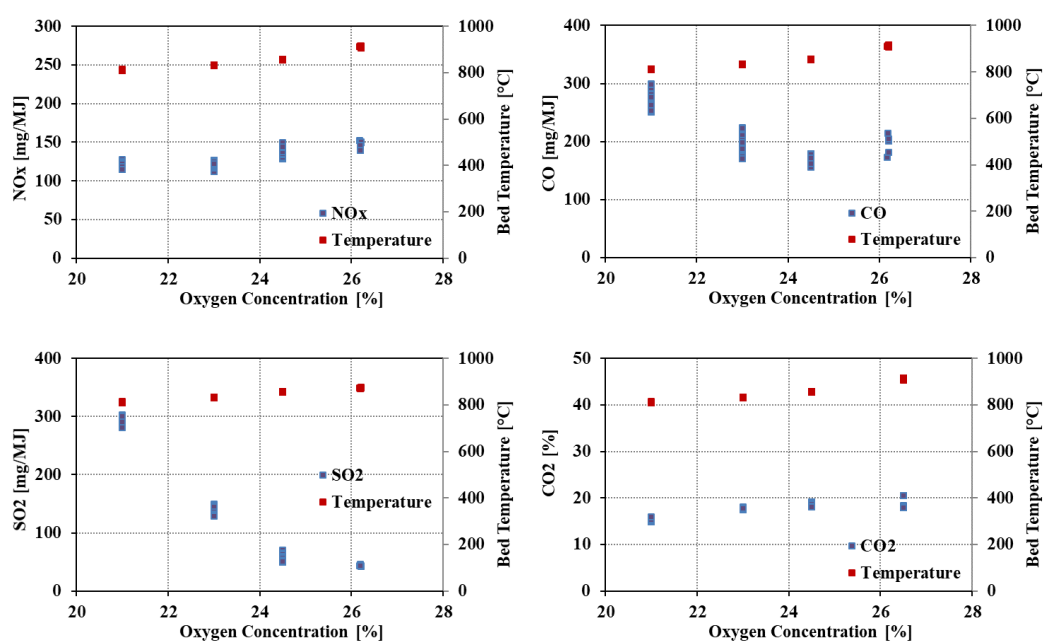


Figure 4.47. Effect of oxygen concentration on flue gas emissions in the combustion of Orhaneli lignite and Çan limestone at Ca/S = 2 and Particle size of 1-2 mm

Table 4.17 summarizes the obtained results for the emissions of the combustion of Orhaneli and Çan limestone at different conditions. It can be seen that increasing the adsorbent particle size and Ca/S ratio enhanced the SO₂ adsorption. Furthermore, at elevated oxygen concentrations, the adsorption of SO₂ was higher. Comparing the obtained results with the results of the combustion with no addition of the Ca-based sorbents (Table 4.16), it can be concluded that in-situ addition of limestone had a significant impact on SO₂ removal. The effect on NO_x, CO, and CO₂ emissions was not noticeable. The only adverse effect of limestone addition was the decrease of carbon-based efficiency of the reactor.

Table 4.17. Emissions of the combustion of Orhaneli lignite and Çan limestone at different conditions

Atmosphere	Particle Size (mm)	Ca/S ratio	NO_x [mg/MJ]	CO [mg/MJ]	SO₂ [mg/MJ]	CO₂ [%]
Air	0-1	1.5	162	165	591	14
23% O ₂	0-1	1.5	166	174	605	15
25% O ₂	0-1	1.5	162	159	724	17
27% O ₂	0-1	1.5	158	155	272	19
Air	0-1	2	162	89	521	14
23% O ₂	0-1	2	164	98	446	17
25% O ₂	0-1	2	156	122	391	19
27% O ₂	0-1	2	143	136	204	19
Air	1-2	1.5	115	121	223	16
23% O ₂	1-2	1.5	126	107	207	18
25% O ₂	1-2	1.5	101	110	201	20
27% O ₂	1-2	1.5	152	146	189	17
Air	1-2	2	121	277	294	15
23% O ₂	1-2	2	121	198	119	18
25% O ₂	1-2	2	142	178	61	19
27% O ₂	1-2	2	149	198	49	19

4.2.2. Combustion of Orhaneli Lignite and Eskişehir Dolomite in Enriched Oxygen Atmosphere

4.2.2.1. Dolomite Particle Size = 0-1 mm; Ca/S Ratio = 1.5

The combustion test of Orhaneli lignite and Eskişehir dolomite adsorbent was performed in the CFBC under different oxygen-enriched environments. At the steady-state condition, fuel feeding rate was about 4.0 kg/h. The superficial velocity inside the bed was 2.50 m/s and the carbon-based efficiency was 85.98%. Dolomite significantly decreased the carbon conversion efficiency due to the fact that dolomite contains MgCO_3 component which does not play a role on SO_2 adsorption but resulted in increase of the unburnt material in the bed. The temperature profiles throughout the reactor and the return leg for the combustion of Orhaneli lignite and Eskişehir dolomite at Ca/S ratio of 1.5 and adsorbent particle size interval of 0-1mm are shown in Figure 4.48. The highest temperature value was measured at about 32cm above the distributor plate for the oxygen concentration of 27% as 875°C. This temperature was lower than the obtained temperature in the presence of limestone by about 35°C. The temperature at the dense region of the bed increased with the increase of the oxygen concentration by about 120°C. The highest temperature at the top of the bed was about 750°C at oxygen concentration of 23%. The measured temperature at the top of the bed were higher than the combustion in the presence of limestone by about 40°C indicating that the combustion process completed at higher levels in the presence of dolomite.

The temperature profiles along the return leg were measured from the bottom of the cyclone down to recirculated gas re-entry. The temperature at the top of the return leg was in the range of 660-720°C at different oxygen concentrations and decreased along the return leg. The highest temperature profile was measured for the 23% oxygen concentration and was about 720°C at the top of the return leg and decreased to 555°C at the re-entry location. The temperature profiles in the return leg were higher than that of using limestone as adsorbent.

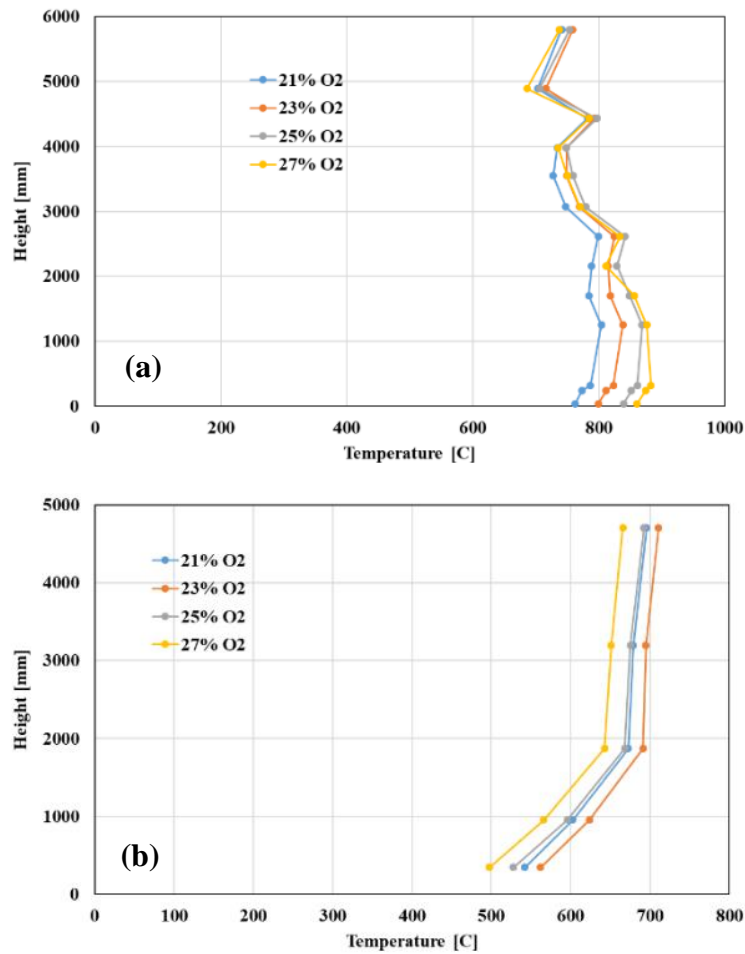


Figure 4.48. Temperature profile along (a) combustor and (b) return leg in the combustion of Orhaneli lignite and Eskişehir dolomite at Ca/S = 1.5 and Particle size of 0-1 mm

The effect of oxygen concentration on NO_x, CO, SO₂, and CO₂ emissions are shown in Figure 4.49. It can be seen that the variation of NO_x emission slightly increased from 141mg/MJ to 152mg/MJ with the increase of oxygen concentration. This can be attributed to the increase of the bed temperature in oxygen-enriched conditions. On the other hand, CO emission showed a decrease from about 151mg/MJ to 92mg/MJ with the increase in oxygen concentrations due to complete combustion. CO emission values were lower in the presence of dolomite than limestone. SO₂ concentration was 1091mg/MJ at 21% oxygen concentration, decreased to 567mg/MJ at 25% O₂, then

showed a slight increase up to 674mg/MJ. Comparing the results with the results of Çan limestone indicated that the dolomite sample had inferior impact on SO₂ adsorption due to the fact that in dolomite the magnesium oxide does not react with sulfur dioxide. The addition of dolomite with the particle size of 0-1 mm and Ca/S ratio of 1.5 resulted in negligible amount of SO₂ removal in 21% O₂ (1223mg/MJ in no dolomite and 1091mg/MJ with dolomite), however, at higher oxygen concentrations a considerable retention of SO₂ was noticed. The insignificant retention of SO₂ at air combustion (21% O₂) can be attributed to poor calcination of dolomite at lower bed temperatures. The small particle size of the adsorbents resulted their fast leaving of the bed before their complete reaction with SO₂ emissions. CO₂ emission increased from 14% to 19% due to increase in oxygen concentration. That was because combustion in oxygen-enriched atmosphere resulted in complete combustion of the fuel.

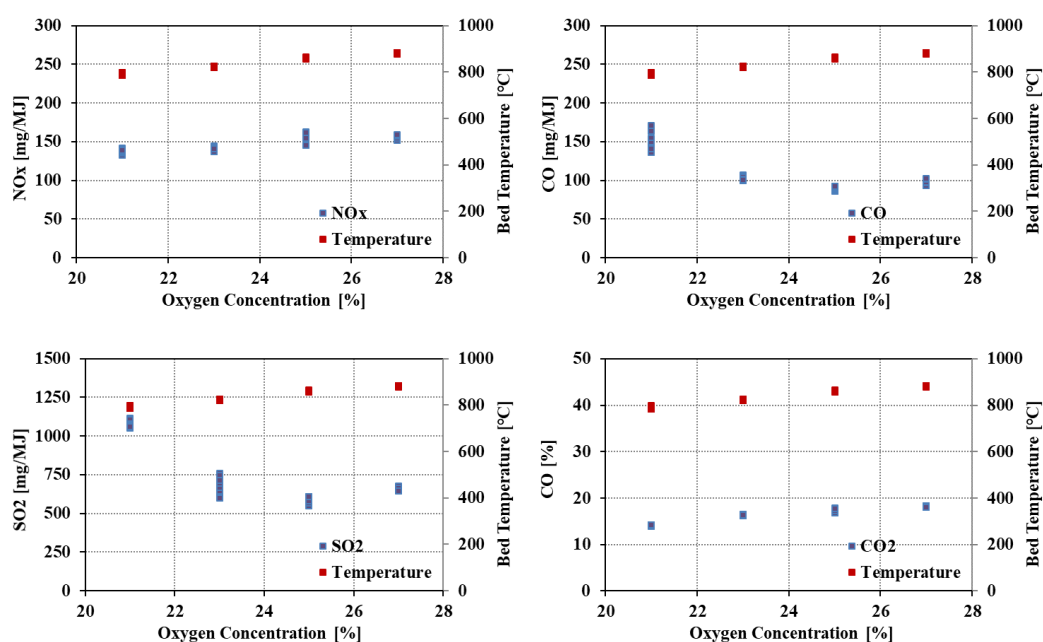


Figure 4.49. Effect of oxygen concentration on flue gas emissions in the combustion of Orhaneli lignite and Eskişehir dolomite at Ca/S = 1.5 and Particle size of 0-1 mm

4.2.2.2. Dolomite Particle Size = 0-1 mm; Ca/S Ratio = 2

In the next case, the Ca/S ratio was increased from 1.5 to 2 while all other parameters were kept the same as before. Figure 4.50 represents the temperature profiles along the combustor and the return leg for the combustion of Orhaneli lignite and Eskişehir dolomite at Ca/S= 2 and adsorbent particle size of 0-1mm. The highest temperature value was measured at about 1.2 m above the distributor plate for the oxygen concentration of 25% as 873°C. The level at which this maximum occurred shifted from 32 cm above the distributor plate to 1.2 m. The temperature at the top of the reactor was in the range of 710°C and 750°C. The temperature profiles at the return leg decreased with the increase of oxygen concentration. Due to increase in the amount of Ca-based sorbent in the bed, the carbon-based efficiency was decreased from 85.98% to 79.55%. This decrease can be attributed to the presence of higher quantities of MgCO₃ in the bed

The effect of oxygen concentration on NO_x, CO, SO₂, and CO₂ emissions are shown in Figure 4.51. NO_x emission values slightly increased from 140mg/MJ to 154mg/MJ with the increase of oxygen concentration due to increase in bed temperature. On the other hand, CO emission values showed a slight decrease from 159mg/MJ to 91mg/MJ with the increase in oxygen concentrations. The lowest value of CO was obtained in 25% O₂. Increasing the Ca/S ratio did not affect the NO_x and CO emissions. SO₂ emission decreased from 1043mg/MJ at 21% O₂ to 356mg/MJ at 25% O₂. Comparison of the Figure 4.49 and Figure 4.51 showed that increasing the Ca/S ratio from 1.5 to 2 resulted the decrease in SO₂ emission be about 35% at higher oxygen concentrations. CO₂ emission increased from about 14% to 19% due to increase in oxygen concentration.

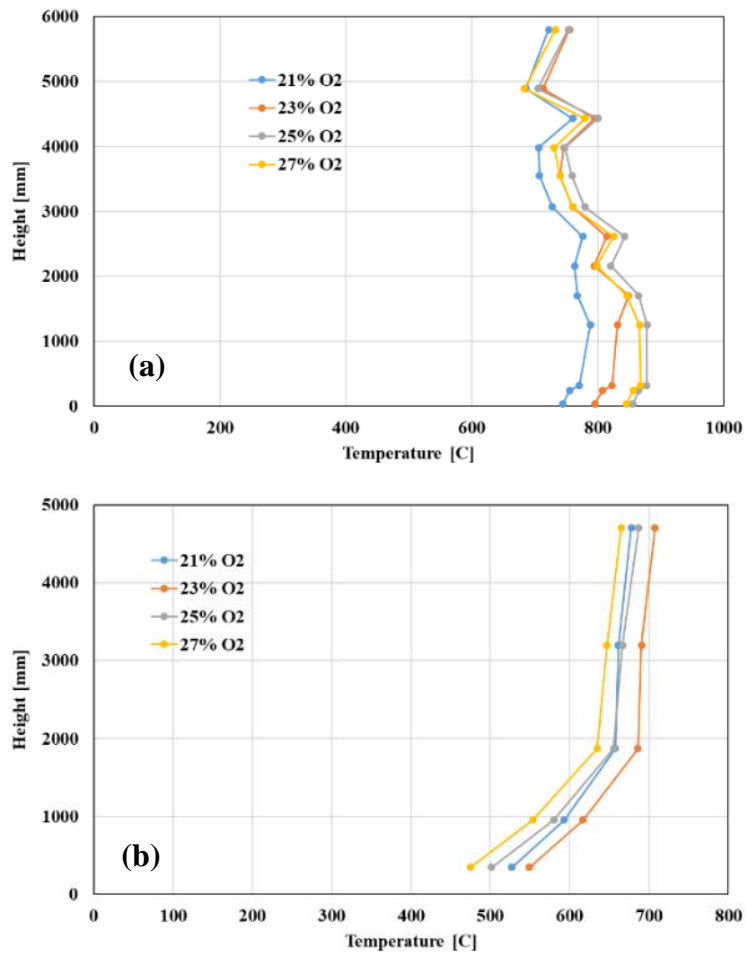


Figure 4.50. Temperature profile along (a) combustor and (b) return leg in the combustion of Orhaneli lignite and Eskişehir dolomite at $Ca/S = 2$ and Particle size of 0-1 mm

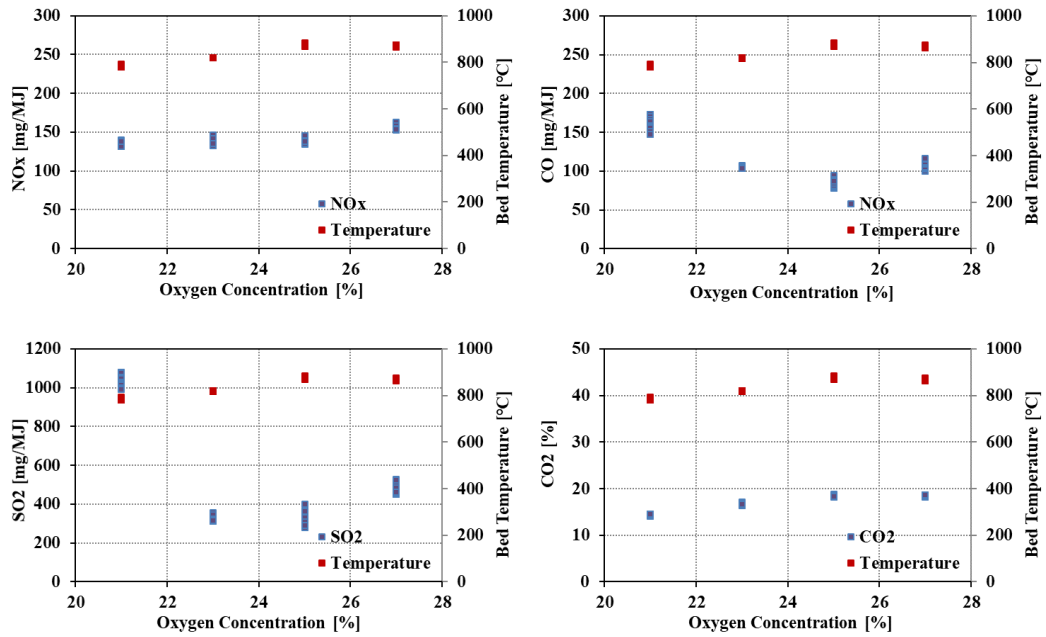


Figure 4.51. Effect of oxygen concentration on flue gas emissions in the combustion of Orhaneli lignite and Eskişehir dolomite at Ca/S = 2 and Particle size of 0-1 mm

4.2.2.3. Dolomite Particle Size = 1-2 mm; Ca/S Ratio = 1.5

In this set of experiments, bigger particle sizes of the adsorbent were used (1-2 mm). The fuel feeding rate was about 6.0 kg/h at steady state condition. The superficial velocity inside the bed was 2.70 m/s and the carbon-based efficiency was 95.06%. Increasing the adsorbent particle size resulted a significant increase in the carbon-based efficiency by about 10%. The temperature profiles throughout the bed and the return leg for the combustion of Orhaneli lignite and Eskişehir dolomite at Ca/S ratio of 1.5 and adsorbent particle size interval of 1-2mm are given in Figure 4.52. The highest temperature value was measured at about 32cm above the distributor plate for the oxygen concentration of 25% as 882°C. The highest temperature at the top of the reactor was about 763°C at oxygen concentration of 23%. The temperature profiles at the return leg decreased with the increase of oxygen concentration. Increasing the adsorbent particle size did not showed a significant effect on the bed temperature

distribution and the results were comparable with the case of smaller particle size experiments.

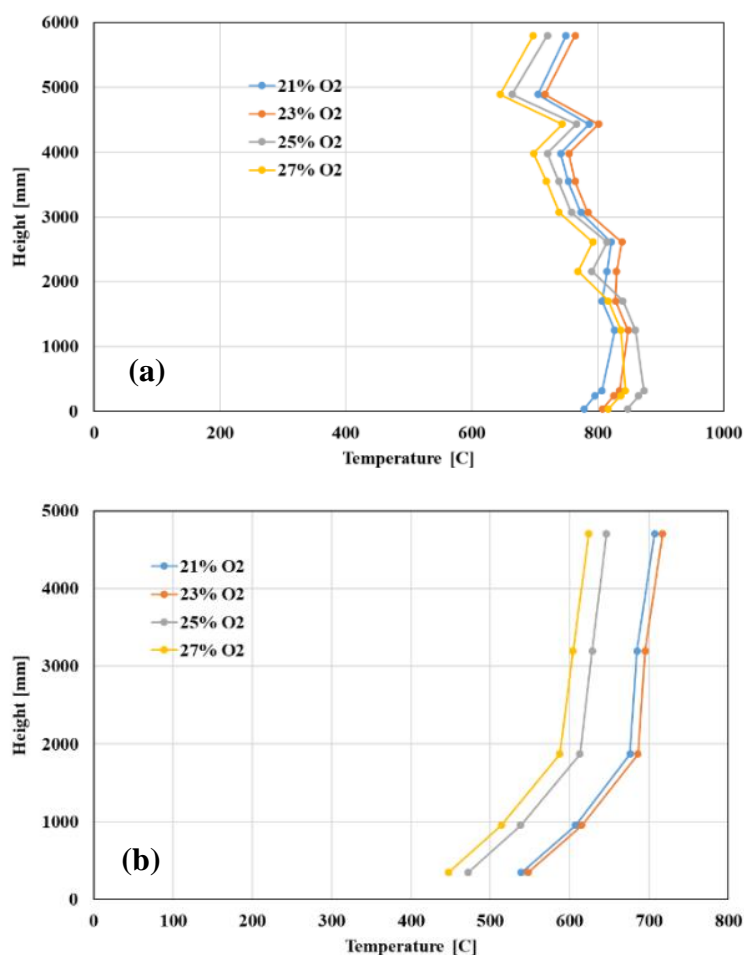


Figure 4.52. Temperature profile along (a) combustor and (b) return leg in the combustion of Orhaneli lignite and Eskişehir dolomite at $Ca/S = 1.5$ and Particle size of 1-2 mm

Figure 4.53 shows the effect of oxygen concentration on NO_x , CO, SO_2 , and CO_2 emissions. NO_x emission increased with the increase of the oxygen concentrations from 141mg/MJ up to 196mg/MJ. Also, the obtained results indicated that CO emissions increased with the increase of the oxygen concentrations from 112mg/MJ

up to 283mg/MJ. This sharp increase in the value of CO was due to incomplete combustion at 27% O₂. As can be seen CO₂ emission was lower at 27 O₂ as well indicating an incomplete combustion. SO₂ emission were at around 160mg/MJ at 21% O₂, 23% O₂ and 25% O₂ but showed a sudden increase up to about 347mg/MJ at 27% O₂. The obtained values in the case of 27% oxygen concentrations were believed to be an experimental error. The larger particle size allowed the dolomite particles to stay longer inside the bed and the SO₂ adsorption enhanced. Comparing the SO₂ results with the results of the 0-1mm particle size showed that the SO₂ emission decreased more than 55%. CO₂ emission was in the range of 16% to 18%.

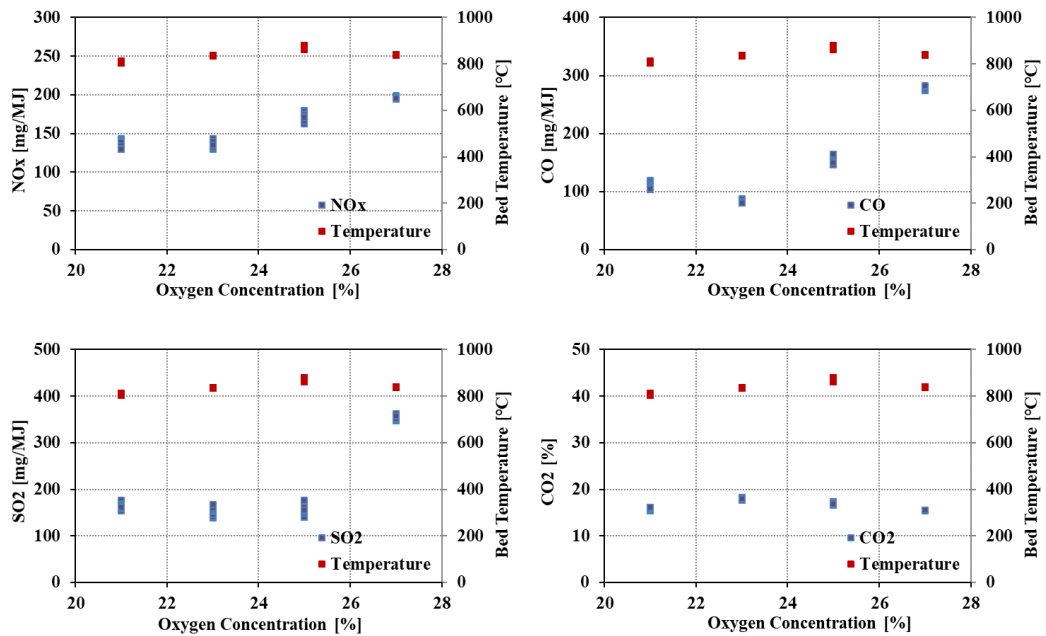


Figure 4.53. Effect of oxygen concentration on flue gas emissions in the combustion of Orhaneli lignite and Eskişehir dolomite at Ca/S = 1.5 and Particle size of 1-2 mm

4.2.2.4. Dolomite Particle Size = 1-2 mm; Ca/S Ratio = 2

In this set of experiments, bigger particle sizes of the adsorbent were used (1-2 mm) and the Ca/S ratio was increased to 2. The fuel feeding rate was about 4.6 kg/h at steady state condition. The superficial velocity inside the bed was 2.80 m/s and the carbon-based efficiency was 89.55%. Increasing the Ca/S ratio showed a negative impact on the carbon-based efficiency and decreased its value by about 5%. Figure 4.54 represents the temperature profiles along the combustor and the return leg for the combustion of Orhaneli lignite and Çan limestone at Ca/S = 2 and adsorbent particle size of 1-2 mm. The highest temperature value was measured at about 32cm above the distributor plate for the oxygen concentration of 27% as 897°C. The highest temperature at the top of the reactor was about 731°C at 23%O₂. The temperature profiles at the return leg decreased with the increase of oxygen concentration. The highest temperature profile was measured for the 23% oxygen concentration and was about 688°C at the top of the return leg and decreased to 523°C at the re-entry location. It can be concluded that increasing the Ca/S ratio resulted in decrease of the bed temperature both at the dense region and top of the reactor.

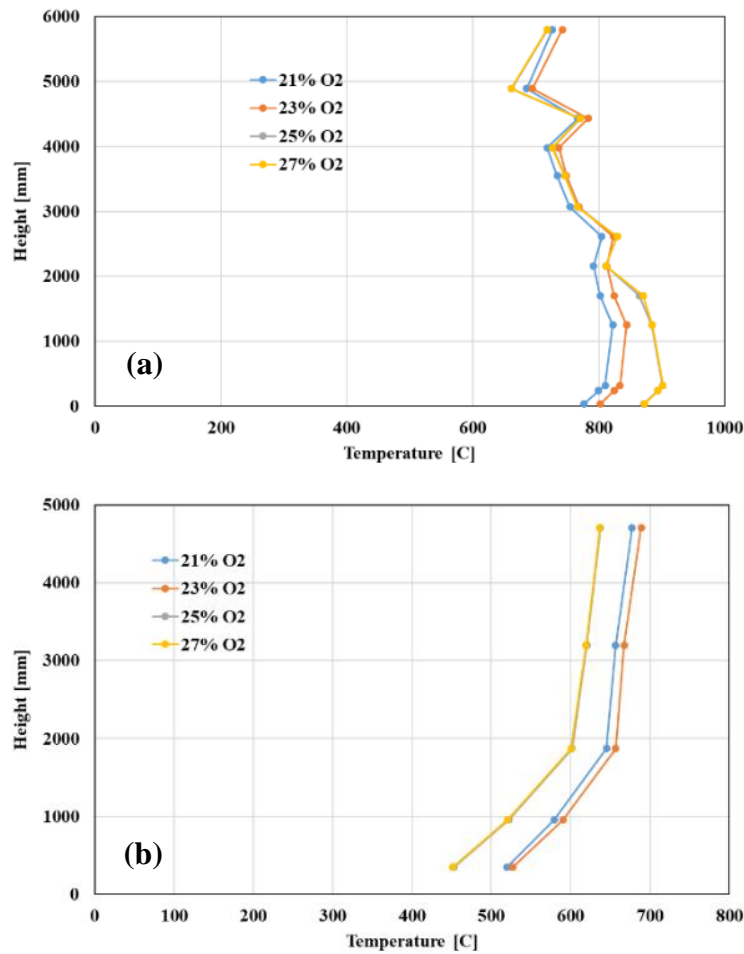


Figure 4.54. Temperature profile along (a) combustor and (b) return leg in the combustion of Orhaneli lignite and Eskişehir dolomite at Ca/S= 2 and Particle size of 1-2 mm

The effect of oxygen concentration on NO_x, CO, SO₂, and CO₂ emissions are shown in Figure 4.55. NO_x emission values were approximately similar to that of the Ca/S=1.5 and changed from 144mg/MJ to 172mg/MJ by increasing the oxygen concentration. On the other hand, CO emission values decreased from 176mg/MJ to 106mg/MJ with the increase in oxygen concentrations from 21% to 23% and increased up to 201mg/MJ at 27% O₂. SO₂ emission decreased dramatically from about 243mg/MJ at 21% O₂ to around 105mg/MJ at 27% O₂. Comparing the results between Ca/S ratios of 1.5 and 2 at particle size of 1-2 mm, it can be concluded that the decrease

in SO₂ adsorption due to increase in Ca/S ratio was not as much effective as it was in the addition of limestone. CO₂ emission increased from about 15% to 18% due to increase in oxygen concentration.

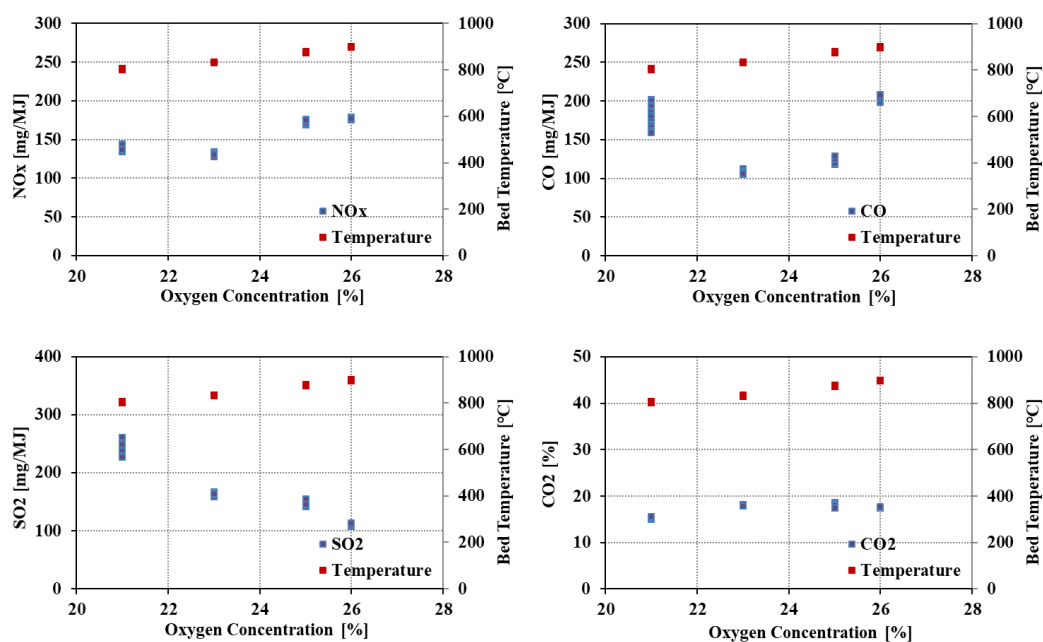


Figure 4.55. Effect of oxygen concentration on flue gas emissions in the combustion of Orhaneli lignite and Eskişehir dolomite at Ca/S = 2 and Particle size of 1-2 mm

Table 4.18 summarizes the obtained results for the emissions of the combustion of Orhaneli and Eskişehir dolomite at different conditions. It can be seen that increasing the adsorbent particle size and Ca/S ratio enhanced the SO₂ retention. Furthermore, at elevated oxygen concentrations, the SO₂ retention was higher. Comparing the obtained results with the results of the combustion with no addition of the Ca-based sorbents, it can be concluded that in-situ addition of dolomite had a significant impact on SO₂ removal. However, it was found that limestone had superior impact on SO₂ retention than dolomite. The effect on NO_x, CO, and CO₂ emissions was not

noticeable. The in-situ addition of dolomite resulted in significant decrease of carbon-based efficiency, especially, at finer particle sizes.

Table 4.18. Emissions of the combustion of Orhaneli lignite and Eskişehir dolomite at different conditions

Atmosphere	Particle Size (mm)	Ca/S ratio	NO_x [mg/MJ]	CO [mg/MJ]	SO₂ [mg/MJ]	CO₂ [%]
Air	0-1	1.5	141	151	1091	14
23% O ₂	0-1	1.5	144	103	682	16
25% O ₂	0-1	1.5	152	92	567	17
27% O ₂	0-1	1.5	152	98	674	19
Air	0-1	2	140	159	1043	14
23% O ₂	0-1	2	144	105	358	16
25% O ₂	0-1	2	145	91	356	19
27% O ₂	0-1	2	154	106	454	19
Air	1-2	1.5	141	112	171	16
23% O ₂	1-2	1.5	141	92	158	18
25% O ₂	1-2	1.5	162	149	162	17
27% O ₂	1-2	1.5	196	283	347	16
Air	1-2	2	144	176	243	15
23% O ₂	1-2	2	138	106	157	18
25% O ₂	1-2	2	167	117	149	18
27% O ₂	1-2	2	172	201	105	18

4.2.3. Oxy-fuel combustion of Orhaneli lignite

The CFBC was retrofitted to operate under oxy-fuel combustion conditions as well. Oxygen and carbon dioxide tanks were installed with their respective mass flow controllers and measurement units. In order to recirculate the exhaust gas into the system, the oxy-fuel combustion line was added after the ID fan. The location of oxy-fuel combustion line can be seen in Figure 3.7. A fan was connected to re-introduce the exhaust gas to the system. The control user interface of the system was modified to incorporate the controls of the mass flow, temperature and pressure transmitters, and fan of the oxy-fuel combustion line as well.

The emission values in the oxy-fuel combustion of Orhaneli lignite at different excess air ratios are given in Table 4.19. These results were obtained when no sulfur adsorbent was introduced to the bed. As can be seen the SO₂ concentrations were in the range of 771mg/MJ and 490mg/MJ and decreased with the increase of the excess air ratio. The carbon-based efficiency was 98.77%. Comparing the results with the data obtained for Orhaneli lignite in air combustion condition (Table 4.16), it was seen that the SO₂ concentration in oxy-fuel combustion condition was lower.

Table 4.19. Emissions of Orhaneli lignite under oxy-fuel combustion conditions at different excess air ratios

Lambda	Bed temperature [°C]	NO_x [mg/MJ]	CO [mg/MJ]	SO₂ [mg/MJ]	CO₂ [%]
1.07	687	29.7	409	771	70
1.13	687	29.9	224	712	74
1.22	695	31.0	149	658	78
1.33	723	34.1	105	613	83
1.35	723	34.1	107	615	84
1.49	688	33.2	99	599	91
1.77	728	35.6	60	490	96

4.2.3.1. Addition of Çan limestone

The oxy-fuel combustion test of Orhaneli lignite and Çan limestone adsorbent was performed in the CFBC under different excess air ratios. The adsorbent particle size was 0-1 mm and Ca/S ratio was 2. At the steady-state condition, fuel feeding rate was about 4.6 kg/h. The superficial velocity inside the bed was 2.80 m/s and the carbon-based efficiency was 92.02%. Addition of limestone resulted in the decrease of carbon-based efficiency in oxy-fuel condition by about 8%. Figure 4.56 represents the temperature profiles along the combustor and the return leg. As can be seen, the temperature increased along the combustor from about 700°C up to 750°C. This was in contrast with combustion in air and oxygen-enriched conditions in which the highest temperatures were seen in the dense region. This was due to the fact that in

this experiment the reactor temperature could not have been risen to temperatures higher than 800°C because of some limitations in the operating system.

The temperature at the top of the combustor indicated that the combustion process was completed at higher levels inside the bed. Increasing the excess air ratio resulted in slight decrease in temperature profile in the combustor. The temperature profile at the top of the return leg was between 702-722°C and decreased to 570°C at the recirculated gas re-entry. Due to the increase in excess air ratio, a slight decrease in the temperature profile was noticed.

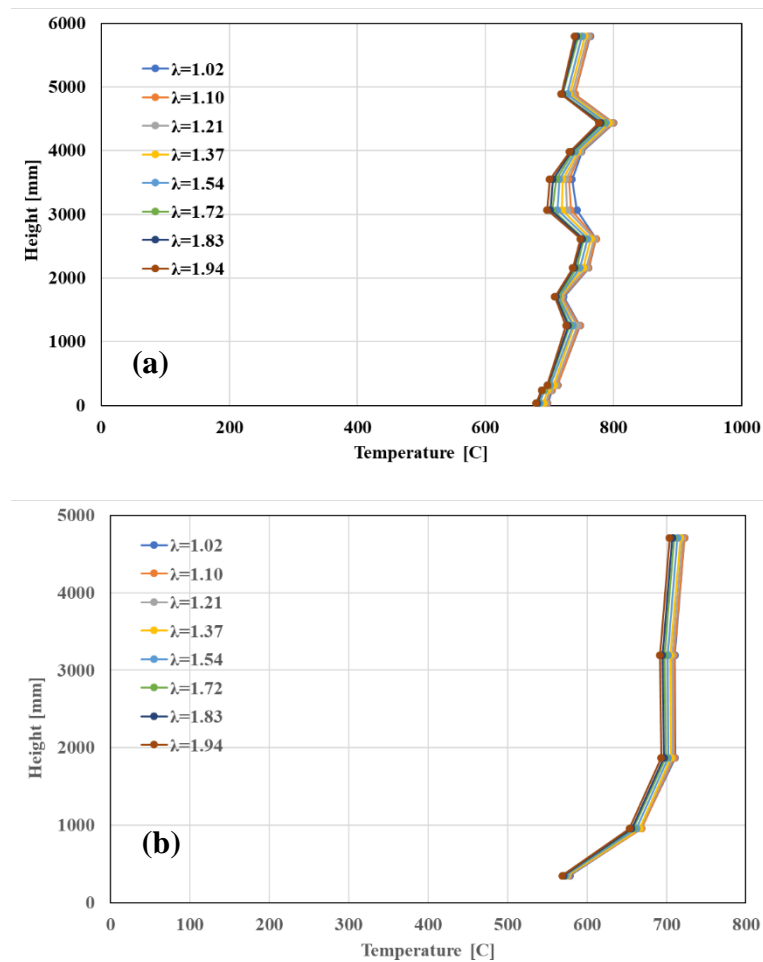


Figure 4.56. Temperature profile along (a) combustor and (b) return leg under oxy-fuel combustion of Orhaneli lignite and Çan limestone at Ca/S= 2 and Particle size of 0-1 mm

Figure 4.57 shows NO_x , CO, SO_2 , and CO_2 emissions and bed temperature for oxy-fuel combustion of Orhaneli lignite and Çan limestone at different excess air ratios. NO_x emission concentration was approximately constant in the range of 26.8mg/MJ to 34.0mg/MJ showing a slight increase with the increase of excess air ratio. The concentration of NO_x was significantly lower than combustion in air due to the fact that in oxy-fuel conditions the nitrogen does not enter into the combustor. The impact of limestone addition on NO_x concentration was insignificant. On the other hand, addition of limestone resulted in CO emission concentration increase due to incomplete combustion which can be attributed to the lower carbon-based efficiency. The decrease of CO emission at higher excess air ratios was due to reaction of CO and oxygen producing CO_2 [101].

The reaction mechanism between SO_2 and limestone is a function of CO_2 partial pressure and bed temperature. In oxy-fuel combustion condition, due to high concentration of CO_2 , the indirect sulfation reaction takes place. The SO_2 concentration was 807mg/MJ at $\lambda=1.02$ and decreased to 349mg/MJ at $\lambda=1.94$. Comparing these results with the results obtained for the case with no addition of adsorbent (Table 2.1), it was seen that SO_2 retention process did not occur. That was because at temperatures around 700°C the sulfation reaction did not take place [50]. CO_2 emission increased from 65% at $\lambda=1.02$ up to 100% at $\lambda>1.7$. Based on the obtained results, it can be concluded that in order to achieve the oxy-fuel combustion with CO_2 concentrations of more than 90% as well as reasonable concentrations of other emissions, the excess air ratio needs to be higher than 50%.

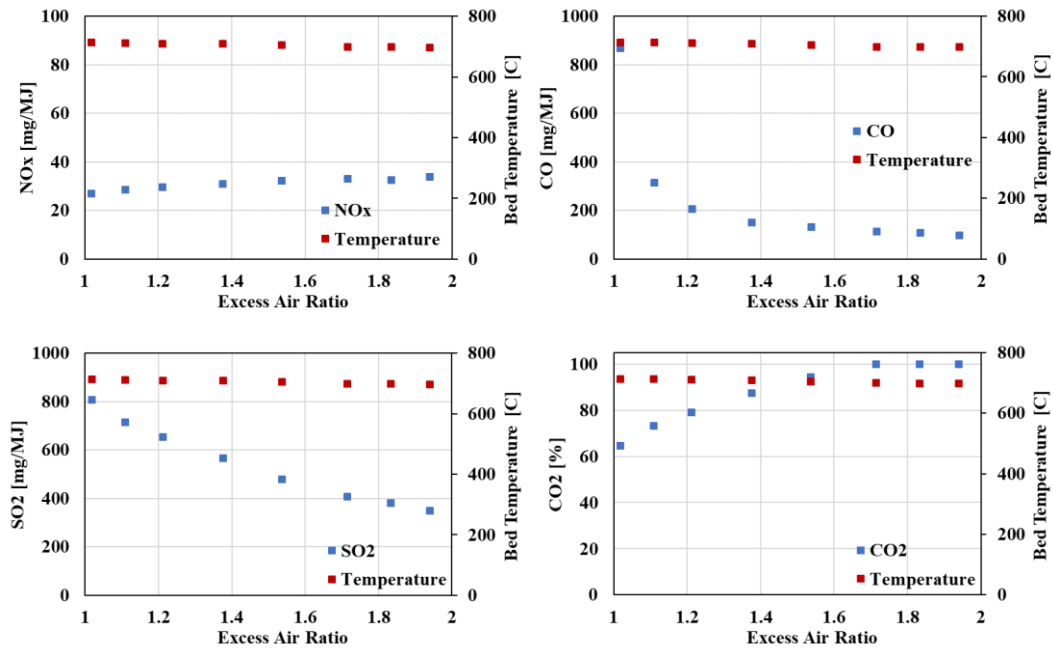


Figure 4.57. Flue gas emissions under oxy-fuel combustion of Orhaneli lignite and Çan limestone at Ca/S = 2 and Particle size of 0-1 mm

4.2.3.2. Addition of Eskişehir Dolomite

The oxy-fuel combustion test of Orhaneli lignite and Eskişehir dolomite adsorbent was performed in the CFBC under different excess air ratios. The adsorbent particle size was 0-1 mm and Ca/S ratio was 2. The fuel feeding rate was about 4.6 kg/h, the superficial velocity inside the bed was 2.80 m/s and the carbon-based efficiency was 91.89%. The carbon-conversion efficiency was similar to the limestone addition. The temperature profiles along the combustor and the return leg are given in Figure 4.58. In this case, the bed temperature could be increased and maintained to temperatures up to 800°C and the steady state operation was obtained. Therefore, the temperature profile in this case was comparable to the air combustion cases. The highest temperature was obtained at 1.7 m above the distributor plate at 810°C. As can be seen, increasing excess air ratio did not have a significant impact on the temperature profile. The temperature at the top of the combustor was at about 745°C. The

temperature at the top of the return leg was 700°C and decreased to 550°C at the recirculated gas re-entry.

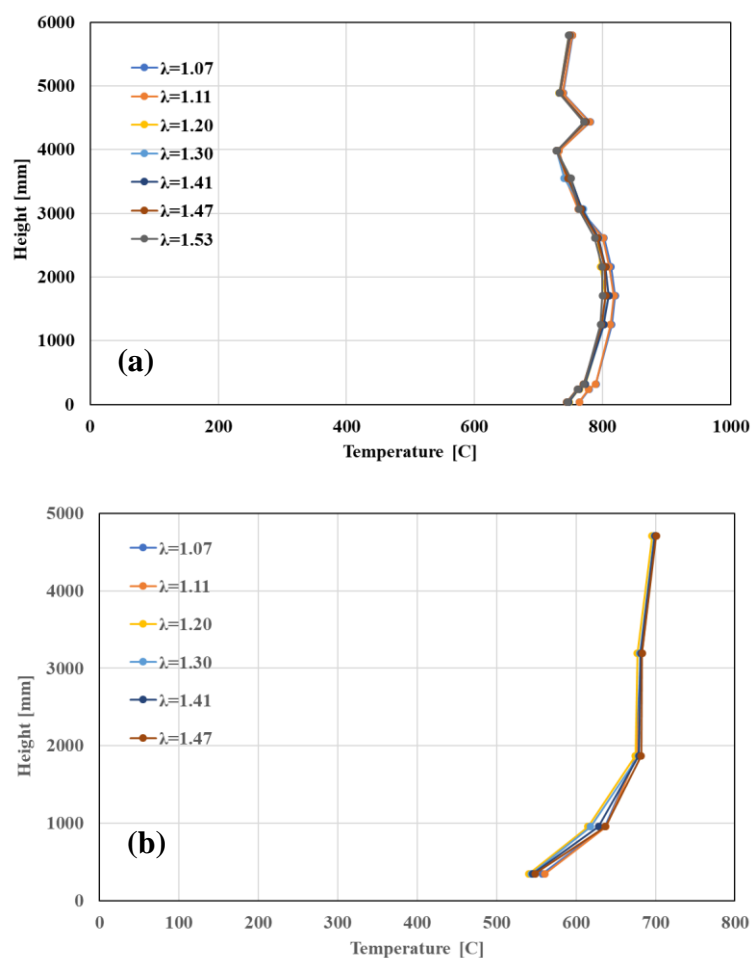


Figure 4.58. Temperature profile along (a) combustor and (b) return leg under oxy-fuel combustion of Orhaneli lignite and Eskişehir dolomite at Ca/S= 2 and Particle size of 0-1 mm

Figure 4.59 shows NO_x, CO, SO₂, and CO₂ emissions and bed temperature for oxy-fuel combustion of Orhaneli lignite and Eskişehir dolomite at different excess air ratios. NO_x emission concentration was 25.4mg/MJ at $\lambda=1.07$ and increased with the increase of excess air ratio up to 53.0mg/MJ at $\lambda=1.53$. While the concentration of

NO_x was significantly lower than combustion in air, addition of limestone resulted in increase of NO_x concentration in oxy-fuel combustion condition especially at higher excess air ratios. CO emission concentration decreased with the increase of excess air ratio from 374mg/MJ to 86mg/MJ and was similar to the case of oxy-fuel combustion with no adsorbent.

Based on CaCO₃ thermodynamic equilibrium curve (Figure 2.7), it can be said that the direct mechanism for SO₂ retention took place inside the bed. The SO₂ concentration was 655mg/MJ at $\lambda=1.07$ and decreased to 461mg/MJ at $\lambda=1.53$. Comparing these results with the results obtained for the case with no addition of adsorbent (Table 2.1), a slight retention of SO₂ was noticed. However, this comparison might not be of great value. It is speculated that if the combustion without addition of sorbent could be conducted and maintained at temperatures around 800°C, the concentration of SO₂ would have been higher, hence the desulfurization process would be more evident. CO₂ emission increased from 36% at $\lambda=1.07$ up to 79% at $\lambda=1.53$.

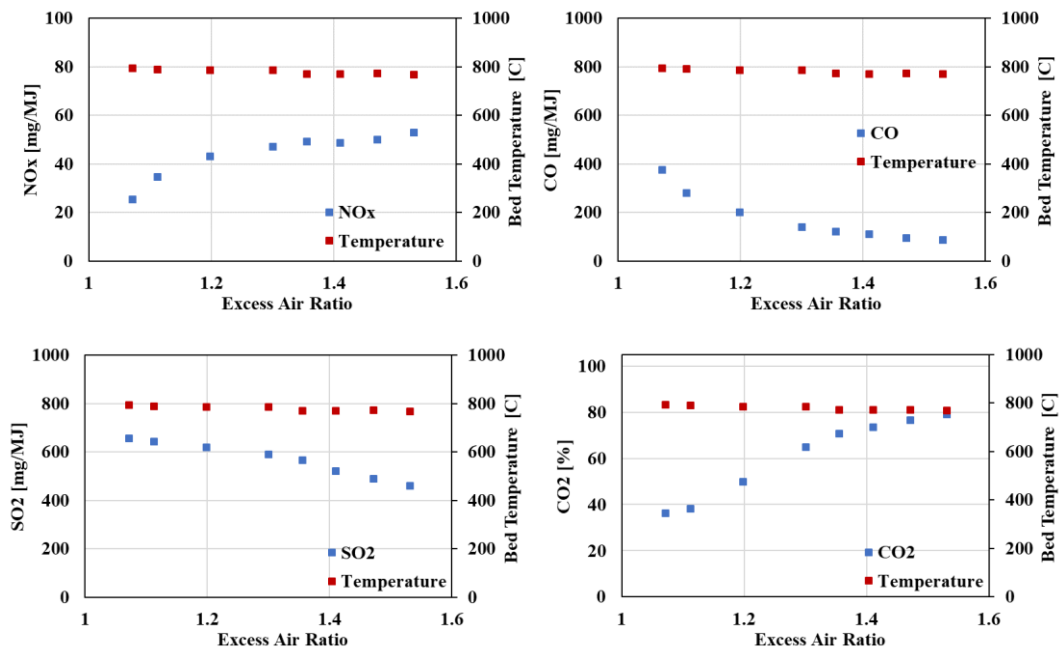


Figure 4.59. Flue gas emissions under oxy-fuel combustion of Orhaneli lignite and Eskişehir dolomite at Ca/S = 2 and Particle size of 0-1 mm

4.3. Circulating Fluidized Bed simulation

The simulation of the CFBC was performed by means of CeSFaMB software. The software has been developed based on fundamental laws of mass, energy and momentum conservations. Also, correlations for kinetics and other auxiliary parameters have been taken from literature and the results of the simulations were proved by stringent experimental data. The main input data required for the software are as follows:

- 1- The ultimate and proximate analysis of the carbonaceous fuels,
- 2- The bulk, true, and apparent densities of the fuels and adsorbents,
- 3- Heating values of the fuels,
- 4- Particle size distribution of the solid fuels and adsorbents,
- 5- Activation energy values of the fuels,
- 6- Geometry of the combustor including height, hydraulic diameter, position of injections and withdrawal of the gases, cyclones geometry, return leg diameter,
- 7- Mass flow, pressure, and composition of the streams injected into the bed.

The input data of the CFBC are summarized in Table 4.20. The simulation and experimental results of temperature profile in the combustor for the combustion of Orhaneli lignite under air atmosphere are presented in Figure 4.60. As can be seen the model was able to predict the evolution of combustor temperature accurately in bed section of the combustor. However, the simulation results deviated from the experimental data in the freeboard region. As can be seen, the experiments showed an increase in the temperature at the top of the freeboard due to particle concentration in the combustor exit. However, due to the fact that the model was a 1-D simulation, it was not able to capture this effect. The maximum discrepancy between the simulation and experimental results were less than 10%. The carbon-based efficiency for the experiment was 96.50% and in simulation this value was obtained as 98.16%. Furthermore, the obtained value for superficial velocity inside the bed was 2.45 m/s which was close to that of the experiments at 2.60 m/s.

Table 4.20. Input data of the CFBC system

Mass flow of the inlet air	<i>0,0115 [kg/s]</i>
Temperature of the inlet air	<i>673 [K]</i>
Pressure of the inlet air	<i>110 [kPa]</i>
Surrounding air temperature	<i>300 [K]</i>
Equipment hydraulic diameter	<i>108 [mm]</i>
Equipment height	<i>6 [m]</i>
Number of orifices on the distributor plate	<i>618</i>
Diameter of the orifices	<i>1 [mm]</i>
Diameter of the cyclone	<i>108 [mm]</i>
Length of the recycling tube	<i>5.5 [m]</i>
Position of the recycling injection	<i>136 [mm]</i>
Orhaneli lignite bulk density	<i>600 [kg/m³]</i>
Orhaneli lignite true density	<i>1270 [kg/m³]</i>
Orhaneli lignite apparent density	<i>750 [kg/m³]</i>

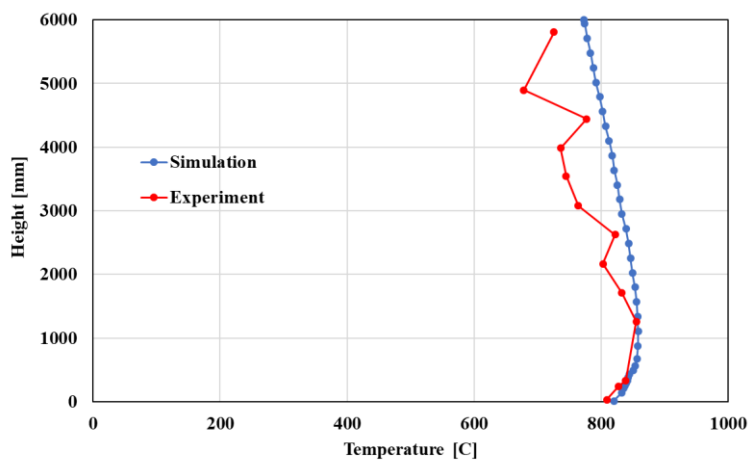


Figure 4.60. Comparison of experimental and simulation results for combustion of Orhaneli lignite under air atmosphere

The simulation results for combustion of Orhaneli lignite under oxygen-enriched atmosphere are given in Figure 4.61. The highest temperature was obtained for combustion in 25% O₂ at 915°C which was similar to the experiments.

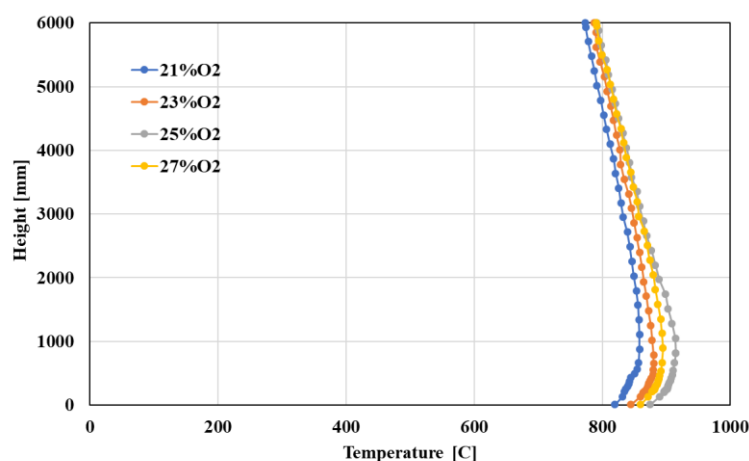


Figure 4.61. Simulation results for the combustion of Orhaneli lignite under oxygen-enriched atmosphere

The evolution of CO₂ and SO₂ emissions in the combustor for the combustion of Orhaneli lignite under oxygen-enriched conditions are given in Figure 4.62. Additionally, the comparison of CO₂ and SO₂ emission data between the simulation and the experiments are presented in Table 4.21. The results showed a good agreement with the experiments. From the evolution of CO₂ emission, it was seen that the major combustion of fuel took place at the bed region of the combustor and the level at which combustion occurred was decreased with the increase of oxygen concentration. The reactions producing SO₂ took place at bed region as well, hence, addition of calcium-based sorbents for in-situ retention of SO₂ can be considered as a suitable removal process.

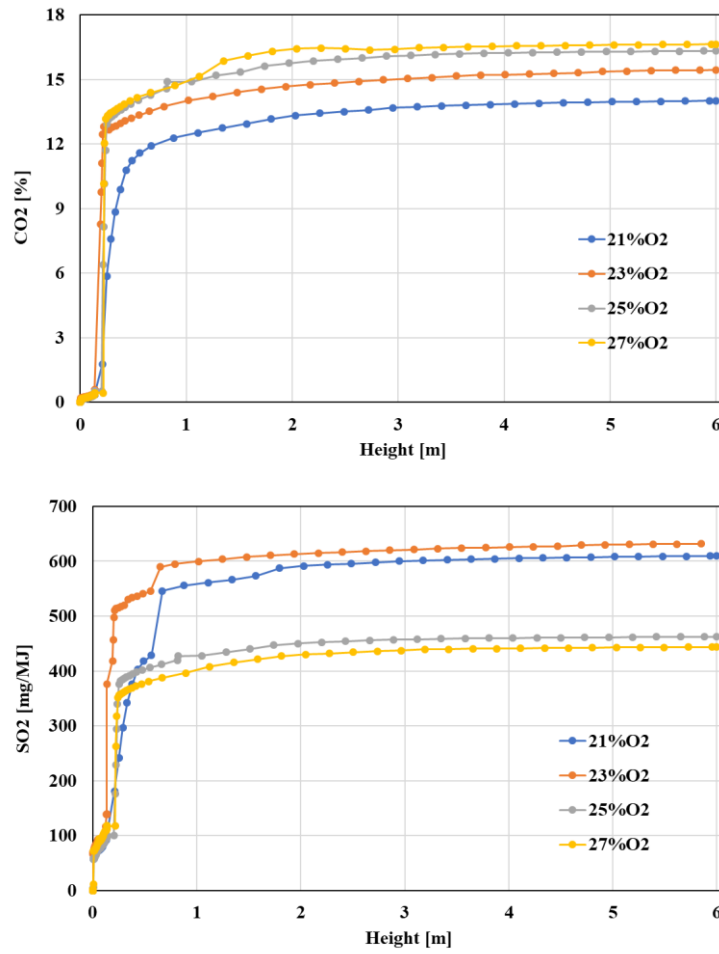


Figure 4.62. Change of CO₂ and SO₂ emissions along the combustor height under oxygen-enriched conditions

Table 4.21. Comparison of CO₂ and SO₂ emission data between the simulation and experiments under oxygen-enriched conditions

Atmosphere	CO ₂ [%]		SO ₂ [mg/MJ]	
	Experiment	Simulation	Experiment	Simulation
Air	14	14	591	610
23% O ₂	15	15.5	605	632
25% O ₂	17	16.3	724	462
27% O ₂	19	16.6	272	444

The mathematical model was used to simulate the oxy-fuel combustion process of the CFBC under different excess air ratios. Comparison of the temperature evolution inside the bed under oxy-fuel combustion condition is shown in Figure 4.63. It can be seen that the model was able to successfully simulate the combustion under oxy-fuel conditions as well. The carbon-based efficiency obtained from the model was 96.43% which was comparable with the data obtained from the experiments (98.77%). The maximum deviation between the simulation and experiments was less than 8%.

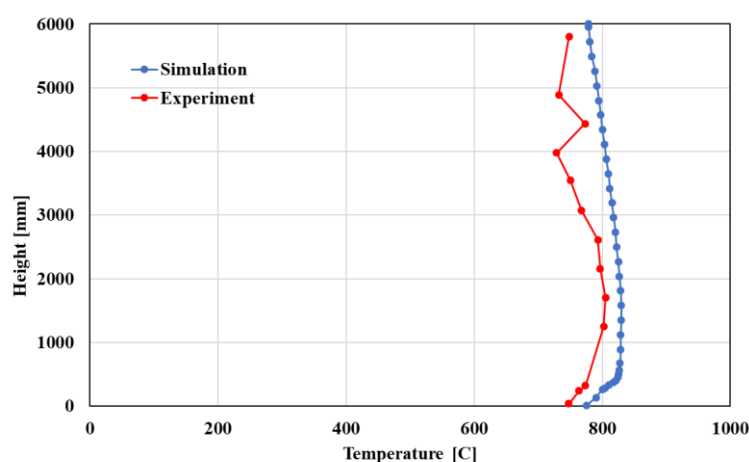


Figure 4.63. Comparison of experimental and simulation results for combustion of Orhaneli lignite under oxy-fuel combustion condition

The simulation results for oxy-fuel combustion of Orhaneli lignite at different excess air ratios are presented in Figure 4.64. As can be seen, increasing the excess air ration resulted in decrease of the temperature inside the combustor. This trend was similar to the data obtained from the experiments proving that the simulation with CeSFaMB software can be used successfully in prediction of overall combustor behavior.

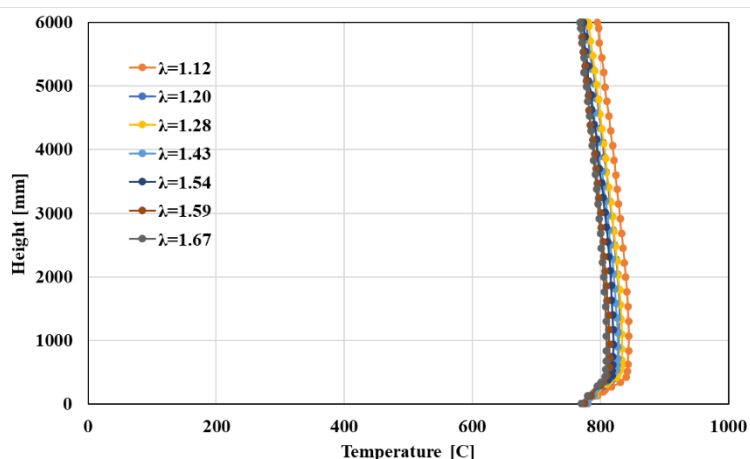


Figure 4.64. Simulation results for the oxy-fuel combustion of Orhaneli lignite at different excess air ratios

The evolution of CO₂ and SO₂ emissions in the combustor for the oxy-fuel combustion of Orhaneli lignite at different excess air ratios are given in Figure 4.65. Additionally, the comparison of CO₂ and SO₂ emission data between the simulation and the experiments are presented in Table 4.22. From the evolution of CO₂ emission, it was seen that at the bed region of the combustor, a reduction in CO₂ concentration was noticed. The simulation results for CO₂ emission was about 81% irrespective of excess air ratio while in the experiments increasing the excess air ratio resulted in increase in CO₂ emission. Therefore, it can be concluded that the model was not able to accurately predict the CO₂ emission at oxy-fuel conditions. The reactions producing SO₂ took place at bed region and the simulation results were at reasonably good agreement with the experiments. The model showed a reduction in SO₂ concentration with the increase in excess air ratio as it was seen in the experimental data.

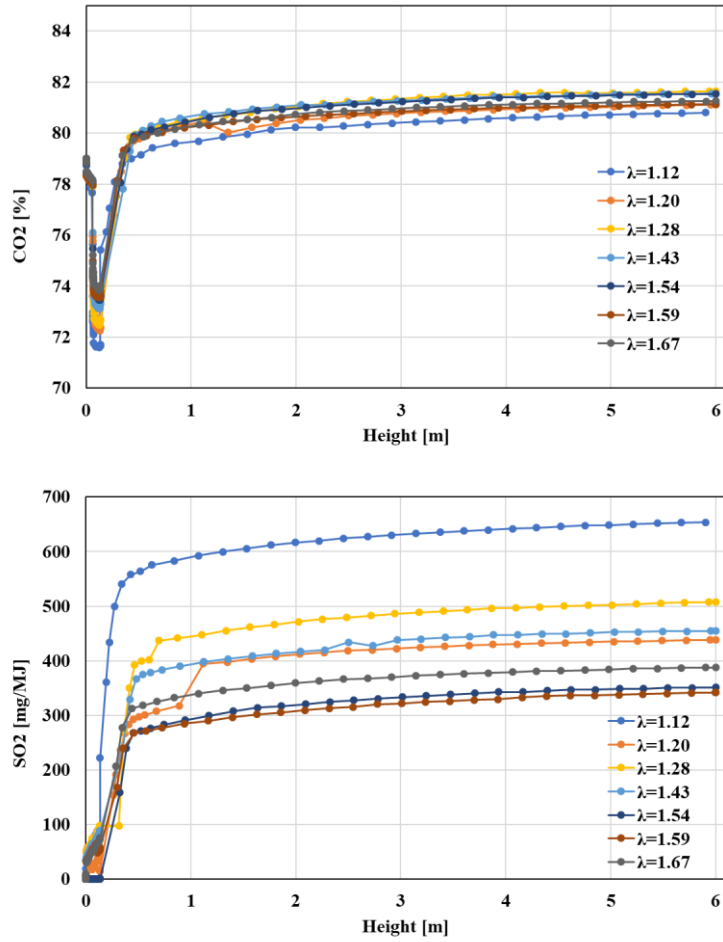


Figure 4.65. Change of CO₂ and SO₂ emissions along the combustor height under oxy-fuel combustion conditions

Table 4.22. Comparison of CO₂ and SO₂ emission data between the simulation and experiments under oxy-fuel combustion conditions

Lambda	CO₂ [%]		SO₂ [mg/MJ]	
	Experiment	Simulation	Experiment	Simulation
1.02	64.6	-	807	-
1.12	73.4	80.8	716	654
1.20	79.0	81.1	655	438
1.28	-	81.7	-	508
1.37	87.3	-	565	-
1.43	-	81.6	-	455
1.54	94.4	81.5	478	351
1.59	-	81.1	-	342
1.67	-	81.2	-	387
1.72	100	-	409	-
1.83	100	-	382	-
1.94	100	-	349	-

Comparison of the obtained data from the simulation with the experiments showed that the mathematical modeling and simulation approaches are reliable and cost-effective tools in CFBC analysis especially in providing information on the behavior of a given system. The fluidized bed boiler design can be supported by the mathematical models. However, the developed models require validation against experimental data. Therefore, both the experiments and numerical models play an important role in the design process.

CHAPTER 5

CONCLUSIONS

This PhD research was aimed at improving the knowledge on oxy-fuel combustion of Turkish indigenous lignite coals, biomass and coal/biomass blends in a laboratory scale Circulating Fluidized Bed (CFB). A thorough investigation on combustion, oxygen-enriched combustion and oxy-fuel combustion of coal, biomass and their blends were experimentally conducted by means of Thermogravimetric analyzer (TGA). Following that, the CFB experiments were conducted in order to investigate the effects of addition of calcium-based sorbents for in-situ SO₂ adsorption. Finally, the obtained data for CFB experiments was used in order to numerically simulate the combustion process in the CFB. The obtained results were summarized under two categories:

5.1. TGA Experiments

Based on the obtained results for combustion and oxy-fuel combustion at elevated oxygen concentrations, the followings were concluded:

- The Orhaneli lignite, which has relatively higher quality than Soma lignite owing to its higher volatile matter, higher fixed carbon, and lower ash contents, displayed a steeper weight loss profile indicating a more rapid combustion process.
- The combustion of volatiles at both combustion and oxy-fuel combustion conditions showed approximately similar behaviors indicating that both N₂ and CO₂ can be considered as inert gases. The last stage of weight loss in air and oxygen-enriched air combustion conditions taking place at temperatures above 700°C was the result of CaCO₃ decomposition. This process was independent of the oxygen concentration and took place when the temperature

reached to a certain threshold. This decomposition process did not take place in oxy-fuel conditions until the temperature was higher than 900°C.

- Elevated oxygen concentrations resulted in a faster combustion of the samples, however, no impact on the weight loss quantity was noticeable and the total weight loss was found to be nearly the same.
- The estimated activation energy distribution between FWO and KAS methods were in a good accordance and produced relatively similar results. The average activation energy values estimated by the three methods were in decreasing order of FWO > KAS > Friedman.
- Combustion in oxy-fuel conditions had higher activation energy values comparing to conventional combustion atmosphere. The activation energy values were similar at $\alpha=10\%$ regardless of oxygen concentration or combustion atmosphere at about 165 kJ/mole and 150kJ/mole for Orhaneli and Soma lignites, respectively.
- At elevated oxygen concentrations, combustion process takes place at lower temperatures resulting increase in activation energy levels.
- For Soma lignite combustion in air and oxygen-enriched air conditions, the activation energy values increased at $\alpha>65\%$ due to decomposition of CaCO_3 .
- The evaluation of uncertainty related to kinetic parameters showed that FWO method had a lower uncertainty in activation energy estimation of both lignites. The calculated uncertainty values were found to be in the range of 5-15% for most of the cases.

The obtained results for combustion of raw and torrefied biomass under air and oxy-fuel conditions can be summarized as follows:

- Torrefaction of biomass resulted in decrease of O/C and H/C atomic ratios.
- The 300°C-30min and 350°C-15min torrefied biomasses were completely embedded in lignite region in van-Krevelen's diagram.

- The oxy-fuel combustion did not affect the hemicellulose decomposition, but delayed the cellulose and lignin decomposition.
- The activation energy values increased with conversion degree during hemicellulose degradation, remained approximately constant during cellulose decomposition and showed a sharp decrease for lignin decomposition.
- The activation energy trends were comparable in both air and oxy-fuel combustion conditions, however slight changes in activation energy values were noticed.
- The highest average activation energy was 183.40kJ/mole for 250°C-30min biomass at and the lowest value was 72.93kJ/mole for 350°C-15min biomass.
- The uncertainty values related to FWO method were lower than KAS and Friedman methods. The uncertainty values for FWO and KAS methods were at the range of 5-15%.

The obtained results for co-combustion of Orhaneli and Soma lignites with raw and torrefied biomass can be summarized as follows:

- The burnout temperature of the blends was seen to be lower in oxy-fuel combustion condition indicating that the completion of combustion occurred faster. This phenomenon was more significant in higher heating rates.
- The decomposition of the lignin in the blend of Orhaneli lignite with the biomass samples occurred at lower temperature indicating a synergetic effect. For Soma lignite blends this effect could not be distinguished because the temperature interval related to lignin decomposition was coincided with the Soma main combustion interval.
- The characteristic temperatures of the 50/50 blend of Orhaneli lignite with biomass samples were lower than its parent fuels under both air and oxy-fuel combustion conditions showing that the blend had higher reactivity than the parent fuels.

- Based on the experimental and calculated DTG curves and their relative error values, the synergetic effect for blends of Orhaneli lignite was noticed. The highest synergism was obtained for the 50/50 blend of Orhaneli lignite and 300°C-30min torrefied biomass with the average relative error of 21.41%. The average relative error regarding 50/50 blend of Soma lignite with 300°C-30min torrefied biomass was about 1.34% showing that the blend had no significant synergetic effect.
- The 50/50 blend of Orhaneli lignite and 300°C-30min torrefied biomass combustion under air and oxy-fuel combustion atmospheres had lower average activation energy values than its parent fuels indicating the higher reactivity of the blend.
- The uncertainty values in the kinetics calculations of the blend combustion and oxy-fuel combustion were higher than their parent fuels. Moreover, the uncertainties of FWO method were lower than KAS and Friedman methods.

5.2. Circulating Fluidized Bed Experiments

- In the combustion process in air and oxygen-enriched air atmospheres, due to calcination of Ca-based sorbents, indirect sulfation of the adsorbents took place. However, in oxy-fuel combustion conditions due to high partial pressure of CO₂ in the bed, direct sulfation process occurred.
- The limestone and dolomite with particle size of 1-2 mm showed superior impact in SO₂ retention. The small particle size of the adsorbents resulted in their fast leaving of the bed before their complete reaction with SO₂ emission. Also, increasing the Ca/S ratio enhanced SO₂ adsorption. The effect of Ca/S ratio on SO₂ emission reduction was more significant in limestone addition.
- At elevated oxygen concentrations, the adsorption of SO₂ was higher.

- Addition of limestone showed no significant impact on NO_x, CO, and CO₂ emissions. The only adverse effect of limestone addition was the decrease of carbon-based efficiency of the reactor.
- In the oxy-fuel combustion tests with the addition of limestone, because the bed temperature was around 700°C, the sulfation reaction did not take place and SO₂ retention process did not occur. In the experiment with the dolomite sample, a slight decrease in SO₂ was noticed.
- Increasing the excess air ratio in oxy-fuel combustion tests resulted in the decrease of CO and SO₂ emission and increase of NO_x emission. In order to achieve the oxy-fuel combustion with CO₂ concentrations of more than 90% as well as reasonable concentrations of other emissions, the excess air ratio needs to be higher than 50%.
- The obtained results for the simulation of CFBC with CeSFaMB software showed that the model was successful at prediction of the evolution of the combustor temperature and carbon-based efficiency. The simulation results under air combustion conditions showed a good agreement with experiments especially at the bottom section of the bed. The maximum temperature deviation between the calculated and measured data was 10%.
- From the emissions perspective, the software was successful at estimation of SO₂ emission trend and the obtained values were comparable with the experiments. Calculation of CO₂ emission in oxygen-enriched combustion condition was in a good agreement with the experiments, however, the model was not able to accurately predict the CO₂ emission under oxy-fuel combustion conditions.

CHAPTER 6

FUTURE STUDIES

The recommendations for future studies are as follows:

- 1- In this study, the combustion and oxy-fuel combustion experiments of lignite and biomass blends were carried out under 21% oxygen concentration. It is recommended to conduct these combustion tests at elevated oxygen concentrations as well.
- 2- Due to some design problems, the oxy-fuel combustion experiments in CFB could not reach to the desired bed temperatures. It is suggested to improve the CFB combustor to operate at higher temperatures under oxy-fuel condition.
- 3- The maximum oxygen concentration in CFB experiments was 27% and it is suggested to study the operation of the CFB at higher oxygen concentrations as well.
- 4- The applied model in this study was not able to successfully simulate the combustion of the CFB under oxy-fuel combustion conditions, especially at predicting CO₂ concentration. It is recommended to develop a model for the simulation of the CFB under oxy-fuel combustion conditions.
- 5- The CFD studies of the CFB systems is recommended.

REFERENCES

- [1] IEA, "World Energy Outlook 2018: Electricity," *Iea*, 2018.
- [2] M. F. Irfan, M. R. Usman, and K. Kusakabe, "Coal gasification in CO₂ atmosphere and its kinetics since 1948: A brief review," *Energy*, vol. 36, no. 1, pp. 12–40, 2011.
- [3] British Petroleum, "Primary energy consumption - leading countries 2014," *Br. Pet.*, no. June, p. 48, 2015.
- [4] K. Burnard and S. Bhattacharya, "Power generation from coal," *Iea*, p. 56, 2011.
- [5] Y. Shi, S. Li, and H. Hu, "Studies on pyrolysis characteristic of lignite and properties of its pyrolysates," *J. Anal. Appl. Pyrolysis*, vol. 95, pp. 75–78, 2012.
- [6] A. F. Ghoniem, "Needs, resources and climate change: Clean and efficient conversion technologies," *Prog. Energy Combust. Sci.*, vol. 37, no. 1, pp. 15–51, 2011.
- [7] J. Koornneef, M. Junginger, and A. Faaij, "Development of fluidized bed combustion-An overview of trends, performance and cost," *Prog. Energy Combust. Sci.*, vol. 33, no. 1, pp. 19–55, 2007.
- [8] R. Chirone, P. Salatino, F. Scala, R. Solimene, and M. Urciuolo, "Fluidized bed combustion of pelletized biomass and waste-derived fuels," *Combust. Flame*, vol. 155, no. 1–2, pp. 21–36, 2008.
- [9] T. F. Wall, "Combustion processes for carbon capture," *Proc. Combust. Inst.*, vol. 31 I, pp. 31–47, 2007.
- [10] T. Fujimori and T. Yamada, "Realization of oxyfuel combustion for near zero emission power generation," *Proc. Combust. Inst.*, vol. 34, no. 2, pp. 2111–2130, 2013.
- [11] N. Selcuk and N. S. Yuzbasi, "Combustion behaviour of Turkish lignite in O₂/N₂ and O₂/CO₂ mixtures by using TGA-FTIR," *J. Anal. Appl. Pyrolysis*, vol. 90, no. 2, pp. 133–139, 2011.
- [12] N. Kimura, K. Omata, T. Kiga, S. Takano, and S. Shikisima, "The characteristics of pulverized coal combustion in O₂/CO₂ mixtures for CO₂ recovery," *Energy Convers. Manag.*, vol. 36, no. 6–9, pp. 805–808, 1995.
- [13] M. B. Toftegaard, J. Brix, P. A. Jensen, P. Glarborg, and A. D. Jensen, "Oxy-fuel combustion of solid fuels," *Prog. Energy Combust. Sci.*, vol. 36, no. 5, pp. 581–625, 2010.

- [14] L. Duan, C. Zhao, W. Zhou, C. Qu, and X. Chen, "O₂/CO₂ coal combustion characteristics in a 50kWth circulating fluidized bed," *Int. J. Greenh. Gas Control*, vol. 5, no. 4, pp. 770–776, 2011.
- [15] T. Czakiert, K. Sztekler, S. Karski, D. Markiewicz, and W. Nowak, "Oxy-fuel circulating fluidized bed combustion in a small pilot-scale test rig," *Fuel Process. Technol.*, vol. 91, no. 11, pp. 1617–1623, 2010.
- [16] L. Jia, Y. Tan, C. Wang, and E. J. Anthony, "Experimental study of oxy-fuel combustion and sulfur capture in mini-CFBC," *Energy and Fuels*, vol. 21, no. 6, pp. 3160–3164, 2007.
- [17] S. C. Pickard, S. S. Daood, M. Pourkashanian, and W. Nimmo, "Co-firing coal with biomass in oxygen- and carbon dioxide-enriched atmospheres for CCS applications," *Fuel*, vol. 137, pp. 185–192, 2014.
- [18] H. Okutan, A. Yozgatlıgil, B. Engin, H. Olgun, and M. Özkaymak, "Oxy-Combustion of Lignite and Torrefied Biomass in a Circulating Fluidized Bed (OXYCOMBUSTION)," 2017.
- [19] S. Avşaroğlu, "Investigation of SO₂ Removal Characteristics with Limestone under Oxycombustion Conditions," Middle East Technical University, 2019.
- [20] IEA, *World Energy Outlook 2013*. 2013.
- [21] WorldCoalInstitute, "the Coal Resource a Comprehensive Overview of Coal the Coal Resource Where Does Coal Come From? What Is It," *World Coal Inst.*, pp. 1–44, 2005.
- [22] Herdem Attorneys At Law, "2013 Turkey Energy Report," no. February, 2014.
- [23] Z. B. Erdem, "The assessment of coal ' s contribution to sustainable energy development in Turkey," vol. 28, no. 2, pp. 117–129, 2010.
- [24] M. Balat, "Turkey's Major Lignite Fields and Significance of Lignite for Energy Necessity," *Energy Sources, Part B Econ. Planning, Policy*, vol. 3, no. October 2014, pp. 13–25, 2007.
- [25] ETKB, "2015-2019 Türkiye Stratejik Planı," *Igarss 2014*, no. 1, pp. 1–5, 2014.
- [26] M. Güneş and S. Güneş, "A study on thermal decomposition kinetics of some Turkish coals," *Energy Sources*, vol. 27, no. 8, pp. 749–759, 2005.
- [27] M. K. Urkan and M. Arikol, "Correlations for the heating value of Turkish coals," *Fuel*, vol. 68, no. 4, pp. 527–530, 1989.
- [28] K. Kaygusuz and A. Kaygusuz, "Renewable energy and sustainable development in Turkey," *Renew. Energy*, vol. 25, no. 3, pp. 431–453, 2002.
- [29] UNFCCC. Conference of the Parties (COP), "Adoption of the Paris Agreement.

Proposal by the President.," *Paris Clim. Chang. Conf. - Novemb. 2015, COP 21*, vol. 21932, no. December, p. 32, 2015.

- [30] T. Wall *et al.*, "An overview on oxyfuel coal combustion-State of the art research and technology development," *Chem. Eng. Res. Des.*, vol. 87, no. 8, pp. 1003–1016, 2009.
- [31] J. Bugge, S. Kjær, and R. Blum, "High-efficiency coal-fired power plants development and perspectives," *Energy*, vol. 31, no. 10–11, pp. 1437–1445, 2006.
- [32] M. M. Abu-Khader, "Recent Progress in CO₂ Capture/Sequestration: A Review," *Energy Sources, Part A Recover. Util. Environ. Eff.*, vol. 28, no. 14, pp. 1261–1279, 2006.
- [33] J. Gibbins and H. Chalmers, "Carbon capture and storage," *Energy Policy*, vol. 36, no. 12, pp. 4317–4322, 2008.
- [34] M. Pehnt and J. Henkel, "Life cycle assessment of carbon dioxide capture and storage from lignite power plants," *Int. J. Greenh. Gas Control*, vol. 3, no. 1, pp. 49–66, 2009.
- [35] K. Damen, M. Van Troost, A. Faaij, and W. Turkenburg, "A comparison of electricity and hydrogen production systems with CO₂ capture and storage. Part A: Review and selection of promising conversion and capture technologies," *Prog. Energy Combust. Sci.*, vol. 32, no. 2, pp. 215–246, 2006.
- [36] J. M. Beér, "High efficiency electric power generation: The environmental role," *Prog. Energy Combust. Sci.*, vol. 33, no. 2, pp. 107–134, 2007.
- [37] C. Descamps, C. Bouallou, and M. Kanniche, "Efficiency of an Integrated Gasification Combined Cycle (IGCC) power plant including CO₂ removal," *Energy*, vol. 33, no. 6, pp. 874–881, 2008.
- [38] M. Kanniche, R. Gros-Bonnivard, P. Jaud, J. Valle-Marcos, J. M. Amann, and C. Bouallou, "Pre-combustion, post-combustion and oxy-combustion in thermal power plant for CO₂ capture," *Appl. Therm. Eng.*, vol. 30, no. 1, pp. 53–62, 2010.
- [39] C. Chen and E. S. Rubin, "CO₂ control technology effects on IGCC plant performance and cost," *Energy Policy*, vol. 37, no. 3, pp. 915–924, 2009.
- [40] D. Singh, E. Croiset, P. L. Douglas, and M. A. Douglas, "Techno-economic study of CO₂ capture from an existing coal-fired power plant: MEA scrubbing vs. O₂/CO₂ recycle combustion," *Energy Convers. Manag.*, vol. 44, no. 19, pp. 3073–3091, 2003.
- [41] R. Notz, N. Asprion, I. Clausen, and H. Hasse, "Selection and Pilot Plant Tests of New Absorbents for Post-Combustion Carbon Dioxide Capture," *Chem.*

- Eng. Res. Des.*, vol. 85, no. 4, pp. 510–515, 2007.
- [42] B. J. P. Buhre, L. K. Elliott, C. D. Sheng, R. P. Gupta, and T. F. Wall, “Oxy-fuel combustion technology for coal-fired power generation,” *Prog. Energy Combust. Sci.*, vol. 31, no. 4, pp. 283–307, 2005.
- [43] S. Nakayama *et al.*, “Pulverized coal combustion in O₂/CO₂ mixtures on a power plant for CO₂ recovery,” *Energy Convers. Manag.*, vol. 33, no. 5–8, pp. 379–386, 1992.
- [44] F. Châtel-Pélage *et al.*, “Applications of oxygen for NO_x control and CO₂ capture in coal-fired power plants,” *Therm. Sci.*, vol. 10, no. 3, pp. 119–142, 2006.
- [45] M. Anhedén, J. Yan, and G. De Smedt, “Denitrogenation (or oxyfuel concepts),” *Oil Gas Sci. Technol.*, vol. 60, no. 3, pp. 485–495, 2005.
- [46] S. Rezvani, Y. Huang, D. McIlveen-Wright, N. Hewitt, and Y. Wang, “Comparative assessment of sub-critical versus advanced super-critical oxyfuel fired PF boilers with CO₂ sequestration facilities,” *Fuel*, vol. 86, no. 14 SPEC. ISS., pp. 2134–2143, 2007.
- [47] M. M. Hossain and H. I. de Lasa, “Chemical-looping combustion (CLC) for inherent CO₂ separations-a review,” *Chem. Eng. Sci.*, vol. 63, no. 18, pp. 4433–4451, 2008.
- [48] J. D. Figueroa, T. Fout, S. Plasynski, H. McIlvried, and R. D. Srivastava, “Advances in CO₂ capture technology-The U.S. Department of Energy’s Carbon Sequestration Program,” *Int. J. Greenh. Gas Control*, vol. 2, no. 1, pp. 9–20, 2008.
- [49] J. Werther, M. Saenger, E.-U. Hartge, T. Ogada, and Z. Siagib, “Combustion of agricultural residues,” *Prog. Energy Combust. Sci.*, vol. 26, pp. 1–27, 2000.
- [50] A. Lyngfelt and B. Leckner, “SO₂ Capture in Fluidized-Bed Boilers: Re-emission of SO₂ Due to Reduction of CaSO₄,” *Chem. Eng. Sci.*, vol. 44, no. 2, pp. 207–213, 1989.
- [51] N. H. Ulerich, R. A. Newby, and D. L. Keairns, “A thermogravimetric study of the sulfation of limestone and dolomite - prediction of pressurized and atmospheric fluidized-bed desulfurization,” *Thermochim. Acta*, vol. 36, no. 1, pp. 1–16, 1980.
- [52] F. Winter and P. Szentannai, “IEA Fluidized Bed Conversion Programme Status Report 2010,” 2010.
- [53] K. Chen, “What are the main characteristics of fluidised bed combustors ? 2 . Bubbling Fluidised Bed Combustors,” pp. 2–7, 2001.

- [54] H. Topal, A. T. Atimtay, and A. R. Durmaz, "Olive cake combustion in a circulating fluidized bed," *Fuel*, vol. 82, no. 9, pp. 1049–1056, 2003.
- [55] A. Batu, "Investigation of Combustion Characteristics of Indigenous Lignite in a 150 KWT Circulating Fluidized Bed Combustor," Middle East Technical University, 2008.
- [56] T. Kiga *et al.*, "Characteristics of pulverized-coal combustion in the system of oxygen/recycled flue gas combustion," *Energy Convers. Manag.*, vol. 38, pp. S129–S134, 1997.
- [57] H. Liu, R. Zailani, and B. M. Gibbs, "Pulverized coal combustion in air and in O₂/CO₂ mixtures with NO_x recycle," *Fuel*, vol. 84, no. 16, pp. 2109–2115, 2005.
- [58] H. Liu, R. Zailani, and B. M. Gibbs, "Comparisons of pulverized coal combustion in air and in mixtures of O₂/CO₂," *Fuel*, vol. 84, no. 7–8, pp. 833–840, 2005.
- [59] L. Jia, Y. Tan., and E. J. Anthony, "Emissions of SO₂ and NO_x during Oxy-Fuel CFB combustion tests in a mini-circulating fluidized bed combustion reactor," *Energy and Fuels*, vol. 24, no. 2, pp. 910–915, 2010.
- [60] J. R. Grace, A. A. Avidan, and T. M. Knowlton, *Circulating Fluidized Beds*. London: Blackie Academic and Professional, 1997.
- [61] J. Marion, C. Bozzuto, H. Andrus, and R. Chamberland, "Greenhouse gas emissions control by oxygen firing in circulating fluidized bed boilers: Phase 1 - A preliminary systems evaluation," 2003.
- [62] Y. Mathieu, L. Tzanis, M. Soulard, J. Patarin, M. Vierling, and M. Molière, "Adsorption of SO_x by oxide materials: A review," *Fuel Process. Technol.*, vol. 114, pp. 81–100, 2013.
- [63] B. Leckner and A. Gómez-Barea, "Oxy-fuel combustion in circulating fluidized bed boilers," *Appl. Energy*, vol. 125, pp. 308–318, 2014.
- [64] S. Li, M. Xu, L. Jia, L. Tan, and Q. Lu, "Influence of operating parameters on N₂O emission in O₂/CO₂ combustion with high oxygen concentration in circulating fluidized bed," *Appl. Energy*, vol. 173, pp. 197–209, 2016.
- [65] B. Leckner, "Developments in fluidized bed conversion of solid fuels," *Therm. Sci.*, vol. 20, pp. S1–S18, 2016.
- [66] H. I. Mathekga, B. O. Oboirien, and B. C. North, "A review of oxy-fuel combustion in fluidized bed reactors," *Int. J. ENERGY Res.*, vol. 40, pp. 878–902, 2016.
- [67] P. Adolphi, M. Störr, P. G. Mahlberg, H. H. Murray, and E. M. Ripley, "Sulfur sources and sulfur bonding of some central European attrital brown coals," *Int.*

- J. Coal Geol.*, vol. 16, pp. 185–188, 1990.
- [68] E. Raask, “Sulphate capture in ash and boiler,” vol. 8, 1982.
- [69] A. Attar, “Chemistry, thermodynamics and kinetics of reactions of sulphur in coal-gas reactions: A review,” *Fuel*, vol. 57, no. 4, pp. 201–212, 1978.
- [70] C. Sheng, M. Xu, J. Zhang, and Y. Xu, “Comparison of sulphur retention by coal ash in different types of combustors,” *Fuel Process. Technol.*, vol. 64, no. 1, pp. 1–11, 2000.
- [71] R. Zevenhoven, P. Yrjas, and M. Hupa, “Sulfur dioxide capture under PFBC conditions: the influence of sorbent particle structure,” *Fuel*, vol. 77, no. 4, pp. 285–292, 1998.
- [72] F. García-Labiano *et al.*, “Calcium-based sorbents behaviour during sulphation at oxy-fuel fluidised bed combustion conditions,” *Fuel*, vol. 90, no. 10, pp. 3100–3108, 2011.
- [73] J. S. Dennis and A. N. Hayhurst, “Mechanism of the sulphation of calcined limestone particles in combustion gases,” *Chem. Eng. Sci.*, vol. 45, no. 5, pp. 1175–1187, 1990.
- [74] A. B. Fuertes, G. Velasco, E. Fuente, J. B. Parra, and T. Alvarez, “Sulphur retention by limestone particles under PFBC conditions,” *Fuel Process. Technol.*, vol. 36, no. 1–3, pp. 65–71, 1993.
- [75] A. B. Fuertes, G. Velasco, E. Fuente, and T. Alvarez, “Study of the direct sulfation of limestone particles at high COE partial pressures,” vol. 38, pp. 181–192, 1994.
- [76] C. Wang, L. Jia, Y. Tan, and E. J. Anthony, “Carbonation of fly ash in oxy-fuel CFB combustion,” *Fuel*, vol. 87, no. 7, pp. 1108–1114, 2008.
- [77] C. Chen and C. Zhao, “Mechanism of highly efficient in-furnace desulfurization by limestone under O₂/CO₂ coal combustion atmosphere,” *Ind. Eng. Chem. Res.*, vol. 45, no. 14, pp. 5078–5085, 2006.
- [78] L. F. De Diego *et al.*, “Optimum temperature for sulphur retention in fluidised beds working under oxy-fuel combustion conditions,” *Fuel*, vol. 114, pp. 106–113, 2013.
- [79] C. Lupianez, I. Guedea, I. Bolea, L. I. Diez, and L. M. Romeo, “Experimental study of SO₂ and NO_x emissions in fluidized bed oxy-fuel combustion,” *Fuel Process. Technol.*, vol. 106, no. x, pp. 587–594, 2013.
- [80] I. Liémans, B. Alban, J. P. Tranier, and D. Thomas, “SO_x and NO_x absorption based removal into acidic conditions for the flue gas treatment in oxy-fuel combustion,” *Energy Procedia*, vol. 4, pp. 2847–2854, 2011.

- [81] A. Kochel, A. Cieplin, and A. Szymanek, "Flue Gas Desulfurization in Oxygen-Enriched Atmospheres Using Modified Limestone Sorbents," vol. 2, no. 2, 2015.
- [82] M. De Las Obras-Loscertales *et al.*, "Morphological analysis of sulfated Ca-based sorbents under conditions corresponding to oxy-fuel fluidized bed combustion," *Fuel*, vol. 162, pp. 264–270, 2015.
- [83] S. Guo, H. Wang, D. Liu, L. Yang, X. Wei, and S. Wu, "Understanding the Impacts of Impurities and Water Vapor on Limestone Calcination in a Laboratory-Scale Fluidized Bed," *Energy and Fuels*, vol. 29, no. 11, pp. 7572–7583, 2015.
- [84] C. Wang and L. Chen, "The effect of steam on simultaneous calcination and sulfation of limestone in CFBB," *Fuel*, vol. 175, pp. 164–171, 2016.
- [85] H. Wang, S. Guo, D. Liu, L. Yang, X. Wei, and S. Wu, "Understanding the Impacts of Water Vapor on CaO Sulfurization in a Laboratory-Scale Fluidized Bed," *Energy and Fuels*, vol. 30, p. 7108–7117, 2016.
- [86] R. Saidur, E. A. Abdelaziz, A. Demirbas, M. S. Hossain, and S. Mekhilef, "A review on biomass as a fuel for boilers," *Renew. Sustain. Energy Rev.*, vol. 15, no. 5, pp. 2262–2289, 2011.
- [87] S. Bachu, "CO₂ storage in geological media: Role, means, status and barriers to deployment," *Prog. Energy Combust. Sci.*, vol. 34, no. 2, pp. 254–273, 2008.
- [88] W. H. Chen and P. C. Kuo, "Torrefaction and co-torrefaction characterization of hemicellulose, cellulose and lignin as well as torrefaction of some basic constituents in biomass," *Energy*, vol. 36, no. 2, pp. 803–811, 2011.
- [89] Q. Bu *et al.*, "Phenol and phenolics from lignocellulosic biomass by catalytic microwave pyrolysis," *Bioresour. Technol.*, vol. 102, no. 13, pp. 7004–7007, 2011.
- [90] L. J. R. Nunes, J. C. O. Matias, and J. P. S. Catalão, "A review on torrefied biomass pellets as a sustainable alternative to coal in power generation," *Renew. Sustain. Energy Rev.*, vol. 40, pp. 153–160, 2014.
- [91] D. Agar and M. Wihersaari, "Bio-coal, torrefied lignocellulosic resources - Key properties for its use in co-firing with fossil coal - Their status," *Biomass and Bioenergy*, vol. 44, pp. 107–111, 2012.
- [92] A. Pirraglia, R. Gonzalez, D. Saloni, J. Wright, and J. Denig, "Fuel properties and suitability of *Eucalyptus benthamii* and *Eucalyptus macarthurii* for torrefied wood and pellets," *BioResources*, vol. 7, no. 1, pp. 217–235, 2012.
- [93] M. Phanphanich and S. Mani, "Impact of torrefaction on the grindability and fuel characteristics of forest biomass," *Bioresour. Technol.*, vol. 102, no. 2, pp.

1246–1253, 2011.

- [94] A. A. Khan, W. de Jong, P. J. Jansens, and H. Spliethoff, “Biomass combustion in fluidized bed boilers: Potential problems and remedies,” *Fuel Process. Technol.*, vol. 90, no. 1, pp. 21–50, 2009.
- [95] P. Sun *et al.*, “Experimental investigation on the combustion and heat transfer characteristics of wide size biomass co-firing in 0.2 MW circulating fluidized bed,” *Appl. Therm. Eng.*, vol. 52, no. 2, pp. 284–292, 2013.
- [96] D. Vamvuka, M. Pitharoulis, G. Alevizos, E. Repouskou, and D. Pentari, “Ash effects during combustion of lignite/biomass blends in fluidized bed,” *Renew. Energy*, vol. 34, no. 12, pp. 2662–2671, 2009.
- [97] M. Varol, A. T. Atimtay, H. Olgun, and H. Atakül, “Emission characteristics of co-combustion of a low calorie and high sulfur-lignite coal and woodchips in a circulating fluidized bed combustor: Part 1. Effect of excess air ratio,” *Fuel*, vol. 117, no. PART A, pp. 792–800, 2014.
- [98] M. Varol, A. T. Atimtay, and H. Olgun, “Emission characteristics of co-combustion of a low calorie and high-sulfur-lignite coal and woodchips in a circulating fluidized bed combustor: Part 2. Effect of secondary air and its location,” *Fuel*, vol. 130, pp. 1–9, 2014.
- [99] L. Duan, Y. Duan, C. Zhao, and E. J. Anthony, “NO emission during co-firing coal and biomass in an oxy-fuel circulating fluidized bed combustor,” *Fuel*, vol. 150, pp. 8–13, 2015.
- [100] M. Kosowska-Golachowska, A. Kijo-Kleczkowska, A. Luckos, K. Wolski, and T. Musial, “Oxy-combustion of biomass in a circulating fluidized bed,” *Arch. Thermodyn.*, vol. 37, no. 1, pp. 17–30, 2016.
- [101] A. T. Atimtay *et al.*, “Co-firing of pine chips with Turkish lignites in 750kWth circulating fluidized bed combustion system,” *Bioresour. Technol.*, vol. 224, pp. 601–610, 2016.
- [102] C. Lupiáñez, M. C. Mayoral, L. I. Díez, E. Pueyo, S. Espatolero, and J. M. Andrés, “The role of limestone during fluidized bed oxy-combustion of coal and biomass,” vol. 184, pp. 670–680, 2016.
- [103] L. Reh, “Development potentials and research needs in circulating fluidized bed combustion,” *China Particuology*, vol. 1, no. 5, pp. 185–200, 2003.
- [104] R. Sotudeh-Gharebaagh, R. Legros, J. Chaouki, and J. Paris, “Simulation of circulating fluidized bed reactors using ASPEN PLUS,” *Fuel*, vol. 77, no. 4, pp. 327–337, 1998.
- [105] E. Desroches-Ducarne, J. C. Dolignier, E. Marty, G. Martin, and L. Delfosse, “Modelling of gaseous pollutants emissions in circulating fluidized bed

- combustion of municipal refuse,” *Fuel*, vol. 77, no. 13, pp. 1399–1410, 1998.
- [106] W. Zhou, C. S. Zhao, L. B. Duan, C. R. Qu, and X. P. Chen, “Two-dimensional computational fluid dynamics simulation of coal combustion in a circulating fluidized bed combustor,” *Chem. Eng. J.*, vol. 166, no. 1, pp. 306–314, 2011.
- [107] L. Huilin, Z. Guangbo, B. Rushan, C. Yongjin, and D. Gidaspow, “Coal combustion model for circulating fluidized bed boilers,” *Fuel*, vol. 79, no. 2, pp. 165–172, 2000.
- [108] N. V. Gnanapragasam and B. V. Reddy, “Modeling of axial bed-to-wall heat transfer in a CFB combustor with abrupt riser exit geometry,” *Int. J. Heat Mass Transf.*, vol. 51, no. 25–26, pp. 6102–6109, 2008.
- [109] A. Gungor and N. Eskin, “Analysis of environmental benefits of CFB combustors via one-dimensional model,” *Chem. Eng. J.*, vol. 131, no. 1–3, pp. 301–317, 2007.
- [110] A. Gungor, “One dimensional numerical simulation of small scale CFB combustors,” *Energy Convers. Manag.*, vol. 50, no. 3, pp. 711–722, 2009.
- [111] A. Gungor, “Simulation of NO_x emission in circulating fluidized beds burning Low-grade Fuels,” *Energy and Fuels*, vol. 23, no. 5, pp. 2475–2481, 2009.
- [112] A. Gungor, “Prediction of SO₂ and NO_x emissions for low-grade Turkish lignites in CFB combustors,” *Chem. Eng. J.*, vol. 146, no. 3, pp. 388–400, 2009.
- [113] N. Selcuk and M. Ozkan, “Simulation of circulating fluidized bed combustors firing indigenous lignite,” *Int. J. Therm. Sci.*, vol. 50, no. 6, pp. 1109–1115, 2011.
- [114] N. Zhang, B. Lu, W. Wang, and J. Li, “3D CFD simulation of hydrodynamics of a 150MWe circulating fluidized bed boiler,” *Chem. Eng. J.*, vol. 162, no. 2, pp. 821–828, 2010.
- [115] R. Wischniewski, L. Ratschow, E. U. Hartge, and J. Werther, “Reactive gas-solids flows in large volumes-3D modeling of industrial circulating fluidized bed combustors,” *Particuology*, vol. 8, no. 1, pp. 67–77, 2010.
- [116] K. Myöhänen and T. Hyppänen, “A three-dimensional model frame for modelling combustion and gasification in circulating fluidized bed furnaces,” *Int. J. Chem. Eng.*, vol. 9, p. nr A25, 2011.
- [117] W. P. Adamczyk, P. Kozolub, G. Wecel, A. Klimanek, R. A. Bialecki, and T. Czakiert, “Modeling oxy-fuel combustion in a 3D circulating fluidized bed using the hybrid Euler-Lagrange approach,” *Appl. Therm. Eng.*, vol. 71, no. 1, pp. 266–275, 2014.
- [118] W. P. Adamczyk, P. Kozolub, A. Klimanek, R. A. Bialecki, M. Andrzejczyk, and M. Klajny, “Numerical simulations of the industrial circulating fluidized

- bed boiler under air- and oxy-fuel combustion,” *Appl. Therm. Eng.*, vol. 87, pp. 127–136, 2015.
- [119] S. Rahiala, K. Myohanen, and T. Hyppanen, “Modeling the behavior of limestone particles in oxy-fuel CFB processes,” *Fuel*, vol. 127, pp. 141–150, 2014.
- [120] K. Luo, F. Wu, S. Yang, M. Fang, and J. Fan, “High-fidelity simulation of the 3-D full-loop gas – solid flow characteristics in the circulating fluidized bed,” vol. 123, pp. 22–38, 2015.
- [121] C. Liu, M. Zhao, W. Wang, and J. Li, “3D CFD simulation of a circulating fluidized bed with on-line adjustment of mechanical valve,” *Chem. Eng. Sci.*, vol. 137, pp. 646–655, 2015.
- [122] S. Banerjee and R. K. Agarwal, “An Eulerian Approach to Computational Fluid Dynamics Simulation of a Chemical- Looping Combustion Reactor With Chemical Reactions,” vol. 138, no. July 2016, pp. 1–9, 2017.
- [123] Y. Guan, J. Chang, K. Zhang, B. Wang, Q. Sun, and D. Wen, “Three-dimensional full loop simulation of solids circulation in an interconnected fluidized bed,” *Powder Technol.*, vol. 289, pp. 118–125, 2016.
- [124] B. Gasifier, M. Biglari, H. Liu, A. Elkamel, and A. Lohi, “Application of Scaling-Law and CFD Modeling to Hydrodynamics of Circulating Biomass Fluidized,” 2016.
- [125] R. K. Thapa, A. Frohner, G. Tondl, C. Pfeifer, and B. M. Halvorsen, “Circulating fluidized bed combustion reactor : Computational Particle Fluid Dynamic model validation and gas feed position optimization,” *Comput. Chem. Eng.*, vol. 92, pp. 180–188, 2016.
- [126] M. Nikku, K. Myöhänen, J. Ritvanen, and T. Hyppänen, “Chemical Engineering Research and Design Three-dimensional modeling of biomass fuel flow in a circulating fluidized bed furnace with an experimentally derived momentum exchange,” vol. 5, pp. 77–90, 2016.
- [127] R. I. Singh and K. Ghule, “Design , development , experimental and CFD analysis of a prototype fluidized bed stripper ash cooler,” *Appl. Therm. Eng.*, vol. 107, pp. 1077–1090, 2016.
- [128] C. Zi *et al.*, “CFD simulation and hydrodynamics characterization of solids oscillation behavior in a circulating fluidized bed with sweeping bend return,” *Chem. Eng. J.*, vol. 307, pp. 604–620, 2017.
- [129] M. V. Kök and M. R. Pamir, “Pyrolysis and combustion studies of fossil fuels by thermal analysis methods,” *J. Anal. Appl. Pyrolysis*, vol. 35, no. 2, pp. 145–156, 1995.

- [130] E. Abbasi-Atibeh and A. Yozgatligil, "A study on the effects of catalysts on pyrolysis and combustion characteristics of Turkish lignite in oxy-fuel conditions," *Fuel*, vol. 115, pp. 841–849, 2014.
- [131] S. L. Niu, K. H. Han, and C. M. Lu, "Characteristic of coal combustion in oxygen/carbon dioxide atmosphere and nitric oxide release during this process," *Energy Convers. Manag.*, vol. 52, no. 1, pp. 532–537, 2011.
- [132] X. Huang, X. Jiang, X. Han, and H. Wang, "Combustion Characteristics of Fine- and Micro-pulverized Coal in the Mixture of O₂/CO₂," vol. 22, pp. 3756–3762, 2008.
- [133] Q. Li, C. Zhao, X. Chen, W. Wu, and Y. Li, "Comparison of pulverized coal combustion in air and in O₂/CO₂ mixtures by thermo-gravimetric analysis," *J. Anal. Appl. Pyrolysis*, vol. 85, no. 1–2, pp. 521–528, 2009.
- [134] F. Meng, J. Yu, A. Tahmasebi, and Y. Han, "Pyrolysis and combustion behavior of coal gangue in O₂/CO₂ and O₂/N₂ mixtures using thermogravimetric analysis and a drop tube furnace," *Energy and Fuels*, vol. 27, no. 6, pp. 2923–2932, 2013.
- [135] M. Wilk, A. Magdziarz, and I. Kalemba, "Characterisation of renewable fuels' torrefaction process with different instrumental techniques," *Energy*, vol. 87, pp. 259–269, 2015.
- [136] B. Mi, Z. Liu, W. Hu, P. Wei, Z. Jiang, and B. Fei, "Investigating pyrolysis and combustion characteristics of torrefied bamboo, torrefied wood and their blends," *Bioresour. Technol.*, vol. 209, pp. 50–55, 2016.
- [137] M. Varol, A. T. Atimtay, B. Bay, and H. Olgun, "Investigation of co-combustion characteristics of low quality lignite coals and biomass with thermogravimetric analysis," *Thermochim. Acta*, vol. 510, no. 1–2, pp. 195–201, 2010.
- [138] D. Vamvuka and S. Sfakiotakis, "Combustion behaviour of biomass fuels and their blends with lignite," *Thermochim. Acta*, vol. 526, no. 1–2, pp. 192–199, 2011.
- [139] A. Skreiberg, O. Skreiberg, J. Sandquist, and L. Sørum, "TGA and macro-TGA characterisation of biomass fuels and fuel mixtures," *Fuel*, vol. 90, no. 6, pp. 2182–2197, 2011.
- [140] G. K. Parshetti, A. Quek, R. Betha, and R. Balasubramanian, "TGA-FTIR investigation of co-combustion characteristics of blends of hydrothermally carbonized oil palm biomass (EFB) and coal," *Fuel Process. Technol.*, vol. 118, pp. 228–234, 2014.
- [141] A. Toptas, Y. Yildirim, G. Duman, and J. Yanik, "Combustion behavior of different kinds of torrefied biomass and their blends with lignite," *Bioresour.*

- Technol.*, vol. 177, pp. 328–336, 2015.
- [142] N. S. Yuzbasi and N. Selçuk, “Air and oxy-fuel combustion characteristics of biomass/lignite blends in TGA-FTIR,” *Fuel Process. Technol.*, vol. 92, no. 5, pp. 1101–1108, 2011.
- [143] N. S. Yuzbasi and N. Selçuk, “Air and oxy-fuel combustion behaviour of petcoke/lignite blends,” *Fuel*, vol. 92, no. 1, pp. 137–144, 2012.
- [144] A. Magdziarz and M. Wilk, “Thermogravimetric study of biomass, sewage sludge and coal combustion,” *Energy Convers. Manag.*, vol. 75, no. 2013, pp. 425–430, 2013.
- [145] A. Rojas, J. Barraza, R. Barranco, and E. Lester, “A new char combustion kinetic model - Part 2: Empirical validation,” *Fuel*, vol. 96, pp. 168–175, 2012.
- [146] P. Pintana and N. Tippayawong, “Nonisothermal thermogravimetric analysis of Thai lignite with high CAO content,” *Sci. World J.*, vol. 2013, 2013.
- [147] Y. Zhang, Y. Guo, F. Cheng, K. Yan, and Y. Cao, “Investigation of combustion characteristics and kinetics of coal gangue with different feedstock properties by thermogravimetric analysis,” *Thermochim. Acta*, vol. 614, pp. 137–148, 2015.
- [148] S. G. Sahu, P. Sarkar, N. Chakraborty, and A. K. Adak, “Thermogravimetric assessment of combustion characteristics of blends of a coal with different biomass chars,” *Fuel Process. Technol.*, vol. 91, no. 3, pp. 369–378, 2010.
- [149] M. V. Gil, D. Casal, C. Pevida, J. J. Pis, and F. Rubiera, “Thermal behaviour and kinetics of coal/biomass blends during co-combustion,” *Bioresour. Technol.*, vol. 101, no. 14, pp. 5601–5608, 2010.
- [150] S. Y. Yorulmaz and A. Atımtay, “Investigation of combustion kinetics of five waste wood samples with thermogravimetric analysis,” *Environ. Earth Sci.*, vol. 90, pp. 511–520, 2011.
- [151] M. V. Gil, J. Riaza, L. Álvarez, C. Pevida, J. J. Pis, and F. Rubiera, “Kinetic models for the oxy-fuel combustion of coal and coal/biomass blend chars obtained in N₂ and CO₂ atmospheres,” *Energy*, vol. 48, no. 1, pp. 510–518, 2012.
- [152] M. V. Kok and E. Özgür, “Thermal analysis and kinetics of biomass samples,” *Fuel Process. Technol.*, vol. 106, pp. 739–743, 2013.
- [153] M. F. Irfan, A. Arami-Niya, M. H. Chakrabarti, W. M. A. Wan Daud, and M. R. Usman, “Kinetics of gasification of coal, biomass and their blends in air (N₂/O₂) and different oxy-fuel (O₂/CO₂) atmospheres,” *Energy*, vol. 37, no. 1, pp. 665–672, 2012.
- [154] B. Engin and H. Atakül, “Air and oxy-fuel combustion kinetics of low rank

- lignites,” *J. Energy Inst.*, pp. 1–12, 2016.
- [155] D. Magalhães, F. Kazanç, J. Riaza, S. Erensoy, Ö. Kabaklı, and H. Chalmers, “Combustion of Turkish lignites and olive residue: Experiments and kinetic modelling,” *Fuel*, vol. 203, pp. 868–876, 2017.
- [156] A. Olajire, C. Zhi, S. Hanson, and C. Wai, “Thermogravimetric analysis of the pyrolysis characteristics and kinetics of plastics and biomass blends,” *Fuel Process. Technol.*, vol. 128, pp. 471–481, 2014.
- [157] C. M. Romero, G. L. A. F. Arce, and I. Avila, “Comparative study on combustion and oxy-fuel combustion environments using mixtures of coal with sugarcane bagasse and biomass sorghum bagasse by the thermogravimetric analysis a,” vol. 92, 2019.
- [158] P. J. Haines, *Thermal Methods of Analysis: Principles, Applications and Problems*, 1st ed. Springer Netherlands, 1995.
- [159] B. Keivani, S. Gultekin, H. Olgun, and A. T. Atimtay, “Torrefaction of pine wood in a continuous system and optimization of torrefaction conditions,” *Int. J. Energy Res.*, vol. 42, no. 15, pp. 4597–4609, 2018.
- [160] M. V. Kök, “Recent developments in the application of thermal analysis techniques in fossil fuels,” *J. Therm. Anal. Calorim.*, vol. 91, no. 3, pp. 763–773, 2008.
- [161] M. G. Grønli, G. Várhegyi, and C. Di Blasi, “Thermogravimetric Analysis and Devolatilization Kinetics of Wood,” *Ind. Eng. Chem. Res.*, vol. 41, no. 17, pp. 4201–4208, 2002.
- [162] A. T. Atimtay, H. Vural, H. Olgun, and G. Bardakçioğlu, “Development of Circulating Fluidized Bed Combustion Technology for Biomass and Biomass/Coal Mixtures,” 2012.
- [163] R. Du *et al.*, “Thermal behavior and kinetic study on the pyrolysis of Shenfu coal by sectioning method,” *J. Therm. Anal. Calorim.*, vol. 125, no. 2, pp. 959–966, 2016.
- [164] M. Heydari, M. Rahman, and R. Gupta, “Kinetic study and thermal decomposition behavior of lignite coal,” *Int. J. Chem. Eng.*, vol. 2015, 2015.
- [165] S. Vyazovkin, A. K. Burnham, J. M. Criado, L. A. Pérez-Maqueda, C. Popescu, and N. Sbirrazzuoli, “ICTAC Kinetics Committee recommendations for performing kinetic computations on thermal analysis data,” *Thermochim. Acta*, vol. 520, no. 1–2, pp. 1–19, 2011.
- [166] J. R. Opfermann, E. Kaisersberger, and H. J. Flammersheim, “Model-free analysis of thermoanalytical data—advantages and limitations,” *Thermochim. Acta*, vol. 391, no. 1–2, pp. 119–127, 2002.

- [167] J. Sestak, "Thermophysical Properties of Solids," *Prague Acad.*, pp. 218–222, 1984.
- [168] S. Vyazovkin and C. A. Wight, "Model-free and model-fitting approaches to kinetic analysis of isothermal and nonisothermal data," *Thermochim. Acta*, vol. 340, pp. 53–68, 1999.
- [169] R. R. Keuleers, J. F. Janssens, and H. O. Desseyn, "Comparison of some methods for activation energy determination of thermal decomposition reactions by thermogravimetry," vol. 385, pp. 127–142, 2002.
- [170] S. S. Idris, N. A. Rahman, K. Ismail, A. B. Alias, Z. A. Rashid, and M. J. Aris, "Investigation on thermochemical behaviour of low rank Malaysian coal, oil palm biomass and their blends during pyrolysis via thermogravimetric analysis (TGA)," *Bioresour. Technol.*, vol. 101, no. 12, pp. 4584–4592, 2010.
- [171] J. Cai, Y. Wang, L. Zhou, and Q. Huang, "Thermogravimetric analysis and kinetics of coal/plastic blends during co-pyrolysis in nitrogen atmosphere," *Fuel Process. Technol.*, vol. 89, no. 1, pp. 21–27, 2008.
- [172] S. Vyazovkin and N. Sbirrazzuoli, "Isoconversional kinetic analysis of thermally stimulated processes in polymers," *Macromol. Rapid Commun.*, vol. 27, no. 18, pp. 1515–1532, 2006.
- [173] L. Duan, J. Chen, Y. Jiang, X. Li, P. Longhurst, and M. Lei, "Experimental and kinetic study of thermal decomposition behaviour of phytoremediation derived *Pteris vittata*," *J. Therm. Anal. Calorim.*, vol. 128, no. 2, pp. 1207–1216, 2017.
- [174] M. J. Starink, "The determination of activation energy from linear heating rate experiments: A comparison of the accuracy of isoconversion methods," *Thermochim. Acta*, vol. 404, no. 1–2, pp. 163–176, 2003.
- [175] A. Soria-Verdugo, E. Goos, and N. García-Hernando, "Effect of the number of TGA curves employed on the biomass pyrolysis kinetics results obtained using the Distributed Activation Energy Model," *Fuel Process. Technol.*, vol. 134, pp. 360–371, 2015.
- [176] C. Earnest, *The Modern Thermogravimetric Approach to the Compositional Analysis of Materials*. 1988.
- [177] J. Cai *et al.*, "Processing thermogravimetric analysis data for isoconversional kinetic analysis of lignocellulosic biomass pyrolysis: Case study of corn stalk," *Renew. Sustain. Energy Rev.*, vol. 82, no. April 2017, pp. 2705–2715, 2018.
- [178] E1641, "Standard Test Method for Decomposition Kinetics by Thermogravimetry Using the Ozawa / Flynn / Wall Method 1," *ASTM Stand. Test Method Decompos. Kinet. by Thermogravim. Using Ozawa / Flynn / Wall Method 1*, pp. 1–7, 2013.

- [179] Marcio L. de Souza-Santos, *Solid Fuels Combustion and Gasification: Modeling, Simulation, and Equipment Operations*, Second Edi. CRC Press, Tylor & Francis Group, 2010.
- [180] M. L. de Souza-Santos, "CSFB applied to fluidized-bed gasification of special fuels," *Fuel*, vol. 88, no. 5, pp. 826–833, 2009.
- [181] A. Żyłka *et al.*, "Numerical simulations of fluidization dynamics in a hot model of a CLC process," in *E3S Web of Conferences*, 2017, vol. 13, p. 04002.
- [182] M. L. de Souza-Santos, *Comprehensive Simulator of Fluidized and Moving Bed Equipment*. 2019.
- [183] P. Brachi, F. Miccio, M. Miccio, and G. Ruoppolo, "Pseudo-component thermal decomposition kinetics of tomato peels via isoconversional methods," *Fuel Process. Technol.*, vol. 154, pp. 243–250, 2016.
- [184] X. Li, Y. Lv, B. Ma, W. Wang, and S. Jian, "Decomposition kinetic characteristics of calcium carbonate containing organic acids by TGA," *Arab. J. Chem.*, vol. 10, pp. S2534–S2538, 2017.
- [185] L. Duan, C. Zhao, W. Zhou, C. Qu, and X. Chen, "Investigation on Coal Pyrolysis in CO₂ Atmosphere," no. x, pp. 3826–3830, 2009.
- [186] E. P. Hyatt, I. B. Cutler, and M. E. Wadsworth, "Calcium Carbonate Decomposition in Carbon Dioxide Atmosphere," *J. Am. Ceram. Soc.*, vol. 61, no. 1943, pp. 70–74, 1955.
- [187] Z. Zhou, X. Hu, Z. You, Z. Wang, J. Zhou, and K. Cen, "Thermochemical Oxy-fuel combustion characteristics and kinetic parameters of lignite coal from thermo-gravimetric data," *Thermochim. Acta*, vol. 553, pp. 54–59, 2013.
- [188] Y. F. Zhang, X. Y. Chen, Q. C. Zhang, C. P. Li, and Q. Zhou, "Oxygen-enriched combustion of lignite," *Therm. Sci.*, vol. 19, no. 4, pp. 1389–1392, 2015.
- [189] G. Lv, S. Wu, and R. Lou, "Kinetic Study of the Thermal Decomposition of Hemicellulose Isolated From Corn Stalk," *BioResources*, vol. 5, no. 2, pp. 1281–1291, 2010.
- [190] W. H. Chen, K. M. Lu, W. J. Lee, S. H. Liu, and T. C. Lin, "Non-oxidative and oxidative torrefaction characterization and SEM observations of fibrous and ligneous biomass," *Appl. Energy*, vol. 114, pp. 104–113, 2014.
- [191] Z. Chen *et al.*, "Characteristics and kinetic study on pyrolysis of five lignocellulosic biomass via thermogravimetric analysis," *Bioresour. Technol.*, vol. 192, pp. 441–450, 2015.
- [192] L. Jia, E. J. Anthony, I. Lau, and J. Wang, "Study of coal and coke ignition in fluidized beds," *Fuel*, vol. 85, no. 5–6, pp. 635–642, 2006.

- [193] L. Xu, Y. Jiang, and L. Wang, “Thermal decomposition of rape straw: Pyrolysis modeling and kinetic study via particle swarm optimization,” *Energy Convers. Manag.*, vol. 146, pp. 124–133, 2017.
- [194] A. G. Barneto, J. A. Carmona, J. E. M. Alfonso, and R. S. Serrano, “Simulation of the thermogravimetry analysis of three non-wood pulps,” *Bioresour. Technol.*, vol. 101, no. 9, pp. 3220–3229, 2010.
- [195] M. Jeguirim, S. Dorge, and G. Trouvé, “Thermogravimetric analysis and emission characteristics of two energy crops in air atmosphere: *Arundo donax* and *Miscanthus giganteus*,” *Bioresour. Technol.*, vol. 101, no. 2, pp. 788–793, 2010.
- [196] G. Jiang, D. J. Nowakowski, and A. V. Bridgwater, “A systematic study of the kinetics of lignin pyrolysis,” *Thermochim. Acta*, vol. 498, no. 1–2, pp. 61–66, 2010.
- [197] R. Barzegar, A. Yozgatlıgil, and A. T. Atimtay, “Combustion characteristics of Turkish lignites at oxygen-enriched and oxy-fuel combustion conditions,” *J. Energy Inst.*, 2018.
- [198] M. Wilk, A. Magdziarz, M. Gajek, M. Zajemska, K. Jayaraman, and I. Gokalp, “Combustion and kinetic parameters estimation of torrefied pine, acacia and *Miscanthus giganteus* using experimental and modelling techniques,” *Bioresour. Technol.*, vol. 243, pp. 304–314, 2017.
- [199] D. A. Tillman, D. N. B. Doung, and N. S. Harding, *Solid Fuel Blending Principles, Practices, and Problems*. Butterworth-Heinemann, 2012.
- [200] S. Krerkkaiwan, C. Fushimi, A. Tsutsumi, and P. Kuchonthara, “Synergetic effect during co-pyrolysis / gasification of biomass and sub-bituminous coal,” *Fuel Process. Technol.*, vol. 115, pp. 11–18, 2013.
- [201] J. L. Goldfarb and S. Ceylan, “Second-generation sustainability: Application of the distributed activation energy model to the pyrolysis of locally sourced biomass – coal blends for use in co-firing scenarios,” *Fuel*, vol. 160, pp. 297–308, 2015.
- [202] D. A. Tillman, A. Dobrzanski, D. Duong, J. Dosch, K. Taylor, and R. Kinninck, “Optimizing blends of Powder River Basin subbituminous coal and bituminous coal,” in *Proceedings PRB users group annual meeting*, 2006.

CURRICULUM VITAE

PERSONAL INFORMATION

Surname, Name : Barzegar, Ramin
Nationality : Iran
Date and Place of Birth : 23 September 1985, Parsabad
Phone : +90 312 210 72 47
E-mail : ramin.barzegar@metu.edu.tr

EDUCATION

Degree	Institution	Year of Graduation
MS	Urmia University, Mechanical Engineering	2010
BS	Urmia University, Mechanical Engineering	2007
High School	Bagher-Olum High School, Parsabad	2003

WORK EXPERIENCE

Year	Place	Enrollment
2018-2019	DETS Dynamics Co.	Consultant
2010-2014	Azad University, Iran	Academic Staff

FOREIGN LANGUAGES

Advanced English, Advanced Azeri, Advanced Persian

PUBLICATIONS

1. **Ramin Barzegar**, Ahmet Yozgatligil, Aysel T. Atimtay, "Combustion characteristics of Turkish lignites at oxygen-enriched and oxy-fuel combustion conditions", Journal of the Energy Institute, Volume 92, Issue 5, 2019, Pages 1440-1450, <https://doi.org/10.1016/j.joei.2018.08.007>
2. **Ramin Barzegar**, Sevil Avsaroglu, Ahmet Yozgatligil, Aysel T. Atimtay, "Pyrolysis characteristics of Turkish lignites in N₂ and CO₂ environments", Energy Sources, Part A: Recovery, Utilization, and Environmental Effects, Volume 40, 2018 - Issue 20, Pages 2467-2475.

<https://doi.org/10.1080/15567036.2018.1502845>

3. **Ramin Barzegar**, Ahmet Yozgatligil, Aysel Atimtay, Hayati Olgun, “TGA and kinetic study of different torrefaction conditions of wood biomass under air and oxy-fuel combustion atmospheres”, *Journal of the Energy Institute*, Accepted for publication (20 Aug 2019).

4. Sevil Avsaroglu, **Ramin Barzegar**, Baris Kaymak, Ahmet Yozgatligil, Aysel T. Atimtay, Investigation of Combustion Kinetics of two Turkish Lignites under Oxy-Fuel Combustion Conditions by Thermal Gravimetry Analysis, *6th Workshop on Cofiring Biomass with Coal*, 14-15 Sep. 2016, Sardinia, Italy.